Hydrodynamic roughness of floodplain vegetation

Nederlandse Geografische Studies / Netherlands Geographical Studies

ISSN 0169-4839

Netherlands Geographical Studies 358

Hydrodynamic roughness of floodplain vegetation

Airborne parameterization and field validation

Menno Straatsma

Utrecht 2007

Koninklijk Nederlands Aardrijkskundig Genootschap
Faculteit Geowetenschappen Universiteit Utrecht

Supervisors:

Prof. dr. Steven M. de Jong	Universiteit Utrecht
Prof. dr. Eduard A. Koster	Universiteit Utrecht
Dr. Hans Middelkoop	Universiteit Utrecht

Examination committee:

Prof. dr. ir. George M. Vosselman	ITC, Enschede, NL
Univ.Prof. Dipl.-Ing. Dr.techn. Norbert Pfeifer	TU Vienna, AU
Prof. dr. Suzanne M.H. Hulscher	Universiteit Twente, NL
Prof. dr. Paul D. Bates	University of Bristol, UK
Dr. Rob S.E.W. Leuven	Radboud Universiteit Nijmegen, NL

ISBN 978-90-6809-399-5

Graphic design, cartography and figures:
GeoMedia (Faculty of Geosciences, Utrecht University)

Printed in the Netherlands by Labor Grafimedia b.v. – Utrecht

Contents

Figures

Tables

Acknowledgements

Water, and rivers in special, have enticed me since childhood. That led to lots of swimming, numerous kayaking trips and rafting competition. During my studies, I was pleased to be able to combine this love for water with a topic for my masters thesis, even though I had to move from playing in main channel to the floodplain, where I studied vegetion. The floodplain vegetation, however, did not yield her secrets easily. Now I know that vegetation mapping and roughness determination comprise an aspect of seduction, which means that much time and money needs to be invested. New tools and methods had to be developed to lure the vegetation in unveiling her secrets. The work in progress included hope and despair, anger and relieve, steadfastness and indulgence, but in the end the thrill of consistent results. Such an insight feels spacious, energetic and connected.

Over the period of my PhD research, I have been supported by many people. Here, I would like to acknowledge your help. First of all, I would like to thank Hans Middelkoop, my co-promotor. He saw the possibilities for further research in my master's research, created a PhD position and contributed significantly to the overall quality of this thesis. Hans, you were always able to meticulously read my manuscripts. Your enthusiasm is infectious and I admire your wit. I look forward to our next project.

I would like to thank my promotores, Steven de Jong and Ward Koster. Steven, you were able to get the idea of societal significance of this project into my belief system. Persistance beats resistance! I value all the work you put into correcting my manuscripts, your support for and interest in a new type of remote sensing data and processing techniques. Ward, I would like to thank you for your long term commitment to the various frameworks of this project ('gremiumwerk' binnen NCR, IGBP en LOICZ).

The department of Physical Geography has been an inspiring place to work with good vibrations and screamingly funny caberets during many PhD graduation parties. Some people I would like to mention in particular. Leo Tebbens, my room-mate for the first two years, thanks for the longer time-scale framework, your community spirit and open-mindedness. Elisabeth Addink, my neighbour during the last years, your optimimal combination of sense with sensitivity is inspiring. It is great to have you as a room mate.

Ivo Thonon, my partner in crime during field work. Let's take more water samples in the main channel and floodplain of the river Waal during gales. Thanks for your help with the float tracking and political diversions. I am also grateful for the assistance of many others during my float tracking field work: Pim van Santen, Mark Gouw, Nico Willlemse, Freek Huthoff, Herman (frames bouwen geeft wellicht de meeste voldoening) and Johanne Straatsma. The encouragements of Martin Baptist (TUD) are greatly valued: 'You should see the scatter on my

lab tests'. John Beijer (WUR) is gratefully acknowledged for lending me their boat generously. The field work would not have been possible without the myth busters of the physical-electronic laboratory: Theo Tiemissen, Chris Roosendaal, Henk Markies, Marcel van Maarsseveen, Bas van Dam and Hassan Aarab.

Data processing would not have been that efficient without the help of Edzer Pebesma (Dat kan ook in R), Kor de Jong (Dat kan ook in Python), Cees Wesseling (Dat doe ik liever in C) and Derek Karsseberg (Dan moet je een beetje hacken in PCRaster)

Many others contributed to a good working environment. I thank
- the early first-floor corridor-dwellers Kim Cohen (paleo) vs. Maarten Kleinhans (ik actuo), Wim hoek, Esther Stouthamer, Gilles Erkens, Loes van Schaik, Antoine Wilbers and Roy Frings.
- the pixel department consisting of Raymond Sluiter (Orde en Netheid), Hansakwast and Wiebe Borren.
- the third floor corridor-dwellers Susanne Quartel, Ton Hoitink and Freek Buschman.
- the hydrology department, Ariën Lam, Daniel Mourad, Wiebe Borren, Reinder Brolsma, Sibren Loos and Hanneke Schuurmans.

Jord Warmink carried out his master's research within the framework of this thesis. He managed to collect and process gigabites of data, which is the core of our paper on vegetation density measurements. Thank and succes with your PhD.

I thank Luc Amoureus of Fugro-Inpark for his assistance in understanding the various differences between the airborne laser scanner datasets and his help in preprocessing the data in a new format ('in the name of science'). I'm also grateful for the alertness of Ardis Bollweg (AGI) for informing me in the last moment of additional FLIMAP options ('Er zit ook een gain-knop op de scanner'). Regine Brügelmann, René Hartmann and Andries Knotters are also thanked for their contribution to this project.

Emiel van Velzen and Peter Jesse helped me understand aspects of vegetation roughness. Claus van den Brink was always prepared to supply further spatial data

Geomedia is greatfully acknowledged for their effort to optimize my figures and layout ('Dat plaatje kan er net zo goed niet in.'): Margot Stoete, Margriet Ganzeveld, Fred Trappenburg and Rien Rabbers.

Here, I would also like to thank my family; Herman, Johanne, Nanne, Anneriet and Wineke Straatsma for proper distractions from work, assisted by Harry Dagelet and Aad Duifhuis.

I thank the Speedies for our countless parties, holidays, dinners and Catan games. The arc-toolbox is again in my possession!

My Ridhwan 'local group' provided excellent opportunities for subjective scientific inquiery. Our regular meetings always had a relaxing and expanding effect. Thanks to Jenny, Bas, Marcel,

Judith, Annet, Puck, Evelien, Frederiek, Hanneke and Nelleke. Additionally our 'large group and teachers served as a community for personal development.

Special thanks go to my paranimfen Maaike Ritzen and Pim van Santen for being my backup during the defence.

Lastly and most importantly Sari Räsänen, my beloved and partner. You always trusted that I would find a solution for my data analysis problems and supported me. You read all the manuscripts and commented on all my presentations, which was greatly valued. More importantly, you showed me beauty in the world where I never expected it.

1 Introduction

Lowland fluvial areas worldwide have proven popular areas for human settlement and include some of the most densely populated areas in the world. With human settlement, flooding became a major problem, which it still is today. Examples of recent flooding catastrophes are the Mississippi flood in 1993, the Oder flood in 1997 and the Elbe and Danube flood in August 2002 and April 2006. In the Netherlands the near-flooding events of 1993 and 1995 had a shock effect with respect to river management. In 1995, the flood led to the evacuation of the inhabitants in a large part of the fluvial area. Worldwide economic losses due to flooding were estimated by Berz *et al.* (2003) to amount to 27 billion US$ in 2002.

River management has primarily focussed on protection against flooding. In addition to drainage of the river basin, river functions include navigation, irrigation and hydropower. Many measures have been taken in the fluvial area to optimize these functions, including the building of dams, stream channelization, direct modification of the riparian ecosystem and landuse changes in the basin (Goodwin *et al.* 1997). Unfortunately, this management style led to the overall degradation of the fluvial ecosystem (Ward & Tockner 2001), caused by the loss of habitat diversity, the decrease of the flood magnitude and frequency due to dams, and discontinuity of the ecosystem along the length of the river. Moreover, climate change is expected to lead to sea level rise and increased variability of river discharge in some catchments (IPCC 2001; Middelkoop *et al.* 2001). Population pressure leads to the desire for housing in the floodplains, which further constrains the river.

In the past decades, we became aware of limitations of the current flood defense strategy namely, increasing the height of the embankments (Van Stokkom *et al.* 2005) and the significance of the fluvial ecosystem. Therefore, modern river management tries explicitly to combine ecological integrity with flood defense (Nienhuis & Leuven 2001). For constrained lowland rivers, such a goal implies that more space must be created for the river to accommodate peak discharges. At the same time ecological integrity requires more succession of vegetation, and therefore, more spatiotemporal variation of vegetation, which needs monitoring. This study contributes to the monitoring of floodplain vegetation and the associated effects on hydrodynamics. Below, the context, research objectives and outline of this thesis are given.

1.1 Context

Figure 1.1 illustrates the hierarchic context in which this study is embedded, and how the spatial characterization of floodplain vegetation structure is important in the entire line from hydrodynamic modeling to integral river management. At the highest level, the most significant

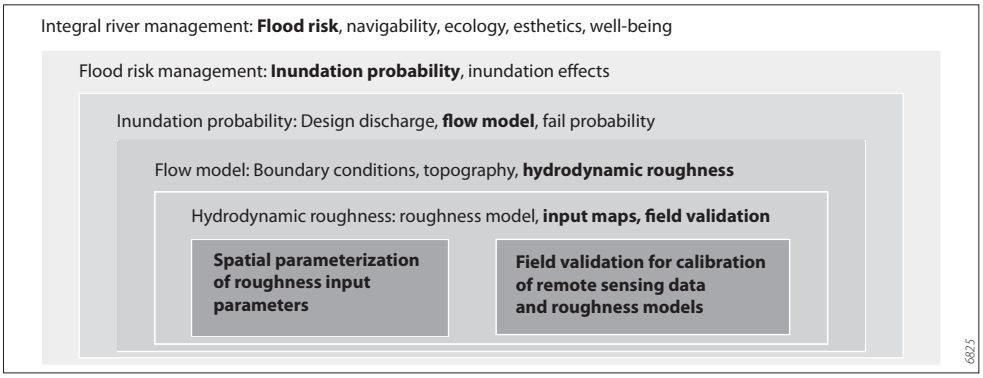

Figure 1.1 Hierarchic context for this PhD thesis

aspects provide an orientation. At lower levels, more fundamental aspects come to the foreground as primary research objectives.

Integral river management
Integral river management (IRM) provides the overall context. IRM *sensu* Esbjörn-Hargens (2005) and Wilber (2000) regards the fluvial area as a multifaceted hierachic system. IRM aims at integrating perspectives on different levels of complexity including physiosphere, biosphere and noösphere to increase the well-being at all levels. It values subjective aspects such as well-being, prosperity, aesthetics, cultural-historic importance, belonging and justice equally to objective aspects of flooding, sediment particles, species, ecosystems and socio-economic systems (Wilber 2000; De Nooij 2006). Currently, IRM is not operational as it is confronted with a number of scientific and institutional problems. Scientific problems include differences in the mono-disciplinary value spheres that are difficult to reconcile (Lenders & Knippenberg 2005; De Nooij 2006). Especially, subjective truth claims are not easily accepted. Institutional problems include the diversity of organisations with conflicting perspectives that have to co-operate at the scale of the river basin (Adams & Perrow 1999). Nonetheless, current river management of the Rhine includes measurable aspects of the river system such as water quality, water availability as well as subjective aspects as sustainability, resilience, ecological integrity and spatial quality (Richter *et al.* 2003; De Bruijn 2005). Within the myriad of goals related to these aspects, flood risk strongly influences landscaping measures as the hydrodynamic effects of the measures are not allowed to increase peak water levels (Silva *et al.* 2001; Nienhuis & Leuven 2001; Van Stokkom *et al.* 2005).

Flood risk management
Flooding poses an important environmental hazard with significant economic damage and human suffering. Flood risk is defined as the product of the probability of inundation and the effects of an inundation (Hall *et al.* 2003; Hooijer *et al.* 2004; Van der Most & Wehrung 2005). Flood risk management includes all measures that are taken to reduce the inundation probability and the effects of an inundation. In the Netherlands, the probability of the design discharge of the River Rhine is once every 1250 years, while the economic damage of a dike breach during design discharge is estimated at around 250.000 euro per hectare for the river area (Van Westen

2005). Flood effects, such as economic loss and casualties may be minimised by the creation of physical compartments to reduce the flood extent, or institutional streamlining of organisations that contribute to the evacuation of flood prone areas (Hooijer & Van Os 2002). Social aspects may include awareness of the inhabitants about the possible effects of a flood at the location of one's house (Wheater 2006), and an internal assessment of how one personally values material goods.

Inundation probability
The probability of an inundation depends on the one hand on the anticipated peak water levels and on the other hand on the fail probability of the weakest link in the flood defense structure of an embanked area (Van Westen 2005). Anticipated water levels are determined by the design discharge and the modeled water levels. The accuracy and precision of the design discharge depend on the length and representativeness of the historical discharge measurements on which the design discharge is based. The longer the period of discharge measurements, the more accurately the magnitude-frequency relation can be extrapolated to discharges that have not been recorded in historical data. Peak discharges and breaching of the embankments are considered stochastic processes. The accepted level of the inundation probability is largely a political question. Local water levels resulting from a flood with the design discharge are computed using a hydrodynamic model such as MIKE21, WAQUA, or Delft3D. The accuracy of the model input, calibration and sensitivity all influence the accuracy of the predicted peak water levels.

Flow modeling
Many hydrodynamic models have been developed (see for example Postma *et al.* 2000; Van der Sande *et al.* 2003; Bates *et al.* 2003; Casas *et al.* 2006). The models may differ in (1) spatial complexity, i.e. 1D, 2D, or 3D model schematization, (2) computational grid i.e. linear, finite-element, curvilinear, orthogonal, and (3) numerical solutions of the flow equations. Nevertheless, all models need data on the upstream discharge and downstream water levels as boundary conditions. River topography and hydrodynamic roughness of the main channel and adjacent floodplains complete the model input.

Hydrodynamic roughness
Roughness determines the retardance of the water flow. The higher the roughness, the slower the water will flow and, hence, the higher the water levels will reach. For the non-vegetated river bed, the roughness depends on the grain size and bedform dimensions (Van Rijn 1994). Vegetation roughness of the floodplains depends on vegetation structure and has been described by many different models (e.g. Kouwen *et al.* 1969; Petryk & Bosmajian 1975; Kouwen & Li 1980; Dawson & Charlton 1988; Klopstra *et al.* 1997; Nepf 1999; Kouwen & Fathi-Moghadam 2000; Baptist 2005). The vegetation structure and its spatial distribution are, therefore, important model input parameters. In addition, field methods supply data on vegetation structure and vegetation roughness, which can be used to validate roughness models and calibrate hydrodynamic models. Hence, the spatial parameterization of roughness input parameters and field validation is important in the entire line from hydrodynamic modeling to inundation probability and integral river management.

1.2 Problem definition and objectives

Like the context of this study, the problem definition can be regarded at different levels as well. Here, I start at the contextual level of the hydrodynamic model (Fig. 1.1). Considerable effort has been undertaken in recent years in the development of 2D and 3D hydrodynamic models that accurately simulate overbank flow patterns and predict extreme flood water levels in rivers and floodplains (Bates *et al.* 1992; Stoesser *et al.* 2003; Nicholas & McLelland 2004; Baptist *et al.* 2005). In addition to surface topography (Marks & Bates 2000), hydrodynamic roughness of the floodplain surface is the key input parameter of these models. The problem is the difficulty to quantify hydrodynamic roughness of the floodplains accurately and spatially distributed. Below, the relevant aspects on roughness, remote sensing and field measurements are presented.

Vegetation roughness
Vegetation roughness is dependent on vegetation structural characteristics like vegetation height and density, rigidity of the stems and the presence of leaves (Kouwen & Li 1980; Dawson & Charlton 1988). Vegetation density is defined as the sum of projected plant areas in side view per unit volume (m^2m^{-3}, which reduces to m^{-1}). Seasonal variation and management that allows vegetation to vary dynamically leads to a high spatiotemporal variation of vegetation structural characteristics and inherent roughness patterns (Baptist *et al.* 2004; Jesse 2004; Van Stokkom *et al.* 2005). To provide hydrodynamic modellers with reliable input, the spatial and temporal distribution of surface characteristics is needed. This requires accurate and fast monitoring methods that can cover large floodplain areas.

Remote sensing
Various remote sensing data may provide information on vegetation type and structure including their dynamics. Promising sensor systems include airborne laser scanning (ALS), optical systems and microwave sensors. This study focuses on the investigation of ALS and optical systems. An important issue to overcome is the translation of remote sensing information, e.g. the intensity and patterns of reflected electromagnetic radiation to relevant parameters to compute patterns of hydrodynamic roughness. Many studies reported successful and accurate mapping of natural vegetation using multispectral or hyperspectral remote sensing data (Ringrose *et al.* 1988; Jansen & Backx 1998; Thompson *et al.* 1998; Mertes 2002; Schmidt & Skidmore 2003; Van der Sande *et al.* 2003;). Recently, spectral information has been combined with height information in vegetation classification schemes (e.g. Hill *et al.* 2002; Dowling & Accad 2003; Ehlers *et al.* 2003; Rosso *et al.* 2006). Even though the spatial resolution and the level of detail of the classification varies with the type of remote sensing data, a lookup table is always required to convert the vegetation classes to vegetation structure values, which leads to undesirable loss of within-class variation. In contrast, ALS enables direct extraction of vegetation structural characteristics such as vegetation height, biomass, basal area, and leaf area index (Davenport *et al.* 2000; Cobby *et al.* 2001; Lefsky *et al.* 2002; Lim *et al.* 2003; Hopkinson *et al.* 2004). However, the vegetation in these studies mostly consisted of vegetation in leaf-on conditions, which is not representative for winter floods.. Dormant vegetation in winter leads to nutrient storage in the plant's root system and for some vegetation types to loss of leaves. This will be referred to as vegetation in leaf-off condition. Furthermore, there is still a lack of studies on the accurate mapping of hydrodynamic vegetation density.

Field measurements

Besides the lack of methods for the automatic mapping of roughness input variables, any mapping strategy requires accurate field reference data for validation of remote sensing data. Vegetation density is a difficult parameter to measure in the field, due to the presence of side branches, complex stem shapes and leaves. Current manual methods to measure vegetation density (Dudley *et al.* 1998) lack objectivity or have a limited spatial support. Current photographic methods (Zehm *et al.* 2003), that potentially have a variable support, provide biased estimates of vegetation density. None of the current field methods generate information on the three-dimensional distribution of vegetation density. This points at the need for accurate field measurements of hydrodynamic vegetation density, both as plot-averaged values and spatially distributed. Moreover, testing of roughness models is mostly carried out in flume facilities, where high flow velocities are used, combined with steep water surface slopes. These circumstances are not representative for flow conditions on lowland floodplains. *In situ* measurements of vegetation roughness still have been carried out (e.g. Van Urk 1981). Freeman *et al.* (1996) note that it is difficult to locate field sites where water depths are sufficient to inundate the floodplain and where a crew can safely perform the measurements. Moreover, field surveys are labour-intensive and timing depends on peak discharges. Therefore, a fast and transportable method is required that measures relevant hydrodynamic parameters such as water depth, water surface slope and the 3D flow field.

Hydrodynamic measurements are also used for the calibration of flow models. These models often suffer from underdetermination (Beven 2006), which means that different combinations of input parameters may generate equal model output. Underdetermination occurs especially when model calibration is carried out using water level measurements at few locations. The same hydrodynamic parameters that are used to derive the *in situ* roughness, depth – water surface slope and the 3D flow field – could also serve in the calibration of flow models. The underdetermination can then be solved using better calibration data instead of computationally intensive calibration strategies like Monte-Carlo simulations.

Research objectives

Based on the problems described above, the research objectives can be summarized as:

1. Is it possible to parameterize floodplain roughness accurately, quantitatively and spatially distributed using airborne remote sensing data? This question is subdivided into the following sub questions:
    a. What are the mapping capabilities of airborne laser scanning (ALS) data with respect to vegetation structure based on the available literature?
    b. Can ALS be used to map accurately the vegetation height and density of herbaceous floodplain vegetation under leaf-off conditions?
    c. Can ALS be used to map accurately the hydrodynamic vegetation density of deciduous floodplain forest?
    d. How can floodplain roughness, including all floodplain land cover classes, be parameterized accurately and automatically using ALS and airborne multispectral data?
    e. What are the effects of different methods of roughness estimation on the flow field and water levels?

2. How can hydrodynamic vegetation density be measured accurately in the field to calibrate airborne remote sensing data?
   a. What method is able to measure vegetation density objectively at the plot level with a variable support?
   b. What method can measure density spatially distributed, and what is the accuracy?

3. Is it possible to derive floodplain roughness from *in situ* measurements? This question is subdivided into:
   a. What method can be easily applied at various locations with different submerged vegetation types, is transportable and requires only a small water depth?
   b. What is the sensitivity of the method?
   c. What roughness is derived?

1.3 Thesis outline

To answer objective 1, I carried out the following steps (Fig. 1.2). In a literature review, I assessed the possibilities of airborne laser scanning to quantify vegetation structural characteristics. A pilot study was carried out in the Duursche Waarden floodplain section in the Netherlands. This review is presented in chapter 2. Mapping vegetation structure from ALS data included two detailed studies on the extraction of vegetation height and density of herbaceous floodplain vegetation in winter (Chapter 3), and of vegetation density of floodplain forest in winter (Chapter 4). These two studies were combined in a study on floodplain roughness parameterization, which integrated ALS data with airborne multispectral data (CASI, Compact Airborne Spectral

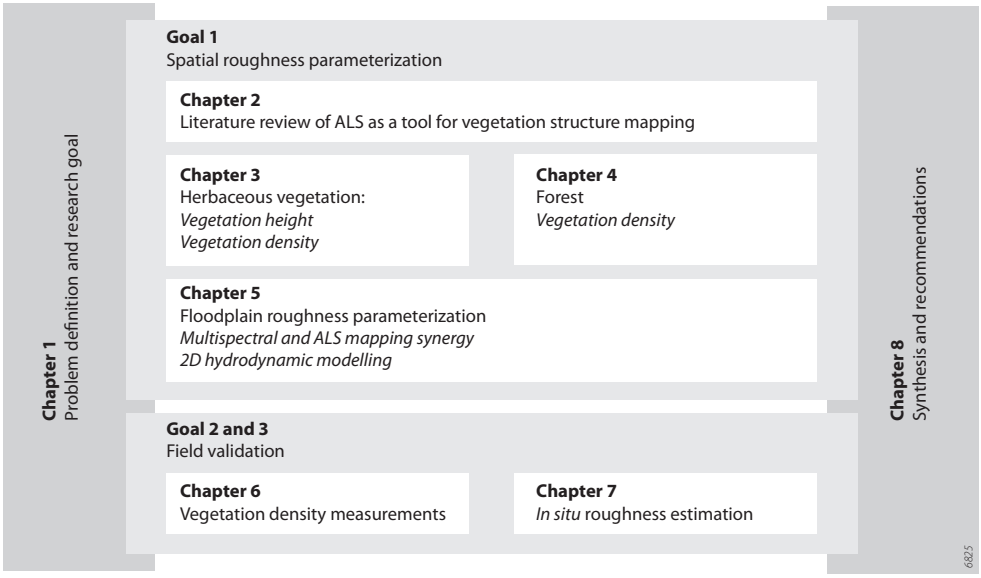

Figure 1.2 Outline of the thesis

Imager) to parameterize roughness of the whole floodplain surface (Chapter 5). The effects of different methods to produce roughness maps were assessed within a 2D hydrodynamic model.

Research objective 2, I pursued using terrestrial laser scanning (TLS) and parallel photography (PP). Both methods were tested on their ability to accurately predict vegetation density. This was carried out in a floodplain forest with straight stems (Chapter 6). With respect to research objective 3 a new method was developed: 3D float tracking (Chapter 7). This method uses a floating tripod that is tracked in three dimensions using an on-shore total station, while a current meter provides flow velocity profiles.

In the synthesis (Chapter 8), I come back to the research questions posed above and sum up the achievements of this study within the framework of the hydrodynamic modeling. An outlook is given into possible future research.

1.4 Thesis foci

Geographically, the focus of this thesis is on the floodplains of distributaries of the river Rhine in the Netherlands, which has a temperate climate. Peak discharges occur mostly in the winter months (Middelkoop & Van Haselen 1999). Fieldwork was carried out on five floodplain sections. The '*Gamerensche Waard*,' the '*Afferdensche en Deestsche Waard*' and the '*Duursche Waarden*' floodplain sections were used in the airborne remote sensing studies. The studies on field measurements of vegetation density were also tested in the '*Gamerensche Waard*' floodplain. 3D float tracking was carried out on the '*Groene rivier*' floodplain in Arnhem and on the '*Dreumelse Waard*.'

Within the myriad of vegetation roughness models, I focussed on the model of Baptist (2005):

$$C_r = \sqrt{\frac{1}{C_b^{-2} + (2g)^{-1} C_d D_v H_v}} + \sqrt{\frac{g}{\kappa}} \ln \frac{h}{H_v} \qquad (1.1)$$

where C_r is the Chézy coefficient representing roughness of bare soil plus vegetation ($m^{½}s^{-1}$), C_b the Chézy coefficient for the bare soil ($m^{½}s^{-1}$), g the acceleration of gravity (9.81; ms^{-2}), C_d the drag coefficient (-), D_v the vegetation density (m^{-1}), H_v the vegetation height (m), κ the Von Kármàn constant, (0.4; -), and h the water depth (m). In case of non-submerged conditions, equation 1.1 reduces to the left part on the right hand side for H_v equals h. This model assumes that vegetation consists of rigid cylinders that can be characterized by height and density, which is essentially an extension of the early work of Einstein & Banks (1950), Kouwen *et al.* (1969), Kouwen & Unny (1973), Klaassen & Van der Zwaard (1974) and Petryk & Bosmajian (1975). This model proved well able to predict the roughness of flexible and rigid vegetation (Baptist, 2005), and has the advantage that its input, vegetation height and density, seem promising to be mapped using remote sensing. Other roughness models may include vegetation flexural rigidity and average stem spacing (Kouwen & Li 1980; Kouwen & Fathi-Moghadam 2000; Armanini *et al.* 2005), but these parameters can not be mapped using remote sensing directly. These parameters have, therefore, been omitted from this study.

With respect to remote sensing data, this study strongly focussed on ALS to document spatial patterns of vegetation structure, because of its ability to extract vegetation structure without the need for a lookup table and its capacity to penetrate the forest canopy. Spectral remote sensing was applied together with the ALS data for its complementary qualities in land cover classification.

2 Airborne laser scanning as a tool for lowland floodplain vegetation monitoring

published as: Straatsma, M. W. & H. Middelkoop. (2006). Airborne laser scanning as a tool for lowland floodplain vegetation monitoring. *Hydrobiologia*, 565, pp. 87-103.

Abstract

Monitoring of three-dimensional floodplain vegetation structure is essential for ecological studies, as well as for hydrodynamic modeling of rivers. Height and density of submerged vegetation and density of emergent vegetation are the key characteristics from which roughness parameters in hydraulic models are derived.

Airborne laser scanning is a technique with broad applications in vegetation structure mapping, which therefore may be a promising tool in monitoring floodplain vegetation for river management applications. This paper first provides an introduction to the laser scanning technique, and reviews previous studies on the extraction of vegetation height and density of forests, low vegetation and meadows or unvegetated areas. Reliable predictions using laser scan data have been reported for forest height (R^2 = 0.64-0.98), parameters related to forest density, such as stem number, stem diameter, biomass, timber volume or basal area (R^2 = 0.42-0.93), and herbaceous vegetation height (summer condition; R^2 = 0.75-0.89). No empirical relations have been reported on density of herbaceous vegetation. Laser data of meadows and unvegetated areas show too much noise to predict vegetation structure correctly.

In a case study for the lower Rhine river, the potential of laser scan mapping of vegetation structure was further explored for winter conditions. Three laser-derived metrics that are often reported in the literature have been applied to characterize local vertical distributions of laser reflections. The laser data clearly show the large structural differences both between and within vegetation units that currently are the basis of floodplain vegetation and roughness mapping. The results indicate that airborne laser scanning is a promising technique for extraction of 3D-structure of floodplain vegetation in winter, except for meadows and unvegetated areas.

Key words: airborne laser scanning, floodplain vegetation, vegetation structure, model input

2.1 Introduction

In the forthcoming decennia, the landscape of the lower Rhine and Meuse floodplains in the Netherlands may undergo major changes. The near-flooding events of 1993 and 1995 combined with the anticipated increase in peak flows due to climate change (Shabalova *et al.* 2003) have raised the awareness that the discharge capacity of the high-water bed of the rivers should be increased. While in previous decennia this has been done by raising the river dikes, a new flood management strategy has been adopted in recent years in the Netherlands, which involves accommodating more room for the river by lowering the floodplain surface, digging side channels, removing small embankments, and various other landscaping measures (Silva *et al.* 2001; Van Stokkom *et al.* 2005). At the same time, river management aims at ecological rehabilitation of the floodplains, which involves the restoration of various natural floodplain habitats, thereby enhancing natural biodiversity (Ward & Tockner 2001; Nienhuis *et al.* 2002). To achieve these objectives – with safety as the primary boundary condition – a strategy of dynamic floodplain management is advocated (Nienhuis & Leuven 2001). Accordingly, flood reduction measures will be carried out as an artificial form of floodplain rejuvenation, followed by a period of renewed sedimentation and vegetation development (Baptist *et al.* 2004). Over the years, this will lead to a higher floodplain level, as well as to an increase of hydrodynamic roughness exerted by the denser vegetation. By the time this would cause excessively high flood water levels, artificial rejuvenation of the floodplain will be undertaken again.

This management practice will lead to a high spatio-temporal variability of floodplain habitats, vegetation structure and related roughness, and demands adequate monitoring techniques. Spatial distribution of vegetation structure is also needed as input for ecological habitat modeling; for example, tree height and the full three dimensional structure of the forest are important parameters for bird habitat modeling (MacArthur & MacArthur 1961). Detailed information of vegetation structure is needed to estimate the changes in hydrodynamic roughness of the floodplain. Furthermore, hydrodynamic roughness is a key variable required for modeling deposition of suspended sediment and associated contaminants within the floodplain.

Currently, vegetation mapping of the lower Rhine and Meuse floodplains is based on ecotopes. Ecotopes are 'spatial landscape units that are homogeneous as to vegetation structure, succession stage and the main abiotic factors that are relevant to plant growth' (Leuven *et al.* 2002). Mapping of ecotopes within the lower Rhine floodplain is based on visual interpretation and manual classification of vegetation units from aerial photographs, scale 1:5000 (Jansen & Backx 1998). Ecotopes are then linked to vegetation structural characteristics related to roughness using a lookup table (Van Velzen *et al.* 2003). This method, however, may become inadequate to monitor the spatio-temporal dynamics of vegetation roughness, since the procedures are time consuming and do not allow documentation of within-ecotope variation of vegetation roughness.

There is clearly a need for a more automated approach to assess hydrodynamic roughness of vegetated floodplain surfaces. Airborne remote sensing is regarded a useful technique for surveying and mapping floodplain vegetation. While successful attempts have been reported to map wetland vegetation using (hyper-) spectral remote sensing data (Thompson *et al.* 1998; Schmidt & Skidmore 2003; Van der Sande *et al.* 2003), airborne laser scanning may provide a useful technique to map 3D vegetation structure as a measure of hydrodynamic roughness.

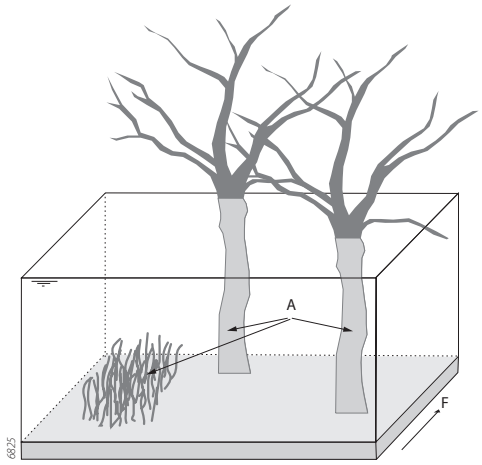

Figure 2.1 Hydrodynamic vegetation density in m^{-1}: the sum of projected plant areas (A) in the direction of the water flow (F) per unit volume (cube).

Airborne laser scanning is an active remote sensing technique that involves high-resolution elevation measurement by means of laser pulses. Over the past years airborne laser scanning has become a widely used technique in the generation of digital elevation models (Oude Elberink *et al*. 2003) and in forest structure mapping, while experiments on mapping of shrub and herb vegetation have been reported as well. A few recent examples have reported on the application of laser scan data in lowland floodplains to map topography (Marks & Bates 2000) and roughness, for use as input of hydrodynamic models (Cobby *et al*. 2001).

The objective of this paper is to review the potential of airborne laser scanning data as a tool for quantitative assessment of floodplain vegetation roughness, which is related to vegetation height and density. First we will introduce the parameters needed for hydrodynamic vegetation roughness. Secondly, we introduce the laser scanning method and review current applications related to vegetation structure, where we will make a distinction between (1) forest, (2) shrubs and herbaceous vegetation and (3) meadows and unvegetated areas. Finally, we present a case study of laser scanning of floodplain vegetation.

2.2 Hydrodynamic vegetation roughness

Hydrodynamic vegetation roughness refers to the resistance force exerted by vegetation on water flowing over or through it. Rough vegetation reduces water flow velocity and leads to higher water levels and thus increases flood risks. A meadow is hydrodynamically smooth, forests and dense shrubs are hydrodynamically rough (Chow 1959). Two types of vegetation are distinguished with respect to roughness modeling; emergent and submerged. The parameter describing emergent vegetation, such as forest, is vegetation density (Petryk & Bosmajian 1975). Hydrodynamic vegetation density is the sum of the projected plant areas (A) in the direction of the flow (F) per unit volume (cube) (Fig. 2.1). The unit is m^2m^{-3}, which reduces to m^{-1}. Under the

assumption that vegetation consists of cylindrical elements, vegetation density is calculated as the product of number of stems per square meter and stem diameter, which also reduces to m^{-1}. The parameters describing submerged vegetation, such as grassland, reed, or herbs are vegetation height and density (Carollo *et al*. 2002). The spatial distribution of these vegetation characteristics is an essential input for hydrodynamic models. Therefore, the challenge is to estimate vegetation density for emergent vegetation and vegetation height and density for submerged vegetation from laser scanning data.

2.3 Airborne laser scanning technique

All airborne laser systems have three components in common (Wehr & Lohr 1999; Fig. 2.2):
1. Differential Global Positioning System (dGPS) to locate the aircraft in space;
2. Inertial Navigation System (INS) to determine the orientation of the aircraft;
3. Laser Range Finder (LRF) to determine the distance between the aircraft and objects below.

Differential GPS consists of 2 components; a base station and a mobile GPS receiver. GPS is a satellite positioning system. The base station remains immobile, hence the positioning error can be calculated, which enables correction of the positioning error of the aircraft. The INS measures acceleration of the aircraft along three orthogonal axes enabling the computation of the pitch, yawn and roll. Data of all three components are synchronized to enable the determination of the location and elevation of the measured object in a local coordinate system.

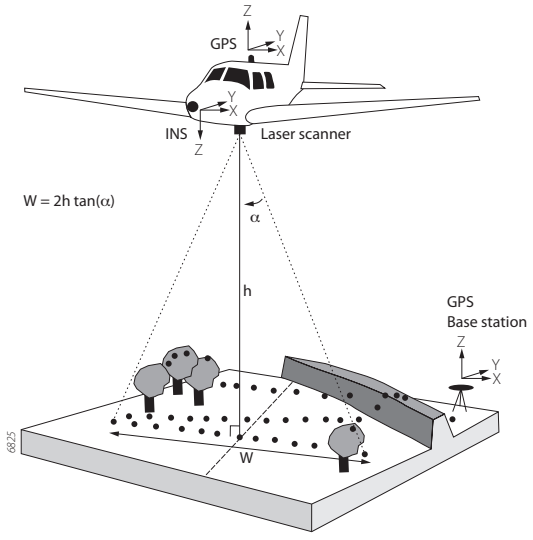

Figure 2.2 Components of an airborne laser scanning system: (1) GPS for positioning in space plus a base station for error correction, (2) INS, Inertial Navigation System, for recording the orientation of the aircraft in space, (3) Laser scanner for measuring the distance between the aircraft and the objects below it. When combined, a 3D point cloud of laser hits is generated.

Two types of LRF exist: (1) Continuous wave (CW) ranging, in which the distance to the target is determined from the phase difference of the return pulse of a continuously emitted laser signal. Since this technique is not widely applied (Baltsavias 1999b) it will not be discussed here. (2) Pulse LRF that fires discrete laser pulses of a few nanoseconds to the earth. The distance is calculated from the pulse travel time between emission and return of the pulse. The laser pulse typically has a wavelength in the near infrared (i.e. 1064 nm; Baltsavias 1999a). Pulse frequencies range from 0.1 to 100 kHz.

The horizontal distribution of the laser hits on the ground depends on the scan pattern of the LRF. Early LRF systems used vertical profiling lasers, resulting in closely spaced points underneath the aircraft only. Modern systems deflect the laser pulses across track, resulting in a wider distribution of points below the aircraft. The scan pattern depends on the motion of the deflection device and aircraft speed (Wehr & Lohr 1999). Figure 2.2 shows a saw-tooth scan pattern. The footprint size refers to the area on the surface that is illuminated by a single laser pulse: a larger footprint increases the chance of hitting more than one object with a single pulse.

The return signal can be recorded in different ways (Fig. 2.3): (1) waveform digitizing (Blair *et al*. 1999; Means *et al*. 1999; Wagner *et al*. 2004) and (2) discrete return (Baltsavias 1999b). A waveform-digitizing scanner records the full reflection profile of the returned laser pulse in a series of equally spaced time bins. Conversely, a discrete return system records only discrete levels in the vertical profile. Typically, discrete return laser scanners record first pulse (FP) and last pulse (LP), but some systems are able to record up to 6 intermediate pulses (IMP). Last pulse is more likely to represent the ground surface, first and intermediate pulse will be reflected from the canopy. However, a minimum vertical object separation of about 1.5 m is needed to register first and last pulse separately, otherwise these two pulses will merge into one (Baltsavias 1999a). Echo detection refers to the reflection intensity at which a pulse is registered. This determines which height of the returned waveform is recorded (Katzenbeisser 2003; Fig. 2.3). The reflection intensity for herbs in winter is slowly increasing towards the ground surface. The exact height recorded by the laser scanner depends on the detection threshold that is used. Varying this threshold may cause large differences in detected vegetation height.

Waveform digitizing scanners often use large footprints, typically with 10 to 25 m diameters (Blair *et al*. 1999; Lefsky *et al*. 1999a). In recent years, little waveform-digitizing data has been available. NASA deployed such scanners in preparation for the space borne Vegetation Canopy Lidar (VCL), but they were not commercially available (Baltsavias 1999b). Recently, a commercial waveform-digitizing scanner has become operational (Hug *et al*. 2004), which opens up new possibilities in vegetation mapping. Blair & Hofton (1999) successfully modeled large-footprint waveforms using small-footprint first pulse data that indicates that no major differences exist between the two types of scanners.

The minimum detectable object size is of specific importance when measuring senescent herbaceous vegetation. Ritchie *et al*. (1993) estimated the minimum detectable vegetation element, leaves in their case, to be 2 to 3 cm, which is still larger than the stalk diameter of herbs in winter. Baltsavias (1999a) listed a number of parameters influencing the minimum object size that can be detected: these include reflectivity, laser power, detector sensitivity and laser

wavelength. Flying height also determines the minimum detectable object size. Due to beam divergence, the footprint will increase with flying altitude, while the energy per unit area will decrease. Nevertheless, Næsset (2004) found no significant difference in forest canopy height estimation when flying altitude varied by 60 %, while using the same laser scanner. Conversely, Yu *et al*. (2004) did report that tree height was progressively under-estimated when the flying altitude increased by a factor 2 to 4.75. Water reflects little energy in the near-infrared (Lillesand & Kiefer 1994). This usually leads to large errors in the height measurement of vegetation emerging above a water body because the water level is not detected properly and the water depth is unknown (Hopkinson *et al*. 2004a). This is particularly important for aquatic vegetation such as reed. However, also using the traditional methods the correct water depth will be difficult to predict.

Laser scanning monitoring of floodplain vegetation should be carried out in the period with the highest chance of flooding, which is winter in the Netherlands, but the floodplain should not be inundated during data acquisition, nor should the floodplains be snow-covered as this will cover part of the vegetation. The presence of leaves may strongly affect the laser return signal (Fig. 2.3). Leaves increase the echo intensity and limit the penetration distance into the vegetation before a significant return is generated. Although the effects of seasonal variations in foliage on the representation of the three-dimensional vegetation structure by laser scanning are widely known,

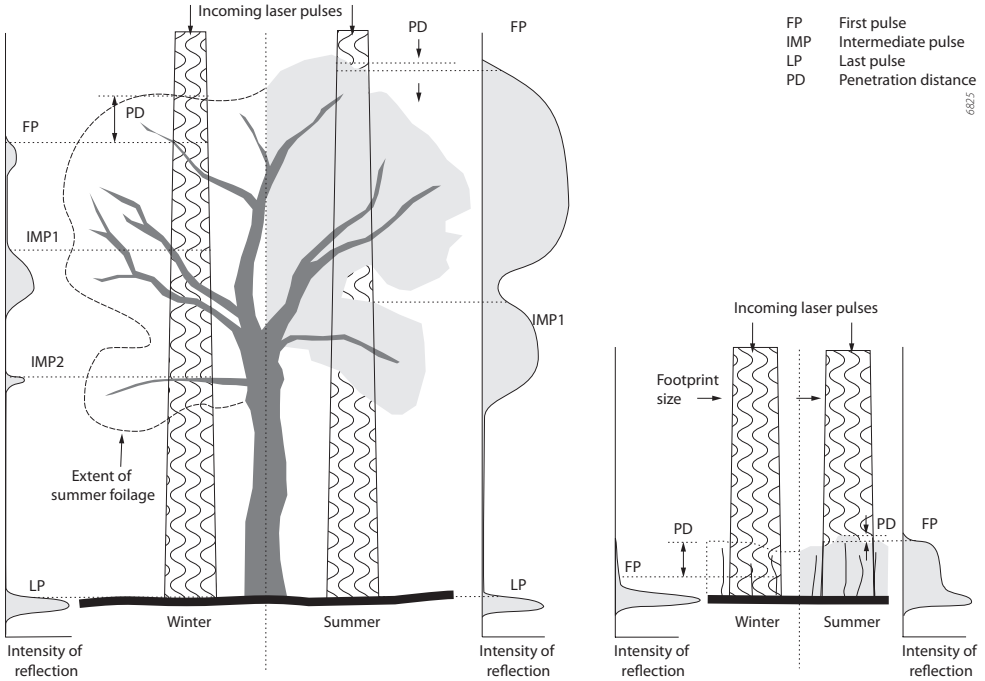

Figure 2.3 Seasonal effects on laser reflection from trees (left panel) and herbaceous vegetation (right panel). Reflection intensity is higher and penetration depth into the canopy is smaller in summer for both forests and herbaceous vegetation.

still little effort has been undertaken to quantify the consequences for the shape of the returned waveform or the vertical point distribution.

2.4 Review: airborne laser scanning of vegetation

The literature review is focused on the prediction of vegetation height and density of three main structural vegetation types in floodplains: (1) forest, (2) herbaceous vegetation and shrubs, and (3) meadows and unvegetated areas. However, the first step is ground surface reconstruction to enable the calculation of the point distribution relative to the ground surface.

2.4.1 Calculation of relative vertical point distribution

The calculation of the vertical point distribution above the ground surface requires a Digital Terrain Model (DTM) describing the ground surface elevation. To determine the surface elevation using laser scanning, the laser data reflected from the ground surface must be separated from the laser data reflected from vegetation or other objects above the ground surface (Kilian *et al*. 1996; Kraus & Pfeifer 1998; Vosselman 2000). Sithole & Vosselman (2004) compared eight different algorithms used to segment the laser point cloud in ground surface and non-ground surface points. Most filter algorithms calculate a measure of discontinuity based on a local neighbourhood. They conclude that all methods perform well in smooth landscapes, but produce errors in rough terrain with dense vegetation. Still, vegetation in smooth terrain can deteriorate the quality of the resulting DTM (Pfeifer *et al*. 2004). Hodgson & Bresnahan (2004) report absolute errors in the DTM under various vegetation types of less than 20 cm. Since floodplain topography is relatively smooth, except ditches, embankments and eroding shorelines, it is expected that laser-based DTMs of the floodplain surface will be sufficiently accurate as a basis for vegetation height determination.

Once a DTM is derived from the laser data, the height above the ground surface can be calculated for each individual point. The result is a three-dimensional point cloud representing heights above ground level. This can be converted to a vertical point height distribution characterized by various statistics such as percentiles, measures of central tendency and shape. These statistics are subsequently related to vegetation structure characteristics, which are determined by field reference data (Næsset 2002; Lefsky *et al*. 1999a).

2.4.2 Forest vegetation structure

Over the last 20 years many papers – mostly originating from forestry research – have reported on extracting forest properties, such as stand height, biomass, timber volume, stem number and stem diameter, from airborne laser scanning data. Lefsky *et al*. (2002) and Lim *et al*. (2003) provide reviews on this subject. Forest stand characteristics have been successfully extracted from laser data over a wide range of forest types and climate zones, from the tropics (Drake *et al*. 2002) and temperate zone (Ritchie *et al*. 1993; Means *et al*. 1999; Lefsky *et al*. 1999a; Lefsky *et al*. 1999b;) to the boreal zone (Nilsson 1996; Næsset 1997a; Næsset 1997b; Magnussen & Boudewyn 1998; Næsset 2002; Morsdorf *et al*. 2004). Initial interest was in forest stand characteristics, but recently single tree mapping and tree species identification are topics of research (Brandtberg *et al*. 2003; Holmgren & Persson 2004). Most studies considered forest under leaf-on conditions.

Since the hydrodynamic roughness of forest is high, extracting floodplain forest stand characteristics from laser scanning data is highly relevant for river management. We will focus on those characteristics of forests that relate to hydrodynamic vegetation density.

Forest height

Estimates of forest height are mostly derived from percentiles of the laser data. It is then assumed that the vertical leaf area distribution in forests is the same as the vertical distribution of laser points (Magnussen & Boudewyn 1998). Consequently, the *n*-percentile of the laser vertical point distribution would correspond to the height above the ground below which *n* percent of the leaf area occurs. The good correspondence between leaf area percentiles and laser data percentiles has been confirmed by various field sampling studies where height distributions were measured for a range of canopy types (Ritchie *et al*. 1993; Næsset 1997a; Næsset & Økland 2002; Means *et al*. 1999). Laser estimates were less than 6% different from field and laser estimates of canopy height. Table 2.1 shows explained variances based on regression analyses from research on forest height prediction.

Forest height can be expressed by different properties, including (1) mean tree height, (2) dominant height, i.e. the arithmetic mean of the 100 largest trees, (3) maximum tree height in a limited sized plot, or (4) Lorey's mean tree height, which is the weighted mean of the canopy height based on the basal area of individual trees, and is used to account for the influence of larger trees on the mean canopy height. The latter three parameters focus on harvestable timber and ignore small trees. The quality of the prediction of forest stand height depends on the way tree height is expressed, as well as on the percentiles used for prediction. Regression models obtained in a number of studies explain on average more than 80 % of the variation in tree height measured in the field (Table 2.1). The studies do not agree on a single laser-derived statistic to predict forest height. Moreover, the correlation between mean tree height and laser derived statistics becomes weaker when the higher trees intercept most of the laser pulses, so

Table 2.1 Overview of explained variances obtained in the prediction of forest canopy height using various laser-derived statistics as independent variable and field canopy heights as dependant variable

Reference	Footprint size (m)	Height (R^2)	Number of reference data	Remarks
Ritchie *et al*. (1993)	small	0.98	8	laser profiler
Næsset (1997a)	0.13-0.17	0.94	36	laser scanner
Magnussen & Boudewyn (1998)	small	0.64	36	laser scanner
Means *et al*. (1999)	10.4	0.95	24	laser scanner
Lefsky *et al*. (1999a)	10.4	0.78	48	laser scanner
Næsset & Bjerknes (2001)	0.21	0.83	39	laser scanner
Næsset (2002)	0.21	0.74-0.95	144	laser scanner
Næsset & Økland (2002)	0.18	0.91	37	laser scanner
Hopkinson *et al*. (2004b)	small	0.86	54	laser scanner
Persson *et al*. (2002)	0.3 – 3.7	0.99	135	individual trees
Brandtberg *et al*. (2003)	0.1	0.68	48	individual trees
Morsdorf *et al*. (2004)	0.30	0.92	918	individual trees

that the smaller trees are not detected by laser scanning (Popescu *et al*. 2002). Næsset (2002), Næsset & Økland (2002) and Holmgren & Jonsson (2004) demonstrated that the overall quality of laser scanning prediction of forest height is better than conventional methods, such as manual interpretation of aerial stereo photos.

Individual tree height estimation has recently become a topic of research. Persson *et al*. (2002) delineated individual coniferous trees using local maxima in a smoothed canopy model. Brandtberg *et al*. (2003) studied deciduous trees in leaf-off condition and used a scale-space technique which smoothes the canopy model at various scales. By identifying height clusters at various scales, the image was segmented to identify individual trees. Morsdorf *et al*. (2004) identified coniferous trees using cluster analyses on the raw 3D laser scanning data.

Forest vegetation density

Several characteristics of forest stands relate to vegetation density, such as stem number, stem diameter, basal area, biomass, or timber volume. Table 2.2 gives an overview of the prediction results for these characteristics using laser-derived parameters based on the vertical distribution of laser points as independent variables. The dependent variable was always field reference data in these studies. Number of stems can also be determined using the methods discussed in the section on individual tree delineation. This is likely to give a minimum value for the stem number, because overtopped trees and undergrowth vegetation are difficult to detect (Maltamo *et al*. 2004). Vegetation density should be computed over the lower part of the vegetation that will be inundated by the water. Hence, information is needed on specific height increments as provided by Lefsky *et al*. (1999b) and Næsset (2002).

Lefsky *et al*. (1999b) reconstructed the canopy height profile (CHP) from large footprint, waveform digitizing, laser-scanning data. The CHP is the 'surface area of all canopy material, woody and foliage, as a function of height'. CHP is based on method of MacArthur & Horn (1969) who assumed that the intensity of light, which travels through a forest canopy, shows an extinction curve depending on the occlusions from the vegetation. This was validated by Aber (1979). Their method computes the leaf area index (LAI) over a specified height interval. For laser scanning data the following formula can be used to compute the LAI between heights h1 and h2:

$$LAI_{h1-h2} = \ln\left(\frac{N_{h2}}{N_{h1}}\right) \tag{2.1}$$

in which N_{h1} and N_{h2} are the number of points below heights $h1$ and $h2$. Lefsky *et al*. (1999b) found excellent agreement between ground and laser measurements of the CHP. Estimates of CHP and LAI are however *vertically oriented* descriptors, while hydrodynamic vegetation density is a measure of *horizontal* obstruction. Næsset (2002), using small footprint data, used canopy density statistics based on the vertical point distribution. In this case canopy densities are 'the proportions of the laser hits above the 0, 10,..... 90 percentiles of the height distributions to the total number of pulses'. These statistics proved useful in predicting mean diameter by basal area, stem number, basal area and volume. A combination of two canopy densities, one at ground level and the second at the height of maximum water level during flood, might be strongly

Table 2.2 Overview of hydrodynamic vegetation density and related forest stand properties based on linear regression analyses. Independent variable was a laser-derived parameter based on the vertical distribution of laser points

Reference	FP size[a] (m)	D_v[a] (R^2)	N[a] (R^2)	D_a (R^2)	BA[a] (R^2)	B/TV[a] (R^2)	Np[a]
Nilsson (1996)	0.75-3.0	– -	– -	– -	– -	0.78	27
Næsset (1997b)	0.13-0.16	– -	– -	– -	– -	0.46-0.89	36
Means *et al*. (1999)	10.4	– -	– -	– -	0.88	0.96	24
Lefsky *et al*. (1999a)	10.4	– -	0.85	0.61	0.87	0.91	22
Lefsky *et al*. (1999b)	10.4	– -	– -	– -	0.69	0.81	48
Næsset & Bjerknes (2001)	0.21	– -	0.42	– -	– -	– -	39
Næsset (2002)	0.21	– -	0.5-0.7	0.39-0.78	0.69-0.89	0.8-0.93	144
Drake *et al*. (2002)	25	– -	– -	0.93	0.72	0.93	25
Asselman (2002)	0.17	0.6	– -	– -	– -	– -	30
Holmgren *et al*. (2003a)	small	– -	– -	– -	– -	0.82-0.9	?

a. FP size= laser footprint size, D_v = hydrodynamic vegetation density, N = stem number, D stem diameter, BA = basal area, B/TV = biomass/timber volume, Np = number of plots

correlated to the hydrodynamic vegetation density. However, this method does not compensate for occlusions from the top of the canopy.

The methods and results reported from these forestry studies, however, do not explicitly relate to hydrodynamic vegetation density, as this was not the focus of these studies. Extraction of vegetation density associated with hydraulic roughness of vegetation from laser-scanning data has been reported only by Asselman (2002). She found the 90-percentile to be negatively correlated with floodplain vegetation density that included forest, reeds and shrubs. Apparently, tall trees more efficiently shade the ground layer and limit understory growth. However, tree height alone can not explain all variation in vegetation density as understory vegetation does occur when the canopy is not closed. In conclusion we could say that laser scanning is a promising technique to map vegetation density because many related parameters have been predicted accurately. However many prediction methods remain to be tested for this application: LAI based on MacArthur & Horn (1969), canopy density based on Næsset (2002) and individual tree delineation.

2.4.3 Structure of herbaceous vegetation and shrubs

Compared to forestry research, few studies have been reported on the extraction of vegetation structure of low vegetation such as reed, natural grassland, herbaceous vegetation or low shrubs. Again we will discuss vegetation height and density as the hydraulically important variables to extract from the laser data.

Height of herbaceous vegetation

Vegetation height is the primary structural characteristic that determines the hydraulic roughness of submerged vegetation. Table 2.3 gives an overview of research on low vegetation types, in which empirical relations were established to predict vegetation height from laser-

scanning data. Ritchie *et al*. (1993) studied low (0.1-0.3 m) desert shrubs using a laser profiler. In a similar approach as used for forested areas, they established empirical relations between percentiles of laser data and vegetation height measured in the field. The 95 percentile of the vertical distribution of the laser points explained 75 percent of the variation of the vegetation height. Weltz *et al*. (1994) and Ritchie *et al*. (1996) compared the vertical point distribution of laser data with the vertical distribution of vegetation height measured in field plots, and found good agreement between the histograms of the laser data and vegetation height distributions.

Various studies used the standard deviation of the laser data in a local window as a predictor for vegetation height. Davenport *et al*. (2000), and Cobby *et al*. (2001) used this statistic for grasslands and agricultural crops, Hopkinson *et al*. (2004b) for shrubs, aquatic marshland vegetation, grassland and herbs. The regression equations established in these studies varied greatly. Cobby *et al*. (2001) used a log-linear regression, which did not give satisfactory results on the data of Hopkinson *et al*. (2004b). Moreover, the slope of the regression equation of Hopkinson *et al*. (2004b) was three times higher than the one from Davenport *et al*. (2000). The high regression slope reported by Davenport *et al*. (2000) might be due to higher density of the crops when compared to the natural vegetation studied by Hopkinson (2004b). Dense crops create a continuous canopy cover and most laser pulses will reflect of the top of the canopy thereby limiting the variation in the vertical distribution. In a comparative study, Hopkinson (2004a) concluded that vegetation height estimation of aquatic vegetation is associated with the largest errors. This is due to the low reflectivity of the water, preventing accurate determination of the ground surface elevation; hence this vegetation height should be regarded as a minimum value. These results indicate that, for individual laser data sets, the explained variance is high. However, the empirical relations differ greatly and therefore must be determined for each survey using ground reference data.

Asselman (2002) estimated vegetation height of meadows and herbaceous vegetation in a floodplain area under winter conditions from laser data with a point density of 10 points m^{-2}. She calculated laser-derived vegetation height as the difference between the actual point height and the minimum value in a local 1 m x 1 m window. She recommended using the median value of the laser data height distribution as predictor of vegetation height for meadows and herbaceous vegetation. However, large scatter was present and no regression analyses were carried out.

When compared to forestry studies (Table 2.1), results on low vegetation in summer (Table 2.3) are of slightly lower predictive quality. This, however, is a major achievement given that the range

Table 2.3 Overview of papers on vegetation height of low vegetation with regression equations

Reference	Footprint size (m)	Height (R^2)	Number of plots	Vegetation type	Height range in the field (m)
Ritchie *et al*. (1993)	small	0.75	7	Desert shrubs	0.13 – 0.27
Davenport *et al*. (2000)	0.15-0.23	0.89	18	crops <1m	0- 0.9
Cobby *et al*. (2001)	0.2	0.8	55	grassland and crops	0 -1.2
Hopkinson *et al*. (2004b)	Small	0.77	14	aquatic, grass, herbs, low shrubs	0 – 1.25

of vegetation heights that are predicted is much smaller. Estimating herb vegetation height under winter conditions remains a challenge.

Vegetation density and coverage of herbaceous vegetation
To date, little progress has been reported on the estimation of density of low vegetation using airborne laser scanning data. Asselman (2002) found only very poor relations between height distribution of laser scan data and the vegetation density of low floodplain vegetation. Therefore she established a lookup table to assign vegetation density values to areas with a specific vegetation height range to enable roughness computation. Mason *et al.* (2003) got around this problem by using vegetation height only as input for their hydrodynamic model. Vegetation coverage can be seen as a parameter that is related sideways to vegetation density, as correct estimation of vegetation coverage is a prerequisite for vegetation density prediction. Weltz *et al.* (1994) concluded for arid and semi-arid vegetation that laser altimetry data consistently overestimated coverage of vegetation lower than 0.3 m and underestimated vegetation cover of vegetation higher than 0.5 m, due to noise in the laser signal and an inaccurate estimation of higher vegetation. Ritchie at al. (1993) concluded that laser estimates of vegetation coverage for vegetation higher than 1 m were consistent with field reports. However, while vegetation cover can be predicted accurately using laser data, predictive models for vegetation density still have not yet been established. Vegetation density determination from laser scanning data thus remains a challenge.

2.4.4 Meadows and unvegetated areas

Meadows and unvegetated areas are both considered as the same land cover type in most papers reporting on laser scanning. The vertical precision of the laser height measurements, expressed as the standard deviation of unvegetated flat terrain, varies between 0.04 m (Davenport *et al.* 2000) and 0.07 m (Hopkinson *et al.* 2004a). The accuracy of laser-derived DTMs of unvegetated areas is 10 to 20 cm according to theoretical considerations (Huising & Gomes Perreira 1998), later confirmed by empirical analysis (Hodgson & Bresnahan 2004). The resulting height range in laser scan data of flat, unvegetated areas will thus be in the order of 20 cm. With this precision, accurate estimation of vegetation height and density for meadows is unlikely using discrete return laser systems. No studies have reported on the use of waveform digitizing laser scanners to estimate very short vegetation or unvegetated areas. Large footprint waveform digitizing lasers are also not suitable for this task, as it will be impossible to distinguish between small irregularities in the ground surface elevation and the vegetation. However, small footprint waveform digitizing laser scanners might improve the vegetation height estimates of low vegetation because ground elevation differences can be ignored over such small areas in case of relatively flat floodplains. Moreover, the errors from GPS and INS do not affect the digitized waveform.

2.4.5 Discussion and conclusion of the review

Airborne laser scanning is an emerging technique with broad applications in vegetation structure mapping. Vegetation height of forests and herbaceous vegetation in summer can be measured reliably. Parameters related to vegetation density have been studied by many studies in forestry, and can be determined almost equally accurately well as forest height. Still, different laser-derived statistics are used to predict the same forest characteristic, and when the same statistic is used in

different areas, regression coefficients with vegetation height and density vary a lot. The same holds for the vegetation height of low vegetation. Extraction of vegetation height and density of herbaceous vegetation under winter conditions still remains to be investigated. This indicates that in the near future field data will remain necessary to establish regression models to predict vegetation structure using airborne laser data. The reasons for this are all the parameters which influence the minimum detectable object as listed in section 3. A solution could be a physically based model in which ray tracing of laser pulses is combined with a 3D vegetation model (Kay & Kajiya 1986). However, such a physically based model would not be trivial as many parameters should be taken into account like: flying height, scan pattern and angle, beam divergence, laser power, detection threshold of the receiver, 3D structure and reflectivity of woody vegetation, reflectivity and orientation of leaves, soil reflectivity and multipath effects of the laser pulse in the vegetation.

2.5 Case study: vegetation mapping of Dutch floodplains

As a first assessment of applicability of laser scanning data for prediction of floodplain vegetation structure in winter conditions, we evaluated different statistics of laser data of a floodplain along the Lower Rhine in the Netherlands.

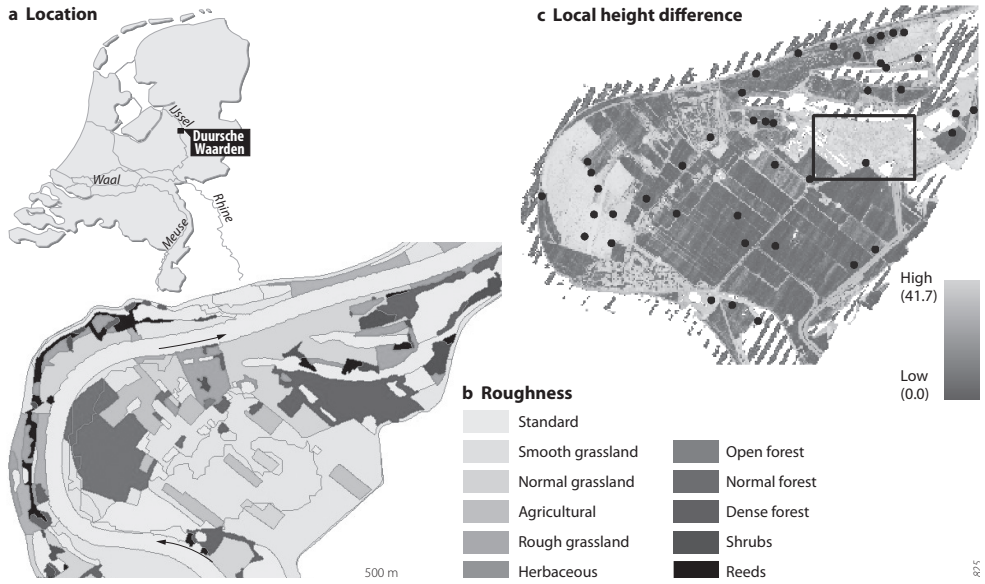

Figure 2.4 'Duursche Waarden' floodplain. a) location, b) roughness map based on ecotopes, c) local height differences from laser scanning data. The black rectangle indicates the location of figure 2.5.

2.5.1 The 'Duursche Waarden' floodplain study area

The 'Duursche Waarden' floodplain (Fig. 2.4) along the IJssel river, the smallest distributary of the river Rhine in the Netherlands, was used as test area for vegetation mapping using airborne laser altimetry. The floodplain consists of a large meander along the concave bank of the main channel, and includes two man-made side channels, and a small river dune. The area is partly used as meadow and arable land, while large areas have become nature area. The vegetation comprises (Koppejan 1998): (1) softwood forest (willow, (*Salix alba, Salix viminalis)*, poplar (*Populus nigra, Populus x canadensis*), (2) hardwood forest (oak (*Quercus robur*), ash (*Fraxinus excelsior*) and a small pine stand (*Pinus sylvestris*) on a river dune, together with (3) reed marshes (*Phragmites australis*), and (4) herbaceous vegetation with sedge (*Carex hirta*), sorrel (*Rumex obtusifolius*), nettle (*Urtica dioica*), thistle (*Cirsium arvense*) and clover (*Trifolium repens*). Within the floodplain, some gravel and clay pits occur. At the upstream side the floodplain is protected from low-magnitude floods by a minor dike. Inundation of the floodplain usually occurs in winter, so surveys of vegetation structure related to hydrodynamic roughness were also undertaken during the winter season.

2.5.2 Data collection

The laser data was collected in winter (March 11, 2001). First pulse, small footprint data was collected from low flying heights (~80 m) using the FLI-MAP system operated from a helicopter. FLI-MAP, Fast Laser Imaging and airborne MApping Platform, is a scanning laser system with a nadir looking laser scanner that has a scan angle of ± 30° (Baltsavias 1999b). Point densities varied between 5 and 12 points m^{-2}. The right panel in figure 2.4 shows height differences in the laser data within a moving window with a 1 m circular radius. Simultaneously with the laser data, vegetation height and density were measured in the field on 39 plots of size 200 m^2 or larger in the same floodplain (Fig. 2.4c). Vegetation density was determined from the product of number of stalks or stems per unit area and the average stalk or stem diameter. The average stem diameter for each plot was based on 30 individual measurements using a sliding gauge.

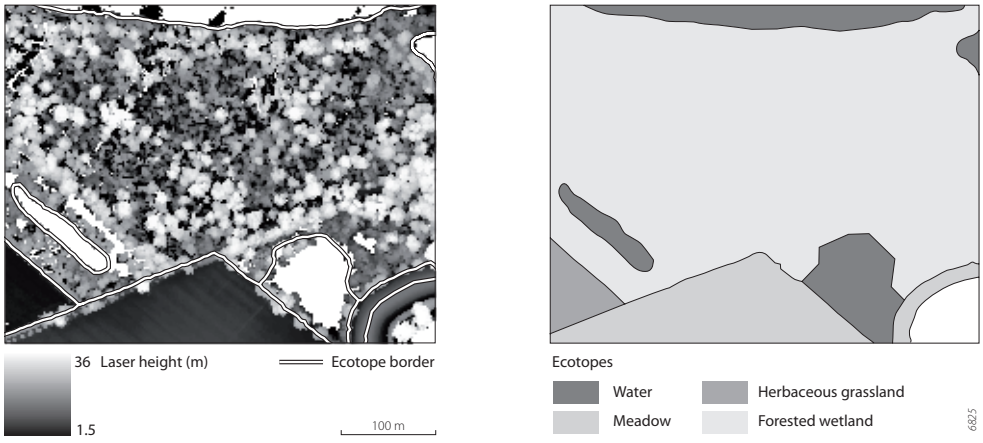

Figure 2.5 Detail of the Duursche Waarden floodplain: laser image (left) and ecotope map (right). The laser image shows much more detail than the ecotope map.

Vegetation height was based on 30 individual measurements using a measuring rod. Vegetation height of forests was not measured as the trees reach above the maximum flood water levels.

2.5.3 Vegetation structure in laser data

Figure 2.4c shows the height differences in a moving local circular window with a 1 m radius, which is based on the unsegmented laser scanning point cloud. Obvious similarities are present in the distribution of forest ecotopes and high values in the laser image. Shrubs and young forests show intermediate values and grasslands are characterized by small local height differences. However, when zooming in, both field and laser data show large variation within specific ecotopes. Table 2.4 compares the vegetation structural characteristics based on the lookup table of Van Velzen *et al.* (2003), which are used in hydrodynamic modeling, with the range of field values of vegetation height and density and the range of three selected laser-derived parameters. Both laser and field data show variation of more than one order of magnitude within a specific ecotope. An example of this difference is given in figure 2.5, where the ecotope 'forest wetland' is classified as having a vegetation density of 0.023 m^{-1}, but includes areas of high and low vegetation with a vegetation density in the field ranging between 0.019 and 0.19 m^{-1}.

Figure 2.6 shows laser point clouds and local histograms of field plots with variable size. Four typical types of vegetation within the floodplain are depicted. Maximum inundation depth during flooding is 5 m at these locations. The difference between open (Fig. 2.6a) and dense (Fig. 2.6b) forests is clearly visible in the laser point cloud (middle column) and the resulting histogram (right). Also the *LAI* values, computed over the 0.5 to 2.5 m height range, increase with increasing vegetation density. *LAI* is 0.015 for open forest and 0.028 for dense forest. The ground surface is also clearly recognizable. Laser scanning also detected herbaceous vegetation in winter (Fig. 2.6c). Here, point density progressively decreases with height above the ground, which indicates that stalks are recognizable. Most laser returns (up to 90%) represent the ground surface. Therefore, the median value of a laser point cloud is not a good parameter to predict vegetation height. The gradual decrease in point density with height indicates that it is difficult to separate laser points reflected from the ground surface from points reflected from vegetation. The point cloud and resulting histogram of a meadow is indicated in figure 6d. The histogram

Table 2.4 Comparison of model input to observed values of vegetation height and density and laser-derived parameters

Hydrodynamic model input			**Range of field values**		**Range of selected laser-derived parameters**		
Ecotope type[a]	**Height**[b] **(m)**	**Density**[b] **(m^{-1})**	**Height (m)**	**Density (m^{-1})**	**st. dev. (m)**	**D_{95}**[c] **(m)**	***LAI***[d] **10^{-2} (-)**
Hardwood forest	– -	0.023	– -	0.005 – 0.056	1.8 – 5.5	10.3 – 22.4	0.3 – 3.8
Softwood forest	– -	0.023	– -	0.015 – 0.19	4.4 – 8.5	5.4 – 27.9	1.4 – 19
Softwood shrubs	6	0.13	5 – 7	0.08 – 0.11	0.7 – 2.3	2.7 – 7.3	9 -20
Natural grassland	0.1	12	0.1 – 0.7	0.0003 – 0.065	0.03 – 0.11	0.16 – 0.38	1.3 – 16
Meadow	0.06	45	0.02 – 0.07	– -	0.015 – 0.035	0.13 – 0.20	0.7 – 3.2

a. Based on Jansen & Backx (1998), b. Based on Van Velzen et al. (2003), c. 95 percentile of the relative height distribution, d. leaf area index

shows an almost perfect Gaussian error distribution. Standard deviation is 4 cm and the range is 30 cm.

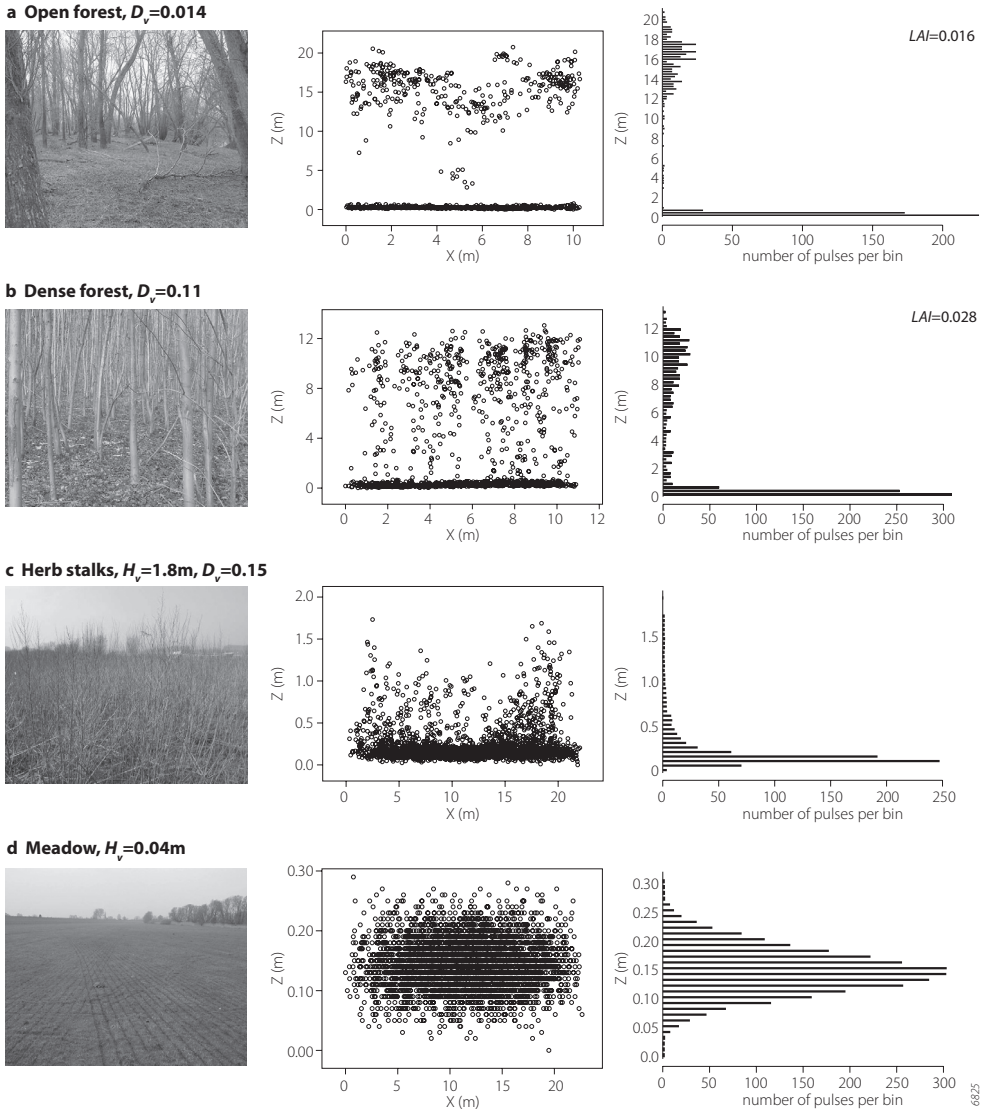

Figure 2.6 Examples of the influence of vegetation characteristics on the vertical point distribution. Open forest (a) shows less laser hits just above the ground surface than dense forest (b). Herb stalks are detectable (c). Meadows show a Gaussian error distribution (d). Explanation of symbols: D_v = vegetation density, H_v = vegetation height, *Z(m)* = height above local zero plane (m), *X(m)* = local easting (m), *LAI* = Leaf Area Index

2.6 Prospects: the future of airborne laser scanning in floodplain management

Floodplain vegetation structure is spatially heterogeneous, and will vary in time due to vegetation succession (Baptist *et al*. 2004; Jesse 2004). Airborne laser scanning is a promising tool to extract vegetation structural characteristics. Typical differences in forest structure within floodplains are easily recognizable from local differences in the laser point cloud, but also the ability to determine vegetation density of forests seems likely. However, a first step in data processing should be the classification of vegetation types, because the empirical relations are vegetation-type specific. Forest, shrubs and herbaceous vegetation are discernable from vegetation heights derived from laser data, but meadows and agricultural lands are not. Therefore, boundaries between vegetation types should be generated using an object-based classification algorithm based on spectral and laser data, for example as in Hay *et al*. (2003).

Vegetation density of floodplain forests could be predicted using the LAI method of MacArthur & Horn (1969), a canopy density based on Næsset (2002) or individual tree delineation. Herbaceous vegetation in winter can be detected by laser scanning. Since previous studies focused on crops and grasslands in summer condition, research into floodplain vegetation roughness should focus on detailed investigation of the relation between the laser scanning data and field measurements of vegetation height and density of herbaceous vegetation under winter conditions. Special attention should be paid to the reconstruction of DTMs under these vegetation types, since a large proportion of the laser points are reflected from the ground surface. Due to the noise in the currently available laser scanning data, it seems impossible to determine vegetation height of floodplain meadows. Full waveform digitizing data may improve these estimates. Thus, from the literature review and the first field assessment for the Lower Rhine floodplain airborne laser scanning data seems a promising tool for hydrodynamic roughness determination for vegetation types other than meadows. Compared to spectral data, laser scanning offers the ability to map the 3D structure of vegetation, avoiding the use of lookup tables with their inherent data loss. Combining laser scanner data with spectral data may provide an adequate solution to classify unvegetated areas and meadows. In this case, a lookup table still needs to be used to convert land cover to roughness values.

Management of floodplains involves comparing costs of different techniques. Laser scanning mapping of vegetation structure is more expensive than traditional airborne photography, but ALS has the potential of more detailed vegetation structure extraction. Hartmann *et al*. (2004) conclude that a combination of multispectral remote sensing and laser scanning is five times more expensive for roughness determination than the traditional method. Increased scan frequency of the laser system would allow acquisition of the laser data from higher altitudes, covering larger areas in a single flight strip while preserving the required point density. In the future, such technical developments may reduce acquisition cost. Laser altimetry data provides useful information for various other applications like floodplain morphology, 3D shape of groynes, location of shorelines and break lines (Bollweg *et al*. 2004). For example, for groyne monitoring and floodplain DTM generation, laser scanning is cheaper than conventional methods like terrestrial height measurements or analytic photogrammetry. This indicates that laser scanning is particularly suitable for floodplain management if multiple end products are derived from the laser data.

3 Extracting structural characteristics of herbaceous floodplain vegetation under leaf-off conditions using airborne laser scanner data

in press: Straatsma, M. W. & H. Middelkoop. Extracting structural characteristics of herbaceous floodplain vegetation for hydrodynamic modeling using airborne laser scanner data. *International Journal of Remote Sensing*.

Abstract

Hydrodynamic models of river flow need detailed and accurate friction values as input. Friction values of floodplain vegetation are based on vegetation height and density. To map spatial patterns of floodplain vegetation structure, airborne laser scanning is a promising tool. In a test for the lower Rhine floodplain, vegetation height and density of herbaceous vegetation were measured in the field at 42 georeferenced plots of 200 m^2 each. Simultaneously, three airborne laser scanning (ALS) surveys were carried out in the same area resulting in three high resolution, first pulse, small-footprint datasets. The laser data surveys differed in flying height, gain setting and laser diode age. Point density of the laser data varied between 10 and 75 points m^{-2}. Point heights relative to the DTM derived from the ALS data were used in all analyses. Laser points were labeled as either vegetation or ground using three different methods: (1) a fixed threshold value, (2) a flexible threshold value based on the inflection point in the point height distribution, and (3) using a Gaussian distribution to separate noise in the ground surface points from vegetation. Twenty-one statistics were computed for each of the resulting vegetation-point distributions, which were subsequently compared to field observations of vegetation height. Additionally, the Percentage Index (*PI*) was computed to relate density of vegetation points to hydrodynamic vegetation density. The vegetation height was best predicted by using the inflection method for labeling and the 95 percentile as a regressor (R^2 = 0.74 – 0.88). Vegetation density was best predicted using the threshold method for labeling and the *PI* as a predictor (R^2 = 0.51). The results of vegetation height prediction were found to depend on the combined effect of flying height, gain setting or laser diode age. The quality of the estimation of vegetation height and density is also affected by point density, for densities lower than 15 points m^{-2}. We conclude that high resolution ALS data allows estimation of vegetation height and density of herbaceous vegetation in winter condition, but field reference data remains necessary for calibration.

Keywords: Airborne laser scanning; floodplains, herbaceous vegetation; leaf-off; vegetation height; vegetation density; hydrodynamic vegetation roughness input.

3.1 Introduction

In response to the increased awareness of the socio-economic importance of river flooding in the past decades, considerable effort has been undertaken in recent years in the development of hydrodynamic models of overbank flow to predict extreme flood water levels for the design of flood defence structures. Hydrodynamic roughness of the floodplain surface is one of the key parameters of these models, and depends on vegetation structure. The role of vegetation roughness in hydrodynamic modeling is becoming increasingly important to assess the implications of ecological rehabilitation measures in floodplain areas for overbank flow patterns and extreme water levels. This is because ecological rehabilitation may involve considerable changes in floodplain vegetation, and may lead to a more extensive use of floodplains, resulting in complex patterns and succession stages of floodplain vegetation (Baptist *et al*. 2004; Jesse 2004; Van Stokkom *et al*. 2005). Although various schemes have been developed to represent vegetation roughness in 2D and 3D hydrodynamic models, and numerous flume experiments have been reported to determine vegetation roughness, there is still considerable lack of quantitative estimates of vegetation patterns and inherent roughness of real floodplains (Darby 1999; Fischer-Antze *et al*. 2001; Stoesser *et al*. 2003; Nicholas & McLelland 2004). Therefore, monitoring floodplain vegetation structure becomes essential for accurately modeling the hydrodynamics of submerged floodplains (Mason *et al*. 2003). Key parameters used in numerical 2D or 3D modeling schemes to calculate hydrodynamic roughness of vegetation are vegetation height and density, average stem spacing and flexural rigidity (Kouwen & Li 1980; Klopstra *et al*. 1997). Vegetation density is the projected plant area in the direction of the flow per unit volume. For cylindrical vegetation, this equals the product of number of stems or stalks per unit area multiplied by the average stem diameter (Fischer-Antze *et al*. 2001; Wilson & Horrit 2002). Numerous models have been presented to convert vegetation structural characteristics to roughness (e.g. Kouwen & Li 1980; Klopstra *et al*. 1997; Baptist 2005).

Traditional methods to map vegetation patterns within the floodplain are based on visual interpretation and manual classification of vegetation units from aerial photographs, as applied for the lower Rhine floodplains (Jansen & Backx 1998; Van Velzen *et al*. 2003). These, however, may become inadequate to monitor the spatio-temporal dynamics of vegetation roughness, since the procedures are time consuming and do not allow to document within-class variation of vegetation roughness. There is thus a need for a faster and more adequate approach to assess hydrodynamic roughness of vegetated floodplain surfaces. In case of the River Rhine in the Netherlands, such approach has to be specifically suited for herbaceous vegetation since these occupy the largest floodplain areas (Duel *et al*. 2001).

For many years, successful attempts have been reported to map vegetation types using multispectral or hyperspectral remote sensing data (Ringrose *et al*. 1988; Mertes *et al*. 1995; Thompson *et al*. 1998; Schmidt & Skidmore 2003; Van der Sande *et al*. 2003, Rosso *et al*. 2005). Recently, spectral information has been combined with height information in classification

schemes (e.g., Hill *et al*. 2002; Ehlers *et al*. 2003). Mertes (2002) gives an overview of different aspects of remote sensing of riverine landscapes. The resulting maps with vegetation classes need to be converted to a vegetation structure map using a lookup table, since vegetation structure cannot be extracted directly from the spectral image. In the classification procedure, spatial detail of vegetation structural characteristics is lost. In contrast, airborne laser scanning (ALS) provides information on the distribution of vegetation directly, and therefore has been used extensively in forestry surveys to estimate forest characteristics (Lefsky *et al*. 2002; Lim *et al*. 2003). It has been used to map vegetation height of floodplains as well, but only in summer when vegetation was in leaf-on condition (Cobby *et al*. 2001; Mason *et al*. 2003). However, in the Netherlands, most floods occur in winter (Middelkoop & Van Haselen 1999). Relations derived for summer vegetation may be unrepresentative as the vegetation structure differs, which will influence the vertical distribution of the ALS point cloud. No multitemporal study of herbaceous vegetation structure is known to the authors.

The main goal of this study was to estimate vegetation height and density of herbaceous floodplain vegetation in senescence on a field plot level using airborne laser scanning data. Flexural rigidity and average stem spacing seems unlikely to be extractable from ALS data in case of herbaceous vegetation. We focused on herbaceous vegetation, as this is the dominant vegetation type in Dutch floodplains. Three different methods to distinguish between ground points and vegetation points were evaluated. We determined a large number of statistical characteristics of the vegetation points and evaluated which of these were the best predictors of vegetation height and density. The study was based on ALS data collected during three scanning surveys in different sections of the lower Rhine floodplain in the Netherlands: one in March 2001 and two in March 2003. Simultaneously with each laser survey, field reference data were collected on vegetation height and density at the same floodplain sections.

3.2 Extraction of vegetation structure of low vegetation from airborne laser scanning data

ALS has been extensively used for various applications, such as aerodynamic roughness determination (Menenti & Ritchie 1994), ice sheet modeling (Krabill *et al*. 2000), and coastal dune morphology (Woolard & Colby 2002). It has been successfully applied to measure vegetation structure (Wehr & Lohr 1999). In forestry, laser scanning has been successfully applied to map forest properties, such as timber volume (Næsset 1997b), tree height (Næsset 2002; Brandtberg *et al*. 2003) or number of stems and stem diameter (Lefsky *et al*. 1999a; Næsset 2004). Lim *et al*. (2003) give an overview of airborne laser scanning of forests.

Only a few papers have reported on documenting and mapping vegetation height of low vegetation. Weltz *et al*. (1994) and Ritchie *et al*. (1996) found good correspondence between field data and airborne laser measurements of plant height, canopy cover and ground cover of low height rangeland vegetation. However, they did not present regression models to estimate these parameters from laser data. Davenport *et al*. (2000) and Cobby *et al*. (2001) used low-resolution (1 point per 9 m^2) laser data to estimate crop height. Since the vegetation density of the crops was very high, they were unable to detect the ground surface in the laser data, and therefore they

used the standard deviation of de-trended laser heights as a predictor. The standard deviation of laser scan height data correlated in a (log-) linear way with crop height determined by field sampling (R^2 = 0.89 in Davenport *et al.* 2000; R^2 = 0.80 in Cobby *et al.* 2001). Hopkinson *et al.* (2004) predicted vegetation height of shrubs, aquatic marshland vegetation, grassland and herbs. Like the previous studies, they used the standard deviation of all laser points, corrected for local ground surface undulations, as a predictor of vegetation height (R^2 = 0.77). All laser data and field data were collected during leaf-on season. The parameters in the regression models in these studies varied greatly. Cobby *et al.* (2001) used a log-linear regression, which did not give satisfactory results on the data of Hopkinson *et al.* (2004b). Moreover, the slope of the regression reported by Hopkinson (2004) was three times higher than the one from Davenport *et al.* (2000). The high regression slope reported by Davenport *et al.* (2000) might be due to higher density of the crops when compared to the natural vegetation studied by Hopkinson *et al.* (2004b). Dense crops create a continuous canopy cover and most laser pulses will reflect off the top of the canopy thereby limiting the variation in the vertical distribution.

In spite of this successful application of ALS laser data to document vegetation height of crops and marshlands in summer, it remains to be evaluated whether these methods are applicable for assessing vegetation structure in Dutch floodplains, when vegetation is leafless, and only the stalks of the grasses and herbs are present. Thus, contrary to Davenport *et al.* (2000) and Cobby *et al.* (2001), the vegetation type to be mapped is very open and consists of thin stalks. Consequently, regression models established in these previous studies might not be valid for winter vegetation. Besides vegetation height, vegetation density is also needed as input to hydrodynamic models. No literature was found that related laser-derived parameters to the vegetation density of herbaceous vegetation.

3.3 Materials and methods

3.3.1 Study area

This study is based on laser data collected in three floodplain sections of the distributaries of the River Rhine in the Netherlands: 'Duursche Waarden' floodplain (DW) along the right bank of the River IJssel, and the 'Afferden en Deestsche Waarden' (ADW) and the 'Gamerensche Waarden' (GW) floodplains along the left bank of the River Waal (Fig. 3.1). In all these floodplains, landscaping measures have been carried out to reduce flood levels and to restore the ecology. For these floodplains, high-density laser data were acquired by the Dutch Ministry of Transport, Public Works and Water Management as a monitoring pilot. Vegetation presently consists of hardwood and softwood forest and shrubs, but is dominated by herbaceous vegetation. Vegetation is characterized by a heterogeneous pattern of vegetation types and structure. Herbaceous vegetation consists mostly of sedge [*Carex hirta L.*], sorrel [*Rumex obtusifolius L.*], nettle [*Urtica dioica L.*], thistle [*Cirsium arvense L.*] and clover [*Trifolium repens L.*]. The vegetation height inside the plots ranged between 0.26 and 1.66 m.

3.3.2 Field measurements

We measured vegetation height and density in 42 field plots of homogeneous vegetation (Fig. 3.1): 12 plots in the DW and ADW floodplain in March 2001, and 30 plots in the GW floodplain

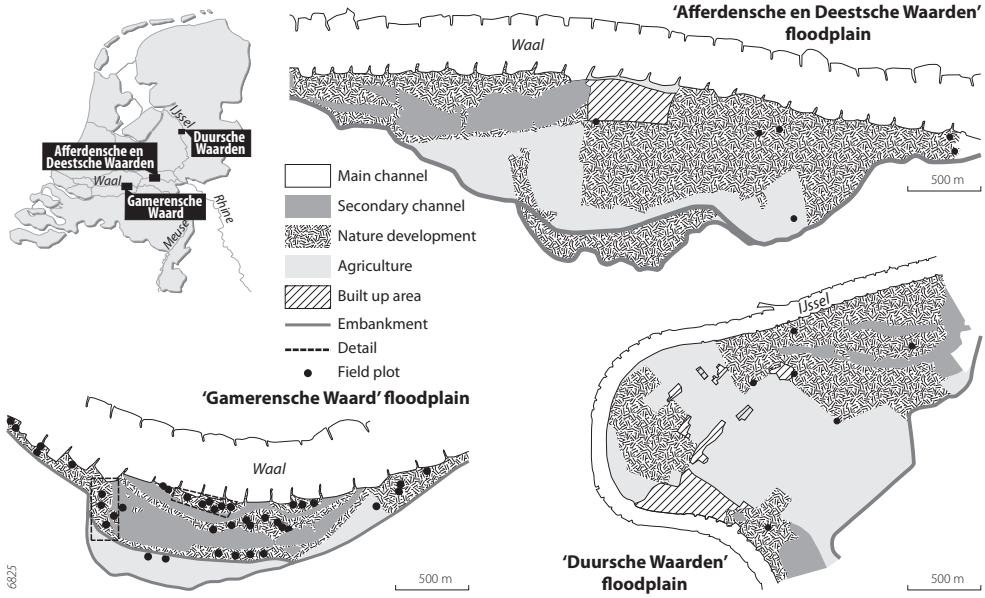

Figure 3.1 Location of the study sites and field plots

in March 2003. The plots represented a large range of herbaceous vegetation types. Plot size was at least 200 m^2, to ensure a sufficient number of laser points available for subsequent analysis. The plots were geo-located using a Garmin GPS12 resulting in a horizontal accuracy of 5 meter, which is the Estimated Positioning Error (EPE) given by the Garmin proprietary software. Vegetation height was measured in two steps: (1) We estimated the average vegetation height as an imaginary plane through the average top of the vegetation and (2) we measured the length of 30 randomly selected stalks reaching at least to half the height of step 1. Mean and standard deviation of the 30 measured heights were registered. Vegetation density was determined from the product of the number of stalks per unit area and the average stalk diameter, which was based on the same 30 stalks using a sliding gauge.

3.3.3 Airborne laser scanning data

The laser data were acquired by Fugro-Inpark using the FLI-MAP II system mounted on a helicopter (Huising & Gomes Pereira 1998; Baltsavias 1999a). FLI-MAP, Fast Laser Imaging and Mapping Airborne Platform, is a scanning laser range finder combined with a dGPS and an Inertial Navigation System for positioning. An overview of the laser scanning technique used is given by Wehr & Lohr (1999). FLI-MAP has an additional option to change the gain setting. The gain is the amount of amplification of the return signal before it is converted to a digital signal. Surveyors may increase the gain to compensate for the declining emission of energy due to ageing of the laser diode.

Table 3.1 summarizes the characteristics of the three laser scanning campaigns and the locations are shown in figure 1. The laser data collected in 2001 in the 'Duursche Waarden' and the

Table 3.1 Metadata for the three laser scanning campaigns

Acquisition Time	Floodplain location	scan angle	nr of sensors	sensor age	Flying height	Gain	Point density	Flight strips
March 2001	DWADW	± 30°	1	old	80 m	100%	12 m^{-2}	Single
March 2003a	GWhigh	± 30°	2	new	80 m	80%	75 m^{-2}	Double
March 2003b	GWlow	± 30°	2	new	55 m	100%	60 m^{-2}	Single

'Afferdensche en Deestsche Waarden' floodplains is referred to as 'DWADW' dataset. Between 2001 and 2003, Fugro-Inpark added a second laser range finder to FLI-MAP, resulting in a doubling of the data collection rate and a re-orientation of the scanners. Instead of one nadir looking scanner, the two scanners were facing 7° forward and backwards to decrease the number of occlusions in built-up areas. With the new FLI-MAP configuration two datasets were collected in the 'Gamerense Waard' floodplain in 2003. One was acquired from a height of about 80 m and with normal gain setting of the receiver, resulting in the 'GWhigh' dataset, the second from a minimum height of 55 m and with the maximum gain, called the 'GWlow' dataset. The GWhigh dataset covers the entire GW floodplain, while each flight line was flown twice to increase the point density resulting in a point density of 75 points m^{-2}. The GWlow dataset only covers 10 field plots (Fig. 3.1). The three datasets enable the evaluation of the resulting regression equations to estimate vegetation height, which are influenced by the different flight parameters (table 3.1).

3.3.4 DTM extraction and labeling

For the determination of the vegetation height, the effect of the undulations of the terrain should be eliminated. This can be done by constructing a Digital Terrain Model (DTM) based on points that are expected to represent the ground. This is the common practice, as reported in most literature. Sithole & Vosselman (2004) give an overview of eight different DTM extraction methods. They conclude that all methods perform well in relatively flat terrain such as lowland river floodplains.

Detailed terrestrial reference heights were collected on five out of six plots of the DWADW. The accuracy of the laser DTM was 7.3 cm for herbaceous vegetation using a different filter (Pfeifer *et al*. 2003). The terrestrial data was not used as a DTM, because the offset between the ALS DTM and the terrestrial DTM would influence the regression equations, which would limit the applicability of the method.

DTM filtering

For this study, only the laser points that were located inside the field plots were considered. For each plot, a DTM was constructed using iterative residual analysis based on a simplified version of the method of Kraus & Pfeifer (1998). In each step, a surface was computed as a local second order trend surface in a moving window. The window radius was 1.5 m to ensure enough points are available for a robust fit. A larger window would lead to a loss of detail. The residual distance to this surface was computed for each point. Points with positive residuals are likely to be vegetation points. Since the range of values for an unvegetated, flat surface was computed and proved to be approximately 30 cm, a simple weight function was applied to compute the

surface in the next iteration: points with an residual value of more than 15 cm were excluded from further analysis in the DTM processing. With the remaining points a new DTM surface was computed. Iterations were continued until all points had residuals less than 15 cm. The final DTM was a smooth surface running through the middle of these ground points. Heights relative to the DTM were used in subsequent computations.

Vegetation labeling

In a second step, a detailed study was carried out to decide which points should be labelled as vegetation. Three different methods were evaluated: (1) a threshold method, (2) an inflection method, and (3) a Gaussian method. The first method is based on a fixed threshold value above the DTM, the other two are based on histogram analysis of heights above the DTM. For the threshold method, we used 15 cm above the DTM as a threshold (Fig. 3.2a), similar to the DTM filtering setting.

For the second and third method laser points were binned in 2 cm vertical bins. Narrower bin intervals led to very spiky histograms, wider intervals to a loss of detail. The vertical point distribution was considered as a combination of a noise distribution of ground points and a uniform distribution of vegetation points. The inflection method finds the point of maximum concave-up curvature in the upper limb of the histogram, the so-called inflection point. The rationale behind the selection of this point as a threshold value is that the sum of a noise distribution of the ground points and the uniform distribution of the vegetation points gives a strong concave up curvature. Any point that lies above the inflection point value is labelled as a vegetation point, all points below are ground points. To find the inflection point, a Harris function was fitted through the upper part of the histogram for each field plot (Fig. 3.2b). The Harris function is defined as:

$$y(h) = \left(a + b * h^{c}\right)^{-1} \tag{3.1}$$

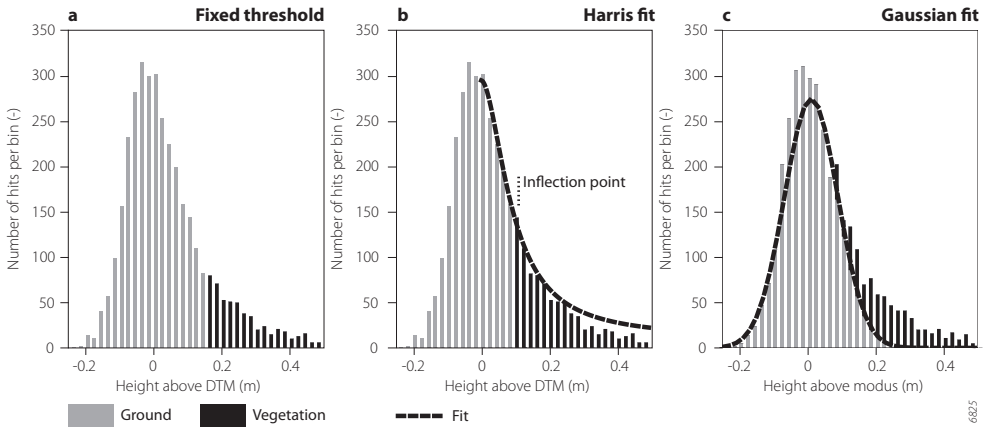

Figure 3.2 Labeling of vegetation points (black bars) and ground points (grey bars); a) threshold value of 0.15 m, b) inflection point, c) difference between Gaussian fit and point distribution.

where y(h) is the frequency of occurrence in a bin at height h. Parameters a, b and c are estimated from a least squares fit using a minimum of 15 bins to ensure stability of the fit. The inflection point was obtained by determining the height at which the second derivative of the Harris function reaches the maximum value. The height of the inflection point in the example is 0.09 m (Fig. 3.2b).

The Gaussian method fits a Gaussian curve to the histogram. The Gauss curve is defined as:

$$p(h) = (2\pi\sigma)^{-0.5} \exp\left(-\frac{1}{2}\left(\frac{h-\mu}{\sigma}\right)^2\right) \tag{3.2}$$

where $p(h)$ is the frequency of noise occurrence at height h, μ is the mean, σ is the standard deviation. Fitting the Gauss curve boils down to finding the mean and standard deviation *of the ground points*. The mean of all points in the plot however also considers the vegetation points. Therefore, we used the mode of the distribution instead of the mean to estimate μ. The disadvantage of the mode is that the data have to be binned which introduces a dependence on the choice of the bin boundaries. Moreover, the mode can be undetermined. To counteract this effect we used the *weighted mode*, the average of the seven most frequent values in the point distribution, weighed by frequency. The standard deviation was based on the points lower than the weighted mode using the 15.9 and 25 percentile. These two standard deviations were averaged to derive the final standard deviation. The Gauss curve was then scaled by the product of twice the number observations below the weighted mode and the bin width (Fig. 3.2c). The difference between the histogram values and the fitted Gauss curve in the range above one standard deviation above the mode provided the number of points per bin that were assumed to represent vegetation. In each bin, points were labelled randomly as vegetation up to the predicted number of vegetation points. This ensured a spatially random distribution of the vegetation points.

3.3.5 Relative point height distribution and comparison with field data

The three methods, described in the previous section, result in three height distributions of vegetation points for each plot. With respect to predicting the vegetation height, each point distribution was described by 21 different statistics:

- Central tendency: mean, median, mode
- Variability: standard deviation and variance
- Shape: skewness and kurtosis
- Percentiles: D_{10}, D_{20},....., D_{100} + D_{95}, D_{96}, D_{97}, D_{98}, D_{99}

The observed vegetation heights in the field were subsequently compared to these statistics using correlation as an indicator of the strength of the relation. Forward stepwise linear regression was subsequently carried out to determine the strongest predictors (Wonnacott and Wonnacott, 1990). The affects of gain setting and flying height were tested using two statistical tests; a t-test on differences in means and a paired sample t-test of the D_{95} percentiles of the GWhigh and GWlow data set. Samples could be paired for these datasets since the same reference plots were used. To gain insight in the effect of laser diode age and the flight parameters, the slopes of the regression models for vegetation height were compared using a single percentile as a regressor using three Student's t-tests.

Table 3.2 Field measurements of vegetation height and density

Floodplain[a]	Plot nr	H_v[b]	D_v[c]	Floodplain	plot nr	H_v[b]	D_v[c]
GW	1	0.69	0.12	GW	35	0.59	0.046
GW	3	0.55	0.088	GW	36	0.91	0.084
GW	7	0.99	0.13	GW	37	0.81	0.034
GW	9	0.66	0.113	GW	39	0.57	0.048
GW	10	0.48	0.015	GW	41	1.66	0.015
GW	11	0.44	0.22	GW	42	0.43	0.065
GW	12	0.77	0.35	GW	45	0.38	0.025
GW	13	0.50	0.082	GW	47	0.30	0.020
GW	15	0.38	0.070				
GW	16	0.84	0.16	ADW	21	1.34	0.20
GW	17	0.69	0.091	ADW	22	0.61	0.17
GW	18	0.70	0.077	ADW	23	0.76	0.72
GW	19	1.18	0.12	ADW	31	0.42	0.037
GW	20	1.49	0.15	ADW	32	0.38	0.0054
GW	23	0.26	0.11	ADW	33	0.30	0.027
GW	24	0.84	0.34				
GW	26	0.73	0.29	DW	21	0.72	0.065
GW	27	0.90	0.067	DW	22	0.70	0.049
GW	29	0.47	0.025	DW	23	0.75	0.0003
GW	31	0.47	0.016	DW	31	0.39	0.011
GW	32	0.52	0.018	DW	32	0.47	0.0020
GW	33	0.71	0.060	DW	33	0.49	0.032

a. GW = "Gamerensche Waard" floodplain, ADW = "Afferdensche en Deestsche Waarden" Floodplain, DW = "Duursche Waarden" floodplain; b. H_v = vegetation height (m); c. D_v = vegetation density (m^{-1})

Vegetation density was predicted using the Percentage Index (*PI*), which computes the percentage of laser hits that fall within the height range of the vegetation ($h1$ to $h2$):

$$PI_{h1-h2} = \frac{1}{h2-h1} \cdot \frac{N_{h1-h2}}{N_{tot}} \tag{3.3}$$

in which $N_{h1\text{-}h2}$ is the number of vegetation points between height 1 and 2 above the ground surface, N_{tot} is the total number of points in the field plot including vegetation points and ground surface points. The height interval for *PI* is equal to the height of the vegetation. The first term in the equation is added, because higher vegetation would increase $N_{h1\text{-}h2}$, but does not necesserily increase the vegetation density. Ideally, $h1$ should be set to zero, and $h2$ to the maximum height of the vegetation. However, $h1$ should not include noise of the ground surface. Therefore we chose the lower limit of the vegetation point height distribution as a minimum value.

3.4 Results

3.4.1 Field measurements of vegetation height and density

Vegetation height in the 42 sample plots ranged from 0.26 to 1.66 m. Vegetation density varied between 0.0003 and 0.72 m^{-1}. Table 3.2 gives the full list of the data collected in the field plots.

3.4.2 Estimation of vegetation height and density from laser data

Figure 3.3 shows a 3D scatter plot of the laser scanning representation of the herbaceous vegetation shown on the photograph. The laser points in this image were labelled using the inflection method. For each plot, the three different labeling methods were applied: threshold, inflection point and Gaussian fit, which resulted in three vegetation point distributions per plot. Each distribution was described by the 21 laser-derived statistics and the *PI* parameter. For each individual dataset (DWADW, GWhigh, GWlow), the correlations between the field vegetation heights and the laser statistics were computed. The average correlation per labeling method and per laser-derived statistics is shown in figure 4. The following parameters showed the highest correlations: (1) D_{30} for the threshold method (r = 0.72), (2) D_{90} to D_{98} plus the standard deviation and variance for the inflection method (r > 0.85), and (3) D_{70} for the Gaussian fit (r = 0.70).

The parameter with the highest correlation was chosen for vegetation height prediction for each labeling method. For the inflection method, a few parameters showed a high correlation. The 95 percentile was selected to maintain congruency in predictors even though the standard deviation and the variance showed a marginally better correlation coefficient. Figure 3.5 shows nine scatter plots depicting the measured vegetation heights versus the predicted heights based on the selected laser percentiles. Forward stepwise regression was carried out to select the best regression

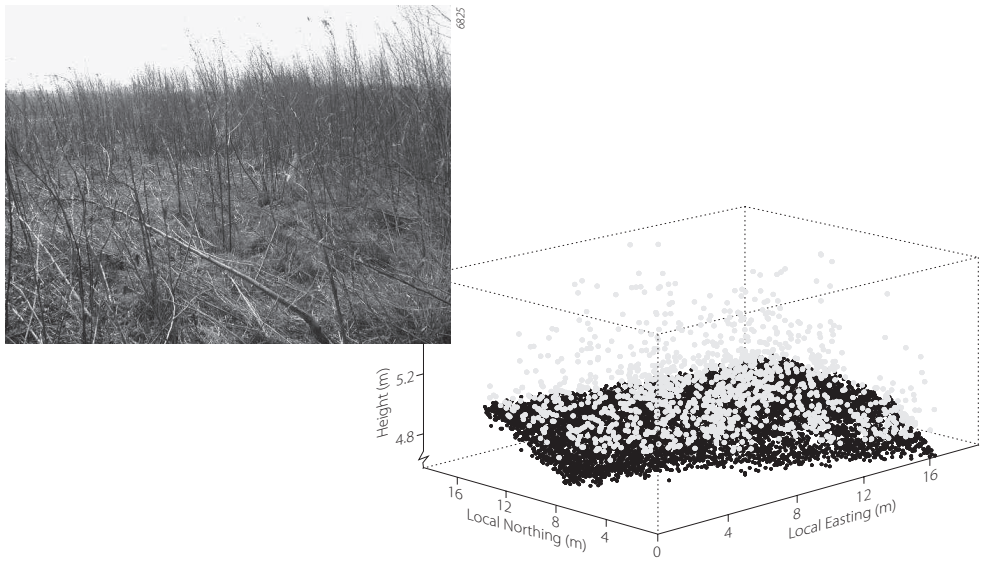

Figure 3.3 3D laser data scatter plot of the herbaceous vegetation on the picture. Vegetation points depicted in grey, ground points in black

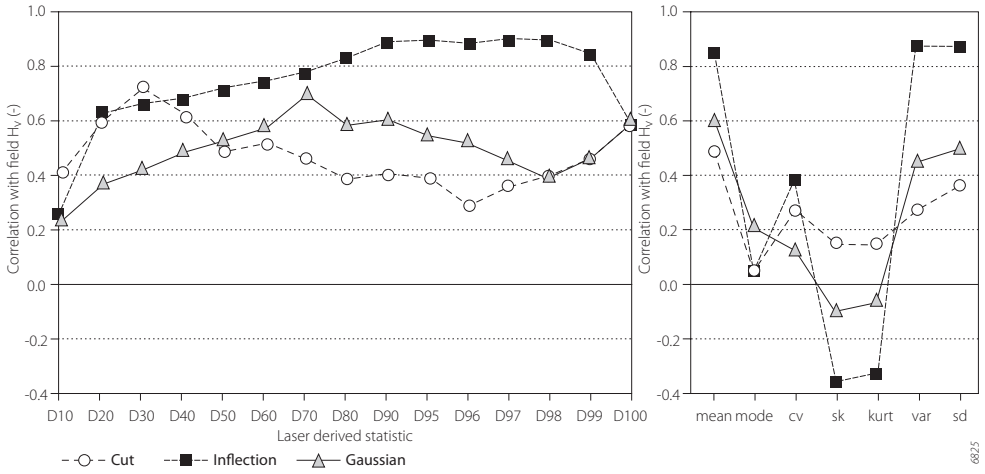

Figure 3.4 Effect of point labeling methods on the strength of correlation between laser-derived statistics and field vegetation heights. D_x = X percentile of the vegetation points, cv = coefficient of variation, sk = skewness, kurt = kurtosis, var = variance, sd = standard deviation

Table 3.3 Regression equations for vegetation height

Labeling method/dataset	Regression equation	R^2	RSE (m)[a]
Threshold			
DWADW	$H_v = 17.20D_{30} - 2.45$	0.58	0.17
GWhigh	$H_v = 10.57D_{30} - 1.26$	0.41	0.24
GWlow	$H_v = 6.98D_{30} - 0.83$	0.57	0.21
Inflection			
DWADW	$H_v = 2.51D_{95} + 0.11$	0.76	0.13
GWhigh	$H_v = 1.47D_{95} + 0.28$	0.74	0.16
GWlow	$H_v = 1.06D_{95} + 0.40$	0.88	0.11
Gaussian			
DWADW	$H_v = 5.13D_{70} - 0.39$	0.37	0.21
GWhigh	$H_v = 2.67D_{70} + 0.02$	0.46	0.23
GWlow	$H_v = 1.80D_{70} + 0.19$	0.65	0.19

a. Residual Standard Error

model, starting with the selected percentile (D_{30}, D_{95}, and D_{70} for the threshold, inflection and Gaussian method respectively). This did not result in the selection of any additional parameters for any of the regression models, due to multicollinearity constrictions. Table 3.3 summarizes the regressions.

Results of the prediction of vegetation density using the Percentage Index *(PI)* are shown as scatter plots (Fig. 3.6). The threshold and Gaussian method show a positive relation with

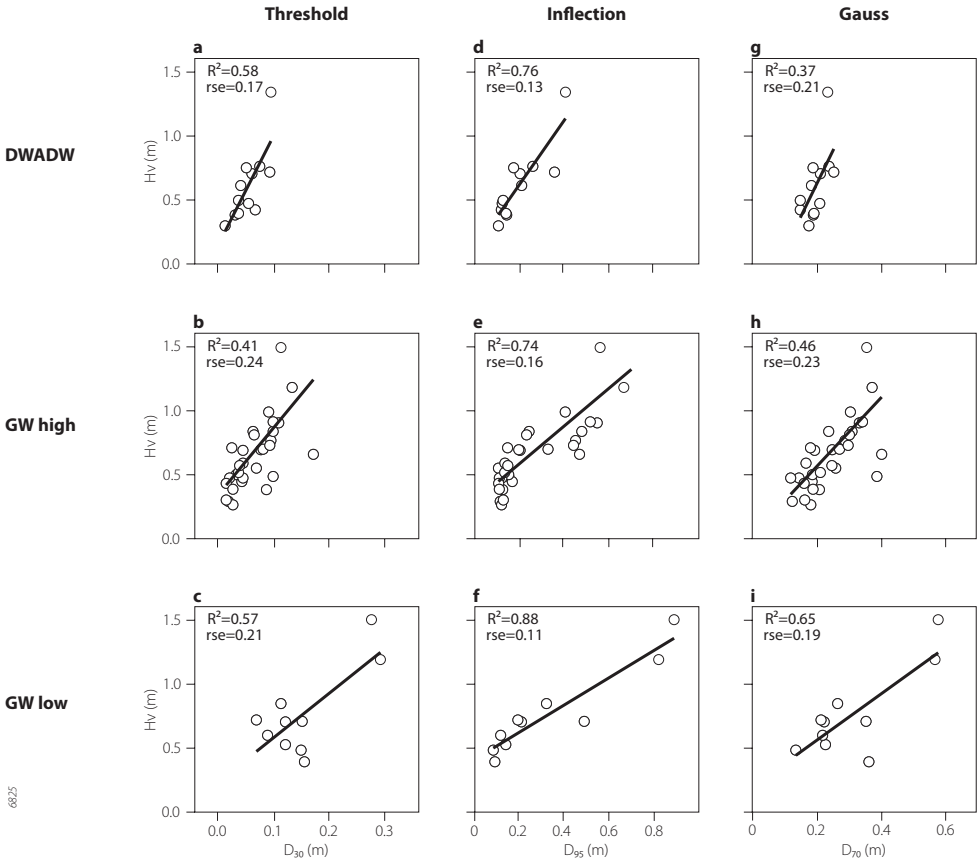

Figure 3.5 Scatter plots of predictions of vegetation height per dataset using three different point labeling methods: a), b), and c) threshold method, d), e) and f) inflection method, g), h) and i) Gaussian method

vegetation density (R^2 = 0.51 and 0.49 respectively). Conversely, prediction based on the inflection labeling shows a weak negative relation (R^2 = 0.09). Table 3.4 summarizes the equations.

3.4.3 Effect of point density

To investigate the effect of varying the point density on the estimation of vegetation height and density, the analyses were repeated for the GWlow dataset that was progressively thinned out. The original point density of 60 points m^{-2} was step-wise reduced to create twelve different datasets with 50, 40, 30, 20, 15, 10, 8, 6, 4, 2, 1, 0.5 points m^{-2}. Point density was reduced by omitting data points at regular intervals from the original dataset, which was in chronological order of data aquisition. This mimics the spatial distribution that would be obtained from a higher flying speed or altitude, with an equal footprint size. For each of the thinned datasets, the D_{95} percentile was calculated using the inflection labeling method and subsequently correlated with observed vegetation height. The *PI* was based on the threshold method and correlated to

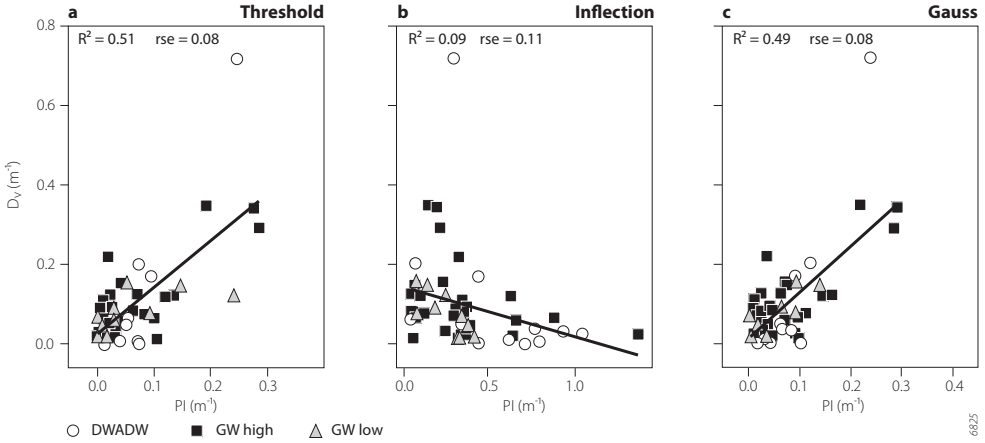

Figure 3.6 Scatter plots of predictions of vegetation density per dataset using three different point labeling methods: a) threshold method, b) inflection method and c) Gaussian method

Table 3.4 Regression equations for vegetation density using three different methods

	Regression equation	R^2	RSE (m^{-1})[a]
Threshold	$D_v = 1.18\,PI + 0.03$	0.51	0.08
Inflection	$D_v = -0.13\,PI + 0.14$	0.09	0.11
Gaussian	$D_v = 1.16\,PI + 0.01$	0.49	0.08

a. Residual Standard Error

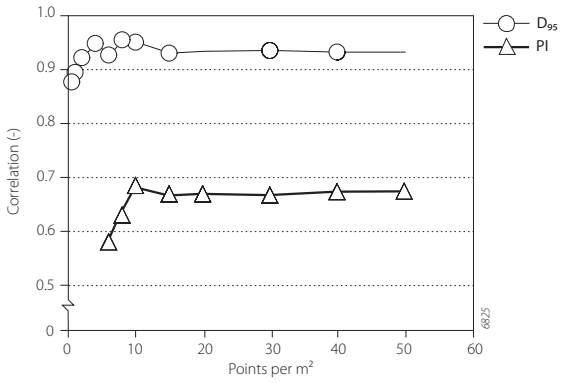

Figure 3.7 Effect of point density on correlation strength for vegetation height (D_{95} in ○) and density (*PI* in △). No variation in correlation is present at point densities higher than 15 points m^{-2}.

Table 3.5 Confidence levels of Student's t-tests on difference in slopes of regression lines.

	DWADW	GWhigh
GWhigh	99.9	
GWlow	99.9	95

the vegetation density. No correlation could be computed for the vegetation density for point densities lower than 6 points m^2 as no vegetations points occurred at some plots. Figure 3.7 shows the effect of decreasing point density on the correlation coefficient between the D_{95} percentile of the laser data and vegetation height plus the correlation between the *PI* and vegetation density as measured in the field. In general, correlations obtained using low point densities are lower (r = 0.85 for vegetation height), but remarkably, correlations do not change for point densities of 15 points m^{-2} or higher. Apparently, a point density of 15 points m^{-2} is most efficient for vegetation height and vegetation density mapping in this study area and for this size of field plots.

3.4.4 Effect of flying altitude and gain setting

The GWhigh and GWlow laser datasets share 10 field plots, which allowed to compare the combined effect of lower flying altitude and increased the gain setting (cf. table 3.1). The following tests were performed using the inflection labeling method and the D_{95} percentile. A t-test on differences in means of both data sets showed no significant difference between the D_{95} percentiles of the GWhigh and GWlow dataset (α = 90%, p = 0.54). These results were in accordance with expectations, since the difference in the average value of the D_{95} percentiles was expected to be low relative to the range of vegetation heights. In contrast, a *paired sample* t-test did reveal significant differences between the height of the D_{95} percentile of the GWhigh and GWlow datasets (α = 90%, p = 0.08). These results indicate that a low flying height, combined with a high gain improves detection of the top of the vegetation.

The slope of the regression lines between laser data and observed vegetation height also indicates the ability of the laser signal to detect the top of the vegetation. A steeper slope indicates a poorer detection of the vegetation top. Figure 3.5 shows the regression lines for the DWADW, GWhigh and the GWlow data sets. The slope of the DWADW is steepest, and the slope of the GWlow dataset is mildest. Three Student's t-tests were carried out to determine whether there were significant differences between the slopes of the regression lines based on vegetation labeling using the inflection method. All differences in slope were significant at the 95 % level of confidence. Table 3.5 gives the significance levels of the three t-tests.

3.5 Discussion

3.5.1 DTM and point labeling

The DTMs for all plots, created using the method of Kraus & Pfeifer (1998), did not show any outliers, and created a smooth surface. Based on visual inspection, the DTMs of the plots seemed very typical of the gently undulating topography observed in the field. However, as Kraus & Pfeifer (1998) stated, it will smooth out terrain jumps, such as erosive river banks.

Sithole & Vosselman (2004) also note in their filtering algorithm test that discontinuities in the terrain surface poses one of the largest problems in point cloud filtering. In case floodplain-wide mapping of vegetation structure is needed, this effect should be taken into account. In this research, laser points from a single dataset, but from different flight strips were combined into one dataset per plot. Height differences between flight strips were checked visually for a few plots, but no systematic errors were detected. Moreover, the combined point distributions did not show a bimodal distribution for any plot. Still, it is advised to create a DTM based on individual flight strips.

Point labeling was done based on the heights relative to the DTM. The three different methods show a varying level of flexibility with respect to discrimination between vegetation and ground points. The threshold method, with the threshold set to 15 cm above the DTM is the most rigid, and identical to the method by which the DTM was created. It assumes that no vegetation points are present below 15 cm above the DTM. The advantage with this method is that point labeling is possible on a per-point basis. The other two methods need a histogram of the point distribution. Both assume that the peak in the point distribution represents the ground surface, an assumption that is not violated in case of herbaceous floodplain vegetation in winter condition. The inflection method defines a threshold value based on the shape of the height histogram as characterized by the Harris function. This function has three fit parameters (a,b,c; eq. 1), which introduces flexibility with respect to height, and width of the point distribution. The height of the inflection point was in all cases lower than 15 cm, and typically around 5 cm. The assumption that underlies this method, is that the ground and vegetation points together generate a point of maximum inflection in the histogram. The disadvantage of this method is that it will also label points as vegetation at sites where no vegetation occurs. The Gaussian method assumes that the ground points show a Gaussian distribution, and labels points as vegetation whenever their frequency in a certain bin exceeds the frequency of the Gaussian distribution. The Gaussian curve (eq. 2) in our case depends on the standard deviation and the weighted mode of the ground points. The number of points labelled as vegetation differ per method. The threshold method labels least points as vegetation, the inflection method most, which is related to the percentile used in the regressions. For example, the inflection method labels most points as vegetation, and therefore a high percentile, D_{95}, correlates best with vegetation height.

3.5.2 Vegetation height and density estimation

Vegetation height of herbaceous floodplain vegetation can be predicted reliably at the plot level using high-density first-pulse airborne laser scanning data (R^2 = 0.74 to 0.88 using the inflection labeling method), while estimation of vegetation density is less accurate (R^2 = 0.51 using the threshold method). The inflection method shows the best predictions of vegetation height for all three datasets (Fig. 3.5). The threshold and the Gaussian method in general selected fewer points, and are therefore more sensitive to outliers in the height distribution. These outliers might result from the relatively low spatial accuracy of the plot boundaries, which was about 5 m. This could have led to the inclusion of laser hits related to other vegetation types. Conversely, vegetation density was predicted better by the threshold and Gaussian method (Fig. 3.6). The *PI* relates point density of vegetation points to hydrodynamic vegetation density. The inflection method labels more points as vegetation than the two other methods, but the *PI* values did not correlate well with field reference values, and are even negatively correlated. This could be caused

by the height at which the vegetation density was measured in the field, which was at least at 13 cm above the ground surface (half the minimum vegetation height). This is well above a typical inflection height of 5 cm. The threshold method performed marginally better than the Gaussian method. The inverse dependence of *PI* on *h*2 minus h1 (eq. 3) could lead to unrealistic values in case h2 nears or equals h1. This should not be a problem for vegetation higher than 25 cm as in this study.

3.5.3 Comparison to other research

In this paper we predicted vegetation height and density of low herbaceous vegetation in winter condition, consisting of open vegetation that generates a weak return. Nevertheless, the quality of prediction of vegetation height in this study is similar to the results obtained in regression models for forests: Means *et al*. (1999), Næsset (2002) and Næsset & Bjerknes (2001) reported regression models explaining 74 to 95 percent of the variance in the field reference data of vegetation height. Given the small range in height of herbaceous floodplain vegetation, it is remarkable that the results obtained in our study are of similar quality as those obtained in forestry surveys.

Davenport *et al*. (2000), Cobby *et al*. (2001), and Hopkinson *et al.* (2004b) studied vegetation height of low vegetation leaf-on condition. However, in our study, we predicted vegetation height of herbs in senescence. This means that the vegetation signal is much weaker, due to the smaller plant surface. Still, the predictive quality of vegetation height found in this study is comparable to the studies on low vegetation in leaf-on condition. The differences found in the regression equations from this study and previous studies (Davenport *et al*. 2000; Cobby *et al*. 2001; Hopkinson, 2004) demonstrate that portability of the derived relations is low. It points to the need for future field reference data and more physical understanding of these relations.

No studies on vegetation density of low vegetation are known to the authors. We chose to relate the vegetation density to the Percentage Index, (R^2 = 0.51 using the threshold method) because of the rationale that denser and higher vegetation should result in more vegetation points in the laser datasets. Although prediction results could be somewhat increased, by including percentiles as additional regressors, we chose not to as percentiles refer to height. Laser-derived parameters from forestry studies that relate to vegetation density, such as stem number and stem diameter explained 39 to 85 percent of the total variance (Lefsky *et al*. 1999a; Næsset 2002). Similar to our study, forestry studies obtained better results for vegetation height than for parameters related to vegetation density.

3.5.4 Effects of flight parameters; flying height, laser diode age and gain setting

Detection of vegetation by laser scanning depends on many factors related to the minimum detectable object (Baltsavias 1999b). Flight parameters for this study are given in table 3.1. The results showed that airborne laser scanning is well able to predict the height of senescent herbaceous vegetation, in a height range order of 0.2 to 2 m (table 3.3). The average stalk diameter of 4 mm of the herbaceous floodplain vegetation apparently exceeds the minimum detectable object size.

The DWADW and GWhigh data sets yielded different slopes of the regression models to estimate vegetation height, which was significant at the 99.9 confidence level (table 3.5). The

reason for this difference might be the age of the laser diode age, the calibration settings or the larger average incidence angle in the GWhigh dataset, due to the reorientation of the laser scanners between 2001 and 2003. The slope of the GWlow dataset was significantly steeper than for the GWhigh dataset. The paired sample t-test also showed significant differences between the GWhigh and GWlow datasets. Remarkably, the increase in the regression slope of the GWhigh and GWlow dataset was significant even though the field and laser data were collected on the same day. The reason for the difference in slope and 95 percentile must therefore be the combination of the reduced flying height and increased gain setting for the GWlow dataset. Together these effects result in a larger amount of energy reaching the analogue to digital converter in the laser scanner from an equally reflective object. Consequently, small objects are detected better, and the regression slopes are lower. With these datasets, it is impossible to assess the influence of the individual parameters. However, as long as the parameters influencing the regression equations are unclear, field reference data will remain necessary to establish the regressions.

Næsset (2004) concluded for spruce and pine forest that the effect of flying altitude is marginal and that the flying altitude can be increased by 60 % without any serious effect on the estimated stand properties. Nilsson (1996) mentions that optimal laser footprint size for forest surveys changes only with acquisition season. These conclusions for forests are contrary to our conclusions for herbaceous floodplain vegetation. The reason for this difference might lie in the shape and structural properties of the vegetation involved. Trees are larger and Næsset's data were collected in leaf-on conditions, which makes detectability of trees better than thin floodplain herbs, which seem at the edge of detectability.

The remaining unexplained variance might result from measurement uncertainties or location errors in the field data. Although the field plots comprised 200 m^2 of homogeneous vegetation each, a 5 m positional error in the location of the plots may influence the height distribution due to spatial heterogeneity of floodplain vegetation. Another source of unexplained variance might be the varying incidence angle resulting from the scanning motion of the laser scanner. The average incidence angle per plot will vary since the plots might be positioned differently with respect to the flight lines. This results in two opposite effects related to the detectability of the vegetation, which change with varying incidence angle: (1) the nadir facing point will have a smaller footprint and therefore a higher amount of energy per unit area, but (2) the vegetation will be hit vertically resulting in a smaller reflective surface in the direction of the pulse. The combined effect on the detectability will depend on the details of the plant structure. Full waveform laser data combined with the incidence angle could give more insight in this issue.

3.5.5 Point density

For point densities lower than 15 points m^{-2}, the correlation between laser data and field reference data becomes unstable. This is the result of two effects: (1) the accuracy of the DTM decreases due to a less accurate representation of small height variations in the floodplain surface, and (2) there are fewer points to determine the histogram to separate ground points from vegetation points, which renders the labeling more noisy. A solution would be to use a larger area for the determination of the histogram, but this larger area should not include shrubs or trees.

3.5.6 Computation of hydrodynamic roughness

The relations to derive vegetation height and density of non-woody herbaceous vegetation from ALS data could be computed in a moving window or per grid cell of the hydrodynamic model. A few issues arise with the computation of hydrodynamic roughness based on ALS data. Firstly, the relations do not hold for other land cover classes, and should therefore not be applied to other land cover classes. Moreover, single trees within the herbaceous vegetation should be delineated separately, see Morsdorf *et al.* (2004) for details). Secondly, some hydrodynamic models need additional information on flexural rigidity, stem spacing, or bottom roughness (Kouwen & Li 1980; Klopstra *et al.* 1997, Baptist 2005), which can not be extracted from ALS data directly. However, the product of stem density and flexural rigidity has heen correlated with vegetation height for both growing and dormant grass up to one meter vegetation height (Kouwen 1988). This relation is not valid for herbaceous vegetation. The bottom roughness, which has a minor effect on the water levels, should be derived from a lookup table. Baptist (2005) provides a model wich can be applied directly using vegetation height and density from ALS data, except for the bottom roughness.

3.6 Conclusions

With airborne laser scanning, a new tool has become available to quantify vegetation height and density of herbaceous vegetation in senescence, which enables the computation of roughness values for hydrodynamic modeling. Laser scanning provides detailed and accurate estimates of vegetation height and to a lesser extent of vegetation density. Three different vegetation labeling methods were evaluated. The threshold method uses a fixed height above the DTM, the inflection method and the Gaussian method analyse the histogram of the height distribution. The inflection method uses the height above the DTM with the strongest concave-up curvature as a threshold. The Gaussian method explicitly takes the noise of the ground points into account by fitting a Gaussian curve to the ground points. The threshold and the Gaussian method selected fewer points, and are therefore more sensitive to outliers in the height distribution. Vegetation height estimation was most successful using the inflection method for point labeling. The 95 percentile proved the best predictor, (R^2 = 0.74 to 0.88). However, regression models differed significantly for datasets that were acquired with different flying height, gain, and laser diode age. The validity range for vegetation height is the height range order of 0.2 to 2 m. Vegetation density was predicted using the Percentage Index *(PI)*, which relates vegetation point density to hydrodynamic vegetation density. The *PI* based on the threshold (R^2 = 0.51) and Gaussian (R^2 = 0.49) labeling method proved better estimators of vegetation density than the *PI* based on the inflection method (R^2 = 0.09). This might be caused by difference in reference heights between field and laser data. The validity range for vegetation density is in the order of 0.001 to 0.7 m^{-1}.

No increase in predictive quality is gained from point densities larger than 15 points m^{-2}. A lower point density might even be possible when larger areas of homogeneous vegetation are present in the study area. Because these herbs in winter are low and thin, the method is sensitive to the combined effect of flying height, gain setting and age of the laser diode. The common factor in these parameters is that they influence the amount of energy at the receiving end of the laser scanner. With increasing energy, the vegetation detection increases too.

We conclude that airborne laser scanning data can be used to map vegetation height and density of senescent floodplain vegetation for floodplain roughness parameterization. Field observations of vegetation structure remain, however, necessary to calibrate the regression models.

Acknowledgements

This work was funded by NWO, the Netherlands Organization for Scientific Research, within the framework of the LOICZ program under contract number 01427004. We would like to thank the Regional Directorate East Netherlands of the Dutch Ministry of Transport, Public Works and Water Management for the free use of all laser altimetry data. Ardis Bollweg and Regine Brügelmann of the AGI are gratefully acknowledged for timely notification of new laser scanning programs, which enabled simultaneous ground truth data collection. Chiel Kollaard and Andries Knotters are thanked for collecting field reference data of surface elevation and vegetation structure. Luc Amoureus of Fugro was very helpful in understanding the differences between the various datasets.

4 Quantitative mapping of hydrodynamic vegetation density of floodplain forests under leaf-off conditions using airborne laser scanning

in press: Straatsma, M.W. Quantitative mapping of hydrodynamic vegetation density of floodplain forests using airborne laser scanning. *Photogrammetric Engineering and Remote Sensing*.

Abstract

In this paper a method is presented to extract hydrodynamic vegetation density from airborne laser scanner data, relevant for exceedance levels of embankments of lowland areas. Two indices to predict vegetation density from the laser data were considered: (1) Percentage Index (*PI*) of points in the height interval inundated by the water, and (2) the Vegetation Area Index (*VAI*) that corrects for occlusion from the crown area. A computer simulation, using a digital forest model, showed a sensitivity of the indices for laser pulses that were sent out, but not detected by the laser receiver. The locations of these invalid points were therefore reconstructed. Two different assumptions were tested to assign new coordinates to all invalid points. Percentage Index, with the invalid points reconstructed by means of thresholding the point density ratio, proved the best predictor (R^2 = 0.66) of vegetation density of deciduous floodplain forests under winter condition.

Key words: airborne laser scanning, floodplains, hydrodynamic vegetation density, forest, simulation

4.1 Introduction

Hydrodynamic vegetation roughness, the retardance of water flow velocity by vegetation, is an important parameter to accurately model water levels and flow velocities of inundated floodplains (Darby 1999; Tsujimoto 1999; Stolker *et al.* 1999; Huthoff & Augustijn 2004). Forest is an important type of floodplain vegetation to be mapped accurately because its roughness is high and therefore strongly influences flood water levels. Moreover, forests grows in space and time in case of natural succession, and the density can change rapidly, especially in young forests (Den Ouden 1993). Various methods have been proposed to compute the roughness of forests.

Petryk & Bosmajian (1975) and Pasche (1984) consider the stems as rigid cylinders and define the hydrodynamic vegetation density and stem drag as the requisite parameters. The hydrodynamic vegetation density (D_v) is defined as the projected plant area (A) in the direction of the water flow (F) per volume of water in which the vegetation stands (Fig. 4.1). Under the assumption of cylindrical vegetation elements, vegetation density equals the product of number of stems per m^2 and average stem diameter (m^{-1}).

Flowing water also has a dynamic effect on the roughness as the vegetation trails downstream due to fast flowing water, thus streamlining the leaves and branches of the vegetation, which reduces the roughness (Kouwen & Fathi-Moghadam 2000; Copeland 2000). Additional parameters that describe these dynamic effects are the tree height, the modulus of elasticity and a parameter that describes all aspects of plant deformation as a result of increasing flow velocity. A roughness model that includes the latter parameters was proposed and tested by Kouwen & Fathi-Moghadam (2000) for coniferous trees. Vegetation parameters that describe the dynamic effects of bending or the drag coefficient seem unlikely to be extractable from remote sensing data, these parameters, therefore, need to be derived from laboratory or field studies. The relative importance of dynamic effects remains to be assessed for deciduous floodplain forest under leaf-off conditions. Klaassen *et al.* (1999), for example, found that bending of submerged vegetation of lowland floodplains under winter conditions did not significant lower the vegetation height. Many roughness models use rigid cylinders as vegetation elements for which vegetation density is an important parameter (Klopstra *et al.* 1997; Van Velzen *et al.* 2003; Mertens 1989; Baptist *et al.* in press; Schröder & Nuding 1986; Darby 1999; Helmiö 2002).

Information on spatial patterns of floodplain vegetation density is essential as input for hydrodynamic flow models based on rigid cylinders. Airborne and spaceborne remote sensing have become well-proven surveying techniques that provide primary information for vegetation classification over various scales (Mertes 2002). Satellite imagery was used to map floodplain

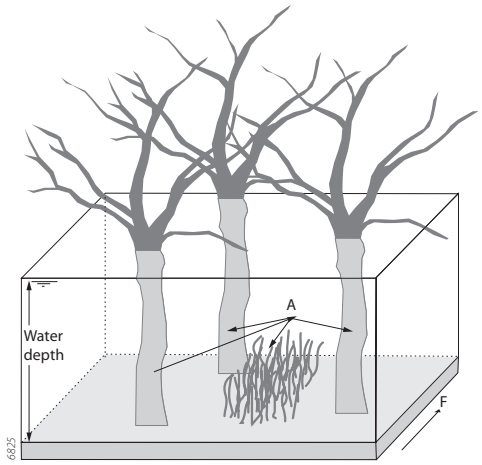

Figure 4.1 Sketch of hydrodynamic vegetation density (D_v); the projected plant area, A, in the direction of the flow, F per unit volume (m^{-1}).

vegetation at a regional scale (Ringrose *et al.* 1988; Mertes *et al.* 1995; Townsend & Walsh 2001; Van der Sande *et al.* 2003), while airborne multispectral images were used for kilometre-scale vegetation classification (e.g. Cusack *et al.* 1999). In the Netherlands, the Ministry of Public Works, Transport and Water Management maps vegetation density based on so-called floodplain ecotopes. Ecotopes are 'spatial landscape units that are homogeneous as to vegetation structure, succession stage and the main abiotic factors that are relevant to plant growth' (Leuven *et al.* 2002). Nevertheless, Ritzen and Straatsma (2002) showed differences in vegetation density of an order of magnitude within single ecotopes. Ecotopes are delineated by manual classification of false color aerial photographs using an interpretation key (Jansen and Backx, 1998). These classified images or ecotope maps can subsequently be converted to vegetation density maps using a lookup table. The disadvantage of lookup tables is that within-unit spatial variability in vegetation density is not considered.

Airborne laser scanning (ALS) has become a tool for the automatic extraction of various forest structural characteristics related to vegetation density: stem number, stem diameter, basal area and/or timber volume (Nilsson 1996; Næsset 1997b; Lefsky *et al.* 1999a, 1999b; Means *et al.* 1999; Næsset and Bjerknes 2001; Drake *et al.* 2002; Næsset 2002; Holmgren and Jonsson 2004). Asselman (2002) related vegetation density to canopy statistics, which does not consider undergrowth. Floodwaters will inundate the lower part of the floodplain forest. Airborne laser scanning, contrary to spectral remote sensing, is well able to penetrate into the forest canopy and detect the forest floor (Baltsavias 1999a), and is therefore also expected to directly supply information about the vegetation density above the forest floor. Recent attempts have been reported of floodplain roughness parameterization using vegetation heights from ALS data (Cobby *et al.* 2001, 2003 Mason *et al.* 2003; Hopkinson *et al.* 2005). They do not include vegetation density in their roughness model. Currently, no method is available to account for the within-unit variation of hydrodynamic vegetation density of floodplain forest. The objective of this study is to assess the predictive quality of ALS for the quantitative mapping of hydrodynamic vegetation density of deciduous lowland floodplain forest with undergrowth under leaf-off conditions in the height interval that can be inundated during peak discharge.

The study was carried out in three floodplain sections along the lower Rhine River during low flow. Field reference data of forest vegetation density were collected and compared to (1) the ecotope approach, (2) laser-derived parameters. Special attention was paid to dropouts: the laser pulses that were emitted, but whose reflection could not be detected.

4.2 Materials and methods

4.2.1 Study area

This study is based on laser data collected in three floodplain sections of the distributaries of the River Rhine in the Netherlands: 'Duursche Waarden' floodplain (DW) along the right bank of the River IJssel, and the 'Afferdensche en Deestsche Waarden' (ADW) and the 'Gamerensche Waarden' (GW) floodplains along the left bank of the River Waal (Fig. 4.2). In these floodplains, the Ministry of Public Works, Transport and Water Management has been taking measures to reduce flood levels and simultaneously restore the ecology by means of digging side channels and

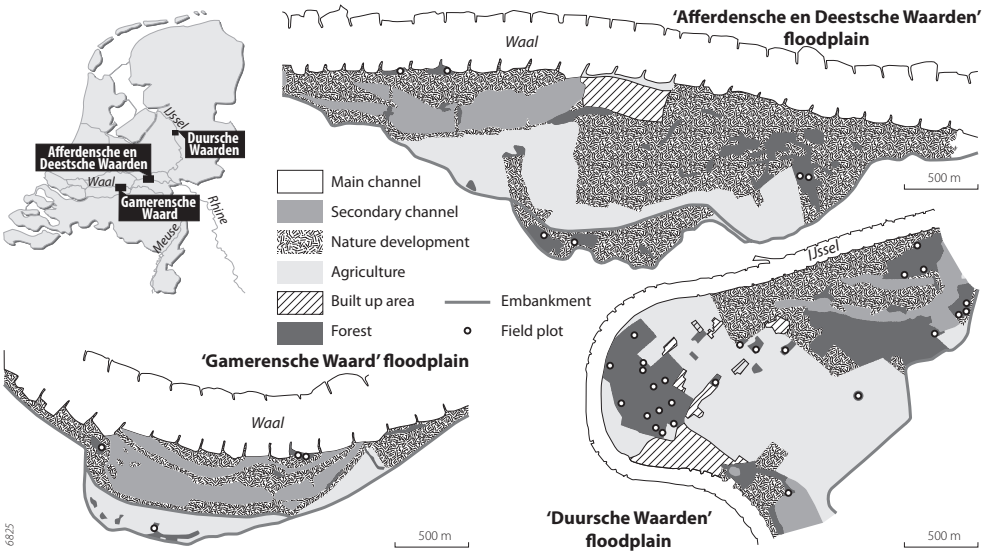

Figure 4.2 Location of the floodplains and the field plots

extensive grazing by cattle (Nienhuis & Leuven 2001; Van Stokkom *et al.* 2005). The ministry also acquired high-density laser data as monitoring pilots. All floodplains are of low slope with micro-topography. Elevation differences are less than 1 m, except for the Duursche Waarden floodplain that contains a few wind-blown ridges of approximately 4 m high. Land cover is a combination of arable land, meadows, open water and nature areas that partly consist of forests. Forests comprise softwood forest (willow, (*Salix alba, Salix viminalis*, poplar (*Populus nigra, Populus x canadensis*)) and hardwood forest (oak (*Quercus robur*), ash (*Fraxinus excelsior*)) in various stages of development, and a small mature pine stand (*Pinus sylvestris*). Forest coverage summed up to 22, 8 and 4 percent of the floodplain surface for the DW, ADW and GW floodplain respectively, according to the ecotope map. All vegetation was in winter condition when the laser data was acquired. The typical inundation depth of these forests is 3 m, but it might rise to 5 m in case of extreme flood events.

4.2.2 Data collection

Ecotope maps

Ecotope maps are available for the whole embanked floodplain area in the Netherlands. They are based on visual interpretation of aerial photographs of 1996, scale 1:5000 (Jansen & Backx, 1998). The smallest detected object was 40 by 40 m in the field, or 2 by 2 mm on the photo, hence any variability at smaller scales is excluded from the map. Each forest ecotope is subsequently labeled with a vegetation density value using a lookup table (Van Velzen *et al.* 2003), based on limited field inventories in the Dutch floodplains. This results in a choropleth map with vegetation density values for the vegetated parts of the floodplain.

Field measurements

Hydrodynamic vegetation density for forests (*Dv*) was measured in the field at breast height (1.5 m above the ground) simultaneously with the laser scanning survey. Visually, the vegetation density did not depend on the height of measurement between 1 and 2 m. Breast height was selected for ease of work. In total 36 plots were outlined in the field, distributed over the three floodplains. Plot size was at least 200 m^2 and varied according to tree size to ensure that at least 30 trees were inside the plot area. Georeferencing of the plots was done using a Garmin 12 handheld GPS system. In case the estimated point error (EPE), as given by the proprietary Garmin software, was more than 15 m the positioning was done using the ecotope map (1:5000). In each plot, the number of stems or shoots per m^2 (N) was counted that cross a virtual horizontal plane and the diameters of the stems were measured manually following (Brown 1971). The average diameter (d) was computed from 30 randomly selected stems, which included understory vegetation. Vegetation density (D_v) was then computed as the product of N and d. Table 4.1 shows a summary of the field data.

Airborne laser scanning data

The laser data were acquired using the FLI-MAP system mounted on a helicopter (Huising & Gomes Pereira 1998; Baltsavias 1999b). FLI-MAP, Fast Laser Imaging and Mapping Airborne Platform, is a small-footprint, first pulse, scanning laser range finder combined with a dGPS and an Inertial Navigation System for positioning. An overview of the laser scanning technique used is given by Wehr & Lohr (1999). Table 4.2 summarizes the characteristics of the two laser scanning campaigns and the locations are shown in figure 4.2. The laser data collected in 2001 in the 'Duursche Waarden' floodplain and the 'Afferdensche en Deestsche Waarden' floodplain was collected with a single, nadir looking laser scanner, which resulted in the DWADW dataset. Between 2001 and 2003, Fugro-Inpark added a second laser range finder to FLI-MAP, resulting in a doubling of the data collection rate and a re-orientation of the scanners. Instead of one nadir

Table 4.1 Summary of sample plot field data. Number of field plots was 36 with at least 30 trees per plot.

Characteristic	Range	Mean
N (m^{-2})	$2.1*10^{-2}$ – 20	0.048
d (m)	$1.1*10^{-2}$ – 0.46	0.11
D_v (m^{-1})	$6.2*10^{-3}$ – 0.24	0.049

N = Number of stems m^{-2}, d = diameter of stem at breast height (1.5 m), D_v = hydrodynamic vegetation density

Table 4.2 Metadata for the two laser scanning campaigns

Acquisition time	Floodplain location[a]	Scan angle	Scan line orientation	No. of sensors	Pulse rate	Flying height	Point density	Flight lines[b]
March 2001	DWADW	± 30°	Nadir	1	10 kHz	80 m	12 m^{-2}	Single
March 2003	GW	± 30°	± 7°	2	2*10 kHz	80 m	75 m^{-2}	Double

a. DW = Duursche Waarden, ADW = Afferden en Deestsche Waarden, GW = Gamerensche Waard
b. For the GW dataset, each flight line was flown two times to increase the point density.

looking scanner, the two scanners were facing 7° forward and backwards to decrease the number of occlusions in built-up areas. With the new FLI-MAP configuration the dataset was collected in the 'Gamerensche Waard' floodplain in 2003 (GW dataset). For this pilot study, each of the flight lines of the GW floodplain was flown twice, to increase the point density even further.

Usual FLI-MAP data products consist of the XYZ of the laser hits in a local coordinate system combined with the optional reflection intensity. Moreover, points are exported only if a significant return is detected by the receiver of the laser range finder. These points will be referred to as *valid* since their coordinates were computed using a valid range value. Points that were emitted, but did not give a significant return were included in the raw data set as well. The low reflection intensity could result from absorption or specular reflection at the object. Hardware causes for a low return include an old laser diode, or a wrong calibration of the focus of the laser receiver, which amplifies the return signal. According to the laser data vendor, the laser range finder is calibrated during each change of laser diode. Malcalibration of the receiver would lead to such a reduction in return intensity that it precludes laser surveying, whereas an aging diode would give a small overall reduction in intensity. No distinction between the two potential error sources could be made from the laser point cloud. A default range value of 300 m was assigned to the pulses without a valid range measurement. These points will be referred to as *invalid* points. Both valid and invalid points were included in the raw datasets. Point validity and time of firing of the laser pulse were added as attributes. In a separate file the positions of the laser scanner were given, which also had a time stamp. The two time stamps were used in subsequent data processing. Temporal frequency of the scanner position output was 50 Hz. Figure 4.3 shows the scanner positions, valid and invalid data of one flight strip.

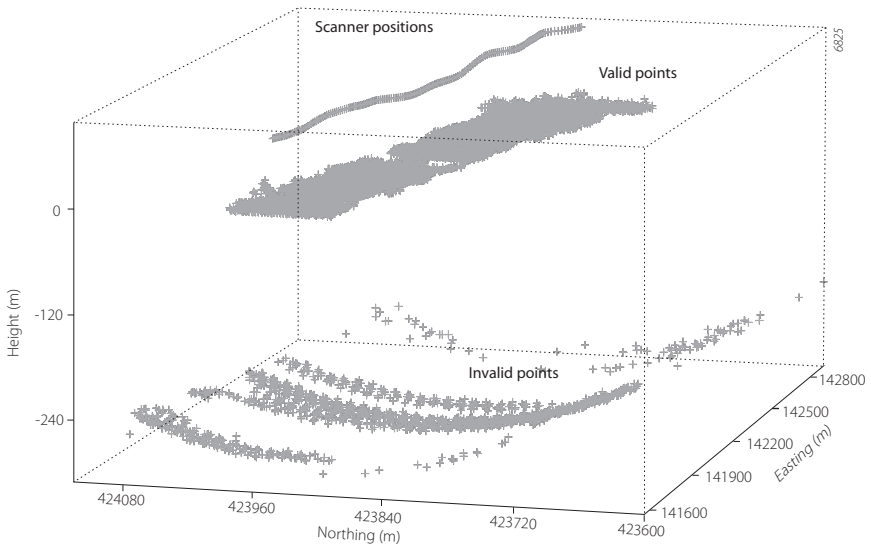

Figure 4.3 Example of the raw data consisting of (1) positions of the scanner, (2) valid points and (3) invalid points (not all points are plotted for visual clarity). All points have a time stamp used for the reconstruction of the path travelled by each pulse.

4.2.3 Indicators for vegetation density

Ecotopes and lookup table
To assess the predictive quality of the method based on ecotope maps, the ecotope type was taken from the ecotope map and the vegetation density was taken from the lookup table presented in (Van Velzen *et al.* 2003). The field reference data were compared to values from the lookup table. The predictive quality of the ecotope approach served as a reference for vegetation density prediction derived from airborne laser scanning.

Laser-derived parameters

DTM processing
Before vegetation indices could be computed, the effect of the topography had to be eliminated by creating a Digital Terrain Model (DTM) for each plot. The first step in the laser data processing was the selection of the points located within the plots laid out in the field. Other laser points were not taken into account for this study. A DTM was constructed using iterative residual analyses based on a simplified version of the method of Kraus and Pfeifer (1998). In each step, a surface was computed as the local average in a moving window. The window radius was 2 m, a larger window would lead to a loss of detail and a smaller window would lead to an erroneous DTM, as in some cases no ground points occurred within the window. The residual distance to this surface was computed for each point. Points with positive residuals are likely to be vegetation points. The range of values for an unvegetated, flat surface was computed and proved approximately 15 cm above and below average, comparable to Davenport *et al.* (2000). Therefore, points with a residual value of more than 15 cm were excluded from further analyses in the DTM processing. With the remaining points, iterations were continued until residuals were less than 15 cm. Heights relative to the DTM were used in subsequent computations.

Percentage Index
Vegetation density was predicted from ALS data by two indices. The percentage index (*PI*) computes the percentage of laser hits that fall within the height range ($h1$ to $h2$) that could be inundated by the water:

$$PI_{h1-h2} = \frac{1}{h2 - h1} \cdot \frac{N_{h1-h2}}{N_{tot}} \tag{4.1}$$

in which N_{h1-h2} is the number of points between height 1 and 2 above the forest floor, N_{tot} is the total number of points in the field plot including canopy and ground surface points. The height interval for *PI* was set to 0.5 to 2.5 m, the region around breast height where the vegetation density was measured in the field, to optimize the representativeness of the laser data. The distance between $h1$ and $h2$ should not be too small, otherwise too few points would be present within the height interval of interest. Moreover, $h1$ was set to 0.5 m to remain well above the noise height of the ground surface points. This method does not take occlusion from the crown area into account. Tree crowns reflect part of the laser pulses, thereby reducing the number of points available for detection of stems or the ground surface. However, the crown density is small (25 percent) under leaf-off conditions.

Vegetation Area Index

The Vegetation Area Index (*VAI*) method, introduced by MacArthur & Horn (1969), compensates for occlusion. Later, it was verified by Aber (1979). This method calculates a Leaf Area Index for specific height increments, in a similar way as the extinction of light in a semi-transparent medium. Recently, Lefsky *et al*. (1999a) successfully modified the MacArthur-Horn method to generate canopy height profiles. Canopy height profiles not only include foliage, but also woody vegetation. The forests considered in the present study were all leafless. The assumption was made that the mechanism of occlusion from trees in leaf-off condition is similarly to occlusion from trees in leaf-on conditions. Laser hits are in this case intercepted by branches instead of leafs. The resulting value is therefore not a *Leaf* Area Index, but a woody *Vegetation* Area Index (*VAI*). Like *PI*, the *VAI* is computed only over the height interval that is inundated by the water using the following equation:

$$VAI_{h1-h2} = \frac{1}{h2 - h1} \cdot \ln\left(\frac{N_{h2}}{N_{h1}}\right) \tag{4.2}$$

in which N_{h1} and N_{h2} are the number of points below heights $h1$ and $h2$ ($h2 > h1$), which includes ground points. The first term in the formula is introduced to make the *VAI* independent of the height interval. However four assumptions underlie this method: (1) all laser pulses enter the forest with an equal incidence angle, (2) no clumping is present, which means that the horizontal distribution of vegetation elements is random (Jonckheere *et al*. 2004), (3) all vegetation elements have an equal angle with a horizontal plain and (4) all elements have an equal probability of detection, which means an equal reflectivity. Strictly speaking, none of these assumptions is fulfilled in the case of floodplain forest and airborne laser scanning observation.

4.2.4 Simulation experiments

To analyze the effects of different laser settings and vegetation densities on *PI* and *VAI*, a computer simulation was carried out using a simplified forest-canopy scheme. The forest scheme consisted of a digital forest model and a ground surface. Trees had a stratified random spatial arrangement and were represented as a beam-shaped stem and a disc-shaped horizontal crown. A full 3D tree-branch model was outside the scope of this study. The crown was simplified to a simple disc since it is above the inundation height. To mimic the occlusion of real a floodplain forest in winter (25 % at 15 m), the crown radius was set to 1.25 m at a tree spacing of 5 m. The crowns were not transparent, which comes close to first pulse characteristics since only 25 percent of the pulses are occluded by the canopy. Tree height was set to 15 m. The ground surface was horizontal. The laser pulse configuration was based on laser scanning settings similar to FLI-MAP; flying height was set to 80 m and the lateral scan angle to ± 30°. The point density was variable. The simulation computes the coordinates of intersection between the 'trees' and simulated laser pulses (Fig. 4.4).

For each simulation, the vegetation density was computed from the stem spacing and thickness. *PI* and *VAI* were computed from the resulting point cloud. The following effects were evaluated quantitatively:

- The relation between vegetation density and *PI* and *VAI*. Using one laser point per m^2, vegetation density was varied stepwise between 0.003 to 0.2 m^{-1}.

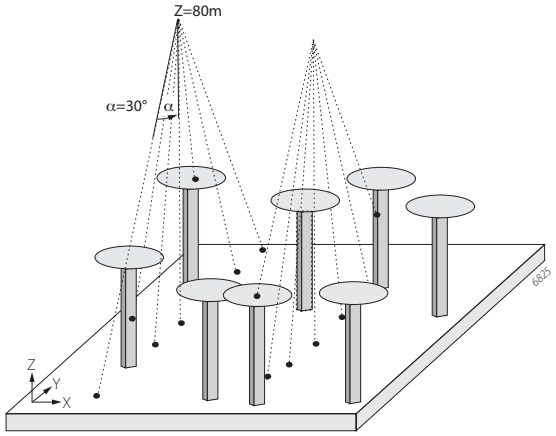

Figure 4.4 Layout of the simplified forest canopy scheme and laser settings used in the simulation.

- The minimum number of laser points needed in the *VAI* interval (0.5-2.5 m) for a robust *VAI* estimation. Due to the random effect in the tree distribution, the resulting *PI* and *VAI* values varied between individual simulations for the same forest setting. Therefore, a suite of simulations was carried out in which point densities were decreased stepwise from 4 points per m^2 to 1 point per 400 m^2. For each point density 30 simulations were run, which enabled the computation of the coefficient of variation as a function of number of points in the height interval h1 to h2.
- The effect of the number of ground points on the *VAI* and *PI* value, allowing to determine the effect of loss of returns from the ground surface.
- The effect of increasing the incidence angle on *VAI* and *PI*.

The incidence angle of the pulse, the angle between nadir and the firing direction, varies over the width of the scan strip. At nadir, a laser pulse will never hit a vertical stem, while along the edges, the probability of hitting a stem proportionally increases due to the longer trajectory through the vegetation and the larger angle between the stem and the laser pulse, which also resulted from a simluation by Holmgren *et al.* (2003b) for canopies. Contrary to the true scan pattern where the scan angle varied over the width of the scan strip, laser pulse in these simulations were generated with equal incidence angles over the whole plot. The incidence angle was, therefore, varied stepwise from 0 to 40° with 2° increments. The upper limit of 40° represents the combination of the scan line orientation (± 7°), scan direction (± 30°), and movement of the helicopter.

4.2.5 PI and VAI computation using invalid points

Both *PI* and *VAI* relate the density of laser points in the inundation height to vegetation density, and assume equal probability of detection for vegetation and ground surface. However, of up to 53 percent of the emitted laser pulses was not detected by the laser receiver due to; (1) low reflectance of the ground surface combined with (2) mirroring away of the laser energy at large scan angles, (3) trapping of the reflected pulse in the tree crown, (4) old laser diode, or

(5) malcalibration of the laser receiver. In some cases large numbers of pulses got absorbed by the ground surface. For example, the spatial distribution of valid ground points showed a stripy pattern in one of the field plots, related to the presence of ditches. The loss of returns could influence *PI* as it affects the number of points within the inundation height or the total number of points ($N_{h1\text{-}h2}$, and N_{tot}; eq. 1), and influences *VAI* through the number of points below height 1 and height 2 (N_{h1}, and N_{h2}; eq. 2). Given the large number of invalid returns, they needed to be incorporated in the computation of *PI* and *VAI*, which consisted of three steps for each plot.

The first step consisted of selecting those invalid points that were absorbed inside the plot areas. To that end, points were converted to ground height. For each plot, all invalid points were selected within a buffer around the boundaries of the field plot. Figure 5a illustrates this with a view in the flight direction. The width for the buffer is determined by the flying height and the scan angle, and was set to 150 m outside the plan-view boundaries of the plot. The timestamps were used to locate the scanner position for each invalid point. The scanner position and the point position give two points of the path that the pulse would have traveled in the absence of a ground surface. To determine whether a pulse indeed passed through the plot, its XY coordinates at the height of the ground surface were determined. The surface elevation of the valid point that is closest *in time* with the invalid point was used as the Z coordinate for each invalid point (Fig. 4.5b). The XY coordinates of the invalid points were found by intersecting the line between point and scanner position with a plane at height Z. As a result, the new position of the invalid points is located on the line that the laser pulse has traveled. Only points whose reconstructed XY values were inside the plot boundary were used in further analyses.

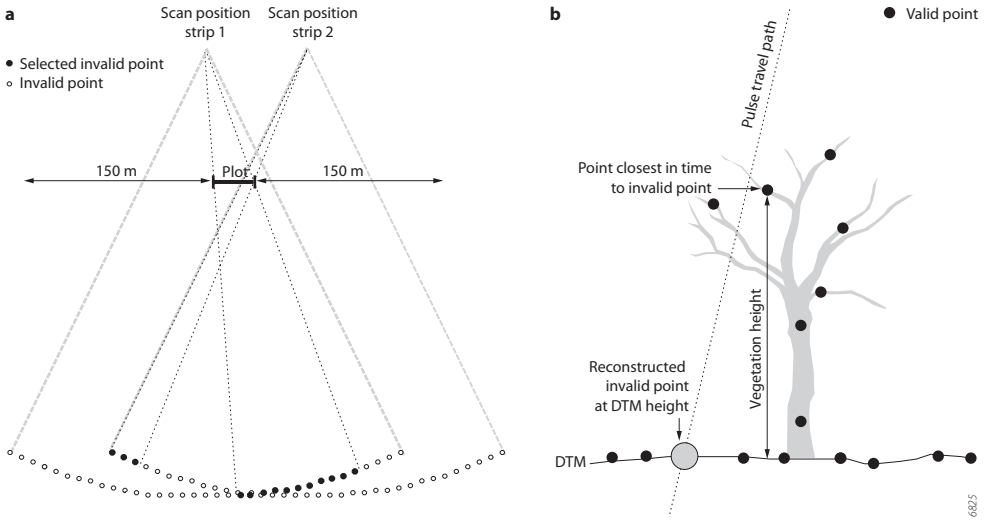

Figure 4.5 Example of the selection and reconstruction of invalid laser points. a) Invalid data points of two different flight strips are visible as concave up slabs of points. Filled black dots (•) were selected. b) The result of the reconstruction of the selected invalid points to the ground surface level, indicated by the large grey circle.

The second step consisted of determining which points were absorbed at the ground surface. Two assumptions were tested. The first assumed that the ground surface absorbed the energy of all invalid points. In this case, XYZ coordinates of the invalid point were assigned using the same method as in the previous step. Figure 4.5b shows the location of the reconstructed point using assumption 1. Visual inspection showed that in a few plots a spatial pattern existed due to the presence of water, for example in ditches or lower areas of the plot. In other plots however, such a pattern was neither visible in the data, nor in the field. The second assumption, therefore, was that the energy got absorbed in the vegetation layer or at the ground surface. To make the distinction between points that got lost by absorption on the ground or within the vegetation layer, the Point Density Ratio (*PDR*) was defined:

$$PDR = \frac{Nlocal_{invalid}}{Nlocal_{valid}} \tag{4.3}$$

where $Nlocal_{invalid}$ are the local point densities of the invalid points reconstructed to the ground level. $Nlocal_{valid}$ refers to the local point densities of all valid points. Both were computed in a local neighborhood using a moving window with a 0.5 m radius to maintain spatial detail in point density differences. When the *PDR* is high, relatively many points in a local neighborhood were absorbed, indicating that a low reflective ground surface was present, which is likely due to water on the ground surface. Points with a higher ratio were therefore assumed absorbed on the ground. Conversely, points with a low *PDR* do not have a specific height of absorption. A range of *PDR* values was tested as a threshold and a *PDR* of 0.7 gave the best prediction results. Invalid points with a *PDR* higher than 0.7 were selected, and their height set to the DTM height of the temporal most proximal point. Invalid points with a *PDR* less than 0.7 were excluded from further analyses.

In the final step, *PI* and *VAI* values were computed for the three different point distributions: (1) valid points only (PI_{valid}, VAI_{valid}), (2) valid points plus all invalid points reconstructed to the ground surface ($PI_{inv.grd}$, $VAI_{inv.grd}$), (3) valid points plus invalid points set to ground level in case the point density ratio was more than 0.7 ($PI_{inv.PDR}$, $VAI_{inv.PDR}$).

4.2.6 Incidence angle and reflection intensity

The time stamp on the scanner positions and the point position facilitated the computation of the incidence angle (α) for each point. The incidence angle was computed by:

$$\alpha = \arccos\left(\frac{\sqrt{(dz)^2}}{\sqrt{(dx)^2 + (dy)^2 + (dz)^2}}\right) \tag{4.4}$$

where *dx, dy* and *dz* are the differences in *X, Y* and *Z* coordinates between scanner and point position in the raw data. The average incidence angle per plot was computed for the hits between *h*1 and *h*2. Additionally, the reflection intensity as registered by the laser scanner was averaged for the valid points between *h*1 and *h*2.

4.3 Vegetation density prediction

4.3.1 Estimates for all field plots

The field data have a likely error of up to 15 percent due to the representativeness of the stem diameter and the number of stems. The error varies with the density and regularity of the understory vegetation. Figure 4.6 shows the scatter plots between the 36 observed vegetation densities (*Dv*) in the field and (1) ecotope approach prediction of *Dv*, (2) the percentage index (*PI*) of laser points in the inundation height and (3) the Vegetation Area Index. Regression analyses showed that all methods explain only a small part of the variance in vegetation density as measured in the field. The ecotope prediction shows four classes. The vertical range per cluster indicates the range of vegetation densities that occur within each ecotope type. *PI* and *VAI* show a linear relation close to the origin, but large outliers are present that underestimate or overestimate vegetation density. The ecotope approach (R^2 = 0.34, residual standard error RSE = 0.040) performs equally well as the *PI* (R^2 = 0.35, RSE = 0.040), but better than the *VAI* (R^2 = 0.15, RSE = 0.046).

4.3.2 Simulation results

The simulation provided insight in the sensitivity of the vegetation density indices to the four effects mentioned in section 2.4. Figure 4.7a shows that *PI* increases from 0 up to vegetation densities of 0.06 m^{-1} and then decreases. *VAI* increases linearly with D_v, over the range of vegetation densities from 0.003 to 0.2 m^{-1}. For vegetation densities up to 0.04 m^{-1}, the curves for *PI* and *VAI* are similar.

The influence of the number of points in the height interval ($N_{b1\text{-}b2}$) on the determination of *VAI* is shown in figure 4.7b. The error bars indicate the standard deviation of the *VAI* of the 30 simulations. With increasing number of points, the standard deviation and coefficient of variation decrease as expected. A coefficient of variation (CV) of 0.15 was arbitrarily selected as a minimum acceptable level, which relates to 50 points for $N_{b1\text{-}b2}$. If the percentage of non-detected ground hits increases, both *PI* and *VAI* become higher (Fig. 4.7c). This implies that if ground returns remain undetected, *VAI* and *PI* will be overestimated, (eq. 1, 2). *VAI* is more sensitive to a loss of ground returns, indicated by the steeper slope of *VAI*. Figure 4.7d shows the dependence

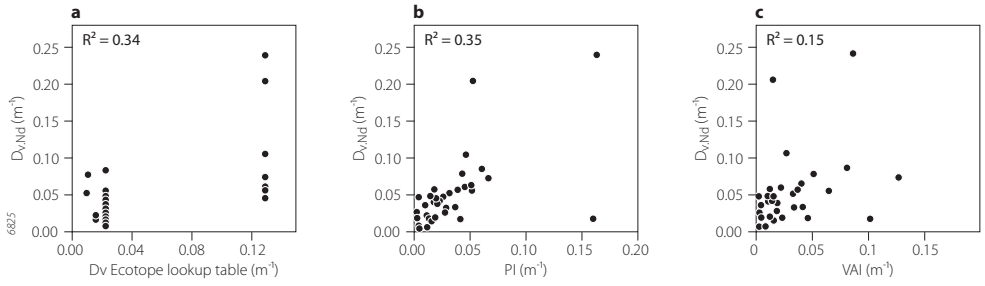

Figure 4.6 Scatter plots of vegetation density values based on a) ecotopes, b) *PI* and c) *VAI* against field reference data for all plots. All three methods explain little of the variance of vegetation densities as measured in the field.

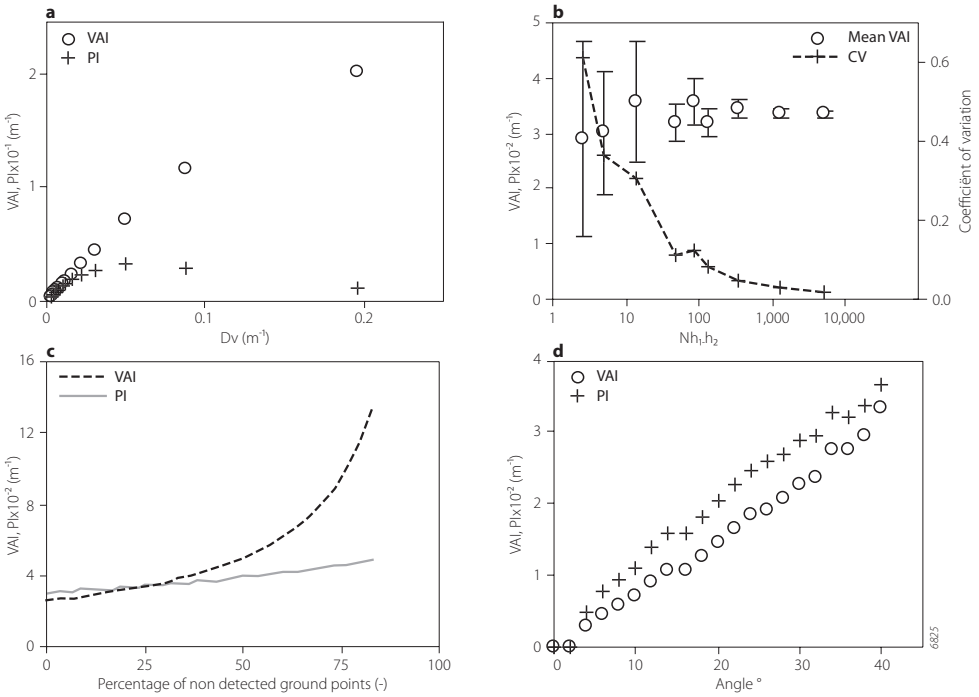

Figure 4.7 Values obtained for *VAI* and *PI* from the simulation, which shows the dependance on a) varying D_v, b) number of points in the inundation height resulting from the varying point density, c) percentage of non detected ground points and d) incidence angles.

of the *PI* and *VAI* on incidence angle. At a vegetation density representative for a normal forest (D_v = 0.022 m^{-1}), *PI* and *VAI* both increase linearly over the 0-40° range. Similar results were found using other vegetation densities.

The simulation showed that large errors can be introduced in the estimation of *PI* and *VAI* due to (1) a low number of vegetation hits in the height range between *h*1 and *h*2, and (2) when a large number of ground points are not detected. These effects have to be taken into account when *PI* or *VAI* are used to predict the hydrodynamic vegetation density.

4.3.3 Estimates for selected plots

Based on the simulation results (Fig. 4.7b), only those plots that included more than 50 points in the inundation height range were considered, which corresponds to a coefficient of variation of 0.15. Twenty-two plots satisfied the above condition. For this subset, the ecotope approach performed slightly worse than for all plots (R^2 = 0.28, RSE = 0.024; table 3). Figure 4.8a shows a 3D scatter plot of a point distribution in case all invalid points are assigned a ground surface height. The stripy pattern of invalid points is related to the presence of ditches in this plot. The number of selected invalid points has a large influence on the vertical point distribution (Fig. 4.8b).

Scatter plots of the relation between field values of vegetation density against *PI* and *VAI* are shown in figure 9. The two left panels show PI_{valid} and VAI_{valid}, based on valid points only. The middle two panels show the results in case all invalid points are assigned a ground height ($PI_{inv.grd}$, $VAI_{inv.grd}$). $PI_{inv.grd}$ and $VAI_{inv.grd}$ estimates are lower than PI_{valid} and VAI_{valid}, most notably for the DWADW plots. The two panels on the right show *PI* and *VAI* under the assumption that only invalid points with a *PDR* larger then 0.7 are ground points ($PI_{inv.PDR}$ and $VAI_{inv.PDR}$). *PI* proved a better predictor of vegetation density than *VAI* even though the index does not correct for occlusion from the canopy. This was the case both before and after the correction using invalid points. Explained variance of *PI* varied between 0.55 to 0.66 when corrections for missed ground points were made compared to 0.27 and 0.36 for *VAI* (table 3). Multiple regression models, using the average incidence angle per plot or intensity as additional parameters did not improve prediction.

Intensity values for the points in the inundation height ranged from 26 to 46 on a 0 to 255 scale for the DWADW dataset and between 71 and 104 for the GW dataset. The difference in intensity

Table 4.3 Regression results for vegetation density prediction

Regression equation (N = 22)	**R^2**	**RSE[a]**
$D_v = 0.27 \cdot Dvecotopes + 0.029$	0.28	0.024
$D_v = 1.18 \cdot PI_{valid} + 0.008$	0.58	0.019
$D_v = 1.33 \cdot PI_{inv.grd} + 0.01$	0.59	0.018
$D_v = 1.36 \cdot PI_{inv.PDR} + 0.008$	0.66	0.016
$D_v = 0.53 \cdot VAI_{valid} + 0.03$	0.33	0.023
$D_v = 0.48 \cdot VAI_{inv.grd} + 0.03$	0.27	0.022
$D_v = 0.56 \cdot VAI_{inv.PDR} + 0.03$	0.36	0.022

a. RSE = Residual standard error (m^{-1})

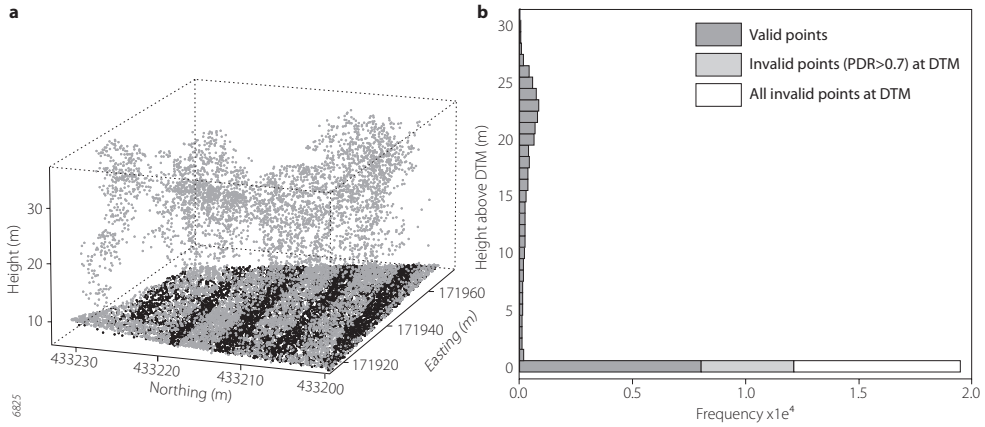

Figure 4.8 a) Spatial pattern of invalid data points reconstructed to ground level due to ditches. The black dots refer to invalid points, the light grey dots to valid points, b) Histogram of vertical point distribution relative to the DTM. The distribution of all invalid points and invalid points with PDR > 0.7 show up as higher frequencies at DTM height.

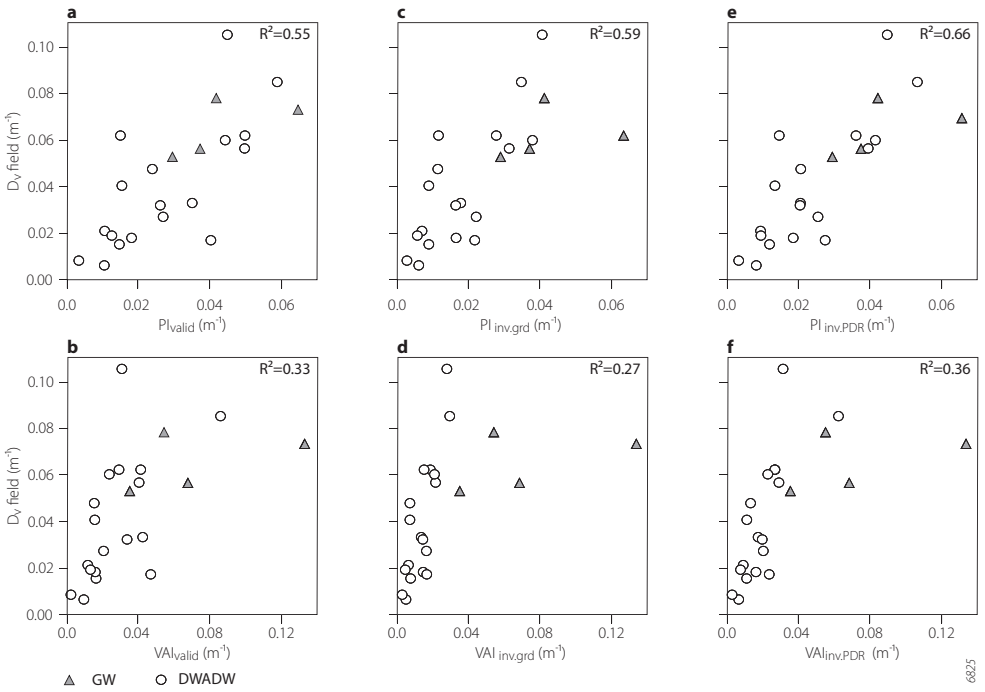

Figure 4.9 Prediction of vegetation density by *PI* and *VAI*. ▲ = DWADW dataset, ○= GW dataset. PI_{valid} and VAI_{valid} are based on valid points only. For $PI_{inv.grd}$ and $VAI_{inv.grd}$ it was assumed that invalid points were lost on the ground surface. For $PI_{inv.PDR}$ and $VAI_{inv.PDR}$ points could have been absorbed at the ground depending on their point density ratio.

values between the two datasets is significant at the 99 percent confidence level. No significant difference in means existed between the average incidence angles between the two datasets. The percentage of invalid points also differs significantly between the two datasets. The number of invalid points varied between 9 and 53 percent for the DWADW dataset and between 0.01 and 1.1 percent for the GW dataset. It is unlikely that this results from the upgrade of the FLIMAP system between 2001 and 2003, because both systems were regularly calibrated. Partly, the difference results from the presence of water on the ground in the DWADW floodplains, either in the form of puddles, or ditches. However, even dry plots showed a minimum of 9 percent invalid data points. The plots in the Gamerensche Waard floodplain (GW) were all dry at the time of laser data acquisition. The large number of invalid points in the DWADW plots explains the sensitivity of these plots to the different estimates of *PI* and *VAI* (Fig. 4.9).

4.4 Discussion

In this paper, field reference data are compared to three vegetation density mapping methods: ecotopes, *PI* and *VAI*. Hydrodynamic vegetation density, as considered in this study, is a

parameter that describes the horizontal obstruction of the vegetation for flowing water, whereas laser point height distribution is a function of detectability in the direction of the laser pulses, which is primarily vertical. With all plots included, straightforward application of the equations for Percentage Index and the Vegetation Area Index (eq. 4.1 and 4.2) to the laser data yielded no improvement over the traditional method based on ecotope mapping, which does not take variability within ecotopes into account. Compared to other laser scanning studies, these results explain little of the field variance as other papers report explained variances between 42 and 96 percent (Nilsson 1996; Næsset 1997b; Means *et al*. 1999; Lefsky *et al*. 1999a; Lefsky *et al*. 1999b; Næsset and Bjerknes, 2001; Næsset, 2002; Drake *et al*., 2002; Asselman, 2002).

The first reason for the low predictive quality of the initial regression models was that the minimum number of points in the interval between $h1$ and $h2$ was not reached for many field plots. Therefore, the simulation was used to decide upon the minimum number of points needed, which appeared to be 50. This improved the results of the laser-derived methods significantly (R^2 was 0.55 for PI_{valid} and 0.33 for VAI_{valid} based on valid points only). The reason for so few laser hits in the inundation height interval can result from a very dense crown layer, from absorption of laser energy by the vegetation, combined with a too small plot size.

The second problem that resulted in low predictive quality was the loss of returns. Lefsky *et al*. (1999a) also addressed the issue of different reflectivity between ground and vegetation surfaces, and simply compensated by multiplying the ground return by two. However, this does not spatial variability in reflectivity into account. Many more invalid points were present in the DWADW dataset than in the GW dataset. The reorientation of the scanner between 2001 and 2003 led to a larger chance of mirroring away of laser energy on a horizontal target as higher incidence angles result from the reorientation. Therefore, it can not be the cause of the lower number of invalid points for the GW dataset. An indication for this difference can be found in the differences in reflection intensities between the two datasets, which also was significantly higher for GW. This indicates that more energy was available due to a newer laser, which improves detection of the returned laser pulse. Reconstructing the position of the invalid points showed unexpected results. The first assumption was that all points got absorbed at the ground surface (Fig. 4.8a and 4.9c, d). However, by assigning the ground height to the invalid point, the reference plots from the GW data set show up as large outliers in the scatter plot ($VAI_{inv.grd}$ in figure 9d, R^2 = 0.27). Due to the large number of invalid points, the *VAI* values for DWADW were underestimated when compared to plots in the GW floodplain with few invalid points. This indicates that absorption of the laser energy indeed did not occur at the ground surface only. The second assumption was, therefore, that only points with a high point density ratio were absorbed at the ground surface while the other points were excluded from the analysis. This results in higher *VAI* values ($VAI_{inv.PDR}$ in figure 4.9f, R^2 = 0.36) as fewer points are assigned to the ground surface. However, the GW plots still shows up as outliers in the scatter plot, reducing the overall explained variance. The Percentage Index, after reassigning coordinates of the invalid points using the point density ratio, appeared the better predictor of hydrodynamic vegetation density (R^2 = 0.66, figure 4.9e), which is valid for deciduous forests with understory under leaf-off conditions. Although this parameter does not take occlusion from the crown area into account, it is less sensitive to the uncertainty in the number of ground points (Fig. 4.7c), resulting in the best overall prediction. Compared to the ecotope approach this is a major improvement as the residual standard error

(RSE) drops by 33 percent. Portability of the method remains to be assessed, but the relation will not hold for forests with a closed canopy, such as pine, as the *PI* does not take occlusion into account. Shrubs have a higher detectability for laser pulses as their stems grow more horizontally, and the established relation will probably overestimate shrub density.

A third source of unexplained variance is the positional error of the field reference plots, resulting from the use of a handheld GPS, with manual correction made using the 1:5000 ecotope map. The forests showed spatial variation in vegetation density, and the field reference density might therefore refer to an area that not fully overlaps with laser-derived *VAI*. A final source of error refers to the assumption of cylindrical vegetation elements of the forest, and that field measurements are taken at breast height, whereas the laser data represents the interval between 0.5 and 2.5 m above the forest floor. More accurate field measurements could be made using photographic techniques (e.g. Zehm *et al.* 2003; Jonckheere *et al.* 2004)

The simulation study showed that the incidence angle potentially has a large effect on both *PI* and *VAI* (Fig. 4.7b). The effect on *PI* and *VAI* of the field plots is potentially large because the size of the field plots was around 20 by 20 m. Therefore, the plots were too small to cover the full width of a scan strip, limiting the range of incidence angles within a single plot. (Holmgren *et al.* 2003b) found in their simulation study that scan angle had a significant effect on laser quantile heights of the canopy of pine and spruce forests. A larger effect was found in forests with a low tree density. The effect of the incidence angle, however, was not confirmed by the field data in this study. Plot-averaged incidence angles varied between 10 and 23°, but adding the incidence angle as a predictor to the multiple regressions did not significantly improve the results. This could be solved by constructing a more realistic model of leafless trees (e.g. Kay and Kajiya, 1986). To make airborne laser scanners more suitable for vegetation density mapping the laser scanner hardware and software should focus on improved detection of vertical stems. Scan angles should therefore be increased by tilting the laser scanner to a more oblique direction, while remaining within the maximum range of the scanner (Skaloud *et al.* 2005). Additionally, waveform digitizing laser scanning might solve the problem of detecting low energy returns from forests, since it does not use a threshold (Wagner *et al.* 2004).

4.5 Conclusions

This paper describes the extraction of hydrodynamic vegetation density from airborne laser scanning data, which can be used for hydrodynamic models that assume rigid vegetation. Two different models to predict vegetation density were tested and compared to the traditional approach, in which manually delineated plots are labeled using a lookup table: (1) Percentage Index (*PI*), which considers the relative number of points in the inundation height interval and (2) the Vegetation Area Index (*VAI*) based on the method of MacArthur and Horn (1969). Both predictors have the advantage that they consider the interval inundated by the water during peak discharges of the river, contrary to any spectral remote sensing method. Both methods relate the vertical point distribution of the laser point cloud to hydrodynamic vegetation density. A minimum of 50 laser points should be included in the laser-estimate to avoid large errors from random sampling of trees. In a novel approach, the emitted laser pulses that did not generate

a significant return were included in the data processing as well. Assessment of the number of invalid points is an important check for any laser-based regression model that uses percentiles, as percentile height will shift with the number of invalid points. Subsequent reconstruction of the location where the energy got absorbed enabled the incorporation of these points into the computation of *PI* and *VAI*. The Percentage Index, with the invalid points reconstructed by means of thresholding the point density ratio, is the best predictor (R^2 = 0.66, RSE = 0.018 m^{-1}) of vegetation density of deciduous floodplain forests including undergrowth under winter condition. This relationship is not valid for pine forests and shrubs. The Percentage Index is an improvement over the current ecotope approach (R^2 =0.28, RSE = 0.024 m^{-1}). Moreover, this method can be applied to map 2D spatial patterns in vegetation density within floodplain forest, which includes an estimate of the prediction error. Both were previously unavailable.

Computer simulation of *VAI* and *PI* based on synthetic data showed that:
- *VAI* increases linearly with vegetation density while *PI* initially increases and then decreases with increasing vegetation density;
- A minimum number of 50 points in the height interval under considerations per estimate is needed for accurate computation of *PI* and *VAI*;
- *PI* and *VAI* increase with higher incidence angles of the laser pulses;
- *VAI* has a stronger dependence on non-returned ground points than *PI*.

To improve vegetation density mapping using airborne laser scanning, the recommendation is to:
- Increase the size of forest field plots for dense canopies to meet the requirement of a minimum number of points in the height interval of interest;
- Use field methods that have a larger physical sampling size and do not need the assumption of cylindrical vegetation;
- Increase the energy of the laser scanner to as much as is legally allowed to limit loss of laser hits on vegetation;
- Change the viewing angle of one of the laser scanners to the maximum forward direction, for example 45°, to increase the detection of vertical stems;
- Investigate in last instance the relation between vegetation density and other parameters such as laser-derived vegetation height, or individual trees, which will have to solve the problem of relating tree crown properties to the vegetation density in the inundation height.

Acknowledgements

This work was funded by NWO, the Netherlands Organization for Scientific Research, within the framework of the LOICZ program under contract number 01427004. I thank the AGI, the Advisory Board on Geo-informatics and ICT of the Dutch Ministry of Transport, Public Works and Water Management for providing the laser scanner datasets. Luc Amoureus of Fugro-Inpark is "in the name of science" gratefully acknowledged for exporting the laser scan data again in its final raw data form.

5 Floodplain roughness parameterization using airborne laser scanning and spectral remote sensing

M.W. Straatsma[a] & M.J. Baptist[b]

resubmitted to *Remote Sensing of Environment*

a Utrecht University, Faculty of Geosciences, Department of Physical Geography, PO Box 80115, 3508 TC, Utrecht, the Netherlands.
b Delft University of Technology, now at IMARES-Texel, PO box 167, 1790 AD, Den Burg, the Netherlands, martin.baptist@wur.nl

Abstract

Floodplain roughness parameterization is one of the key elements of hydrodynamic modeling of river flow, which is directly linked to exceedance levels of the embankments of lowland fluvial areas. The present way of roughness mapping is rather laborious; floodplain vegetation types are schematized as cylindrical elements of which the height (m) and the vertical density (the projected plant area in the direction of the flow per unit volume, m^{-1}) have to measured. This paper presents a novel method that can be used as an automated roughness parameterization. It delivers a spatially distributed roughness parameterization in an entire floodplain by fusion of CASI multispectral data with airborne laser scanning (ALS) data. The method consists of three stages: (1) pre-processing of the raw data, (2) image segmentation of the fused dataset and classification into the dominant land cover classes (KHAT = 0.77), (3) determination of hydrodynamic roughness characteristics for each land cover class separately. In stage three, a lookup table provides numerical values that enable roughness calculation for the classes water, sand, paved area, meadows and built-up area. For forest and herbaceous vegetation, ALS data enables spatially detailed analysis of vegetation height and density. The vertical vegetation density of forest is mapped using a calibrated regression model. Herbaceous vegetation cover is further subdivided in single trees and non-woody vegetation. Single trees were delineated using a novel iterative cluster merging method, and their height is predicted with an R^2 of 0.41. The vegetation density of single trees was determined in an identical way as for forest. Vegetation height and density of non-woody herbaceous vegetation were determined using calibrated regression models. A 2D hydrodynamic model was applied with the results of this novel method, and compared with a traditional roughness parameterization approach. The modeling results showed that the

new method is well able to provide accurate output data, it provides an easier way of obtaining floodplain roughness and it yields a high spatial detail.

Keywords: data fusion, multispectral data, ALS data, object-oriented classification, tree detection, floodplain vegetation, hydrodynamic modeling

5.1 Introduction

Over the last decade, flooding has become a large environmental hazard with significant economic damage and human suffering. Examples of flooding catastrophes are the Mississippi flood in 1993, the Oder flood in 1997 and the Elbe and Danube flood in August 2002 and April 2006. Understanding flood events and predicting flood prone areas and potential damage have become important issues in river management. In this context, hydrodynamic modeling is a tool, not only to compute water levels for unprecedented discharges to assess the design levels for embankments, but also to assess the possible effects of future climate change and ecological river restoration measures on flood water levels. Therefore, considerable effort has been undertaken in recent years in the development of 2D and 3D hydrodynamic models that accurately simulate overbank flow patterns and predict extreme flood water levels in rivers and floodplains (Bates *et al.* 1992; Stoesser *et al.* 2003; Nicholas & McLelland 2004; Baptist *et al.* 2005). In addition to surface topography (Marks & Bates 2000), hydrodynamic roughness of the floodplain surface is the key input parameter of these models. It is common practice to calibrate hydrodynamic models by tuning the hydraulic roughness until model predictions fit observations. This method is suspect, as shortcomings in the model scheme, computation method or model input can be compensated using roughness values that are physically not representative. Therefore, accurate estimates of roughness input parameters help to constrain the range of input parameters that should be allowed during calibration of such models. This is especially important as these models are routinely used to compute water levels for the design of embankments with discharges far exceeding the range of observed data.

Hydrodynamic roughness of the non-vegetated river bed is a function of grain size and bed form (Van Rijn 1994). Vegetation roughness is dependent on vegetation structural characteristics like vegetation height and density, rigidity of the stems and the presence of leaves (Dawson & Charlton 1988; Kouwen & Li 1980). Seasonal variation and dynamic management of floodplains lead to a high spatiotemporal variation of vegetation structural characteristics and inherent roughness patterns (Baptist *et al.* 2004; Jesse 2004; Van Stokkom *et al.* 2005). To provide hydrodynamic modelers with reliable input, the spatial and temporal distribution of surface characteristics is needed. This asks for accurate and fast monitoring methods that can cover large floodplain areas.

Considerable progress has been reported on mapping of natural vegetation using multispectral and hyperspectral remote sensing data (Ringrose *et al.* 1988; Thompson *et al.* 1998; Mertes 2002; Schmidt & Skidmore 2003; Van der Sande *et al.* 2003). In several studies, spectral information has been combined with height information in vegetation classification schemes (e.g. Hill *et al.* 2002; Dowling & Accad 2003; Ehlers *et al.* 2003; Rosso *et al.* 2006). In the Netherlands, floodplain

vegetation units are distinguished based on visual interpretation and manual classification of false-color aerial photographs (Jansen & Backx 1998). Even though the spatial resolution and the level of detail of the classification may vary with the type of remote sensing data, a lookup table is always required to convert the qualitative vegetation classes to vegetation structure values. The use of a lookup table, however, leads to undesirable loss of within-class variation. Airborne Laser Scanning (ALS), has proven its ability to quantitatively map vegetation structural characteristics such as forest vegetation height, biomass, basal area, and leaf area index (Lefsky *et al.* 2002; Lim *et al.* 2003) and vegetation density (Chapter 4). Successful applications have also been reported in mapping of vegetation height of low vegetation in summer (Davenport *et al.* 2000; Cobby *et al.* 2001; Hopkinson *et al.* 2004b) and vegetation height and density in winter (Chapter 3). A recent study has parameterized floodplain roughness using vegetation height derived from ALS data (Mason *et al.* 2003). Due to the noise level of ALS data, which is around 4 cm (Davenport *et al.* 2000; Hopkinson *et al.* 2004b), these relations can not be applied to all floodplain land cover classes. The extraction of surface properties of, for example, sandy surfaces or meadows will still be inaccurate if based on ALS data.

In this paper, we present a novel method that combines spectral and ALS remote sensing data to map floodplain surface characteristics relevant for hydrodynamic modeling. The method comprises (1) image segmentation and object-based classification into the main hydrodynamically relevant land cover types, and (2) determination of roughness characteristics of various land cover types using direct analysis of vegetation structure using ALS and a lookup table. The roughness map resulting from this novel method is compared to the roughness map based on a lookup table for vegetation units. The effects on 2D flow patterns and water levels within a river and floodplain segment are assessed using the Delft3D hydrodynamic model (Gerritsen & Verboom 1994; Postma *et al.* 2000; Kernkamp *et al.* 2005).

5.2 Roughness formulations

Roughness determines the friction of the water flow exerted by the underlying surface. In practice, roughness is a model parameter that is calibrated to account for any loss of momentum of the water flow, which can be due to bed friction, vegetation friction, discrepancies in elevation data, the exchange of mass or momentum between the main channel and the floodplains, the presence of obstacles in the flow, or any other momentum loss (Baptist *et al.* 2005). Since the presence of vegetation adds considerably to the bulk floodplain roughness, we here focus on the description of vegetation roughness.

One of the ways to express roughness is by the Chézy coefficient. This coefficient (C in $m^{1/2}s^{-1}$) relates depth averaged flow velocity (u in ms^{-1}) to the hydraulic radius of a water course (R in m), and the energy gradient, or slope, (i in $m \cdot m^{-1}$) by:

$$u = C\sqrt{Ri} \tag{5.1}$$

Note that the higher the Chézy value, the lower the roughness, or resistance to flow is. There is general agreement that the roughness of subaqueous non-vegetated areas depends on the grain

size and the size and shape of the bed forms, although the scatter of the derived relations is large (Van Rijn 1994). Chézy values for sandy beds can then be calculated based on the Nikuradse equivalent grain roughness (k in m) as defined by the Colebrook-White formula (Keulegan 1938):

$$C = 18 \log \frac{12R}{k} \tag{5.2}$$

For vegetated areas we use the vegetation height and vertical density for roughness parameterization, which builds on the early work of (Einstein & Banks 1950; Kouwen *et al.* 1969; Kouwen & Unny 1973; Klaassen & Van der Zwaard 1974). A distinction should be made between submerged and emergent vegetation (Fig. 5.1). For emergent conditions, the friction of the vegetation against flow is derived from a force balance, in which vegetation stems are considered as rigid cylinders. This yields (Petryk & Bosmajian 1975; Stone & Shen 2002; Baptist *et al.* in press):

$$C_r = \sqrt{\frac{1}{C_b^{-2} + (2g)^{-1} C_d D_v h}} \tag{5.3}$$

where C_r is the composite Chézy coefficient representing roughness of a vegetated bed ($m^{1/2}s^{-1}$), C_b is the Chézy roughness of the bed ($m^{1/2}s^{-1}$), g is the gravitational acceleration (ms^{-2}), C_d is the drag coefficient for vegetation (-), D_v is the vertical vegetation density (the projected plant area in the direction of the flow per unit volume, m^{-1}) and h is the water depth (m).

For submerged conditions, the derivation of an analytical equation for vegetation resistance proves to be more difficult (Dawson & Charlton 1988). In this study we make use of the equation

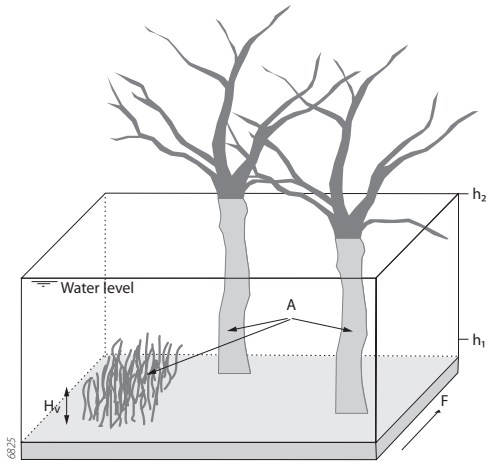

Figure 5.1 Hydrodynamic parameters; vegetation density in m^{-1}: the sum of the projected plant areas (A) in the direction of the water flow (F) per unit volume (cube), and vegetation height (Hv). Heights $h1$ and $h2$ were used for vegetation density computation for forest.

of Baptist *et al.* (in press), which considers resistance of both rigid and flexible submerged vegetation in a simple, but accurate way:

$$C_r = \sqrt{\frac{1}{C_b^{-2} + (2g)^{-1} C_d D_v H_v}} + \sqrt{\frac{g}{\kappa}} \ln \frac{h}{H_v} \tag{5.4}$$

where H_v is the vegetation height (m) and κ is the Von Kármàn constant (0.4). Recent studies showed that the underlying assumption of equation 5.4, the squared relationship between drag force and flow velocity derived for rigid stems, does not hold for flexible vegetation (Kouwen & Fathi-Moghadam 2000; Armanini *et al.* 2005). However, taking the plant flexibility into account requires additional model parameters that would increase uncertainty and the streamlining of vegetation due to hydraulic shear is not significant in case of lowland floodplains such as in the Netherlands (Klaassen *et al.* 1999). Furthermore, it should be noted that the drag coefficient is a property that can not be measured directly in the field, while it influences the roughness of both rigid and flexible vegetation. The drag coefficient for smooth cylinders is known from experimental studies and theory (Schlichting 1962) and depends on the value of the Reynolds number of the flow, which is a measure for turbulence. In model applications on vegetation roughness the drag coefficient is set to different values for submerged and emergent vegetation, which involves an arbitrary choice. This is done, for example, in an effort to account for rough vegetation surfaces or for the leaves on the branches.

To map spatial patterns of surface and vegetation roughness, we need to map different land cover types on which to apply the roughness models, either for non-vegetated parts (eq. 5.2), emerged vegetated parts (eq. 5.3), or submerged vegetated parts (eq. 5.4). Accordingly, we need to map vegetation density for forest patches, and vegetation height and density for herbaceous vegetation.

5.3 Field and airborne data collection

5.3.1 Study area

This study uses airborne remote sensing data collected over the Gamerensche Waard (GW) floodplain, situated on the left bank of the embanked river Waal, the main distributary of the river Rhine in the Netherlands (Fig. 5.2). After a near-flooding event in 1995, the river managers took measures to reduce flood levels and to restore the ecology by means of digging side channels, relocating the embankment, and implementing low density grazing by large herbivores. The Large secondary channel is perennial, the East channel and the West channel are ephemeral. The GW floodplain is essentially flat, except for the embankments and eroding shorelines of the side channels. Land cover is a combination of meadows, open water and nature areas that partly consist of forests as shown in the map and field pictures of figure 5.2. These comprise of willow (*Salix alba*, *Salix viminalis, Salix triandra*) and poplar (*Populus x canadensis*) in various stages of succession (Van Gennip & Bergwerff 2002). In addition to the forest patches, single trees of variable age were present. All vegetation was in winter condition when the laser data was acquired (March 11, 2003) and in summer condition at the moment of CASI data collection (July 11, 2003). The inundation depth of the one-year flood is 2 m, but it might rise up to 6 m

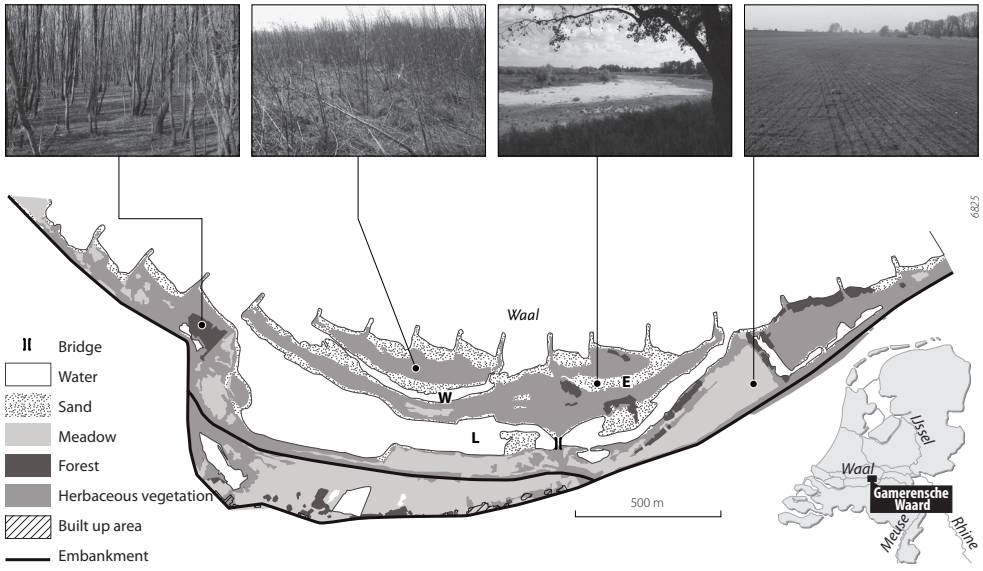

Figure 5.2 Map of the Gamerensche Waard floodplain with field photographs. L is the perennial Large Channel, W the West Channel, and E the East Channel.

in case of the once every 1250-year flood for which the embankments are designed. The typical water surface slope is 10 cm·km^{-1}.

5.3.2 Field data

To derive a regression model for tree heights of individual trees based on ALS data, the location and maximum tree height of 213 single trees on the island north of the western side channel were determined in the field in June 2004. Locations of the trees were determined using a dGPS in real time kinematics mode. Maximum tree height, which ranged between 1.5 and 7.5 m, was measured using a leveling beacon. Estimated accuracy was better than 5 cm.

Discharge measurements were obtained from Jans (2004), who applied an Acoustic Doppler Current Profiler (ADCP) on board a small vessel. For each discharge measurement, 5 to 10 channel crossings were made. Measurement locations were at the bridge in the Large Channel, and halfway the East and West Channel.

5.3.3 Ecotope maps

Ecotope maps are available for the whole embanked floodplain area in the Netherlands. Ecotopes are 'spatial landscape units that are homogeneous as to vegetation structure, succession stage and the main abiotic factors that are relevant to plant growth (Leuven *et al.* 2002). They are based on visual interpretation of aerial photographs of 1996, scale 1:5000 (Jansen & Backx 1998). The smallest detected object was 40 by 40 m in the field, or 2 by 2 mm on the photo, hence any variability on smaller scales is excluded from the map. Each forest ecotope is subsequently labeled with a vegetation density value using a lookup table, submerged vegetation types are

labeled with vegetation height and density (Van Velzen *et al.* 2003), based on limited field inventories in the Dutch floodplains. This results in choropleth maps of vegetation height and density for the vegetated parts of the floodplain.

5.3.4 Remote sensing data

CASI multispectral image
On July 11, 2003, a multispectral image was acquired with the Compact Airborne Spectral Imager (CASI). This system is an along-track scanner and acquires data in 10 channels between 400 and 900 nm, programmable at 2-nm spectral intervals (Lillesand & Kiefer 1994). For this flight campaign, 10 bands were specified, of which six in the near infrared to optimize discrimination of various vegetation types. The image was georectified by the data vendor, using the on-board gyroscope and GPS. Table 5.1 and 5.2 give the specific settings for this flight.

Airborne laser scanning
The ALS data of the GW floodplain were acquired using the FLI-MAP II system mounted on a helicopter (Huising & Gomes Pereira 1998; Baltsavias 1999b). FLI-MAP, Fast Laser Imaging and Mapping Airborne Platform, is a small-footprint, first pulse, scanning laser range finder combined with a dGPS and an Inertial Navigation System (INS) for positioning. An overview of the laser scanning technique used is given by (Wehr & Lohr 1999). Table 5.3 summarizes the characteristics. In 2003, the FLI-MAP system consisted of two laser range finders, resulting in

Table 5.1 Metadata for the CASI mission

Acquisition date	11-7-2003
Acquisition time	11:45
Flying height	1700 m
Strip width	1046 m
Pixel size at nadir	2 m
No. of bands	10

Table 5.2 Spectral properties of the CASI image

Band no.	Band middle (nm)	Band width (nm)	Description
1	450	20	Blue
2	552	10	Green
3	670	10	Red
4	700	10	NIR[a]
5	710	10	NIR
6	740	10	NIR
7	750	10	NIR
8	780	10	NIR
9	820	10	NIR
10	865	10	NIR

a. NIR = Near Infra Red

Table 5.3 Metadata for the laser scanning mission

Acquisition date	11-03-2003
Scan angle	± 30°
Scan line orientation	± 7°
No. of sensors	2
Pulse rate	2*10 kHz
Footprint size	20 by 3 cm
Flying height	80 m
Point density	75 m^{-2}

a combined pulse rate of 20 kHz. The two scanners were facing 7° forward and backward to decrease the number of occlusions in built-up areas. Additionally, FLI-MAP II has acquired true-color, high-resolution photographs simultaneously with the laser data. Photographs were taken in the downward looking direction with a frequency of one image per second and a ground resolution of 5 cm. A georeferenced photo-mosaic was supplied together with the laser data. The photo-mosaic proved unsuitable for vegetation classification, since channels were lacking in the near infrared. Moreover, illumination differences between individual images showed significant contrast changes within the mosaic, hampering vegetation classification. Nevertheless, the photo-mosaic proved useful to georeference the CASI data to the ALS data.

On March 11, 2003, the FLI-MAP II system was deployed over the GW floodplain by Fugro-Inpark. To increase the point density, each of the flight lines was flown twice. The data vendor also filtered the ALS data and labeled points as either terrain points, or non-terrain points. Non-terrain points consist mainly of vegetation, but could also be related to buildings, or outliers. Filtering has been carried out using proprietary software, which included a combination of the slope-based filtering of Vosselman (2000) and contour line analysis (Fugro-Inpark, Luc Amoureus, pers. com.).

5.4 Data processing of spectral and ALS data

To derive roughness values covering the whole floodplain, we combined the discriminative power of the spectral gridded data to classify different land cover types with the direct vegetation structure mapping capabilities of the ALS point data. The three main steps that were successively taken (Fig. 5.3) are (1) preprocessing: merging of the multi-spectral image with a normalized digital canopy model (nDCM) derived from the laser data, (2) supervised classification of image objects to discriminate between water, sand, paved, meadow, herbaceous vegetation, forest and built-up area and (3) application of specific methods to herbaceous vegetation and forest estimate the roughness input parameters. Other classes are assigned roughness input values from a lookup table

5.4.1 Stage 1: Pre-processing

The CASI data were combined with the ALS data to enable object-oriented classification. Both datasets were represented as raster layers with identical extent and with cell size of 1.5 m.

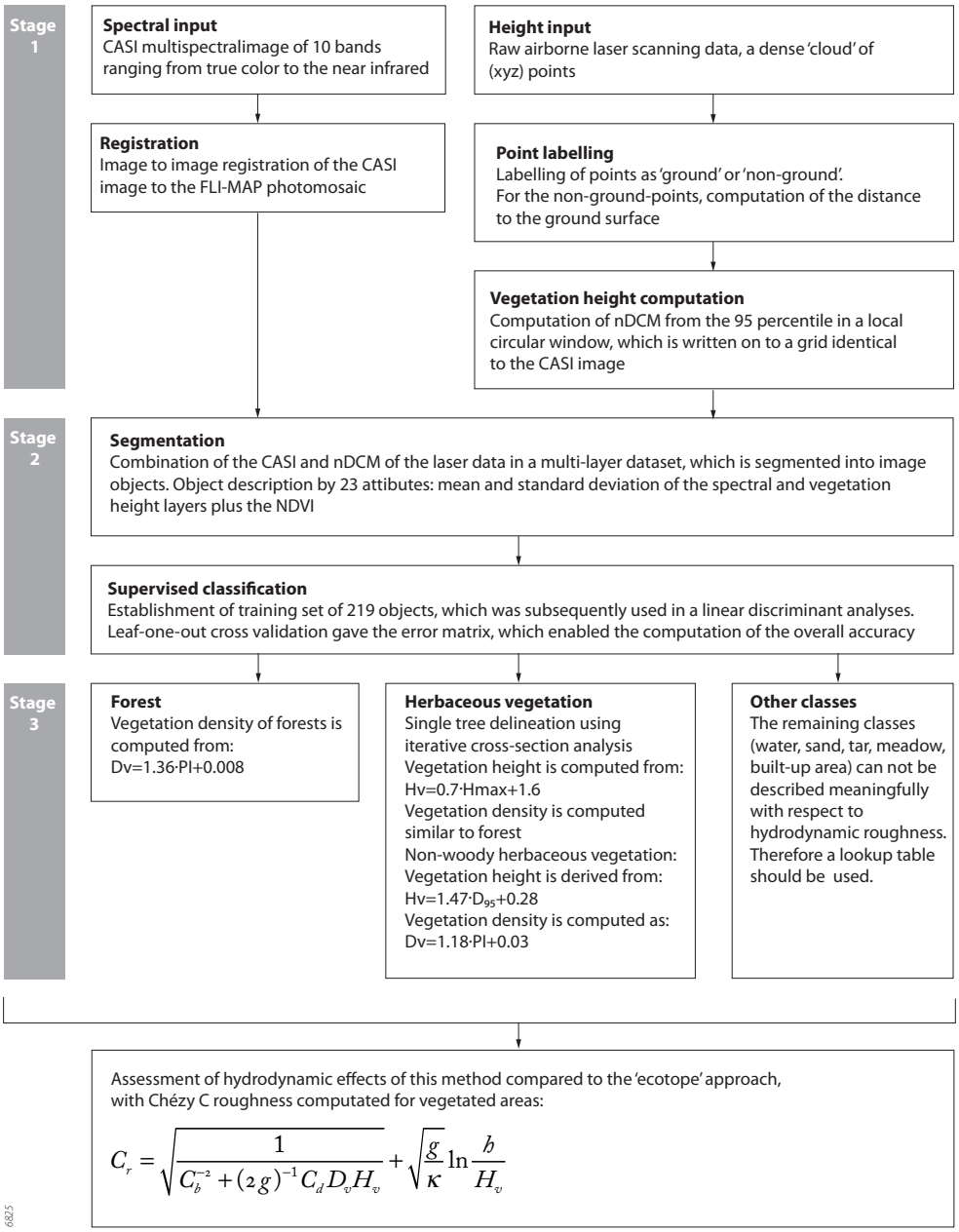

Figure 5.3 Flow chart of the method to map floodplain surface roughness. A Digital Surface Model, describing the vegetation height is combined with the spectral CASI data to derive seven different land cover classes. Each class is described using the appropriate method, which enables the implementation of the Chézy C roughness in a hydrodynamic model.

The CASI data was subsampled to make optimal use of the ALS data. It turned out that the CASI data was not well georeferenced by the vendor of the CASI image, as it did not match geometrically with the *spectral* data acquired by FLI-MAP. Therefore, additional image registration was carried out using rubber sheeting with 300 tie points (Hartmann *et al.* 2004).

A Digital Terrain Model (DTM) was computed from the ALS data based on the terrain points derived from the data vendor, which previously showed a 7 cm absolute accuracy (Huising & Gomes Pereira 1998). The DTM accuracy proved vegetation-class dependent based on terrestrial height measurements using dGPS (Pfeifer *et al.* 2003). Their DTM was created using a different filter and resulted in a DTM accuracy of 7.3 and 11.6 cm for herbaceous vegetation and mature forest. The root mean square error (RMSE) proved 8.4 cm for herbaceous vegetation and 11.7 cm for mature willow forest. Visual inspection showed that the forest floor was well sampled by the laser scanning, as the forest was in leaf-off condition. Similar errors are expected for the DTM generated by the data vendor.

For all non-terrain points, the terrain elevation was computed in a local window with a 1.5 m radius. Within this local window, the terrain was described by fitting a second order trend surface to the terrain points, and a prediction was made for the location of the non-terrain point. Subsequently, the normalized height, the difference between the point height and terrain height was computed. A gridded Digital Canopy Model (nDCM) was computed as the 95 percentile of the normalized heights per cell. The grid of the nDCM matched the grid of the CASI data. The 95 percentile was chosen since it represents the vegetation height well, but excludes outliers from the nDCM (Chapter 3).

5.4.2 Stage 2: Segmentation and classification in land cover types

The software package eCognition (Definiens 2000) was used to segment the floodplain area into image objects *sensu* Hay *et al.* (2003). An object oriented image classification was preferred over a per-pixel approach, because the spectral confusion is lower for objects than for pixels. Spectral confusion is the amount of overlap in feature space between the different classes in the training dataset. Image objects were extracted using the Fractal Net Evolution Approach: FNEA (Baatz & Schäpe 2000b). This procedure uses a bottom-up region merging approach based on 'local mutual best fitting' (Baatz & Schäpe 2000a). It starts with the assumption that each pixel forms an individual image object. In a sequence of steps, pairs of image objects are merged into larger objects based on the local similarity of adjacent objects with respect to form, spectral values and texture. The procedure also incorporates a dimensionless, user-specified 'scale parameter' that describes the minimum degree of fitting needed for a merge. Hence, the segmentation process yields image objects at a specific landscape scale. Additionally, the weight assigned to similarity in the various bands of the fused image and object shape must be specified with this algorithm. The resulting objects are described by various descriptors including spectral and texture information, and relational and contextual features.

The nDCM was fused with the CASI data into a multi-source dataset aiming at floodplain land cover classification. Table 5.4 gives the weights assigned to the individual layers during the segmentation. The weight of the ALS layer was set equal to the summed weights of the spectral layers. The weights for the CASI data were distributed based on a roughly equal weight

Table 5.4 Segmentation weights for the individual layers of the multi source dataset.

Layer	CASI Band middle (nm)	Weight
CASI 1	450	2
CASI 2	552	3
CASI 3	670	2
CASI 4	700	1
CASI 5	710	1
CASI 6	740	2
CASI 7	750	2
CASI 8	780	1
CASI 9	820	1
CASI 10	865	1
ALS	– -	16

for color and near infrared bandwidths. Band 4 and 5 are highly correlated with band 3, and band 8 to 10 correlate strongly with band 6 and 7. Therefore band 4, 5, and band 8 to 10 were given a relatively low weight (Hartmann *et al.* 2004). Additional weights have to be assigned to either the combined information of spectral and height data and to the shape of the segments. A weight of 0.9 was assigned to fused data and a weight of 0.1 was assigned to shape. Different scale settings were tested during image segmentation, and visual inspection showed that a scale parameter of 10 resulted in small segments which was most appropriate for the identification of the vegetation distribution as observed in the field.

The supervised classification of image objects was carried out using linear discriminant analysis (Davis 1986). The discriminant function was based on a training data set, which was created by manual classification of 219 randomly selected image objects. The classification of these objects was based on visual inspection of the CASI and ALS data, field knowledge, and the vegetation maps, scale 1:5000 of (Van Gennip & Bergwerff 2002). Of each class, at least 15 objects were classified. The following classes were discerned based on their different roughness and spectral attributes: water, wet sand, dry sand, paved area, meadow, herbaceous vegetation, dry herbaceous vegetation, forest, and built-up area. Wet sand and dry sand have different spectral signatures, but the same roughness, and these classes were merged after classification. Likewise, herbaceous vegetation and dry herbaceous vegetation were merged into one class. The accuracy of the classification was tested using a leave-one-out cross validation (Wonnacott & Wonnacott 1990). The results are presented in an error matrix, and are summarized by the KHAT statistic to give a conservative estimate of the overall accuracy (Lillesand & Kiefer 1994).

Segmenting herbaceous vegetation into single trees and non-woody vegetation
The class "herbaceous vegetation" comprises a wide range of vegetation types in the succession stage between meadow and forest. Consequently, it includes non-woody vegetation as well as young trees for which different algorithms are used to describe their vegetation structure. Therefore, a single tree delineation method was applied first to segment the laser vegetation points in woody and non-woody herbaceous vegetation segments.

Different tree delineation methods are available in the literature. Persson *et al.* (2002) and Brandtberg *et al.* (2003) developed gridded digital canopy models, smoothed at different scales. In each of the scale levels, they subsequently detected local watersheds, and carried out an automatic selection of the proper scale for each individual tree. Alternatively, single tree delineation can be applied on raw laser data, having the advantage that no data points are lost due to gridding. Andersen *et al.* (2002) presented a Bayesian object recognition method in which ellipsoid crown shapes were fitted to the laser points. This is a computationally intensive method that is difficult to apply to large areas. Morsdorf *et al.* (2004) delineated trees using a k-means clustering technique on laser point data. K-means clustering minimizes, in an iterative way, the overall distances of the points to their cluster centroids. Morsdorf *et al.* (2004) stated that the k-means clustering is highly dependent on the seed points, or initial centroids, of the clustering, which should therefore be located at the tree tops. They derived the seed points from local maxima in a gridded nDCM of 0.5 m resolution.

In the present study of floodplain vegetation, we tested the k-means clustering method of Morsdorf *et al.* (2004). The results were unsatisfactory, because the clustering resulted often in two cluster centroids for a single large tree, while adjacent small trees were not identified as a separate cluster. The initial position of the centroid was located at the tree top, but the final cluster represents a statistical optimum, which often was not related to a single tree. To overcome this problem, we propose a new procedure: cluster merging using iterative cross-section analysis. This method generates many clusters based on seed points that over-represent large tree and k-means clustering. Clusters are subsequently merged depending on the characteristics of the cross-section between the maxima of adjacent clusters. Details of the method are described below.

Firstly, points with a normalized height less than 1.5 m, or with 2 or less neighboring points within 1 m radius were considered to represent herbs and were therefore excluded from further analyses. The 1.5 m threshold was chosen as a tradeoff between missing small trees and selecting too many laser points that represent herbs. Field observations showed that herbaceous vegetation might reach a height of 2 m, while young trees were occasionally smaller than 1.5 m. The second threshold, more than 2 neighboring points, was set to distinguish between herbs and trees of the same height. Due to the laser point density of 60 points per m^2, a young tree is represented by a cluster of points, whereas a stalk of senescent herbaceous vegetation is more likely represented by a single laser point.

Secondly, a k-means cluster analysis was carried out using local maxima as seed points. Local maxima were identified by moving a local window over each laser point and by testing whether the central point was the highest. The 0.7 m radius of the local window was selected because it was the average tree radius as observed in the field. The k-means clustering resulted in too many clusters for large trees; this was solved in the third step. By analyzing cross sections between cluster maxima, it was determined whether these clusters belong to the same tree, or to different trees. For each cluster maximum, the cluster maximum of the nearest neighboring cluster was selected, and the 1 m wide cross section between the maxima was described by the following parameters (Fig. 5.4):

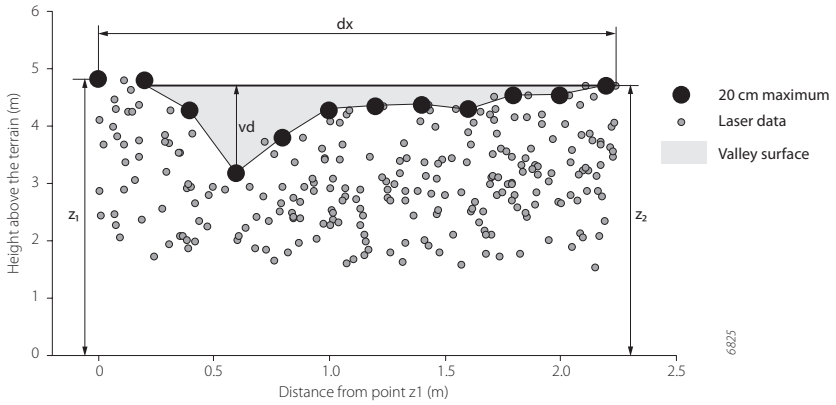

Figure 5.4 Side view of a 1 m wide cross section between two cluster maxima with descriptive parameters: *z*1, *z*2 = highest points of clusters 1 and 2, *dx* = distance between cluster maxima, *vd* = valley depth

1. Horizontal distance between the maxima (*dx*)
2. Height difference between the maxima *z*1 and *z*2 (*dz*)
3. Valley depth between the maxima (*vd*)
4. Valley surface
5. Valley ratio: valley depth/height of the lowest maxima
6. Ground width (nDCM touching the ground, which is zero in figure 5.4)

The first two parameters are based on the original point data. For the other parameters, the point data were resampled on a 20 cm interval. The highest point in that interval was selected to create a local, one-dimensional nDCM of the cross section between the cluster maxima. The 1 m width was a tradeoff between too few selected points for a narrower section and missing details of the linear cross-section in case too wide a section was chosen. A leafless forest will be represented by about three vegetation points per 20 cm distance along the cross section with the point density of this study. A training set of cross-sections that either represents one or two trees was generated by manual classification of 280 cross-sections using an automated visualization of the cross sections. For each vegetation type, this training set has to be created. In our case, the training set represented open vegetation dominated by willow (*Salix alba*). Visual inspection of the scatter plots revealed that a cross section between two trees was best characterized by a nDCM that touched the ground. This means that an open space of at least 20 cm between the clusters should exist to separate two trees. Finally, clusters were merged iteratively until all cross sections satisfied the specified condition. The 2D convex hull of the final merge gives the polygon that describes the outline of a tree. Figure 5.5 shows the cluster merging process in three consecutive products.

5.4.3 Stage 3: Determination of hydrodynamic surface characteristics

The third step consisted of specific methods to estimate the hydrodynamic surface characteristics of different classes. ALS data were used to map vegetation structure of forest, individual trees and herbaceous vegetation. A lookup table provided input data for the other classes: meadow, sand, paved area, and built-up area.

Forest

Airborne laser scanning enables the automatic extraction of various forest structural characteristics related to vegetation density: stem number, stem diameter, basal area and/or timber volume (Nilsson 1996; Naesset 1997b; Lefsky *et al.* 1999a; Drake *et al.* 2002; Naesset 2002; Holmgren & Persson 2004). To map the hydrodynamic vegetation density of the floodplain forest, we used the percentage index (*PI* in m^{-1}) based on chapter 4. The *PI* computes the percentage of laser hits that fall within the height range ($h1$ to $h2$ shown in figure 5.1) that is typically inundated by a flood, and is defined as:

$$PI_{h1-h2} = \frac{1}{h2-h1} \cdot \frac{N_{h1-h2}}{N_{tot}} \tag{5.5}$$

in which N_{h1-h2} is the number of points between height 1 and 2 above the forest floor, N_{tot} is the total number of points in the field plot including canopy and ground surface points. The height interval for *PI* was set from 0.5 to 2.5 m. The $h1$ was set to 0.5 m to avoid inclusion of noise from the ground surface, $h2$ was set to 2.5 m to include enough points to compute a robust value for *PI*. The *PI* was computed in a moving window with a 3 m radius to ensure that a sufficiently large value for N_{h1-h2} was reached (≥ 50), which is needed for an accurate assessment of *PI*. The linear regression model described in chapter 4, was used to predict the hydrodynamic vegetation density (D_v in m^{-1}, eq. 6). The calibration data were collected by manual measurements of stem density and stem diameter. This regression model is based on data of the GW floodplain, combined with two other floodplains, using FLIMAP ALS data (Chapter 4).

$$D_v = 1.36 \bullet PI + 0.008 \ (R^2 = 0.66, \text{RSE} = 0.016\ m^{-1}, n = 22) \tag{5.6}$$

Single trees

Single trees need to be characterized by vegetation height and density, similar to non-woody herbaceous vegetation since the young trees are easily submerged. Vegetation density of the trees was computed using the same regression model as for forest. Tree height was predicted using the regression model derived in this study (eq. 5.9). To that end, field observations of maximum tree had to be related to delineated trees from the laser data, which was carried out manually. The maximum normalized height of the cluster was regressed against field tree height.

Non-woody herbaceous vegetation

Extraction of vegetation structural characteristics of non-woody herbaceous vegetation in the same area was studied in detail in chapter 3. The key issue in vegetation structure mapping of non-woody herbaceous vegetation is the labeling of laser points as ground or vegetation, since the thin stalks of herbs in senescence are difficult to detect by ALS. The DTM height derived from ALS data is relatively insensitive to erroneous labeling of points, because only a small percentage of the laser point represents vegetation. Conversely, the distribution of vegetation points is strongly influenced by the number of laser points labeled as vegetation. Therefore, the point labeling of herbaceous vegetation was carried out following the methodology of chapter 3 using the histogram of the normalized heights. This vertical point distribution is considered as the sum of a noise distribution of the ground points and a uniform distribution of the vegetation points. The point of maximum upward concavity, the inflection point on the upper limb of the

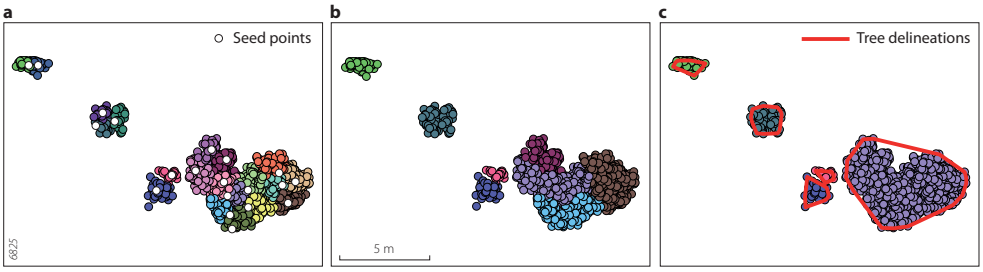

Figure 5.5 Single tree delineation from ALS data using a) seed points from local maxima and k-means clustering. The colors indicate the different clusters, b) Iterative cross section analysis, displaying the merged clusters after two iterations and c) the result after six iterations, with the convex hull delineating the individual trees as observed in the field.

histogram, is used as a threshold to separate ground points from vegetation points. All points above the threshold were labeled as vegetation. This histogram analysis of all normalized laser point heights was applied separately to each image object segmented in stage 2 to avoid large influences on the normalized histogram of erroneous DTM filtering. Vegetation height (H_v) and density (D_v) were computed from regression models determined for the same area in chapter 3. These regression models are valid for vegetation heights ranging from 0.3 to 2 m and vegetation densities ranging from $3 \cdot 10^{-4}$ to 0.7 m^{-1}.

$$H_v = 1.47 \cdot D_{95} + 0.28 \ (R^2 = 0.74, \text{RSE} = 0.16 \text{ m}, n = 31) \quad (5.7)$$

$$D_v = 1.18 \cdot PI + 0.03 \ (R^2 = 0.51, \text{RSE} = 0.08 \text{ m}^{-1}, n = 43) \quad (5.8)$$

where D_{95} is the 95 percentile of the vegetation points labeled using the inflection method, and PI is the Percentage Index computed over the height of the vegetation. This resulted in a spatially distributed map of non-woody vegetation height and density.

Other land cover classes

A lookup table provided input data for the remaining classes: meadow, sand, paved area, and built-up area. The lookup table was needed here, because no method is available to extract the hydrodynamically relevant surface characteristics of these classes from either ALS or CASI data. A point of consideration is whether vegetation height and density of meadows can be mapped using ALS data. Some researchers included meadows in their regression models for the prediction of vegetation height (Davenport *et al.* 2000; Cobby *et al.* 2001). However, with a standard deviation of laser data representing unvegetated flat terrain of 4 cm and a range of 30 cm (Davenport *et al.* 2000), we believe ALS does not allow accurate mapping of vegetation height and density of meadows. Roughness in built-up areas also varies on a small spatial scale due to hedges, grass, trees and fishing garden gnomes with variably sized hats. Moreover, no methods are available in the literature relating ALS data to vegetation structure of gardens. Therefore, a lookup table was used for built-up area as well.

5.5 Hydrodynamic modeling

A hydrodynamic model of the GW floodplain was set-up with the Delft3D-flow model that was applied in a 2D-Horizontal mode (2DH) to compute depth average flow fields and water levels. Delft3D-flow is a numerical hydrodynamic model, which solves the shallow water equations on a staggered curvilinear computational grid (Gerritsen & Verboom 1994; Postma *et al.* 2000; Kernkamp *et al.* 2005). Required input data are the river bathymetry and floodplain topography, boundary conditions for the upstream discharge and the downstream water level and information on the hydraulic roughness, i.e. surface roughness (C_b), height (H_v) and density (D_v) of vegetation, and drag coefficient (C_d).

5.5.1 Model set-up

A curvilinear model grid was defined for a 7.5 km long reach of the river Waal, with an average width of 1.5 km. The GW floodplain is located at approximately 3.5 km from the upstream boundary and 2 km from the downstream boundary to minimize boundary effects. The grid consists of 32,750 active grid cells, sized roughly 30 m long by 10 m wide within the GW floodplain. The bathymetry of the river Waal and the topography of the floodplain section upstream and downstream of the GW floodplain were derived from measurements from 1995, conducted by the Dutch Ministry of Public Works, Transport and Water Management (RIZA). The floodplain topography of GW was derived from detailed measurements in 2000 (Jans 2004). Hydrodynamic boundary conditions were taken from daily discharge measurements at (1) the 'Zaltbommel' station within the model domain and (2) the 'Vuren' station downstream of the model domain. The model was run for a series of stationary discharges between 1000 and 4500 m^3s^{-1}, with a 500 m^3s^{-1} step-wise increase. The maximum discharge is a common flood discharge, with a return period of 5 years (Silva 2003). At this discharge the GW floodplain is inundated by approximately 1.5 to 2 m depth.

5.5.2 Model applications

Two sets of input data were compared within the model set-up. Model 1 was based on the traditional 'ecotope approach', where land cover is manually delineated and classified into ecotopes based on false color aerial photographs. The resulting ecotope map was converted to roughness input parameters using a lookup table (Jansen & Backx 1998; Van Velzen *et al.* 2003). Non-vegetated units were assigned a fixed Nikuradse *k*-value for bed roughness. Vegetated units are assigned cylinder characteristics height (m), density (m^{-1}) and drag coefficient (-) (table 5.5). The drag coefficient and bed roughness can not be measured in the field. In this study we followed (Van Velzen *et al.* 2003), who suggest a C_d value of 1.8 for all vegetation types with a height smaller than or equal to 1.0 m and a C_d of 1.5 for taller vegetation. The bed roughness was chosen as 0.1 m Nikuradse roughness length, corresponding to a Chézy C roughness of 42.8 $m^{1/2}s^{-1}$ at 2 m water depth (eq. 5.2).

Model 2 comprises the new approach in which height and density of herbaceous vegetation, and vegetation density for forest were derived from the ALS data, see table 5.6. Only the GW floodplain section was updated with this new vegetation input. For both models, the data are transferred into the numerical grid.

5.5.3 Model calibration

Model calibration was carried out on discharge measurements in the three secondary channels (Fig. 5.2). Since the discharges through the channels are dependent on the channel roughness, each model run for each stationary discharge required a certain spin-up period.

Model calibration runs for Model 1 firstly required an adjustment of the level and dimensions of the bridge crossing the Large Channel and, secondly, in an adjustment of the Nikuradse roughness of the non-vegetated parts. The bed roughness in the secondary channels may change under changing hydrodynamic conditions, since bed forms may develop. However, we chose to keep the calibration as simple as possible and kept the roughness values fixed for the complete range of discharges, see table 5.5. The bed roughness for the secondary channels was calibrated at a rather high value in order to decrease the discharges of the Large Channel at high discharges of the River Waal. The bathymetry, calibrated bed roughness and all other parameter, such as horizontal eddy viscosity, were held the same for both models. The Chézy value for the vegetation resistance (C_r) was for both models calculated using equation 5.4. Therefore, the only

Table 5.5 Land cover characteristics for model 1, vegetation characteristics after Van Velzen *et al.* (2003)

Land cover class	H_v (m)	D_v (m^{-1})	C_d (-)	C_b ($m^{1/2}s^{-1}$)	k_N (m)
Pioneer vegetation	0.15	0.15	1.8	42.8	– -
Canary reed grass	1.00	0.40	1.8	42.8	– -
Meadow	0.06	45	1.8	42.8	– -
Natural grassland	0.10	12	1.8	42.8	– -
Creeping thistle	0.30	3	1.8	42.8	– -
Dry herbaceous	0.56	0.23	1.8	42.8	– -
Softwood shrub	6.00	0.13	1.5	32.0	– -
Hardwood shrub	5.00	0.17	1.5	32.0	– -
Sofwood prod. forest	10.00	0.010	1.5	34.3	– -
Hardwood forest	10.00	0.023	1.5	32.0	– -
Softwood nat. forest	10.00	0.028	1.5	28.8	– -
Main channel	– -	– -	– -	– -	0.15
Oxbow lake	– -	– -	– -	– -	0.15
Secondary channel	– -	– -	– -	– -	0.40
Lake/Harbour	– -	– -	– -	– -	0.05
Groyne field beach	– -	– -	– -	– -	0.15
Paved/Built-up area	– -	– -	– -	– -	0.60

Table 5.6 Vegetation characteristics in GW for model 2

Class	H_v (m)	D_v (m^{-1})	C_d (-)	C_b ($m^{1/2}s^{-1}$)
Meadow	0.06	45	1.8	42.8
Herbaceous vegetation	eq. 5.7, eq. 5.9	eq. 5.8	1.8	42.8
Forest	10	eq. 5.6	1.5	32

difference in the models was in the detail of the vegetation characteristics resulting in a different vegetation roughness map.

5.6 Spatial roughness input and hydrodynamic modeling results

5.6.1 Land cover map and distribution of vegetation structural characteristics

The result of the classification of image objects is shown in figure 5.6a. The error matrix is given in table 5.7. The largest errors occur in the distinction between meadow and herbaceous vegetation. The overall accuracy is 81 percent and the KHAT statistic is 0.77. After merging wet and dry sand into a single class, and merging herbs and dry herbs into herbs, the overall accuracy increased slightly to 82 percent, and the KHAT statistic to 0.78.

Tree heights of the 213 trees measured in the field ranged from 0.5 to 7.5 m, the average was 3.6 m. Trees lower than 1.5 m were excluded from further analyses, as they were lower than the herbaceous vegetation. The spatial arrangement of the trees in the field is similar to the tree locations extracted from the ALS data. Vegetation height of the individual trees (H_{max}) was estimated using a regression model derived from the field observations as shown in figure 5.7, which reads as:

$$H_{max} = 0.70 \bullet H_{max.laser} + 1.59 \ (R^2 = 0.41, \text{RSE} = 0.84 \text{ m}, n = 86) \qquad (5.9)$$

The vegetation density map of forest derived from ALS data is given in figure 5.6b. Average vegetation density was 0.018 m^{-1}, equaling the standard deviation. Differences in vegetation density within single forest patches are clearly visible. The outlines of individual trees are also depicted in figure 5.6b, which shows a detailed pattern of trees within the herbaceous vegetation.

Table 5.7 Error matrix resulting from leave-one-out cross validation based on 219 manually classified reference segments

	Surface area (%)[a]	Water	Wet sand	Dry sand	Paved	Meadow	Herbs	Forest	Dry herbs	Built-up	Row total	Users accuracy
Water	9.5	**30**	0	0	0	0	0	0	0	0	30	1.00
Wet sand	8.2	1	**10**	1	2	0	3	0	0	0	17	0.59
Dry sand	8.3	0	0	**13**	0	0	0	0	0	0	13	1.00
Paved	0.6	0	3	1	**10**	0	0	0	0	0	14	0.71
Meadow	25.0	0	2	0	0	**25**	8	0	0	1	36	0.69
Herbs	38.7	1	0	0	1	11	**45**	2	2	0	62	0.73
Forest	5.4	0	0	0	0	0	1	**17**	0	0	18	0.94
Dry herbs	4.5	0	0	0	1	0	0	0	**13**	0	14	0.93
Built-up	0.7	0	0	0	1	0	0	0	0	**14**	15	0.93
Column total	– -	32	15	15	15	36	57	19	15	15		
Prod. accuracy	– -	0.94	0.67	0.87	0.67	0.69	0.79	0.89	0.87	0.93		**0.81%**

a. Total surface area amounts to 100 hectares

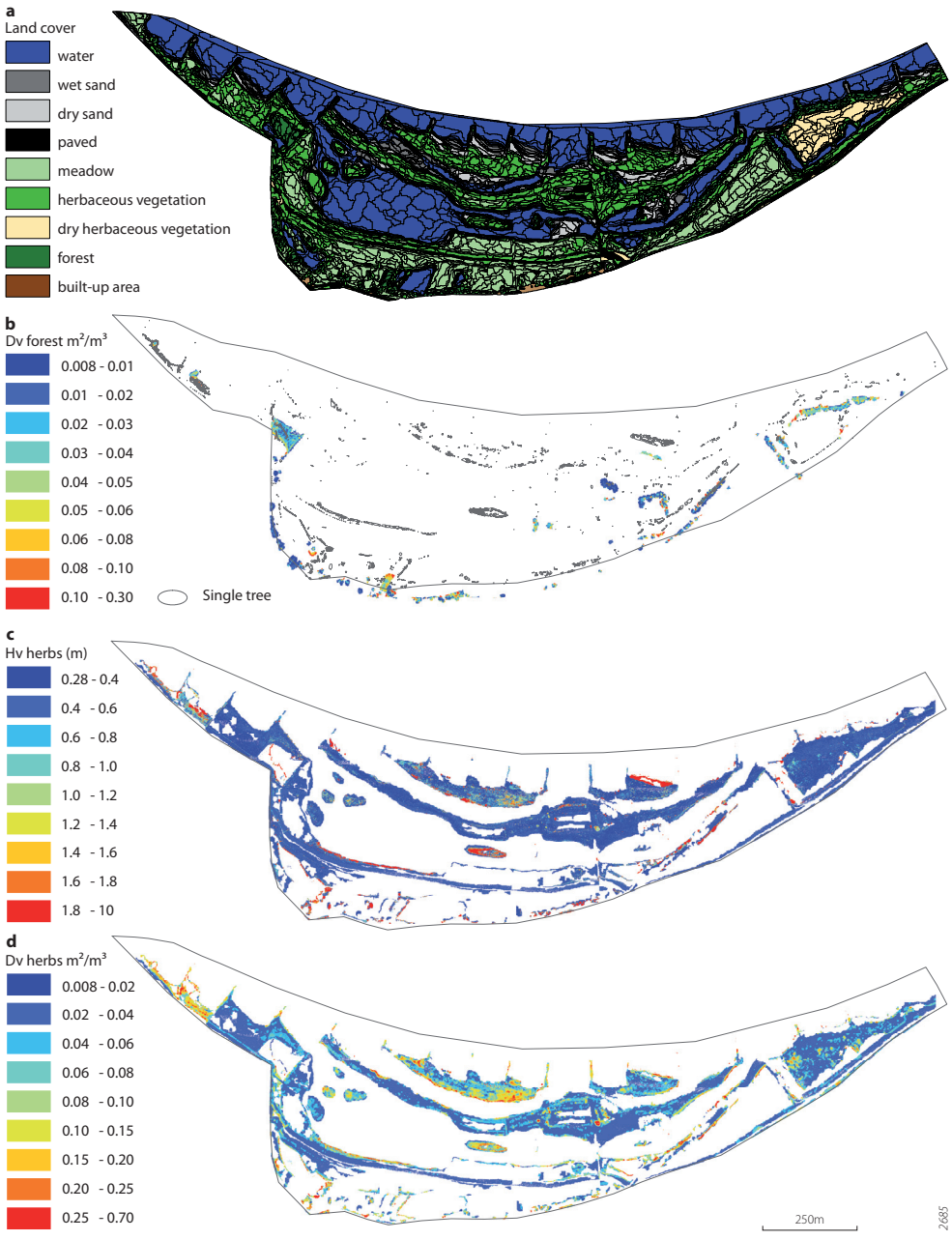

Figure 5.6 Map stack describing the surface properties of the Gamerensche Waard floodplain. a) classified land cover map, b) vegetation density of forest (m^{-1}), c) vegetation height of herbaceous vegetation (m), d) vegetation density of herbaceous vegetation (m^{-1})

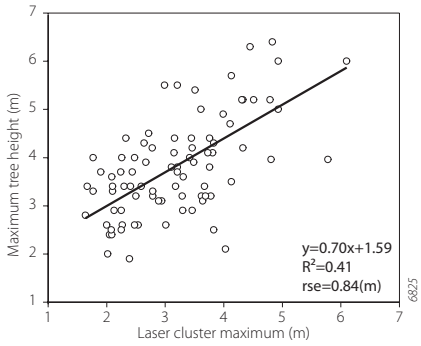

Figure 5.7 Scatter plot of laser-derived single tree heights verses tree heights from field data.

For example, along the northern shore of the western side channel trees line up along the shoreline. Small trees that grew close together were merged, resulting in an under-representation of the number of trees. However, this does not influence the resulting map of the vegetation density. The vegetation height and density maps of herbaceous vegetation are presented in figure 5.6c, and 6d. Both show a high level of detail and much spatial variation. The averaged values for vegetation height and density of herbaceous vegetation are 1.8 m and 0.072 m^{-1} respectively, with 3.6 m and 0.068 m^{-1} as standard deviation, which shows the large within-class variation.

5.6.2 Calibration results and comparison of hydrodynamic patterns

Comparison of calculated and measured water levels at the location of Zaltbommel showed a good fit (Fig. 5.8), but it has to be noticed that the range of water level for a given discharge is large, partly because of hysteresis effects of bed form development and dynamic waves. The measured channel discharges for the Large Channel and the East Channel are reproduced reasonably well (Fig. 5.9), considering that only the roughness of the non-vegetated parts was

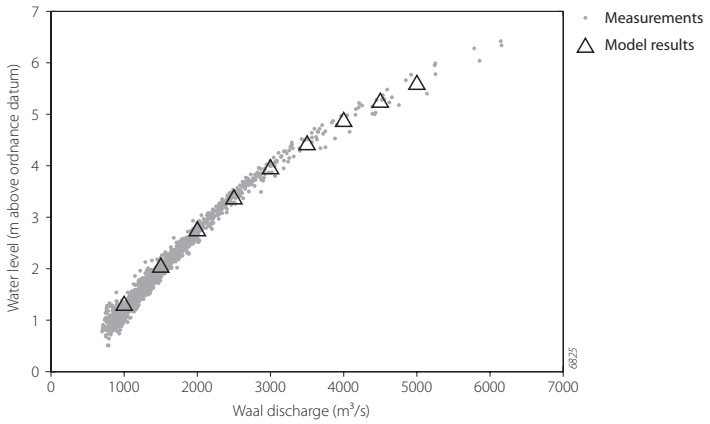

Figure 5.8 Comparison of measured and modeled water levels at location Zaltbommel for Model 1.

used for calibration. The discharge through the West Channel however, seems to be off. We suspect that an error in the bathymetry causes this. The results for Model 2 show small changes in channel discharges compared with Model 1. At low Waal discharges, there are no effects, since the floodplain is not flooded. At higher Waal discharges, the discharge through the East Channel and West Channel increases for Model 2. For the Large Channel, there is no clear indication for an increase or decrease of the discharge. Expressed as RMSE for the modeled versus measured values, Model 2 is performing slightly better for the West Channel and Large Channel, but worse for the East Channel, see table 5.8.

Results from the hydrodynamic computations are shown for the maximum modeled discharge of 4500 m^3s^{-1} (Fig. 5.10). It is important to realize that the Chézy roughness value expresses differences in water depth as well as differences in vegetation structure or bed roughness. The

Table 5.8 Root mean square errorrs for the discharges through the secondary channels.

Channel	Model 1 (m^3s^{-1})	Model 2 (m^3s^{-1})
East	6.1	8.0
West	27.6	25.5
Large	17.5	16.3

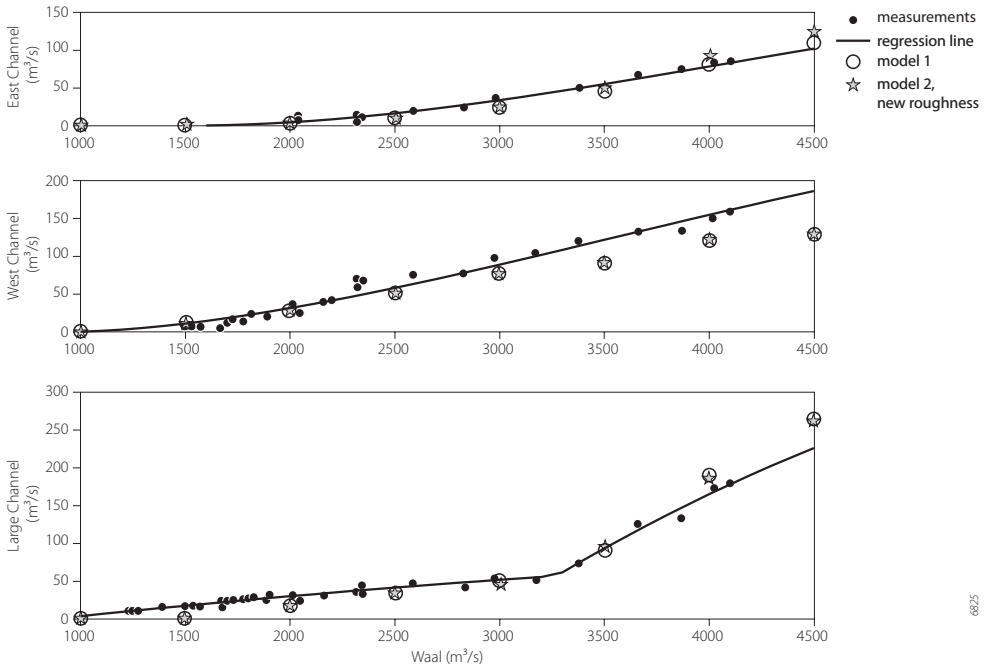

Figure 5.9 Model results, discharge measurements and regression line through measurements (from Jans, 2004) in a) East channel, b) West channel, and c) Large channel.

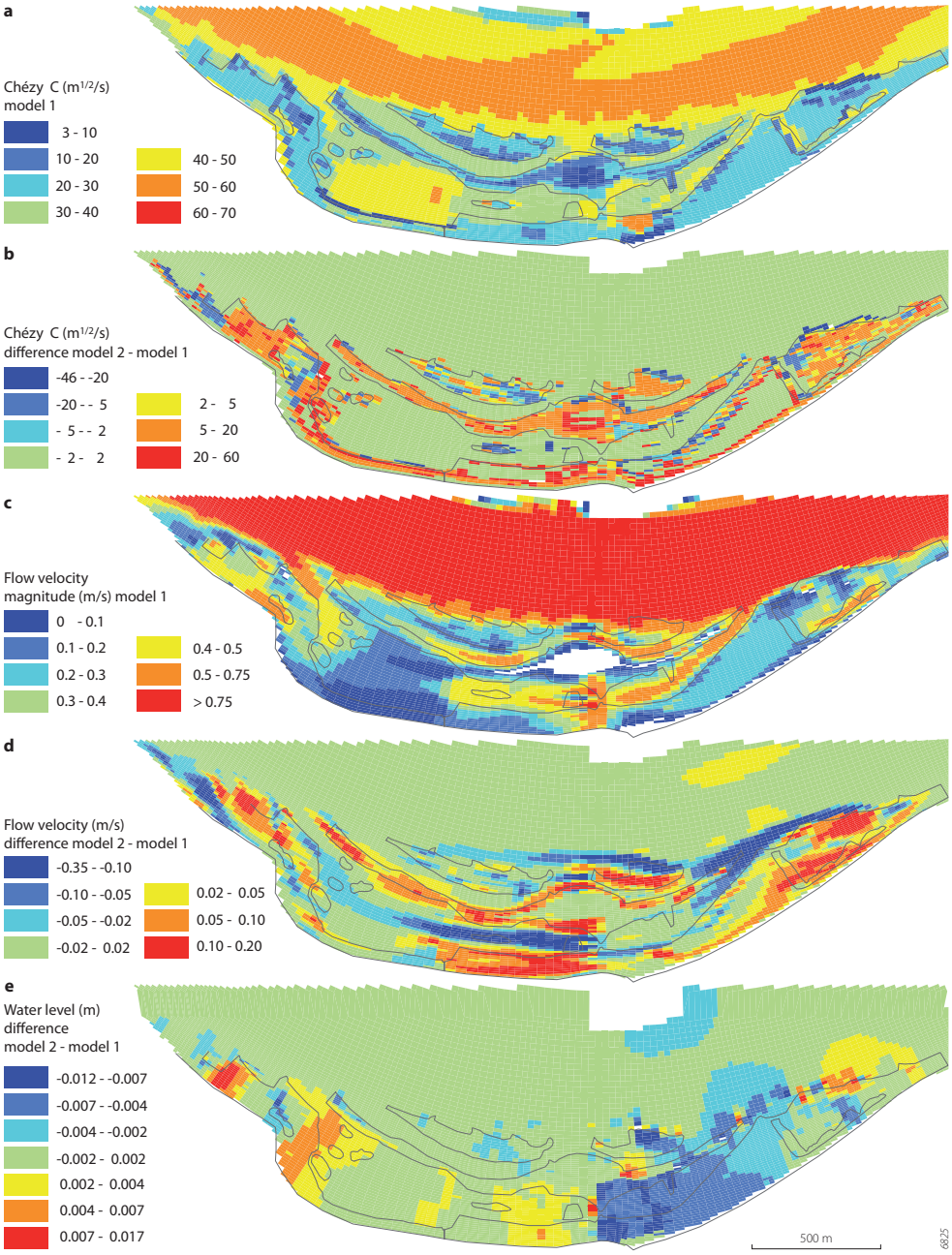

Figure 5.10 Model results a) Chézy *C* roughness values ($m^{1/2}s^{-1}$) based on model 1, b) difference in Chézy *C* roughness values ($m^{1/2}s^{-1}$) between model 2 and model 1, c) magnitude of flow velocity (ms^{-1}), d) difference in flow velocity (ms^{-1}) between model 2 and model 1, and e) difference in water level (m) between model 2 and model 1.

effect of the water depth leads to high *C* values for the main channel, and low values for the higher parts of the floodplain, for example north of the bridge. The Chézy *C* distribution of Model 1 (Fig. 5.10a) is rather smooth, resulting from the uniform vegetation structure values in the lookup table. Still, the herbaceous vegetation north of the West Channel and forest patches show up as low Chézy values and hence a high roughness. Figure 5.10b shows the difference in roughness between Model 1 and Model 2. A negative difference denotes a lower Chézy *C* value for Model 2 than for Model 1. The roughness difference map shows an overall tendency towards higher Chézy *C* values for Model 2, indicating a lower roughness. Nonetheless, regionally significantly lower *C* values are present. For example, the island north of the West Channel, consisting of herbaceous vegetation with many individual trees (Fig. 5.6), has lower *C* values on average for Model 2. The roughness of Model 2 shows more local variation in the distribution of Chézy *C* values.

The magnitude of the flow velocity for Model 1 is shown in figure 5.10c, the flow direction is roughly East to West. The difference between Model 2 and Model 1 is given in figure 5.10d. The flow velocity magnitude clearly differs between models. The differences are typically in the order of 0.1 to 0.2 ms^{-1}, which is significant. The velocity difference inside the West and the East Channel is small. For the riparian zones bordering these channels, there are significant changes. In the Large Channel, the flow changes considerably. Compared to Model 1, Model 2 shows a lower velocity in the middle of the channel and higher velocities on the riparian sides. Higher flow velocities are found for Model 2 on most vegetated parts due to the lower roughness.

The water level differences between Model 2 and Model 1 are in the order of 0.5 cm (Fig. 5.10e), which is small compared to the range in water level measurements in Zaltbommel (Fig. 5.8). Again, a negative difference denotes lower water levels for Model 2 compared to Model 1. Lower water levels can be found in the upstream section of the Large Channel. In Model 2, the upstream water level has decreased by about 0.5 cm compared to Model 1 because of lower vegetation resistance. A slight set-up of the water level can be found at the downstream end of the Large Channel where the flow enters a floodplain forest. The forest extent is slightly larger for Model 2, and the edges of this forest patch are particularly dense (Fig. 5.6b). It has a lower Chézy value in Model 2 (Fig. 5.10b) and, therefore, gives more resistance to flow.

5.7 Evaluation of input data and modeling results

This paper presents a method for automatic floodplain roughness parameterization using a combination of multispectral data, and airborne laser scanning data. The method is innovative in (1) the segmentation of a fused dataset and the classification based on object attributes and (2) the extraction of vegetation characteristics from ALS data, which largely avoids the use of a lookup table. With the Delft3D-flow model a comparison is made between the method based on a lookup table and the new method.

5.7.1 Remote sensing data processing

Segmentation and classification is a prerequisite for floodplain roughness parameterization. ALS data appeared unsuitable to distinguish between land cover classes that are not characterized

by significant local height differences, such as water, paved areas, beaches or meadows. Spectral data is complementary to ALS data in this respect as these classes have significant differences in spectral signatures. The timing of CASI campaign, four months after the ALS campaign could affect the mapping of the spatial distribution of herbaceous vegetation, as the ALS data represents the stalks of the vegetation of the previous growing season, and the distribution of the high herbs could easily change due to grazing. Therefore, spectral data acquired in the preceding summer would be ideal. Classification of the image objects using a linear discriminant analysis proved successful given the overall accuracy of 81 percent. Linear discriminant analysis has the advantage that it can take many parameters into account in the discriminant function, since it assumes the variance per layer to be equal for each group. This limits the required size of the training dataset, which is especially important when an a-select sampling strategy is applied in which classes with a low occurrence are not well represented. The distinction between herbaceous vegetation and meadows proved difficult as their spectral signatures overlap and the user accuracy is relatively low (70 percent). Large parts of the floodplain consist of these two land cover types and this classification error might, therefore, have a large influence on the hydrodynamic characteristics.

The single tree delineation using the iterative cross section analysis is an extension of a point-based clustering method. It combines the clustering of laser points starting at local maxima with the analysis of the profile between the maxima of the clusters. Profile analysis is a powerful tool to discriminate between trees as extra parameters can be derived from the profile (Koch *et al.* 2006). In this study a single attribute of the cross section was used, namely whether or not the 'valley' between the two cluster maxima was lower than the threshold value of 1.5 m. Alternatively, more features of the cross section could be taken into account by using a discriminant analysis to classify the cross sections. This makes the procedure highly flexible for different vegetation types and laser point densities, but the method will have to be trained for each vegetation type. The explained variance of the regression model for tree height (R^2 = 0.41) is relatively low when compared to other studies (Persson *et al.* 2002; Brandtberg *et al.* 2003). The reason might be the small range of tree heights present in the class herbaceous vegetation (up to 7.5 m), and the time delay between the laser campaign and the field inventory of 1.5 year. Young trees might be included in the field data, but not in the laser data. Alternatively, dead trees could have been removed or washed away during a minor flood peak in 2004.

The vegetation density map is used in roughness equation 5.3, which does not take tree flexibility into account. The regression model for *PI* and D_v have to be established using field reference data as the portability of empirical relations between laser data and vegetation structure is still low. The increase of the portability is, therefore, a challenging issue to facilitate large-scale use of ALS data for vegetation analysis. Explained variance of the *PI* for forest vegetation density mapping (R^2 = 0.66) is larger than using ecotopes (R^2 = 0.34; chapter 4). *PI* requires a minimum number of laser pulses in the local window for an accurate estimate. For that reason, the radius of the window was set to 3 m, which led to at least 50 laser hits in the local window, except for the very open parts of the forest. In future studies, the window size could be increased at the cost of less spatial detail. For single trees, the *PI-Dv* relation might differ slightly from forests in case a single tree has no neighboring tree close by, because it will be hit by more laser pulses than a tree in a dense forest. This might lead to higher *PI* values. Conversely, the local window in which

the vegetation density is computed also covers the area outside the tree canopy, which reduces the point density within the window. This leads to underestimation of the *PI*. No reference data were available on density of single trees. Still, the modeled values were within the expected range of 0.01 to 0.7 m^{-1}, whereas D_v values in the lookup range from 0.023 to 0.17 m^{-1}.

Vegetation height (R^2 = 0.78) and density (R^2 = 0.51) of herbaceous vegetation are based on the laser-derived D_{95} and *PI* respectively. These relations also have to be calibrated, and are season-dependent. Vegetation height ranges from 0.28 to 7 m for single trees based on ALS data, compared to 0.15 to 1 m based on the lookup table. Conversely, for vegetation density the lookup table shows a larger range (0.15 to 3 m^{-1}) than the ALS data (0.08 to 0.7 m^{-1})

The class built-up area has been assigned a representative bed roughness (k = 0.6 m). It is, however, possible to extract buildings from a combination of spectral and ALS data (Baltsavias 2004). Buildings could then be added separately to the hydrodynamic model.

5.7.2 Hydrodynamic modeling

In hydrodynamic modeling, there is always a process of calibration involved. This paper provides a method that restricts the range of roughness values that can be assigned to vegetated parts of the floodplain. The roughness values derived from the calibration procedure should be converted back to vegetation characteristics to ensure that the vegetation height and density do not deviate from the predicted value by more than the residual standard error of the regression equation. If this check fails, the source of the discrepancy should be sought in other model parameters such as bathymetry, topography or horizontal eddy viscosity. It thus makes an important step in the independent treatment of roughness values for floodplains, which is important for the computation of water levels for the design discharge and the related height of the embankments outside the range of validation data.

The data transfer from the laser derived vegetation structure maps to the computational grid of the hydrodynamic model led to a loss of detail due to the simple averaging over each grid cell. However, the orientation of the roughness elements relative to the direction of the flow influences the total energy loss over that cell (Van Velzen *et al.* 2003). The laser-derived maps, combined with the modeled flow pattern from an initial model run, enables the appropriate computation of the cell roughness since such a high level of detail is available in the data.

Our modeling results show that disaggregation of roughness values leads to significant changes in the flow patterns and small differences in water levels. When the interest is in flow velocities for physical habitat mapping, or when the interest is in morphodynamic modeling, this disaggregation is of high importance. The limited effect on water levels is caused by the relatively low fractional discharge of the floodplains of the River Waal. For the design discharge of the River Waal, around 10,000 m^3s^{-1}, the hydrodynamic effects are more pronounced as the proportion of discharge over the floodplain is larger. Another cause for the small effect on water levels is the geographical position of the GW floodplain section, 92 km upstream of the mouth of the river. The water levels at such a location are less sensitive to differences in local roughness as the local water levels are governed to a larger extent by the tidally influenced water levels at the river mouth and flow velocities are relatively low. Conversely, rivers with wide floodplains

with a high fractional discharge of the floodplains are more sensitive to correct mapping of vegetation structure.

An important question that arises from the ability to generate detailed vegetation maps is whether such detail is necessary. In other words, what is the lower limit of disaggregation? A study by (Werner *et al.* 2005) claims that a higher spatial segmentation in floodplain roughness values has only limited ability to improve model performance. However, they calibrated their model based on water levels and flood extent, which is prone to equifinality with respect to model input. Nonetheless, we agree that disentangling the separate roughness contributions from the bulk roughness is a daunting task, and that this is of limited value to predict water levels in the GW floodplain section. This points at a major problem for many of the high resolution hydraulic modeling studies, whether they focus on high resolution topography (Marks & Bates 2000; Bates *et al.* 2003; Casas *et al.* 2006) or vegetation characteristics (Cobby *et al.* 2001; Cobby *et al.* 2003; Mason *et al.* 2003). Detailed hydraulic calibration data are necessary to assess the true lower limit of disaggregation of input with respect to model discretization. This requires an extensive field study, which should include spatially distributed measurements of flow velocity profiles, local water surface slopes, and water level measurements that are combined with a bathymetric survey. Such a modeling study needs a probabilistic assessment of the error propagation and may start with the error contribution in the high-resolution input data such as the classification error and residual standard error of the empirical relations. Likewise, drag coefficient, horizontal eddy viscosity and turbulent viscosity should be assessed to determine the largest contribution to the uncertainty in the output in the hydrodynamic model. Given the limited field data for the GW floodplain, such a sensitivity analysis was not carried out. In this respect, ALS contributes detailed input maps to a new generation of high-resolution hydrodynamic models.

5.8 Conclusions

Earth observation techniques may contribute significantly to generate accurate input for a new generation of high-resolution hydrodynamic models. This paper describes a new method to derive hydrodynamically relevant surface characteristics based on airborne laser scanning and multispectral data. This method restricts the range of vegetation input values that should be assigned to vegetated floodplains as the error in the vegetation structure estimate is known.

The fused dataset allowed classification of image objects into seven classes (water, sand, paved, meadow, herbaceous, forest and built-up area) with a KHAT statistic of 0.78. In spite of the good results of the classification, the distinction between meadows and herbaceous vegetation is still difficult.

Airborne laser scanning was well able to map the spatial distribution of vegetation density of forest (R^2 = 0.66). Moreover, ALS provided detailed maps of vegetation height and density of herbaceous vegetation based on simple regression models (R^2 = 0.78 for vegetation height, R^2 = 0.51 for vegetation density). However, these regression models have to be calibrated for the specific laser sensor and vegetation type. A new single tree delineation method is presented: iterative cluster merging based on cross section analysis (R^2 = 0.41 for tree height). The resulting

tree map represented the tree distribution well, but detecting small and narrow trees that grow close together remains a challenge. The result of the combined mapping methods is a highly detailed map stack of surface properties of the floodplain. A lookup table was used to assign surface characteristics cover classes sand, meadow, paved area and built-up area as no reliable relations are available to map the surface characteristics of these classes show too much spatial variation of surface structure. The resulting roughness map showed a high level of spatial detail.

The comparative hydrodynamic modeling study showed better estimates from the new method for two out of three discharge measurements in the secondary channels, and comparable water levels. It also showed that the disaggregation of floodplain roughness leads to significantly different flow patterns, which is of value to for example morphodynamic models. Future studies should include high quality hydrodynamic field measurements to enable quantitative assessment of the error contribution from bathymetry, roughness formulation, spatial distribution of vegetation characteristics and model resolution. The fusion of airborne multispectral and ALS data may supply the detailed vegetation characteristics.

Acknowledgements

This work was funded by NWO, the Netherlands Organization for Scientific Research, within the framework of the LOICZ program under contract number 01427004. I thank the AGI, the Advisory Board on Geo-informatics and ICT of the Dutch Ministry of Transport, Public Works and Water Management for providing the ALS and CASI data.

6 Two novel methods for field measurements of hydrodynamic density of floodplain vegetation using terrestrial laser scanning and digital parallel photography

M.W. Straatsma, J. Warmink, H. Middelkoop
submitted to *International Journal of Remote Sensing*, contribution to the "3D forestry" special issue

Abstract

Hydrodynamic vegetation density, the sum of the projected plant area per unit volume, is an important parameter for floodplain flow models. This paper compares two novel techniques to quantify this parameter in the field using Terrestrial Laser Scanning (TLS) and digital Parallel Photography (PP). Field reference data consisted of (1) a stem map, describing the position and diameter of 650 trees in a single forest patch (2) 17 manually measured plots distributed over forest and herbaceous floodplain vegetation. PP consists of a series of digital photographic images of vegetation against a contrasting background. The centre columns of all images were merged into a single composite parallel image. This mosaic was thresholded to determine the fractional coverage of the vegetation, which is converted to vegetation density using the optical point quadrate method. TLS was carried out using a Leica HDS3000 time of flight laser scanner. Data processing of TLS data consisted of slicing the points around breast height. In a polar grid the vegetation density was predicted, using the optical point quadrate method corrected for missing points. Both methods were compared to the field reference data. PP (R^2 = 0.996, RSE = 0.0037) performed better than the TLS (R^2 = 0.77, RSE = 0.022). Advantage of the TLS method is the ability to provide a detailed 2D or even 3D distribution of the vegetation density. PP is cheaper, faster, and data processing is limited. We conclude that TLS and PP are two complementary techniques that show high accuracies for field measurements of vegetation density.

Keywords: hydrodynamic vegetation density; terrestrial laser scanning; parallel photography; vegetation area index

6.1 Introduction

Accurate calculation of water levels and flow velocities of inundated floodplains, as carried out using 2D or 3D hydrodynamic models, relies not only on detailed input of floodplain topography, but also on accurate estimates of 2D patterns of hydraulic roughness exerted by floodplain vegetation (Darby 1999; Tsujimoto 1999; Huthoff & Augustijn 2004; Stolker *et al.* 1999). Vegetation roughness is the retardance of the water flow velocity due to vegetation. High roughness, resulting from tall and dense vegetation, may substantially slow down flow velocity, causing water levels to rise. The key vegetation parameters that determine vegetation roughness are vegetation height and density, and its flexural rigidity (Kouwen & Li 1980). Flexural rigidity of a plant is the resistance to bending under shear stresses of water, which in the case of grass decreases with vegetation height (Kouwen 1988). Roughness is, therefore, also dependent on the shear stress. Klaassen *et al.* (1999) found that for most vegetation types occurring within e.g. the lower Rhine floodplains, bending of submerged floodplain vegetation under winter conditions was negligible. Accordingly, Klopstra *et al.* (1997), Van Velzen *et al.* (2003) and Baptist *et al.* (in press) only considered vegetation density in their roughness models, and disregarded flexural rigidity. Hydrodynamic vegetation density is defined as the sum of the projected plant areas in the direction of the flow per unit volume (Petryk & Bosmajian 1975). Roughness models that consider vegetation as rigid cylinders use vegetation height and density as the structural parameters for roughness computation in case of submerged vegetation, and vegetation density for emergent vegetation. Hydrodynamic models require 2D spatial patterns of these parameters as input.

Airborne and spaceborne remote sensing have become well-proven surveying techniques for vegetation mapping and characterisation over various different scales (Mertes 2002). Satellite imagery has been used to map floodplain vegetation at a regional scale (Ringrose *et al.* 1988; Mertes *et al.* 1995; Townsend & Walsh 2001; Van der Sande *et al.* 2003), while airborne multispectral images have been employed at the scale of floodplain sections (Cusack *et al.* 1999). At more detailed scale, floodplain vegetation mapping has been based on visual interpretation of airborne photographs (Jansen & Backx 1998), or high-resolution stereo imagery (Ehlers *et al.* 2003). In recent years, airborne laser scanning (ALS) has been introduced as a novel tool in combination with spectral data for landcover analysis of floodplains and estuaries (Hill *et al.* 2002; Dowling & Accad 2003). In Chapters 2 to 5 we used high-resolution ALS data to map 2D patterns of height and density of floodplain vegetation. Still, for all these remote sensing applications field reference data remain necessary to (1) relate remotely sensed data to vegetation classes, (2) to quantitatively convert these data to structural characteristics and (3) to obtain an accuracy assessment of the results.

Over the past decennia, various quantitative methods have been established to measure vegetation structure in the field. Vegetation *height* can be easily measured in the field, for example by directly measuring the length of shoots or stems (Chapter 2), or by using a frame with an array of pins pointing straight downward from a rail installed above the vegetation (Ritchie *et al.* 1996). In contrast, vegetation *density* is far more difficult to measure. When assuming that vegetation can be considered as vertical cylinders, its density would be readily determined by manually measuring the diameter of all stems within the area of interest. The vegetation density

is then the product of number of stems (N) and the average diameter of the stems (d) divided by the surface area of the field plot. However, this approach becomes inaccurate in most real-world vegetation types, due to the presence of side branches, complex stem shapes and leaves. Therefore, alternative methods using point frames have been employed (Zehm *et al.* 2003). Since these manual methods are laborious and usually provide density estimates only for small plots, photographic methods have been proposed in which photographs of vegetation are taken against a contrasting background. Vegetation density is then estimated from the vegetation cover on the digitised image (Zehm *et al.* 2003). Vegetation density can be derived from the Leaf Area Index (LAI), which is traditionally determined in vertical direction for canopy coverage (Jonckheere *et al.* 2004), but can also be determined in a horizontal direction. Current photographic methods still provide biased estimates of vegetation density. Firstly, they disregard the effects of the central projection of the photograph images: consequently, vegetation elements close to the camera take a larger space than the same element at a larger distance due to the opening angle of the camera. This may lead to an overestimation of the fractional coverage of the vegetation, which depends on the distance to and the size of the first vegetation element. Furthermore, these photographic methods do not generate information on three-dimensional distribution of vegetation density.

Terrestrial laser scanning (TLS) is a promising method to map 3D vegetation structure by acquiring extremely dense point clouds (Lichti *et al.* 2002). It has recently been applied in forestry studies to characterize trees using shape fitting (Thies *et al.* 2004; Hopkinson *et al.* 2004; Watt & Donoghue 2005), filter operations in the 3D raster domain (Gorte & Winterhalder 2004), and diameter-height profiles (Bienert *et al.* 2006). So far, these studies have focused at detecting individual tree shapes, which is still problematic for thin twigs. However, for the determination of hydraulic density, it is not particularly necessary to identify each tree *individually*, but to determine the *average vegetation density* over a certain volume of forest. The performance of TLS for the latter purpose has still remained unexplored.

The aim of the present study was to assess the accuracy of two new methods to determine the hydrodynamic vegetation density of floodplain vegetation: digital parallel photography (PP) and terrestrial laser scanning (TLS). The PP method aimed at improving the existing techniques developed by MacArthur & MacArthur (1961) and Zehm *et al.* (2003), by obtaining digital photographic images with a parallel projection, in which there is no over-estimation of vegetation close to the camera. The TLS method consists of the computation of aggregated vegetation density values. The study was carried out in two floodplain sections along the lower Rhine River distributaries in the Netherlands. The PP and TLS method were tested in a floodplain forest with straight stems, in which reference data of vegetation density could be reliably determined by manual measurement in field plots. The PP was subsequently applied to various floodplain vegetation types.

6.2 Current field methods of vegetation density measurements

Different field methods have been developed to determine vegetation density: (1) the point frame method, (2) the cover board method, and (3) the optical point quadrat method. The horizontal point frame method uses a frame with three parallel diagonal rails with holes punched at regular

intervals (Dudley *et al.* 1998). Through each hole, a pin with length L_p is put horizontally into the vegetation, and the number of hits with the vegetation is recorded for each position. The vegetation density is then derived from:

$$Dv = L_p^{-1} \bullet N_{hits}/N_{holes} \tag{6.1}$$

where L_p is the pin length, N_{hits} the total number of hits and N_{holes} the total number of holes. This method requires flexible or penetrable vegetation to record more than one hit per pin. The support is limited to the size of the frame, and the length of the pins. No additional assumptions need to be made about the distribution of the vegetation, which makes the point frame method reliable.

The cover board method of MacArthur & MacArthur (1961) was originally applied vertically. It uses a white board marked with a grid, which is moved away from the observer until the distance L_b is reached at which 50 percent of the board is covered by vegetation. After some rearrangements, the vegetation density is then computed as:

$$Dv = -L_b^{-1} \ln(0.5) \tag{6.2}$$

This method has the advantage that it is rapid, and needs simple equipment. The support is limited by the size of the board. The disadvantage is the subjective estimate of the fractional coverage of the board by the surveyor. To limit the subjective estimate of the fractional coverage of the cover board method, (Ritzen & Straatsma 2002) used a digital camera to photograph the vegetation against a white background for this purpose. However, due to the central projection of the vegetation on the camera the vegetation close to the camera is overestimated.

MacArthur & Horn (1969) developed the optical point quadrate method, in which a photo camera is used as a vertical range finder. At 16 points in a grid that is put on the lens of the camera, the height of the lowest leaf is measured. The Leaf Area Index (*LAI*) between height *f1* and *f2* is then computed from:

$$LAI = \ln(N_{f1}/N_{f2}) \tag{6.3}$$

where N_{f1} and N_{f2} are the number of points sighted above height *f1* and *f2* respectively. The *LAI* can be converted to vegetation density when divided by the distance between *f1* and *f2*. This method was verified by Aber (1979) for foliage height profiles. The disadvantage is the low number of points, and the time consuming procedure. The latter two methods assume a Poisson distribution of vegetation elements perpendicular to the viewing direction, parallel light rays and should include no missing values for any of the distance measurements. The method is also sensitive for a sufficiently large number of observations for N_{f2} (Aber 1979). Parker *et al.* (2004) applied the method of MacArthur & Horn (1969) using a portable profiling laser range finder, connected to a field laptop. With this system they sampled various forest types by walking 31 parallel transects of 30 m length. They found good correlations with foliage profiles derived from the optical point quadrate method, but noted that the laser system overestimated the foliage coverage in all cases, probably due to the large emergent beam size of 12.4 cm^2.

6.3 Site descriptions

This study is based on data collected in two floodplain sections of the distributaries of the River Rhine in the Netherlands: 'Duursche Waarden' floodplain (DW) along the right bank of the River IJssel, the 'Gamerensche Waarden' (GW) floodplain along the left bank of the River Waal (Fig. 6.1). In both floodplains, the Dutch Ministry of Public Works, Transport and Water Management has been taking measures to reduce flood levels and to restore the ecology by means of digging side channels and low intensity grazing by cattle (Silva *et al.* 2001). Elevation differences in both floodplains are mostly less than 1 m, except for a series of wind-blown ridges in the Duursche Waarden floodplain, which are approximately 4 m higher than the rest of the floodplain. Land cover is a combination of arable land, meadows, open water and nature areas that partly consisted of forests. Forests comprise softwood forest (willow, (*Salix alba, Salix viminalis*), poplar (*Populus nigra, Populus x canadensis*)) and hardwood forest (oak (*Quercus robur*), ash (*Fraxinus excelsior*)) in various stages of development, and a small mature pine stand (*Pinus sylvestris*). The typical inundation depth of these floodplains is 3 m, but water depths may rise to 5 m in case of extreme flood events.

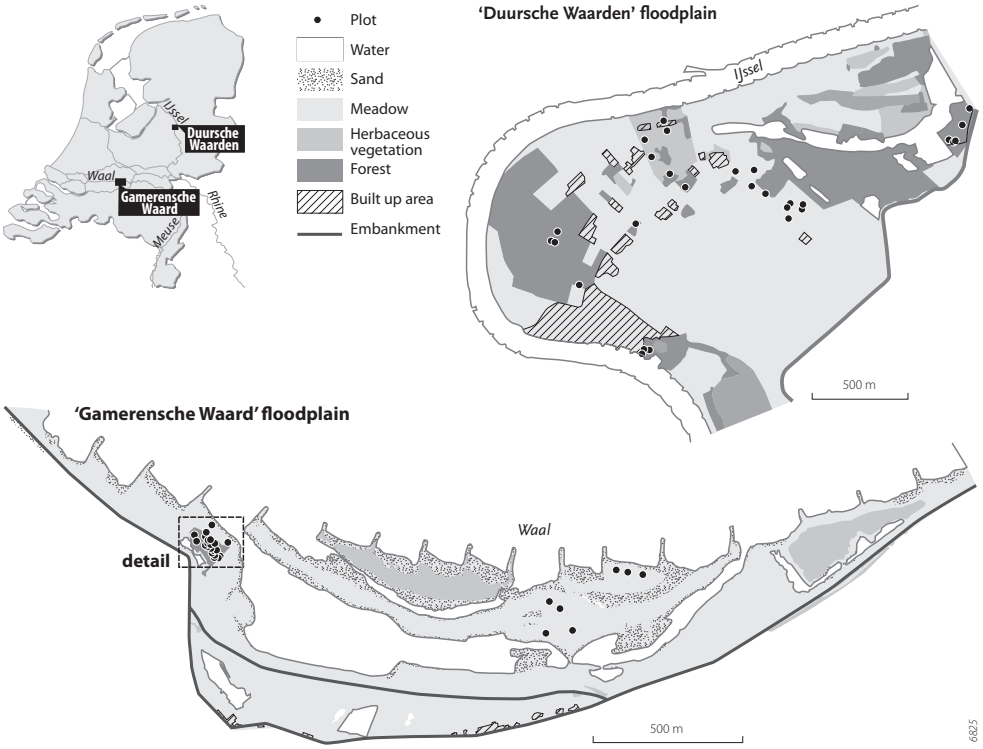

Figure 6.1 Location of floodplain sections of the Gamerensche Waard (GW) and Duursche Waarden (DW) within the Rhine distributaries

6.4 Vegetation density measurements using parallel digital photography

6.4.1 Field reference data

To test the parallel photographic (PP) method, field reference data of vegetation density were collected on rectangular field plots (black dots in figure 6.1), both in forest and herbaceous vegetation. In each plot, the number of stems or shoots (*N*) and the average diameter (*d*) of the stems that cross a virtual horizontal plane following Brown (1971) were determined manually. The average diameter was computed from 30 randomly selected stems. In forest plots, the virtual plane was positioned at breast height, i.e. 1.5 m above the ground surface. This height was chosen for ease of work and small variations in density between 1 and 2 m. For herbaceous vegetation, the plane was positioned at half the vegetation height to measure a representative density. The digital photographs were taken at the same height. Vegetation density $D_{v.Nd}$ was then computed as the product of *N* and *d*, divided by the plot area. This *Nd*-method is valid under the assumption of cylindrical vegetation. Therefore, we selected forest plots with straight stems with few or no side branches for validation of the PP method. After validation of the PP method, we applied it on forest plots with leaves and herbaceous vegetation in summer and winter, where the assumption of cylindrical vegetation is not valid. Results were compared to the *Nd*-method to estimate the underestimation of the *Nd*-method.

6.4.2 Experimental setup and data processing

The PP method uses an array of digital images, all taken with the camera axis in the same direction. The experimental setup consisted of a Canon Powershot A520 digital camera that was moved sideways along a 6 m long guide rail that was horizontally mounted on tripods. By adjusting the tripod heights and the setscrews to rotate the rail along its longitudinal axis, it was assured that all camera positions along the rail were in a horizontal plane. At fixed intervals – 5 cm for forest and 1 cm for herbaceous vegetation – a digital photo was made of the vegetation in front of the camera, against a contrasting background screen (Fig. 6.2). A white background was used for forest plots, a red one for herbaceous vegetation. The background was placed parallel to the guide rail. We used the highest resolution of the camera (2272 by 1704 pixels). Data processing consisted of (1) the creation of a digital photo mosaic, (2) the discrimination between vegetation and background on the digital image, and (3) computation of vegetation density.

A single parallel photo mosaic was created from the series of digital images by clipping the centre columns of each of the images and pasting them next to each other into a single composite image (Fig. 6.2c, d). The number of columns (*c*) to be clipped represented the displacement of the camera between subsequent images, and was computed as:

$$c = n_m \bullet d \tag{6.4}$$

$$n_m = n_{tot}/(2 \bullet L_c \bullet \tan \tfrac{1}{2} \gamma) \tag{6.5}$$

$$\gamma = 2 \bullet \arctan(\tfrac{1}{2} \bullet ccd/f) \tag{6.6}$$

where n_m is the number of pixels m^{-1}, d the distance between two subsequent images, n_{tot} the total number of pixels along the horizontal axis of the image, L_c the distance between camera and

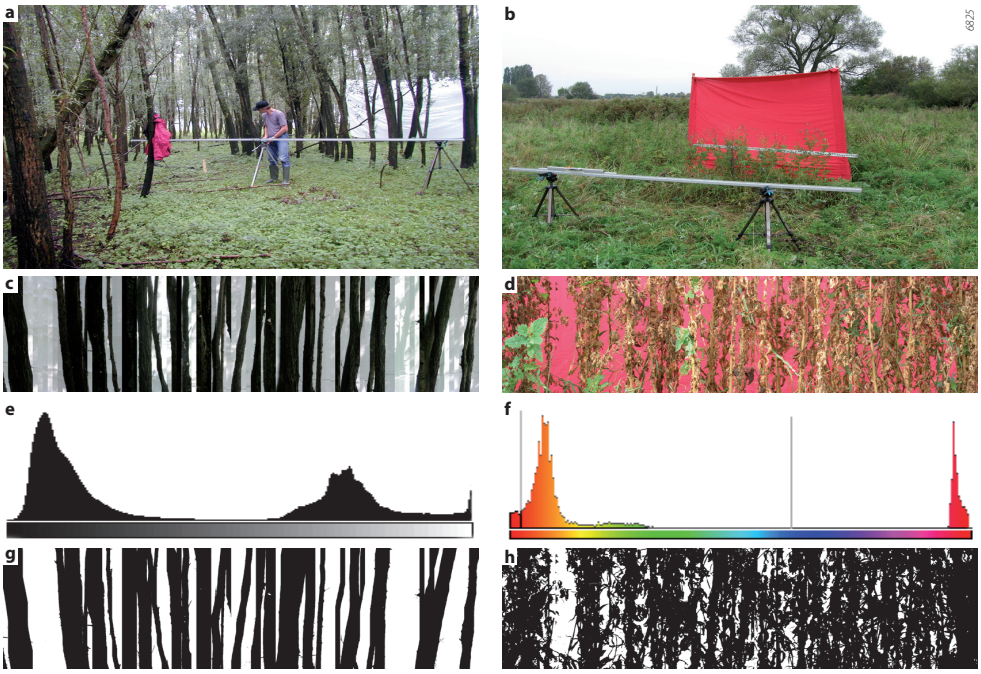

Figure 6.2 Parallel Photography (PP) methods: a,b) setup of the guide rail for the camera and background for forest and herbaceous vegetation, c,d) derived parallel photo-mosaics, e) histogram of intensity values (0 to 255) with threshold, f) histogram of hue values (0 to 360) with thresholds, g,h) thresholded images

background screen (m), γ = opening angle of the camera (°), *ccd* = horizontal size of the recording sensor (5.69 mm), and *f* = focal length of the lens (mm).

To determine the fractional coverage of the vegetation on the composite images, pixels representing vegetation were separated from pixels showing the background screen by means of digital thresholding. Thresholding of the images taken in the forest using the white background screen occurred on the intensity values. Tree stems showed a lower intensity than the white background and the histogram displayed a clear bimodal distribution of the intensities of the image (Fig. 6.2e). The threshold was not determined by the same value for all images, but had to be determined after visual inspection of the histograms, since in several cases illumination of the vegetation by the sun could generate a higher intensity than shadow parts of the background screen creating spectral overlap between the classes. For herbaceous vegetation, a red background screen was used which enabled successful thresholding on hue value of the image (Fig. 6.2f). This has the additional advantage that intensity differences in the image do not affect the estimate of the fractional coverage as the hue is not influenced by shadow. Since the hue of the red background screen is known, the thresholding was carried out with a standard threshold at 10 and 270°.

The vegetation density value was subsequently estimated using the method of MacArthur & Horn (1969), rearranged to:

$$D_{v,PP} = -D_p^{-1} \bullet \ln(1-fc) \quad (6.7)$$

where D_p is the depth of the plot (m) between camera and screen, and fc is the fraction of the image covered by vegetation.

The quality of the PP method to predict vegetation density was evaluated by comparing the results with the densities determined by the manual *Nd*-method in the plots with straight stems using regression analysis.

6.4.3 Sensitivity analysis

The sensitivity of the PP method was determined for (1) the number of selected centre columns, (2) errors in plot depth measurements, (3) camera displacement length, and (4) photo resolution. Firstly, the influence of the number of centre columns on the derived fractional coverage of the vegetation was determined for one plot of herbaceous vegetation. The correct *c* value was 12, and the sensitivity was determined by a stepwise increase of the c value from 6 to 48 pixels. Secondly, D_p was in some cases not clearly determined due to overhanging herb stems. The effect on the resulting vegetation density of a 5, 10 and 20 cm error in D_p was determined as a function of plot depth. Thirdly, the minimum spacing between subsequent photos to derive an accurate estimate of vegetation density is determined. For this purpose, sub samples at regular intervals were taken, and the standard data processing was carried out on each of the sub samples. Finally, the effect of image resolution was evaluated for a single plot by taking photos at three different resolutions, with 2272, 1600 and 1024 pixels horizontally. The resolution of the resulting photo-mosaics was reduced in a stepwise manner to further increase the number of different resolutions.

6.5 Vegetation density measurements using TLS

6.5.1 Field reference data

The TLS measurements required georeferencing of the laser scans and the stem map. For this purpose, fifteen wooden pickets were placed around the forest patch in the GW floodplain section. The position of these pickets relative to ordnance datum was determined by a Trimble dGPS resulting in a 2 centimetre precision. A stem map was created, comprising 650 trees covering 50 percent of the area of the forest patch (Fig. 6.3). Stem locations were measured using a Trimble 5600 tacheometer with a Geodimeter 600 control unit. Position and northing of the tacheometer were derived by measuring the relative position of at least two pickets with known coordinates. The position of the stem centre at breast height was determined by combining the angle measurement of the position of the reflector in front of the tree, and the distance measurement of the reflector next to the centre line of the tree. Due to the limited visibility from the trees, the tacheometer had to be placed at six different positions in the forest to be able to map all trees in this area. Of each tree, the number of side branches at breast eight was determined. The vegetation density was computed for 23 plots based on the stem map plus the number of side branches for each stem (Fig. 6.3). The diameter of the side branches was not

Figure 6.3 Data collection for TLS, with dGPS pickets (5 of 24 depicted), scanner locations, stem locations, and polygons outlining the field plots and stem-based plots.

measured, but set to an estimated value of 1 cm. The vegetation density was based on the stem map. Twenty-three plots were defined inside the area of the mapped stems (Fig. 6.3). Trees inside each plot were selected, and the vegetation density was computed using the *Nd*-method based on stems plus side branches.

Additional pickets were placed in the forest at all positions of the laser scanner. The accuracy of the derived stem map was determined by predicting the position of the scanner positions pickets from two tacheometer positions. The predicted position of these pickets differed less than 10 cm.

6.5.2 Experimental setup

The terrestrial laser scanning was carried out in August 2005 using the Leica HDS3000 time of flight laser scanner (table 6.1). This instrument was chosen for its large range (100 m) and large field of view (360° horizontal by 270° vertical). A disadvantage of this scanner is the relative low pulse repetition rate (Fröhlich & Mettenleiter 2004). Before each scan, digital photos were made using the on-board 1 Mpixel camera, which covered the whole field of view of the scanner. Colour information of these photos was used for visualisation of the resulting point cloud.

Nine different scans were made from eight different scanner positions (see table 6.2; figure 6.3). The effective scan distance appeared to be 25 m due to the occlusion by the trees. Therefore,

Table 6.1 Specifications of the Leica HDS3000 time of flight laser scanner

Field of view	360˚ by 270˚ (two windows)
Vertical field of view of the lower window	-45º to +32.5º
Pulse rate	up to 1800 H2
Spot size	6 mm at 50 m distance
Positional accuracy	6 mm at 50 m distance
Minimal angle increment	60 µrad
Optimal effective range	1 – 100 m
Digital camera	24˚ by 24˚ 1 Mpixel camera
Total weight	~ 28 kg[b]

a. dependent on resolution and field of view; b. 16 kg for scanner, 12 kg for power supply unit

Table 6.2 Point densities per scan

Scan position	no. of points horizontally	no. of points vertically[a]	Percentage of missing points
1	3500	1000	0.71
2a	1876	1500	5.40
2b	1500	1000	1.76
3	1500	1000	1.15
4	3440	1250	0.72
5	2000	1000	1.52
6	4000	1000	2.07
7	2500	1000	0.49
8	2500	563	4.94

a. The vertical range was limited to -45˚ to +32.5˚ deviation from the horizontal plane for this study.

scanning positions were spaced about 15 m apart to maintain enough overlap between the scans. From each scanner position, detailed scans were made of the visible pickets. This was used for initial georeferencing of the point clouds.

6.5.3 Data processing

Pre-processing of the data consisted of registration of the separate scans using the iterative closest point algorithm of Besl & McKay (1992) as implemented in the proprietary software of the data vendor, Delfttech. The data was converted to Dutch ordnance datum, and separated by scan position. Additionally, the scanner position, rotation and scan resolution were listed.

Similar to the PP method, data processing consisted of the computation of the vegetation density based on equation 6.3 of MacArthur & Horn (1969), now written as:

$$D_{v,TLS} = (d2 - d1)^{-1} \bullet \ln(N_{d1}/N_{d2}) \tag{6.8}$$

where N_{d1} and N_{d2} are the number of laser hits occurring behind distances *d1* and *d2* from the scanner, respectively. The first term was introduced to enable the computation of the vegetation density locally over the interval between *d1* and *d2*. Two problems arise while applying this

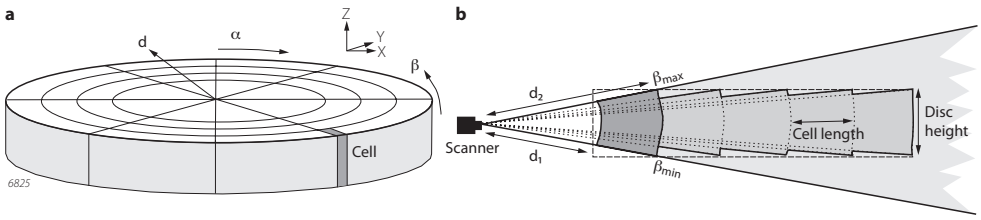

Figure 6.4 Terrestrial laser scanning methods: a) conversion of XYZ coordinates to polar coordinates around the scanner ($\alpha\beta d$), and the selection of points within the disc-shaped space around breast height, b) side view of the cell structure to compute the $D_{v.TLS}$. Cell height remains equal, but β_{min}, and β_{max} vary with distance d.

model. Firstly, some pulses are emitted, but do not return since they do not hit any target, or the targets reflectivity is too low. Secondly, the model assumes a random distribution of vegetation elements perpendicular to the viewing direction at a certain distance away from the scanner, an assumption that does not hold in a forest with few trees.

The following steps were taken to compute spatially distributed vegetation density values. To enable comparison with the field reference data, which was collected at breast height, only the points around breast height were selected. Figure 6.4a shows a 3D scheme of the disc, encompassing the field sampling range at breast height. A polar grid was constructed with the scanner position as the origin and with the disc as the vertical boundaries. The polar grid had curved cells with a horizontal increment of 4°, and a cell length of 0.5 m. The height of the disc

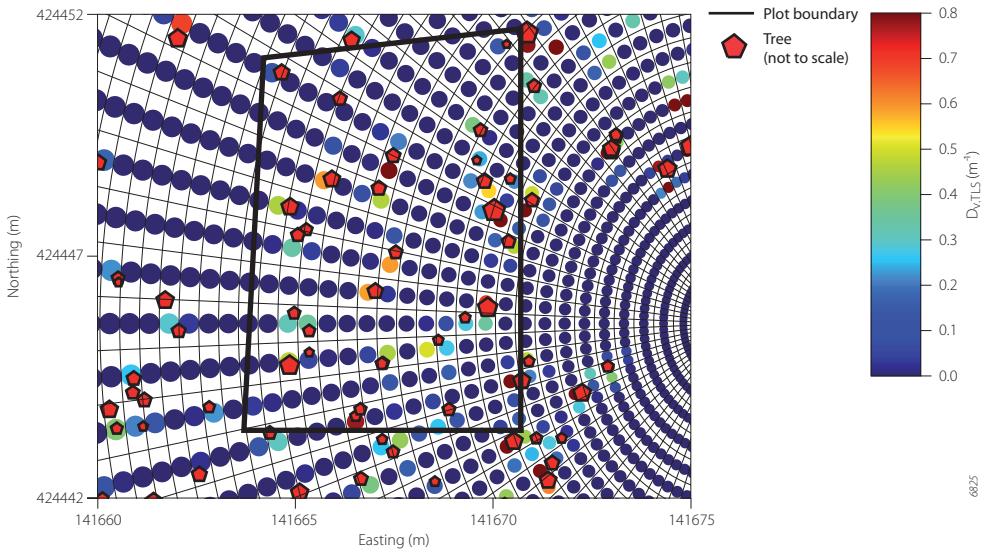

Figure 6.5 Plan view of $D_{v.TLS}$ values per polar cell, tree locations (trees are sized with diameter, but not to scale), and outline of a field plot

was set to 1 m, the vertical angular boundaries of the cells (β), therefore, declined with distance to the scanner (d; figure 6.4b). The data was converted from the orthogonal ordnance datum (XYZ) to a polar coordinate system around the scanner position ($\alpha\beta d$). Missing points were taken into account by computing the total number of emitted laser pulses that passed through the distal boundary of a cell in case no obstruction was present ($N_{tot,i}$), computed as:

$$N_{tot,i} = NED_h \bullet (\alpha_{max,i} - \alpha_{min,i}) \bullet NED_v \bullet (\beta_{max,i} - \beta_{min,i}) \tag{6.9}$$

where NED_h and NED_v are the number of emitted pulses per degree in horizontal and vertical direction respectively, $\alpha_{max,i}$ and $\alpha_{min,i}$ are the horizontal angular boundaries of cell i (a difference of 4° for all cells), $\beta_{max,i}$ and $\beta_{min,i}$ are the vertical angular boundaries of the distal boundary of cell i (°). $N_{d1,i}$ for cell i was derived from:

$$N_{d1,i} = N_{tot,i} - N_{d0\text{-}d1,i} \tag{6.10}$$

where $N_{d0\text{-}d1,i}$ is the number of points in the wedge between the scanner (at d=0 m) and the proximal boundary of cell i. Likewise, $N_{d2,i}$ was computed. The final equation to predict the vegetation density per cell becomes:

$$D_{v.TLS,i} = \frac{1}{d2_i - d1_i} \cdot \ln\left(\frac{N_{tot,i} - N_{d0-d1,i}}{N_{tot,i} - N_{d0-d2,i}}\right) \tag{6.11}$$

The radial cells were subsequently back transformed to the Dutch ordnance datum to obtain the vegetation density map.

To validate the density estimates determined using the TLS, the cell centres were overlain with the field plots. To compare the $D_{V.TLS}$ values with the density estimates of the plots based on the stem map, the non-random positioning (clumping) of the trees perpendicular to the viewing direction had to be taken into account. Figure 6.5 gives an example of the polar grid with $Dv_{TLS,i}$ values, the plot boundary, and the position of the trees. It is clear that at a specific cell distance only one or two cells contain vegetation. Since the method assumes equal density in all equidistant cells, the vegetation density was computed over all cells with an equal distance to the scanner ($Dv_{TLS,d1\text{-}d2}$) by:

$$D_{v.TLS,d1-d2} = \frac{1}{d2,i - d1,i} \cdot \ln\left(\frac{\sum_{d1,i}^{d2,i} N_{tot,i} - N_{d0-d1,i}}{\sum_{d1,i}^{d2,i} N_{tot,i} - N_{d0-d2,i}}\right) \tag{6.12}$$

which combines all hits within the cells within the plot with equal distance from the scanner. The $D_{v.TLS,d1\text{-}d2}$ values was assigned to all cells with an equal distance within the plot. A weighted average of the cells per plot was used to compare with the reference density value based on the stem map. Weights were based on the surface area of the cells.

6.6 Results

6.6.1 Parallel photographic method

Figure 6.6a shows the scatter plot of the manually measured $D_{v.Nd}$ for the field plots against the $D_{v.PP}$ values. The PP method proved well able to predict vegetation density of floodplain forest: the linear regression model explains 99.6 percent of the variance. The regression function is given by:

$$D_{v.Nd} = 1.0059 \bullet D_{v.PP} \qquad (n=17, R^2=0.996, RSE = 3.7\ 10^{-3}\ m^{-1}) \qquad (6.13)$$

A Students t-test proved that the slope of the regression model did not significantly differ from the line of identity at the 99.9 percent confidence level. Figure 6.6b shows the results of applying of the PP method to herbaceous vegetation in summer (n = 9) and in winter (n = 5), and to forest with leaves (n = 12). Summer vegetation displays the largest deviations from the line of identity, since the manual reference data (*Nd*-method) does not include leaves and side branches, thus giving under-estimates for the true D_v. Senescent herbaceous vegetation seemed slightly overestimated by $D_{v.PP}$.

Results of the sensitivity analyses are displayed in figure 6.7. The accuracy of the vegetation density estimate $D_{v.PP}$ depends on the spacing between the subsequent photos (Fig. 6.7a). For the forest plot, D_v estimates become unreliable when the spacing becomes larger than 20 cm. For the herbaceous plot, the largest deviation occurred also at the largest spacings, but some variation remained at the smaller spacings. Fractional coverage of the vegetation varied less than 1 percent from the average when the number of centre columns selected for the composite was varied between 6 and 48 (Fig. 6.7b), the standard deviation was 0.0013. Resolution strongly influences the derived vegetation density estimates (Fig. 6.7c): a coarser resolution leads to considerably higher estimates of D_v using the fixed hue threshold for this herb plot. The two peaks of the bimodal histogram of the hue values became wider, which resulted from more mixed hue pixels.

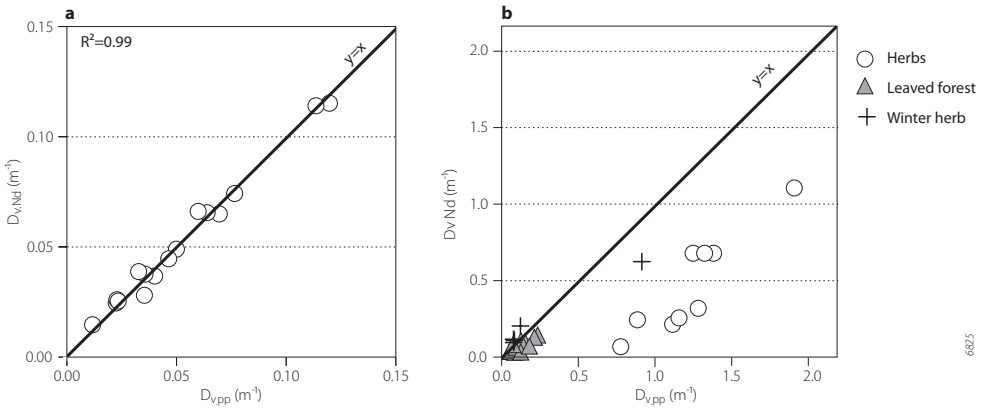

Figure 6.6 Results of the PP method: a) prediction of the vegetation density (D_v), b) application of the PP method to leaved forests, shrubs, and herbs

The step-wise decrease resulted from sub sampling the original mosaics, which smoothed the columns based on subsequent images. Errors of 5, 10, or 20 cm in the measured distance between the camera and the screen, D_p, result in increasingly large errors in the estimate of Dv when D_p is smaller than 2 m (Fig. 6.7d). When the error in D_v is expressed as a percentage of D_p, then it appears that a 10 percent error in D_v results from a 12 percent error in plot depth.

Figure 6.8 TLS point cloud, with the points coloured using the built-in camera.

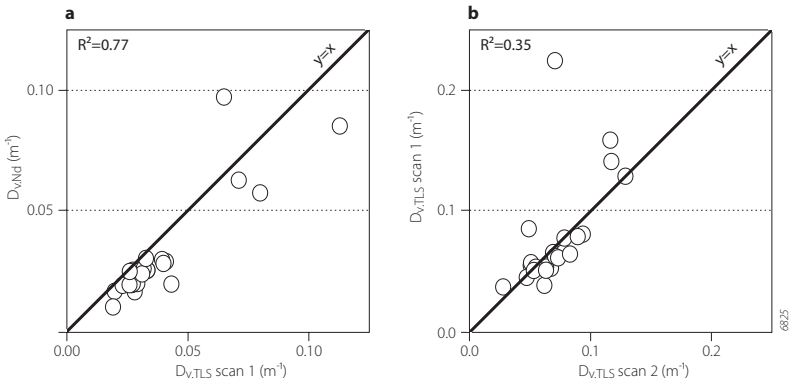

Figure 6.9 a) scatter plot of vegetation density prediction using Terrestrial Laser Scanning, b) comparison of predicted values for plots scanned from two angles

6.6.2 TLS method

Figure 6.8 shows a part of the point cloud of scan number 8 with the points coloured by the on-board photo camera. The scanner position is just behind the viewpoint of this point cloud. The hiding effect of the trees shows as linear black stripes. Figure 6.9a shows the results of the comparison of the $D_{v.TLS,d1\text{-}d2}$ values with the D_v values obtained by the *Nd*-method on plot level (eq. 6.13). The linear regression model

$$D_{v.Nd} = 0.87 \cdot D_{v.TLS} - 0.005 \; (n = 23, R^2 = 0.77, RSE = 0.022) \tag{6.14}$$

fits well with the data, but the higher density values show larger residuals. These are based on the relatively small plots (10 m^2) at large scan distances (15-20 m). A Student's t-test on differences in slope showed that the regression slope does significantly differ from the line of identity at the 99.9 percent confidence level. A leave-one-out bootstrap procedure showed that the regression slope varied between 0.75 and 1.02. On average, the $D_{v.TLS}$ values were 0.015 higher that the $D_{v.Nd}$

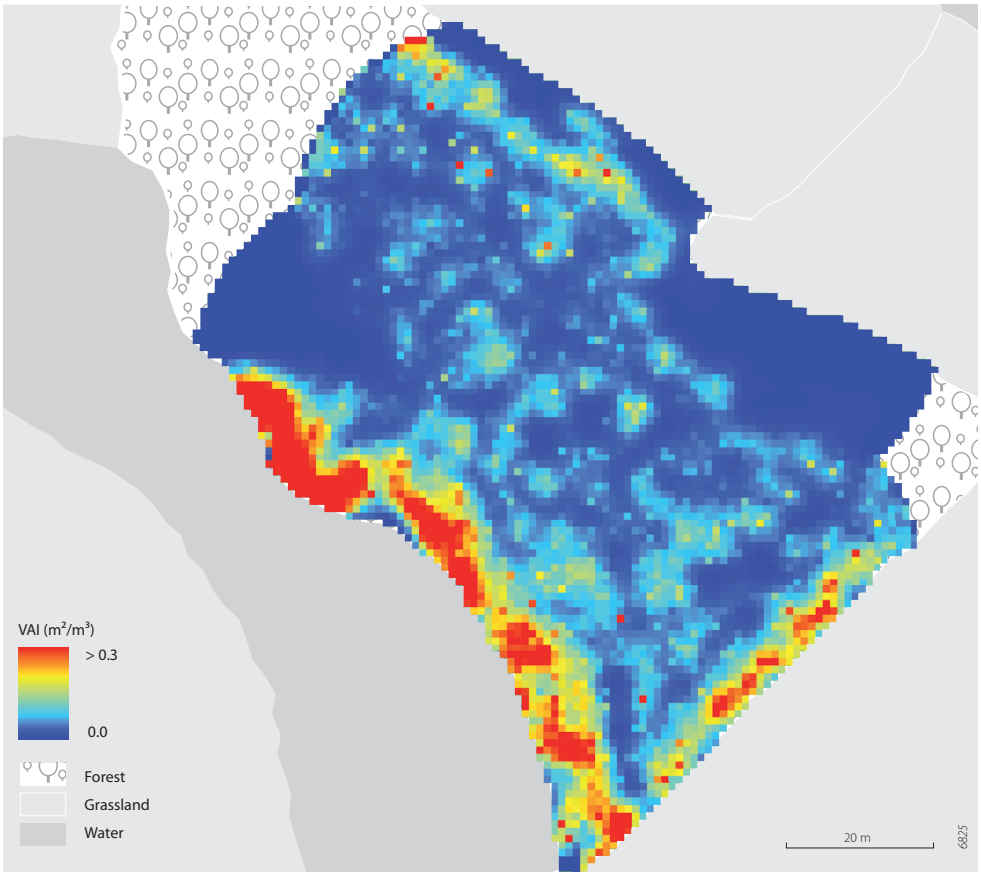

Figure 6.10 Spatial distribution of vegetation density at breast height ($D_{v.TLS,i}$) of the forest patch. Dense forest edges show up along the southern side.

values. The vegetation density prediction for field plots that were scanned from multiple angles shows a weak correlation (R^2 = 0.31; figure 6.9b), again the largest outliers are from small plots at large distances. All scans combined resulted in a 2D map of the vegetation density at breast height (Fig. 6.10). The southern borders of the forest patch show up as a denser part, which was also observed in the field.

6.7 Evaluation of the methods

6.7.1 PP method

The PP method predicted the vegetation density of the reference plots very well (R^2 = 0.996; RSE = 3.7 10^{-3}). The slope of the regression line did not deviate from the line of identity at the 99.9 confidence level. This means that the PP method directly gives the vegetation density, without the need of calibration, for vegetation densities up to 0.12 m^{-1}, which is dense forest. The support of the PP method is easily changed by increasing the distance to the screen, and the length of the guide rail for the camera. The results were consistent when this method was applied to leaved forest plots, and herbaceous vegetation as the PP method showed much higher density values than the manual *Nd*-method. The resolution of the raw images influences the vegetation density estimates, but the maximum camera resolution of 2272 pixels in horizontal direction appeared sufficient in the applied sample configurations in both forest and herbaceous floodplain vegetation. The *Dv* estimates derived from the PP method proved largely insensitive to the correct number of centre columns from which the composite image was established, but when all columns are selected, the vegetation elements close to the camera are over sampled. This overestimates the vegetation density with a 0.008 residual standard error to the line of identity, and the regression slope did deviated from the line of identity at the 99.9 level of confidence (Warmink 2007.). The plot depth (D_p) should be accurately measured. Especially herbaceous vegetation was prone to falling over when space was created to put the guide rail and background in place. This could be avoided by placing a frame of fixed size (e.g. 3 m wide and 1 m deep) around the vegetation plot to be photographed. The spacing between subsequent photos from which the composite is established should not be too large, at most 20 cm.

The white colour of the background screen that was used for forest generated well interpretable bimodal histograms of the intensity value, but spectral overlap remained present between illuminated vegetation and shadows on the screen. Consequently we had to determine the threshold value in the image segmentation manually. While Zehm *et al.* (2003) suggested to using a black background instead of a white screen to avoid erroneous thresholding, we successfully avoided illumination differences by using a red background and subsequently thresholding on the hue value of the images. After evaluating the histograms of all images, it seems that a purple screen might be even more adequate for this purpose, as this hue is virtually absent in vegetation (Fig. 6.2f).

Since the validation in the manually sampled reference plots with a simple vegetation structure has demonstrated that the PP method performs well, the PP can now be well applied in complex and herbaceous vegetation types, with irregularly shaped stems and shoots, where manual sampling becomes a tedious operation. Still, the PP method is time consuming (30 minutes

per plot), while the plot size for which the method yields D_v estimates are bounded by the dimensions of the slide rail and the distance to the background screen.

6.7.2 TLS method

Terrestrial laser scanning of vegetation density also proved successful (n = 23, R^2 = 0.77, RSE = 0.022), with the additional advantage that it results in a full 2D distribution of the vegetation density. The TLS method has been applied to a forest with straight stems, where the vegetation density varied between 0.01 and 0.19 m^{-1}. Again, the method does not involve calibration. The leaves present in the height interval around breast height cause higher estimates of the vegetation density from the TLS method. The leaves were not included in the manual reference data obtained using the *Nd*-method. Additionally, the optical point quadrate method assumes that the range measurements are infinitely thin, whereas the TLS data have a spot size of 6 mm at 50 m distance. This could over-sample the vegetation when only the side of a pulse hits a stem or twig. Compensation could be made using the intensity value of the reflected pulse, but the laser scanner used did not have that capability. A possible source in the prediction errors may be the fact that we compared vegetation density values computed in a radial grid with field plot boundaries. The edges of the radial grid did not fully coincide with the field plots. Consequently, individual trees just outside a field plot might be included in the TLS grids and contributed to the DV_{TLS} estimate.

Computationally, the current method can easily be extended to 3D when the vegetation density is computed for all cells in the polar grid, instead of only the cells around breast height that were used for in this study. With the current dataset, full 3D analysis was impossible as the vertical angle ranged between -45° and +32.5° relative to the horizontal plane.

The time of flight scanner was chosen for its 100 m effective range, but the actual penetration distance into the forest was rarely more than 25 m due to occlusion. Therefore, we advise to use a phase-based scanner in future studies as their 50 m effective range suffices, and the scan rate is much higher, 150 kHz at least (Fröhlich & Mettenleiter 2004) compared to 1.8 kHz of the scanner used in this study. The lower positional accuracy of the phase-based scanners will not affect the bulk vegetation density value extracted. Such a phase based scanner could be placed at more positions within the vegetation leading to increased detail, which would facilitate registration of the scans, and opens up the possibility of deriving vegetation density values for denser vegetation types like shrubs and herbs. The drawback is the increased computation time due to the high number of points.

6.7.3 Comparison

Both the parallel photographic method and the terrestrial laser scanning method were well able to predict the vegetation density of the floodplain vegetation reference plots, but the PP method showed a higher predictive quality and no significant deviation from the line of identity. The PP method is best used to calibrate airborne and space borne remote sensing data, or to fill lookup tables with accurate hydrodynamic vegetation density values. The TLS method is more appropriate to generate spatially distributed vegetation density values, whereas the PP method only provides a bulk density value averaged over a field plot. The 3D mapping abilities of TLS, for example, are more suited to compare spatial patterns in forest structure mapped using airborne laser scanning.

The time required for a single and experienced surveyor to measure a field plot using the PP method consists of 20 minutes to set up the equipment and to take the photos, and another 10 minutes for the data processing. TLS is more labour-intensive and computationally intensive. It needed 8 hours to scan 0.6 hectares of relatively open forest using the Leica HDS3000 time of flight scanner. Registration took the data vendor 3 days since no pickets were mapped for the two first scans and 'all trees looked alike'. Placing the pickets around the forest and georeferencing by dGPS took 4 hours. Data processing using Python code took 2 hours on a Pentium 4 desktop computer with a 1.6 GHz processor and 512 Mb RAM memory. TLS is also more expensive. The costs of buying the PP equipment amounts to 1000 euro, the 1-day rent of the TLS scanner totalled 3500 euro, which included scan registration.

6.8 Conclusions

Hydrodynamic vegetation density is an important input parameter for floodplain flow models, but the current manual field methods to obtain reference data assume cylindrical stems or lack in spatial support. In this paper, we describe two new methods to derive accurate and objective field reference data of hydrodynamic vegetation density, which assumes rigid vegetation: (1) the Parallel Photographic (PP) method, and (2) the Terrestrial Laser Scanning (TLS) method. Both methods are based on the optical point quadrate method. The PP method involves the computation of the fractional coverage of vegetation against a contrasting background on a digital photo mosaic of parallel images. We showed that the PP method predicts the vegetation density very well (R^2 = 0.996; RSE = 0.0037) up to vegetation densities of 0.12 (m^{-1}), which is a dense forest, without the need for calibration. The method is also flexible as the support is easily changed by increasing the distance to the screen, and the length of the guide rail for the camera. The sensitivity analyses showed that the resolution of the raw images should be as high as possible, and that an accurate estimate of the plot depth that is photographed is the most important parameter. Hue transformation of the composite images showed that a background of a dark blue or purple hue would be most appropriate for future studies instead of white or red.

The TLS method performed slightly less (R^2 = 0.77, RSE = 0.022) up to vegetation densities of 0.19 m^{-1}, and deviated from line of identity, probably due to leaves. Nevertheless, the TLS method has the advantage that (1) it does not require calibration, (2) it results in a spatial distribution of vegetation density, (3) is easily extended to 3D, and (4) the support has a variable size. The PP method is more efficient to collect reference data with respect to costs and time.

Acknowledgements

This study was financially supported by NWO, the Netherlands Organization for Scientific Research, within the framework of the LOICZ program under contract number 01427004. We would also like to thank Norbert Pfeifer and Romain Auger for their constructive comments and field assistance.

7 3D float tracking: In-situ floodplain roughness estimation

To be submitted

Abstract

This paper presents a novel technique to quantify *in situ* hydrodynamic roughness of submerged floodplain vegetation: 3D float tracking. This method uses a custom-built floating tripod that is released on the inundated floodplain and tracked from shore by a robotic total station. Simultaneously, an Acoustic Doppler Current Profiler (ADCP) collects flow velocity profiles and water depth data. Roughness values are derived from three methods based on (1) run-averaged values water depth, slope and flow velocity to compute the roughness based on the Chézy equation, assuming uniform flow, (2) the equation for one-dimensional free surface flow in a moving window, and (3) the zero plane displacement of the flow velocity profiles. A sensitivity analysis using synthetic data proved that the median value of the roughness, derived using method 2, is independent of (1) the noise in water levels, which ranged from 1 to 9 mm, (2) bottom surface slope and (3) topographic undulations with a sinusoidal shape and an amplitude of up to 1 m. Field measurements were carried out on two floodplain sections with a vegetation height of 0.030 (Arnhem) and 0.043 m (Dreumel). Method 1 resulted in a Nikuradse roughness value of 0.08 m for both locations. Method 2 gave 0.12 m for Arnhem and 0.19 m for Dreumel. Contrary to the sensitivity analysis, the derived roughness values showed a skewed log-transformed distribution. In Arnhem, a spatial pattern of roughness values was present, which might be related to fractional vegetation cover or vegetation density during the flood peak. Method 3 generated unrealistically high roughness values. 3D float tracking proved a flexible and detailed method for roughness determination in the absence of waves.

Key words: hydrodynamic roughness, submerged vegetation, total station, ADCP, *in situ* measurements

7.1 Introduction

Floodplain vegetation is a key issue in current river management (Tsujimoto 1999). It provides numerous niche habitats for fauna, which is positive for a high biodiversity, but a succession of natural vegetation in regulated rivers will lead to an increase in of roughness and, hence, to a decrease of floodplain discharge and consequently an increase in flood water levels (Nienhuis & Leuven 2001; Baptist *et al.* 2004; Van Stokkom *et al.* 2005). Besides topography, floodplain

vegetation roughness is the key hydrodynamic parameter controlling the floodplain flow pattern during peak discharges. Referring to Kouwen & Li (1980 and Baptist (2005), the most important parameters that determine vegetation roughness are (1) vegetation structural characteristics height, number of stems per m^2, stem diameter and (2) hydraulic parameters such as water depth, shear stress or flow velocity. Numerous flume experiments have been reported to verify predictive models of vegetation roughness. For example, Kouwen & Fathi-Moghadam (2000) and Armanini *et al.* (2005) measured the instantaneous drag force of flowing water on vegetation directly. Others measured hydrodynamic parameters like water surface slope, flow velocity profiles and water depth to derive the roughness, (e.g. Klaassen & Van der Zwaard 1974; Kouwen & Li 1980; Carollo *et al.* 2002; Järvelä 2002; Järvelä 2004). These flume experiments are typically characterized by low water depths and high water surface slopes, which are conditions that do not occur during flooding of lowland floodplains.

Relatively few studies have been carried out to estimate *in situ* floodplain roughness during overbank flooding. Freeman *et al.* (1996) note that it is difficult to locate field sites where water depths are sufficient to inundate the floodplain and where a crew can safely perform the measurements. Moreover, field surveys are labour-intensive and timing depends on peak discharges. Nonetheless, Van Urk (1981) summarizes roughness values from three field campaigns in which roughness of meadows was derived from either the Chézy equation or flow velocity profiles. He also indicates the sensitivity of the obtained roughness values on the water surface slope (WSS), which was derived from water level measurements at gauging stations at the upstream and downstream ends of an 850 m long floodplain section that was laterally separated by an embankment from the main channel. An alternative for gauge measurements of WSS was presented by Dietrich & Smith (1983) who used a leveller to characterize the water surface topography in a small meander bend. The beacon with a sharply pointed base was held 80 cm upstream of the surveyor wading the stream, resulting in a 2 mm precision. This method improves the spatial detail of the water height distribution compared to gauging stations, but it can not be employed for larger water depths or flow velocities. Therefore, Biron *et al.* (2002) measured water heights along a 30 m long river section encompassing a confluence using a total station to survey the position of a reflector mounted on a custom built raft. The raft was tethered by cross-stream tie lines. Five water levels were measured for each cross section of approximately 10 m wide. Vertical resolution of the reflectors position was accurate to less than 1 mm at distances less than 30 m. This resulted in a high spatial resolution, but for large channels, cross-stream tie lines are inconvenient, and surveying a large area would be time consuming.

The aim of this research was to determine the *in situ* hydrodynamic vegetation roughness of submerged vegetation on a large scale in lowland floodplains using a method that is easily applied at various locations. To that end, a new method was developed: 3D float tracking (Fig. 7.1), which comprises a reflector, mounted on a custom-built floating tripod that floats along with the current. The reflector is automatically tracked using a shore-based total station and an Acoustic Doppler Current Profiler (ADCP) mounted underneath the float that collects data on flow velocity profiles and water depth. Three methods to obtain roughness from this data, based on the Chézy equation, based on the equation for free surface flow, and vertical flow velocity profiles, are compared (Van Rijn 1994).

7.2 Deriving roughness values from field data

Three different methods were tested to derive roughness values from 3D float track data. The first method (M1) assumes uniform flow conditions, and uses the Chézy formula:

$$u = C(hi)^{1/2} \tag{7.1}$$

in which u = depth averaged flow velocity (ms^{-1}), C = Chézy friction coefficient ($m^{1/2}s^{-1}$), h = water depth (m), i = downriver water surface slope (-). For the M1 method run-averaged values for u, h and i are derived from the float track data. The second method (M2) assuming one dimensional free surface flow under subcritical conditions is described by the momentum equation (Van Rijn 1994):

$$\frac{dQ}{dt} + \frac{d}{dx}\left(\alpha \frac{Q^2}{A}\right) + gA\frac{dz_s}{dx} + \frac{Og\,\bar{u}^2}{C^2} = 0 \tag{7.2}$$

in which Q = discharge (m^3s^{-1}), t = time (s), x = distance along channel (m), α = integration constant, assumed to be 1, A = cross-section averaged area (m^2), g = acceleration of gravity (ms^{-2}), z_s = water surface level above horizontal plane (m), O = wetted perimeter (m), $\bar{u}$ = cross-section averaged flow velocity (ms^{-1}), For wide channels, O equals the channel width, and for stationary flow dQ/dt becomes zero. Under these conditions, equation 2 simplifies to

$$u\frac{du}{dx} + \frac{gu^2}{hC^2} - gi = 0 \tag{7.3}$$

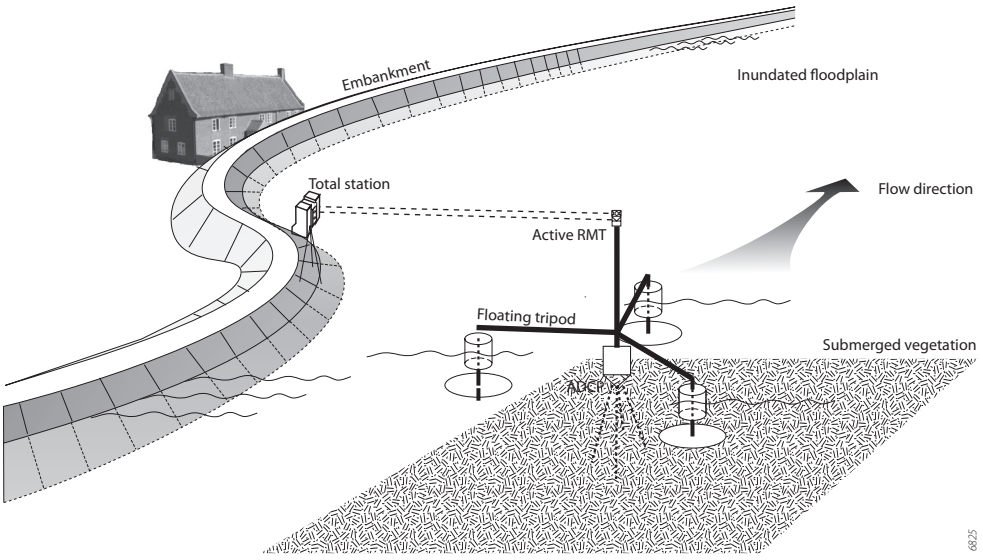

Figure 7.1 3D sketch of the method

where u is the depth averaged flow velocity. The Chézy coefficient is then computed as:

$$C = \sqrt{\frac{gu^2}{h\left(gi - u\frac{du}{dx}\right)}} \tag{7.4}$$

Equation 4 will be referred to as the gradually varied flow equation. All parameters on the right hand in equation 7.4 will be derived locally from the float track data. The Chézy coefficients resulting from the M1 and M2 method were converted to the Nikuradse roughness length, k (m), according to the White-Colebrook formula (Keulegan 1938):

$$C = 18 \log(12h/k) \tag{7.5}$$

The third method (M3) is based on the zero plane displacement of the logarithmic velocity profile, which is based on the validity of the Kármàn-Prandtl expression for hydraulically rough flow, and assumes that the velocity profile is logarithmic in the lower part of the water column (Van Rijn 1994):

$$u_z = \frac{u_*}{\kappa}\ln\frac{z}{z_0} \tag{7.6}$$

where u_z = flow velocity at height z (m) above the bed (ms^{-1}), u = shear velocity (ms^{-1}), κ = Kármàn constant (-), z_0 = roughness length (m). In this research, the flow velocity measurements in the lower half of the water depth are used to increase the number of flow measurements for the fit of the flow profile. The roughness length is the height above the bed at which u_z = 0, and is converted to k roughness by

$$z_0 = 0.033\ k \tag{7.7}$$

For the M3 method, therefore, vertical flow velocity profiles need to be measured, preferably close to the river bed. In this research velocity profiles are measured using the ADCP.

7.3 Materials and methods

7.3.1 Site selection and description

High demands were put on the hydrodynamic characteristics of the field sites. The float needs at least 0.5 m of free flowing water above the submerged vegetation, but the required discharge had to be as low as possible to increase the opportunity for field measurements. The total station needed an unrestricted view from the shore to the float to enable tracking of reflector. Moreover, the downstream end of the measurement section should not be covered with forest to maintain safety for the surveyors. Site selection was carried out using the ecotope map of the Dutch Ministry of Transport, Public Works and Water Management (Jansen & Backx 1998) to select different vegetation types. Predictions of the local hydrodynamic conditions at various

flood stages were derived from a 2D hydrodynamic model of all Rhine distributaries, which was calibrated to a flooding event with discharges varying between 5800 and 11900 m^3s^{-1} at Lobith.

Two floodplains along the Rhine distributaries were selected as field sites (Fig. 7.2). Both are inundated only during high discharges. The 'Green River' in Arnhem is a 700 m long and 200 m wide secondary channel within a large meander pointbar of the Nederrijn river. The upstream end of the Arnhem site is connected to the main channel of the Nederrijn and the downstream end feeds into a floodplain nature reserve (Fig. 7.2(2)). The minimum required discharge for measurements is 6500 m^3s^{-1} at Lobith to provide a sufficient water depth and flow velocity for the measurements. Land cover consisted of meadow (dominated by *Lolium perenne*), which was mowed before the winter. The topographic height differences are less than 0.4 m with a maximum terrain slope 0.003 $m \cdot m^{-1}$. In the middle of the floodplain section a fence was present, which restricted the length of the measurable flow path to 350 m. The second

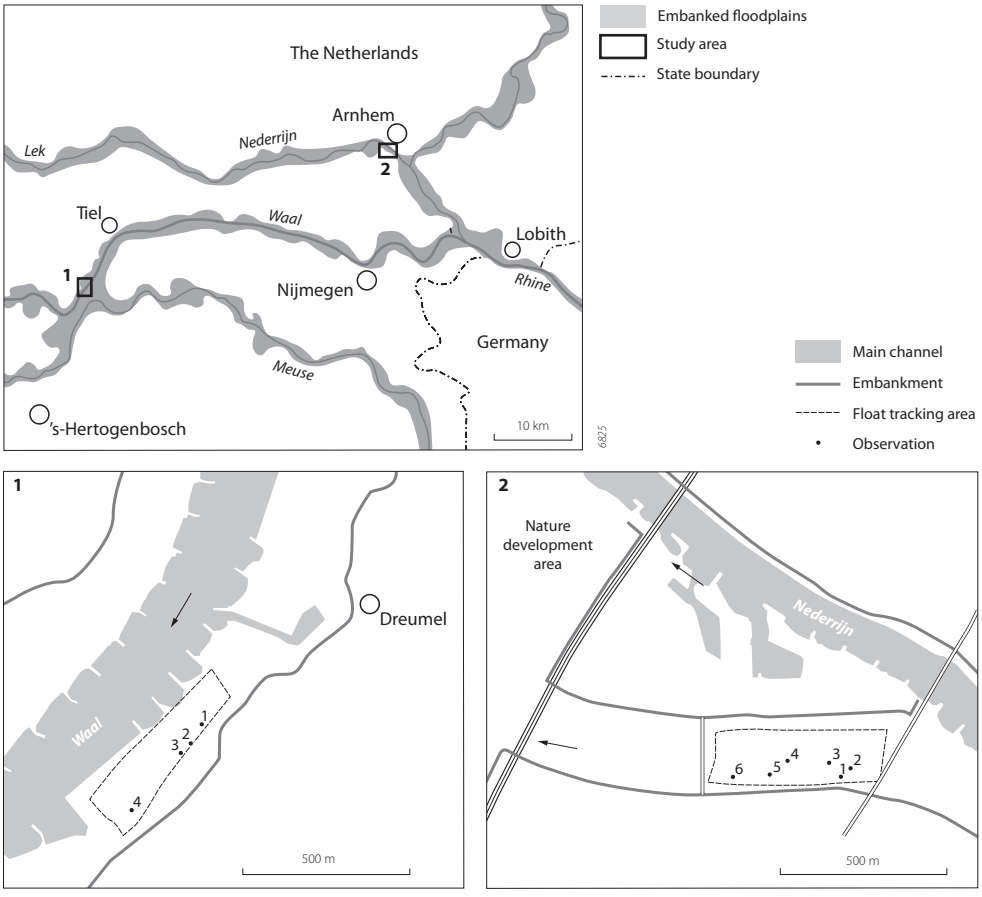

Figure 7.2 Field locations. Measurements were carried out within the dashed areas, vegetation observations were at the numbered points

site was situated along the left bank of the river Waal close to the village of Dreumel (Fig. 7.2). The whole floodplain section was laterally connected to the main channel. Minimum discharge needed for measurements was 6000 m^3s^{-1} at Lobith. Land cover was identical to the Arnhem site, but the vegetation was not mowed before the winter, but it was grazed intensively. Therefore, some scattered stalks of herbaceous vegetation were present up to 30 cm high (*Molinea caerulea, Rumex obtusifolius, Rumex acetosa*). The topographic height differences were larger (up to 1 m) with steeper slopes (maximum 0.02 $m \cdot m^{-1}$).

After the flood peak, vegetation height was measured at 6 locations in Arnhem, and 4 locations in Dreumel (Fig. 7.2). At each location, 30 individual observations were taken to determine the vegetation height, measured using a measuring rod. The average was used to compare with the hydrodynamic data. The hydraulic stress on the vegetation was obviously not present during the post-flood vegetation measurements. This would lead to an overestimation of the vegetation height as the grass was flexible. Vegetation height is also influenced by the thickness of newly deposited sediment, which could lead to an underestimation of the vegetation height. Real time vegetation mapping was not possible with the present equipment.

7.3.2 3D float measurements

The measurements were carried out using a tripod with an Acoustic Doppler Current Profiler (ADCP) and an on-shore total station. The float was transported to the upstream end of the floodplain section using a boat with a 15 horsepower outboard engine, and it was released to flow freely with the current. At the end of the section it was picked up and transported back upstream. This procedure was repeated around ten times on a single measuring day. The float consisted of three horizontal aluminium bars, each connected to a vertical rod with buoyant foam, a horizontal disc to limit vertical movement and a vertical plate to reduce the displacement due to wind (Fig. 7.3). In total, the float weighed 35 kg.

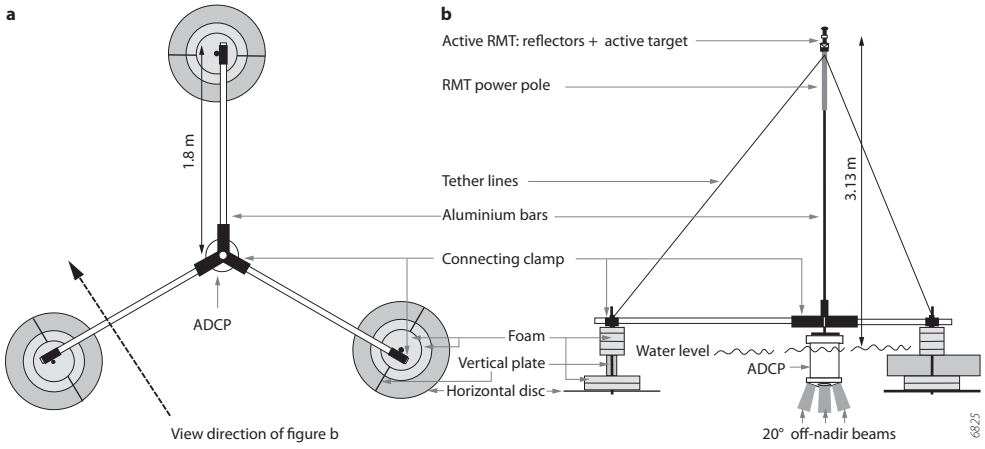

Figure 7.3 Float with equipment a) top view of the float, and b) side view. RMT is the remote target of the total station, ADCP the Acoustic Doppler Current Profiler

ADCP measurements

Flow velocity profiles and relative bottom displacement were measured using a stand-alone broadband ADCP manufactured by RD-Instruments. This ADCP, which included a built-in thermometer, tilt meter and compass, was mounted underneath the float (Fig. 7.3b). A broadband ADCP measures the propagation delay between two consecutive acoustic bursts, so-called pings, to determine the velocity of acoustic scatterers such as sediment particles (RDInstruments 1996). The propagation delay, which is equivalent to the Doppler shift, is measured in four beams, configured in a Janus configuration, with one beam in each of the four main directions under a 20° off-nadir angle (Fig. 7.3b). Each beam is subdivided in vertical bins of a user-specified height. By combining the flow direction of three beams in a specific bin, the three-dimensional flow vector is computed at that specific depth below the ADCP. Since the ADCP has four beams, flows vectors are computed based on four different combinations of three beams. This redundant information enables the computation of the error velocity and correlation between the four flow vectors. Due to the acoustic side lobe effect and the beam angle of 20°, the flow velocity in the lower 6 percent of the profile can not be determined (RDInstruments 1996). Consecutive pings are averaged into 5 s ensembles in this study to reduce noise. The blanking distance, which is the part of the water column directly below the ADCP that can not measured, amounted to 26 cm. Table 7.1 gives an overview of the ADCP settings used in the present study. The ADCP was used to determine (1) the float velocity using the bottom track option, (2) deviations from the float velocity in the water column and (3) the water depth.

Water surface height

The water surface height was measured using a shore-based total station that locks on the active Remote Measuring Target (RMT) mounted on the float (Fig. 7.3b). This configuration is also known as a robotic total station. The Trimble 5602 total station used, had an angular accuracy, expressed as the standard deviation, of 0.5 mgon and a distance accuracy of ± 5 mm plus 2 $mm \cdot km^{-1}$ (Trimble 2006). The RMT is a 360° remote target (Trimble RMT606) suitable for

Table 7.1 Settings for the stand-alone ADCP

Acoustic frequency	1200 kHz
Configuration	4 beams, convex, down looking
Beam angle	20°
Beam divergence	1.2°
Pressure sensor	yes
Bottom tracking	yes
Velocity accuracy (according to specifications)	0.3 % of the velocity relative to the ADCP ± 0.3 cm s^{-1}
Ping rate	10 Hz
Bin height	10 cm
nr of depth cells	50
Ensemble interval	5 s
Bottom track mode	5 (shallow water)
Profiling mode	1 (dynamic sea state)
Bottom track pings	20
Pings per ensemble	20
Ping duration	0.03 s

measurements over distances up to 350 m. It consisted of six prismatic reflectors and an active target. The six prisms are configured in a circle. Therefore, always one of the prisms is oriented towards the total station. The active target emits a coded control signal, which is detected by the total station and is powered by the power pole (Fig. 7.3b). This gives additional range information that is used in the internal software for range verification. The RMT needed to be employed high above the water surface to prevent erroneous height measurements due to multipath effects reflected via the water surface. In addition, the total station was positioned just above the water level, to ensure that the RMT was higher than the total station. The float was positioned in a local coordinate system, and the positioning frequency was 2 Hz. Additionally, time was exported for each position to allow merging of the total station data with the ADCP data during data processing. A compass indicated the north direction, which was used as the zero horizontal angle of the total station. The position of the total station relative to the Dutch ordnance datum was determined using a handheld GPS with an estimated point error of 5 m. The absolute elevation of the total station was determined using a nearby water-gauge.

7.3.3 Extraction of roughness values from float data

Pre-processing of the total station data consisted of conversion of the local coordinate system to ordnance datum, and computation of the cumulative distance travelled from the start (x in m). Depth averaged flow velocity per ensemble was computed using the ADCP data. However, the ADCP profile did not cover the whole water column due to side lobe effects at the bottom, and the blanking distance of 26 cm plus the transducer depth of 25 cm at the top. The height of the side lobe effect was determined by analysis of the average correlation per bin. In case the correlation was less than 100 (scaled to 255), the bins were discarded. Such low correlations were obtained for two or three bins above the ground surface. Four computationally separate

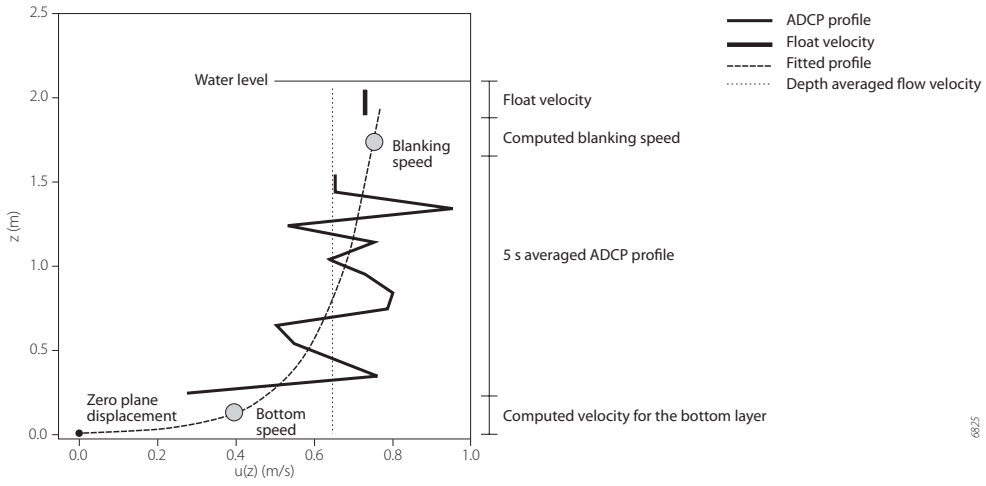

Figure 7.4 Example of a flow velocity profile from the Dreumel floodplain section showing the depth ranges with the associated (1) float velocity, (2) computed blanking speed, (3) 5 s averaged ADCP profile, and (4) the computed velocity for the bottom layer. Reconstructed velocities are based on the fitted logarithmic velocity profile with a 6.6 mm zero plane displacement.

intervals are present in the flow vertical (Fig. 7.4). The bottom track of the ADCP equalled the float velocity derived from the total station data. This float velocity was assumed to represent the averaged water flow velocity over the upper 30 cm of the profile, which is the depth below the water surface of the vertical plates of the float. The flow velocities of the blanking distance and the bottom range were computed using the logarithmic flow velocity profile (eq. 7.6). The roughness length related to the zero plane displacement was assumed to be 0.2 m following Van Urk (1981), thereby setting the zero plane height to 6.6 mm (eq. 7.7). The flow profile was fitted on the ADCP data and float velocity, but was constrained by forcing it through the zero plane height. The resulting logarithmic profile was used to compute the velocity at the middle of the blanked height interval and the middle between the ground surface and the lowest bin boundary. The depth averaged flow velocity was computed as the mean of the flow velocities weighed by the height interval they represented. Data of the total station and the ADCP were merged using the time tag of both datasets.

To compute roughness values using method M1, water surface slope, flow velocity and water depth were averaged over the whole length of each individual run. The slope was determined using a linear regression of distance travelled from the start versus water surface height. The M2 method was applied in a 1D moving window and for each position of the float, the Chézy coefficient was computed (eq. 7.4). Acceleration (du/dx) and slope were computed within a moving window of 80 m long for Arnhem, and 200 m in Dreumel to avoid negative values under the root sign (eq. 7.4). The depth-averaged velocity was also averaged within the window to reduce noise.

7.3.4 Sensitivity analysis

A sensitivity analysis was carried out to estimate the sensitivity of the derived roughness value to noise in the water level measurements, varying window size, bottom slope and ground surface undulations. The sensitivity analysis consisted of (1) numerical computation of a backwater curve using the predictor-corrector method (Van Rijn 1994), (2) adding uniformly distributed noise to the water surface and (3) computation of the Nikuradse roughness in a local window based on the hydrodynamics derived from the backwater curve. The computation of the backwater curve using the predictor-corrector method needs a ground surface profile, downstream water depth and a bottom roughness as input. The downstream flow velocity was computed using equations

Table 7.2 Standard input parameters for water surface curve computation, see figure 7.5 for explanation of the parameters

Parameter	Setting
length	500 (m)
downstream bottom slope	10 ($cm \cdot km^{-1}$)
water depth	1.5 (m)
Nikuradse roughness	0.15 (m)
cell length	0.5 (m)
amplitude	0.3 (m)
noise	4 (mm)
window size	40 (m)

7.5 and 7.1. The ground surface profile was represented by 0.5 m long 1D cells. For each of the cells, the water depth was predicted using the hydrodynamic data of the downstream cell plus the bottom slope, which was subsequently corrected using the same hydrodynamic characteristics for the cell itself. This method is known as the predictor-corrector method (Van Rijn 1994). Flow velocities per cell result from the water depths as derived from the backwater curve and the continuity equation:

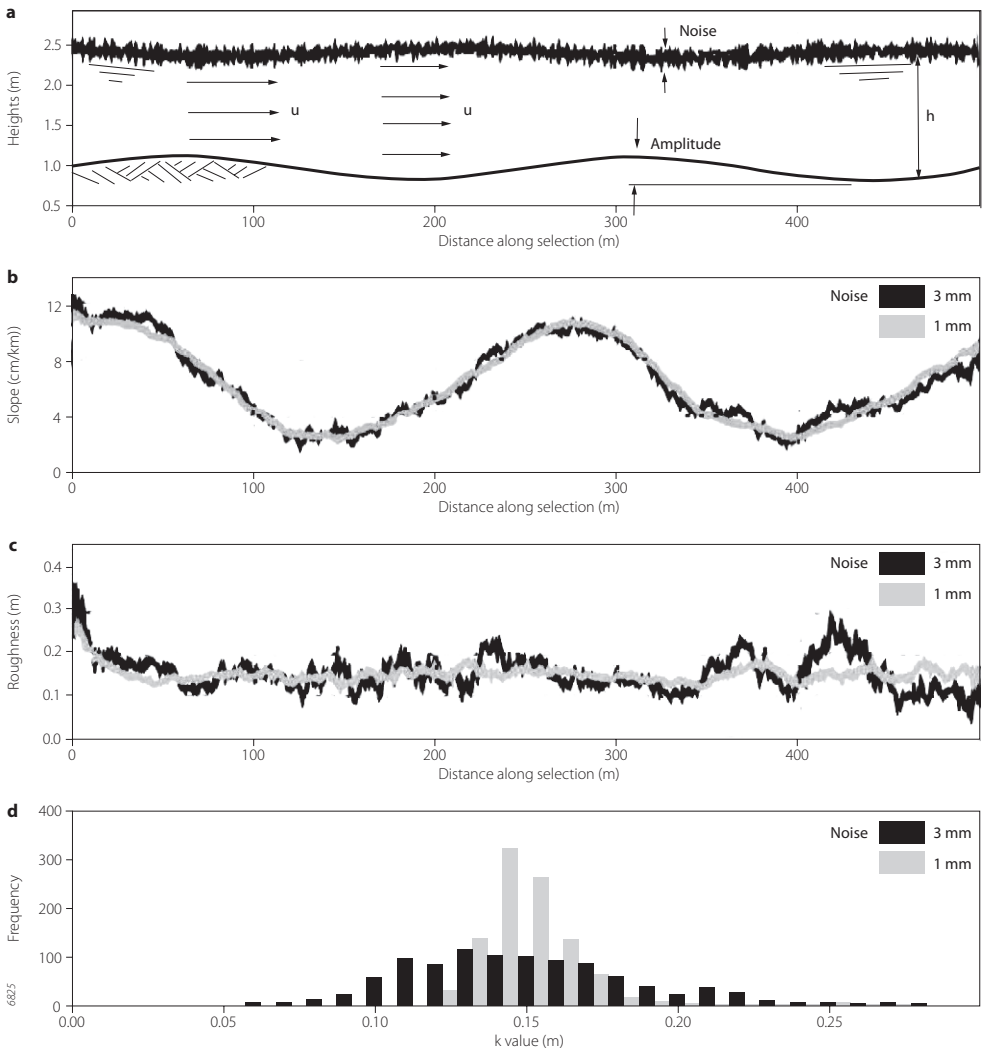

Figure 7.5 Methods of the sensitivity analysis a) Computation of the backwater curve based on the ground profile, water depth, roughness (k = 0.15 m) and at the downstream boundary, b) resulting water surface slopes based on 1 and 3 mm uniform noise added to the water levels, c) derived k values in a local window, d) histogram of the derived k-values.

$$u_1 h_1 = u_2 h_2 \quad (7.8)$$

With these data, the roughness was computed in a local window for each cell using equation 7.4. The path length of 500 m, combined with a cell length of 0.5 m resulted in 1000 roughness estimates. The sensitivity analysis was carried out using settings comparable to the field situation. The range of noise, as measured in Arnhem, equalled 4 mm in the absence of waves, with a standard deviation of 0.7 mm. The bottom slope was superimposed with a spatially correlated undulation of the ground surface (Fig. 7.5a). Table 7.2 gives the standard input parameters.

Figures 5b-d show examples of WSS, roughness and roughness distribution obtained using two different noise levels. The amount of spatial correlation in the noise determines the effect on the WSS and consequently the derived roughness. The slopes derived from the run with 1 mm uniform noise are less spiky, which translates to a narrow distribution of the derived k values. The procedure described above was used to evaluate the effect on the median and interquartile range (IQR) of the derived k values as a function of noise level, bottom slope, window size, and amplitude of the bottom surface. Nine or ten different runs with a stepwise increase in each variable were carried out. This procedure was used to assess the minimal window length for roughness computation.

7.4 Results

7.4.1 Sensitivity analysis

The dependence of the median value and the interquartile range of the derived roughness values on the range of uniform noise, bottom slope, window size and height of the ground undulations is shown in figure 7.5. Variation of the median value of the derived roughness is less than 2 cm for differences in uniform noise, bottom slope, and undulation amplitude (n = 1000 cells). The median values coincide with the assigned roughness of 0.15 m. The IQR increases with increasing noise, is negatively correlated with bottom slope, and independent of the amplitude of the ground surface variations. However, the median value increases for smaller window sizes, and the distribution of the k values becomes skewed and wider. Nikuradse roughness lengths are normally distributed for window sizes of 30 and higher. This shows that window sizes smaller than 40 m are not appropriate to determine roughness based on local hydrodynamic conditions with a 4 mm uniform noise on the water surface levels.

7.4.2 Field measurements

In January 2004 the method was tested under field conditions in Arnhem and Dreumel during a flood wave with a peak discharge of 6650 m^3s^{-1} and a peak water level of 14.3 m above ordnance

Table 7.3 Key characteristics of the two floodplain sections

Floodplain	Date	Vegetation height (m)	WSS ($cm \cdot km^{-1}$)	Water depth (m)	Flow velocity (ms^{-1})
Arnhem	18-01-2004	0.030	5.9	1.2	0.41
Dreumel	20-01-2004	0.043	8.8	2.5	0.74

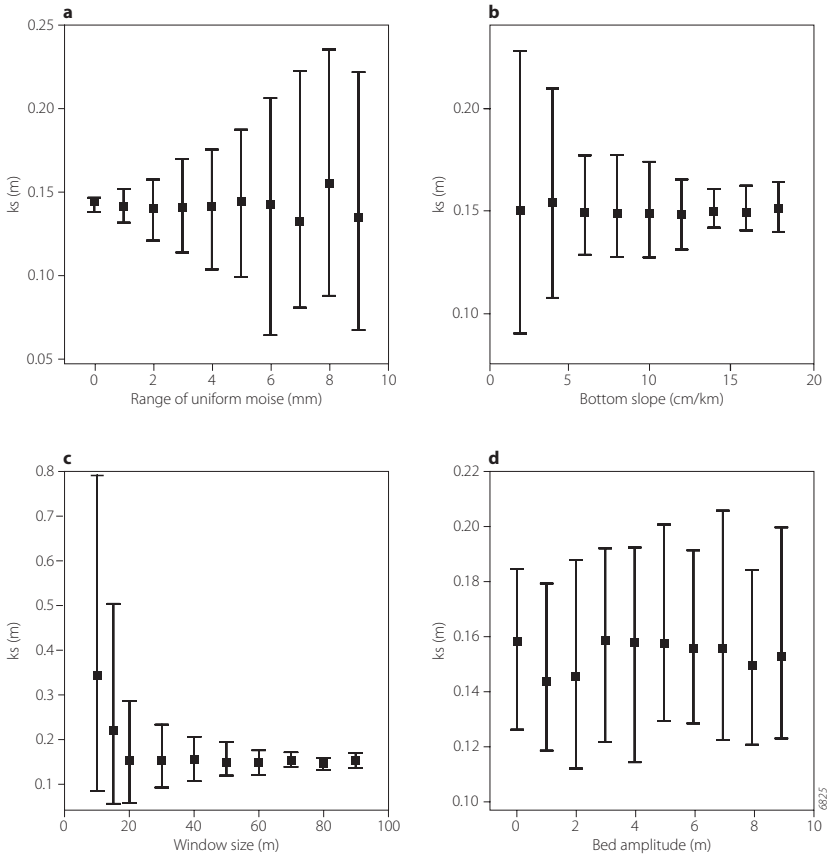

Figure 7.6 Results of the sensitivity analyses using the gradually varied flow equation showing the median (■) and interquartile range of the roughness as a function of a) the range of uniform noise on the water levels, b) bottom slope, c) window size, and d) amplitude of the elevation of the river bed elevation. Assigned roughness was 0.15 m.

Table 7.4 Vegetation heights and standard deviation (between brackets) of 30 individual height measurements (cm), see figure 7.2 for observation locations.

point	Arnhem	Dreumel
1	4.1 (1.9)	3.9 (1.4)
2	4.2 (1.7)	3.4 (1.1)
3	3.6 (1.3)	4.6 2.5)
4	1.9 (2.1)	5.4 (1.6)
5	2.1 (2.1)	
6	2.3 (1.9)	

Table 7.5 Derived roughness values using three different methods.

	Arnhem	Dreumel
M1 D_{50} k (m)	0.08 (IQR = 0.04, n = 7)	0.08 (IQR = 0.06, n = 11)
M2 D_{50} k (m)	0.12 (IQR = 0.15, n = 9573)	0.19 (IQR = 0.30, n = 12082)
M3 D_{50} k (m)	6.7 (IQR = 11.8, n = 1065)	6.0 (IQR = 7.2, n=1187)

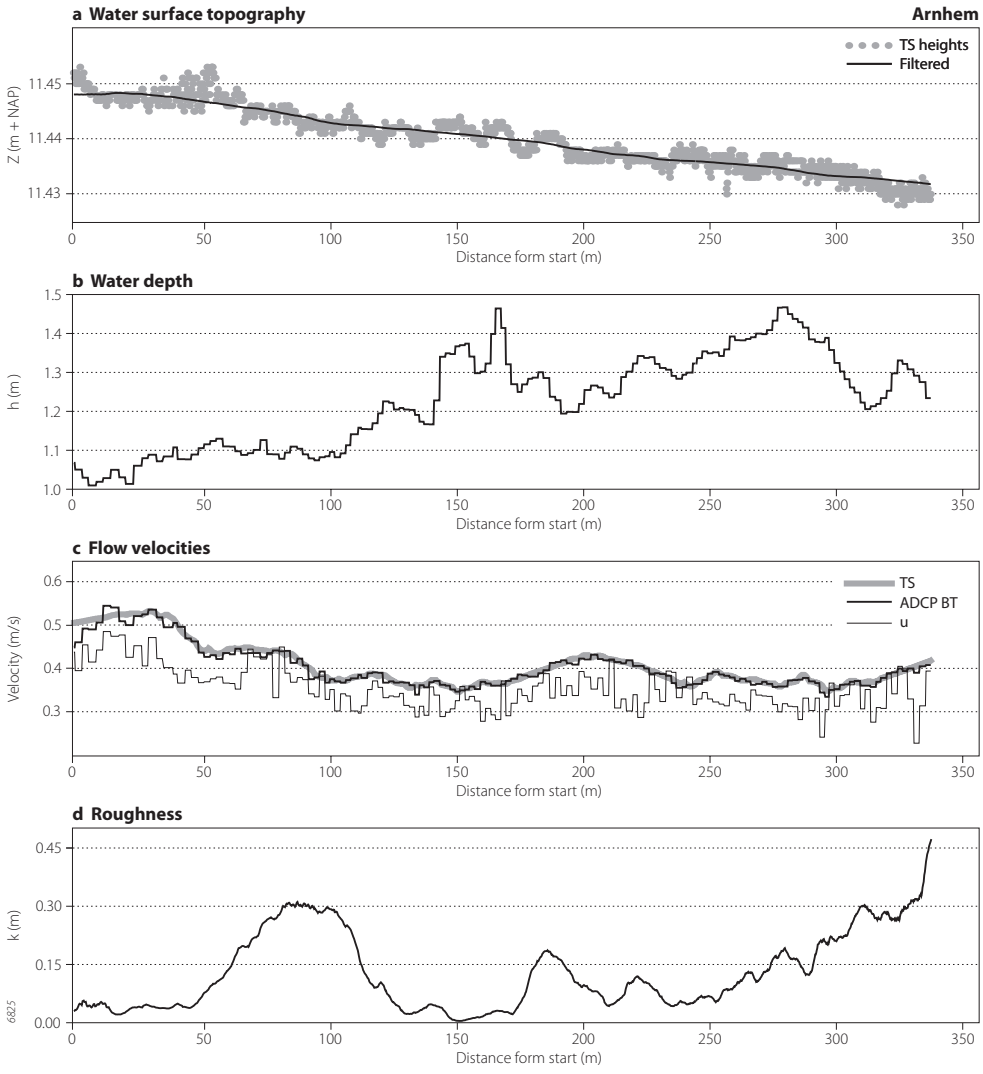

Figure 7.7 Data collected for run 7 in Arnhem a) water surface topography of the raw total station (TS) data and the filtered water levels, b) water depth, c) flow velocities from total station, bottom track option (BT) of the ADCP and depth averaged flow velocity (u), and d) derived roughness using the gradually varied flow equation and a 80 m window length.

datum at Lobith. The recurrence time of this discharge is 2.5 years (Silva 2003). Table 7.3 shows the key hydrodynamic characteristics of the two floodplains. Vegetation heights after the flood are listed in table 7.4. Both measuring days were characterised by low wind speed and clear vision.

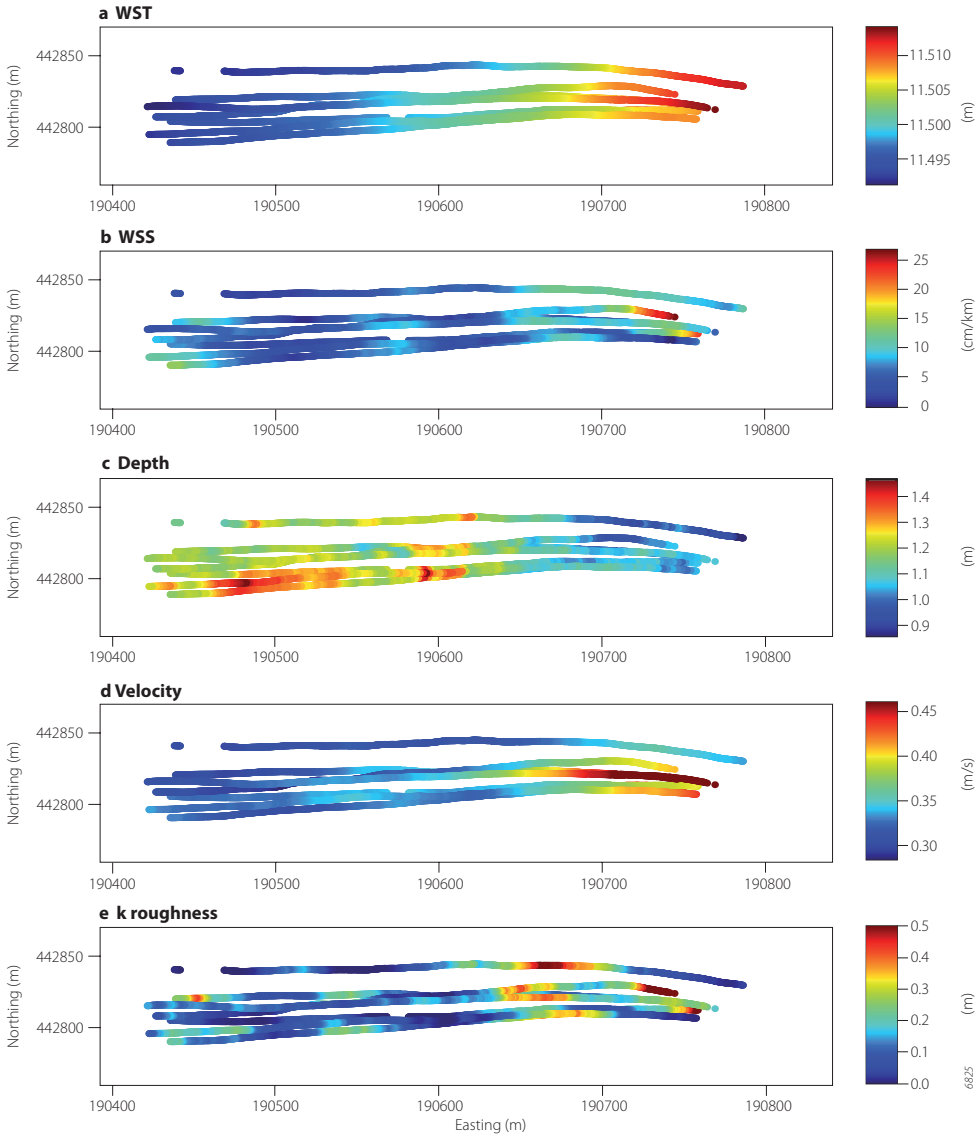

Figure 7.9 Plan view of smoothed data of Arnhem using a 80 m window size a) water surface topography (WST), b) water surface slope (WSS), c) water depth, d) depth averaged velocity, e) Nikuradse roughness using the gradually varied flow equations.

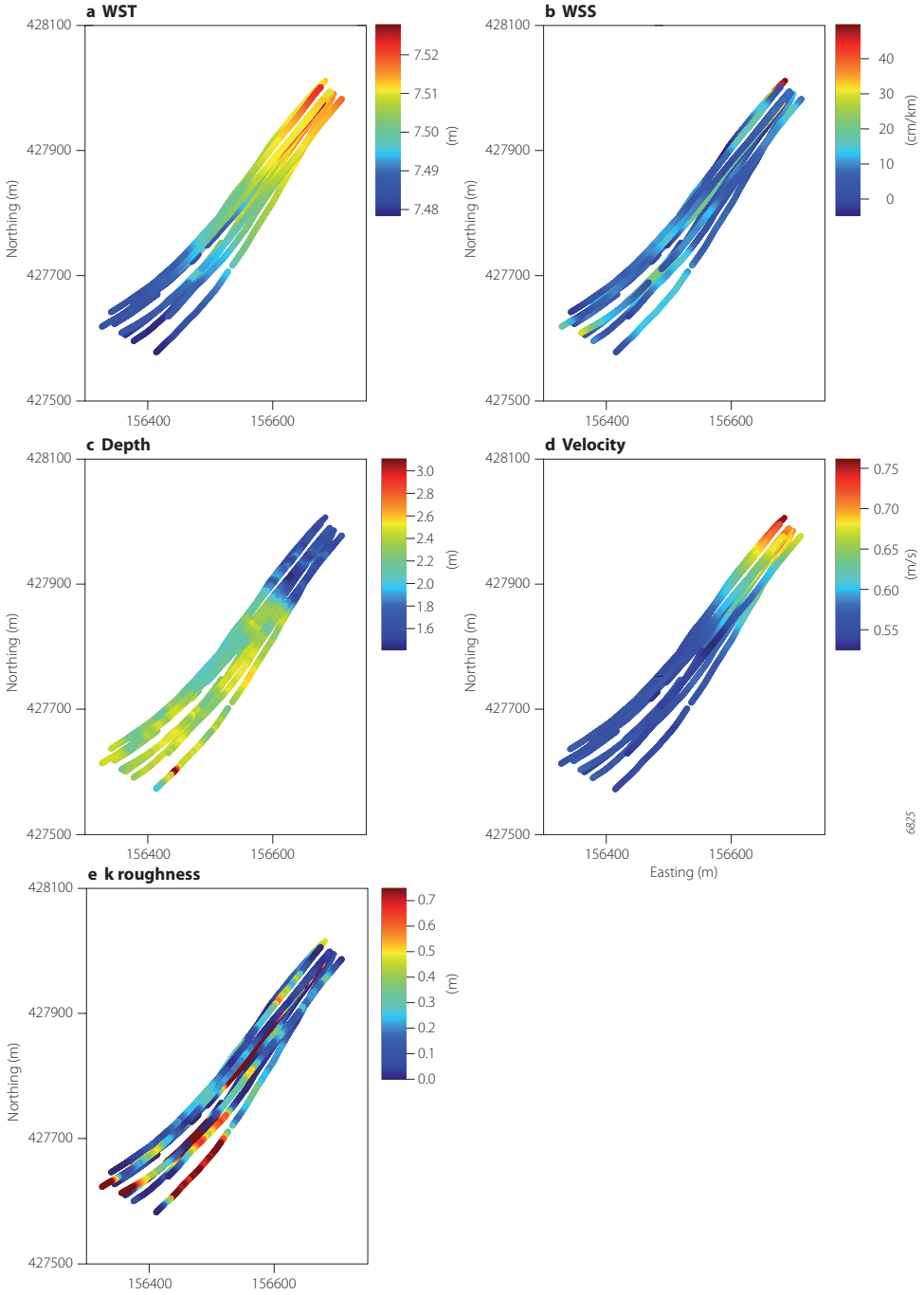

Figure 7.10 Plan view of smoothed data of Dreumel using a 200 m window size a) water surface topography (WST), b) water surface slope (WSS), c) water depth, d) depth averaged velocity, e) Nikuradse roughness using the gradually varied flow equations

Roughness values based on the M1 method gave a median value for k of 0.08 m for both floodplains (table 7.5). The M2 method gives spatially detailed information on water surface topography, water depth, flow velocities and the derived roughness values. Figures 7.7 (page 141) and 7.8 show the details for the Arnhem and Dreumel site respectively. The noise level as well as the spatially correlated undulations of the water surface height were larger in Dreumel than in Arnhem, which is due to the intense navigation on the river Waal and the open lateral

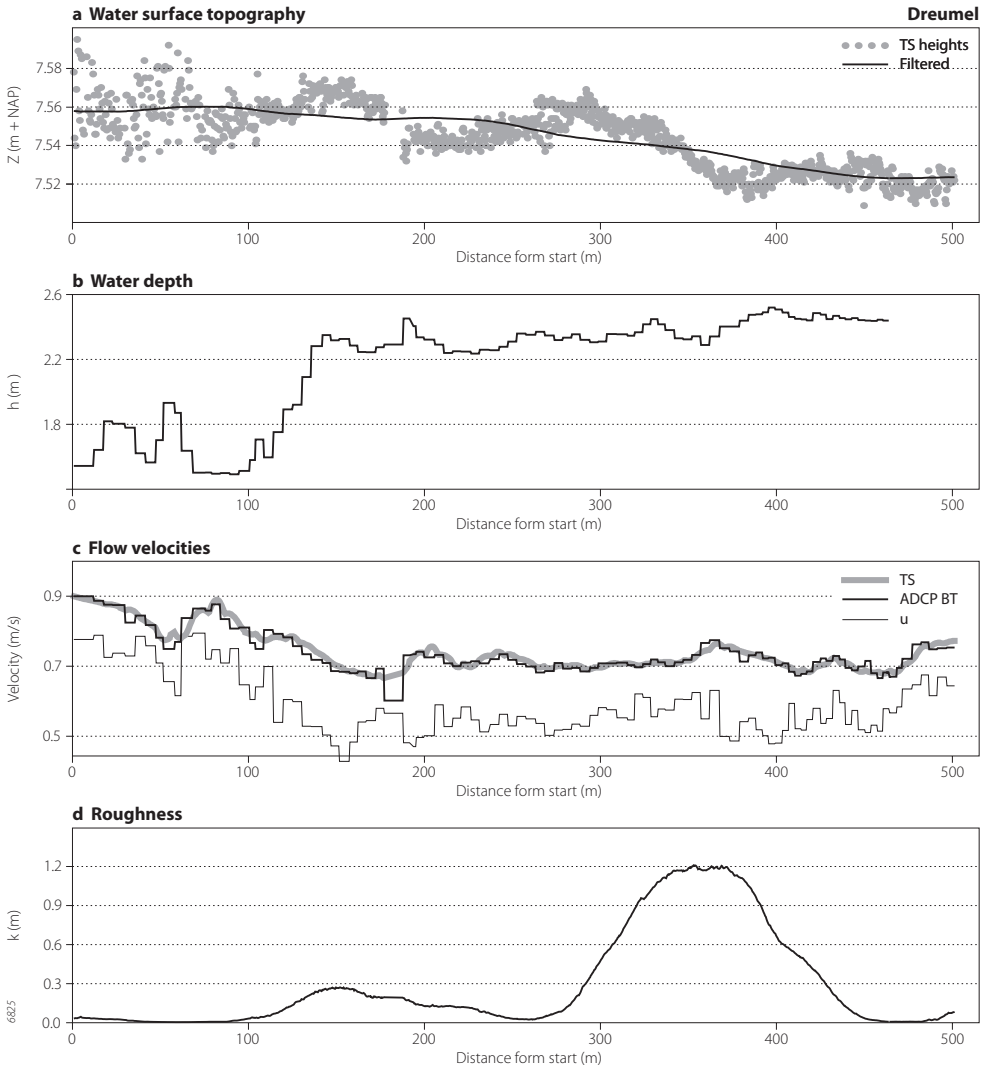

Figure 7.8 Data collected for run 2 in Dreumel a) water surface topography of the raw total station (TS) data and the filtered water levels, b) water depth, c) flow velocities from total station, bottom track option (BT) of the ADCP and depth averaged flow velocity (u), and d) derived roughness using using the gradually varied flow equation and a 200 m window length.

connection between the main channel and the floodplain. Figure 7.7c shows that the bottom track velocity of the ADCP correlates well with the velocity derived from the total station data. The depth-averaged velocity shows a 0.1 ms^{-1} variation per ensemble, which is attributed to turbulence. Plan view images of the smoothed hydrodynamic parameters are given in figures 7.9 and 7.10 (see page 142 and 143). For visualisation purposes, the water surface topography in figure 7.9a and 7.10a has been corrected for variation in water level over the days of measurement, which was 5 cm. Due to the absence of ship-induced waves, the data of Arnhem contain a lot of detail (Fig. 7.9). Downstream of easting 190600, a local topographic high is present of 0.2 m, which led to a decrease of water depth and an increase in the water surface slope. The derived roughness values show spatial correlation. A north to south band of high k-values is visible downstream of easting 190700. Also, at the average northing of the start positions of the individual runs, higher k-values were computed than along the sides.

The normal roughness lengths as well as the log-transformed lengths show a skewed distribution for Arnhem and Dreumel (Fig. 7.11). The range of k-values is larger for Dreumel. The skewed distribution of the field data is contrary to the roughness length distributions of the sensitivity analysis with these window sizes, which are normally distributed. The distribution of log-transformed k-values based on the M_3 method is less skewed for both sites, but the median values are 25 times higher, and the IQR of derived k-values is 11.8 and 7.2 m for the Arnhem and Dreumel sites respectively (table 7.5, figure 7.11).

7.5 Discussion

Float tracking in three dimensions enables the computation of roughness in three different ways. Improvements over current methods (Van Urk 1981; Biron *et al.* 2002) include the increase in accuracy of the local water surface slope. The method generates data with much spatial detail on key hydrodynamic parameters like WSS, depth averaged flow velocity, flow velocity profiles, and water depth.

The sensitivity analysis showed that the noise on the water surface topography does not significantly influence the median value of the derived roughness, even for noise levels twice the measured noise of 4 mm. For the field conditions met in this study, the window size should not be smaller than 40 m based on the sensitivity analysis.

The derived roughness values differ both between the three methods and spatially. The roughness based on the Chézy equation (M_1) is lower than the roughness based on the equation for free surface flow (M_2). This is due to the underlying assumption of uniform flow, which is not valid as both field sites show significant deceleration of the flow (Fig. 7.9d, 7.10d). The M_2 method shows higher roughness values, which was expected by taking the deceleration into account. Derived roughness values show a spatial clustering of high and low values, which can not be explained by noise only. Nor can the differences in roughness of a factor 10 be explained by variation in vegetation height since the site was mowed before winter, and vegetation height measurements after the flood peak showed differences of only a factor two (table 7.4). However, the *fractional cover* of the vegetation also varied along the run trajectories. In the lower lying

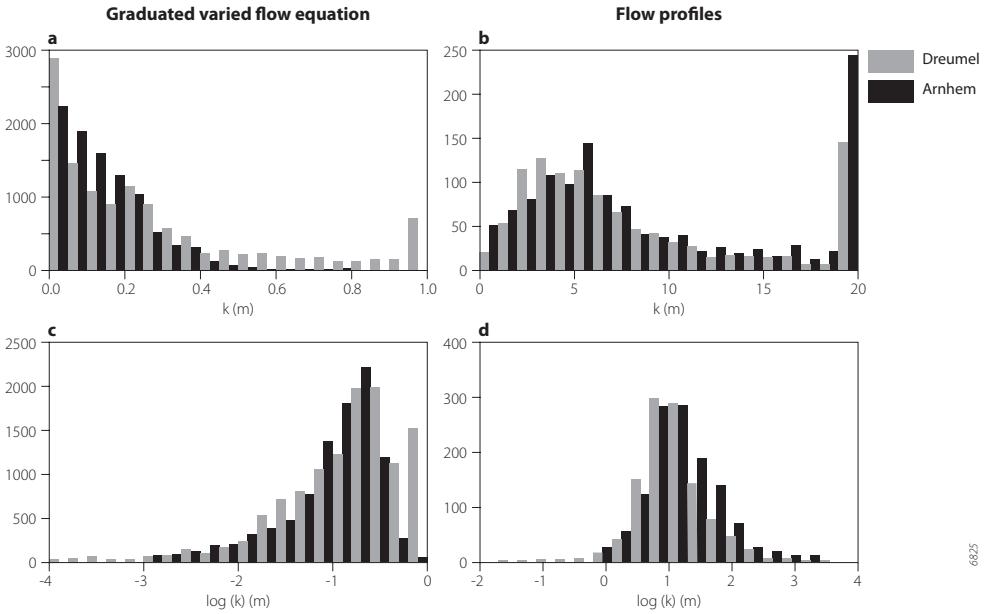

Figure 7.11 Histogram of derived roughness values based on a) 1D equation for gradually varied flow, b) zero plane displacement from flow velocity profiles, c) and d) are the log-transformed histograms of the same data.

parts of the floodplains, much more sediment was deposited, which buried the vegetation to a large extent. This was observed in the field after the flood. Therefore, part of the roughness should be attributed to grain roughness of the sediment rather than vegetation roughness. As the grain size of the sediment was low, the roughness of these areas will also diminish. The area at the start of the section and around 190550 m east (Fig. 7.9), are relatively high, and showed a high fractional coverage of grass. This could explain the higher roughness values at these locations. More detailed information on the fractional coverage could be acquired using post-flood airborne images, or real time data from a pencil-beam acoustic altimeter.

Lateral non-uniform flow, like divergence in plan view, might also lead to errors in roughness computation. A divergent flow pattern was present at the start of the measurement section in Arnhem with higher flow velocities in the centre (Fig. 7.9d). This led to a decrease of the specific discharge, and higher slopes since water is extracted from the flow line. Applying the 2D equation of free surface flow, which needs information on the lateral flow velocity distribution and lateral water surface slope, could solve this. Adding three horizontal ADCPs to the float would allow collection of instantaneous lateral flow measurements. Lateral water surface elevation measurements might be possible by dragging the float in the cross-stream direction. For this purpose, the float would need to be more streamlined to reduce the drag force of the water on the float, and the sensitivity analysis should be extended to 2D. A 2D flow model should be applied in that case to generate the water surface elevation.

The M_3 method resulted in roughness values that were unrealistically high. This resulted from inaccurate flow measurements in the lower 20 to 30 cm of the flow vertical due to the side lobe effect of the acoustic beams. RDInstruments (1996) specified that the lower 6 percent of the water column can not be sampled, but this only holds for infinitely small bins. The accuracy of the flow measurements close to the top of the vegetation could be improved by using a smaller bin height at the expense of more noise in the measurements. Additionally, the small water depth at Arnhem resulted in few bins available for the fit of the flow profile. The ensemble length of 5 s improved the spatial detail of the measurements, but also resulted in large deviations from the logarithmic profile due to turbulence. Muste *et al.* (2004) showed that *static* ADCP measurements generated a stable flow velocity profile only after 15 minutes averaging. In this research, *moving* ADCP measurements were used resulting in different water depths and flow velocities, which decreases the homogeneity of the measurements. Computing the run-average flow profile did not result in better estimates of the zero plane displacement.

3D float tracking was applied to meadows with a low vegetation height. With higher and denser vegetation, the data will be slightly different. The WSS will be higher, which increases the signal to noise ratio of the height measurements by the total station and this may decrease the IQR of the distribution of the obtained roughness values. The water depth as derived from the ADCP becomes unreliable, since it is computed using proprietary software that analyses the intensity profile. Moreover, the ADCP beams have a footprint of 8.65 cm at the transducer and a beam divergence of 1.2°, which limits the penetration capacity in herbaceous vegetation. This problem might be solved by using a pencil beam altimeter with a small beam divergence, a high sampling rate and full storage of the backscatter intensity profile (Marine-electronics 2006). This ensures a higher penetration depth through the submerged vegetation. The full intensity profile might give detailed information on vegetation height under flow conditions and vegetation fractional coverage.

The ADCP flow velocity profile is only valid down to the height of the vegetation. In case of high submerged vegetation, reliable flow measurements inside the vegetation layer that are needed for the depth averaged flow velocity can not be derived from the ADCP, and have to be modeled, or measured by deploying a flow velocity instrument inside the vegetation layer.

7.6 Conclusions

Roughness is an important input parameter for hydrodynamic models, but the past years have shown little progress in field validation of roughness of submerged vegetation. In this study, 3D float tracking showed the ability to map the *in situ* spatial distribution of the water depth, water surface elevation and depth averaged flow velocities along the trajectory of the float. Vertical precision of the water surface height, measured by the total station in robotic mode, proved 4 mm in range with a 0.7 mm standard deviation in the absence of waves. Using these data, roughness values could be determined using three methods based on (1) run-averaged values to compute the roughness based on the Chézy equation, assuming uniform flow, (1) the equation for one-dimensional free surface flow, and (3) the zero plane displacement of the flow velocity profiles.

The sensitivity analysis proved that the *median* value of the roughness, derived using method 2, is independent of (1) the noise in water levels ranging from 1 to 9 mm, (2) bottom surface slope and (3) topographic undulations up to 1 m amplitude. The resulting set of roughness values is normally distributed. Window size, which is used to compute water surface slope and acceleration, influences the median value and should thus not be less than 40 m as method 2 is sensitive to the accurate estimation of the water surface slope.

Field measurements in two floodplain sections, with a vegetation height of 0.030 and 0.043 m, resulted in a Nikuradse roughness length of 0.08 m for both locations using method 1, which is an underestimation. Method 2 gave 0.12 m for Arnhem and 0.19 m for Dreumel, using window sizes of 80 and 200 m. In Dreumel, ship-induced waves on the floodplain necessitated a large window length. Contrary to the roughness values derived in the sensitivity analysis, method 2 showed a skewed distribution of roughness lengths. In Arnhem, a spatial pattern of roughness values was found, which might be related to the fractional vegetation cover during the flood peak. Low roughness values were obtained in the areas with a low vegetation cover. Real time vegetation analysis during flood was not possible with the ADCP. Method 3 generated unrealistically high roughness values, as the lower 20 to 30 cm of the water column could not be sampled using the ADCP due to the acoustic side lobe effect. Reducing the ADCP bin height might partially solve this problem at the expense of more noise in the flow measurements.

3D float tracking is a flexible and detailed method that generates spatially detailed hydrodynamic information, suitable for roughness estimation using the locally solved equation for gradually varied flow. Potential improvements to the technique used in the present study are (1) measurements of lateral flow velocity gradients, (2) detailed echo sounding, which might enable *in situ* vegetation structure analyses and (3) static ADCP measurements.

Acknowledgement

This research has been carried out within the Land Ocean Interaction in the Coastal Zone (LOICZ) program of the Netherlands Organisation for Scientific Research (NWO) under contract number 01427004. I would also like to thank the laboratory for Physical Geography of the Utrecht University for continuous support in refinement of the float model. Claus van den Brink is gratefully acknowledged for the flood wave modeling. I thank Ivo Thonon, Chris Roosendaal, Herman Straatsma, Pim van Santen, Marc Gouw, Martin Baptist and Frederik Huthoff for their field support. John Beijer (WUR) is greatfully acknowledged for lending me their boat.

8 Synthesis and conclusions

The accurate, spatial and quantitative parameterization of floodplain roughness provides important input for hydrodynamic models, which are used to compute peak water levels during overbank flow. These models play an essential role in determining the height of the embankments and hence, in the safety of the people living in the area protected by embankments. In this thesis the possibilities of airborne laser scanning (ALS) combined with multispectral data to generate input maps for floodplain roughness are investigated. In addition, field methods were developed to measure vegetation density and to determine *in situ* hydrodynamic characteristics to compute the vegetation roughness. In the following section the achievements with respect to the objectives of the study are summarized. Where possible, recommendations for further research are given.

8.1 Vegetation structural characteristics

Data on vegetation height and density based on field measurements have been collected for all chapters in this study. Table 8.1 gives an overview of the structural values found. Compared to the ecotope lookup table (Van Velzen *et al.* 2003), the range of values found for vegetation density of herbaceous vegetation is much lower. The maximum density is 0.72 m^{-1} in this study, whereas the lookup table gives a density of 3 m^{-1} for thistle. Conversely, the range of vegetation density values of forest is much larger in this study. According to the results found in this study, the density is both lower and higher than presented in the ecotope lookup table. These differences do not necessarily show a bias of the lookup table. However, the lookup table lacks substantial field measurements, which may partially be solved by data from this study. The vegetation height of herbaceous vegetation varies spatially, especially when single trees are present within the class herbaceous vegetation. The vegetation height of meadows found in this study is comparable to the value in the lookup table. The spatial distribution of these vegetation characteristics is illustrated in figures 5.6 and 6.10 based on ALS and TLS (Terrestrial Laser Scanning).

Table 8.1 Overview of the vegetation structural characteristics derived from field measurements.

	Vegetation height (m)				**Vegetation density (m^{-1})**			
	min	**max**	**median**	**σ[a]**	**min**	**max**	**median**	**σ[a]**
Meadow (n=6, ch. 7)	0	0.13	0.04	0.021	– -	– -	– -	– -
Herbaceous vegetation (n=42, ch. 3)	0.26	1.66	0.64	0.31	$3{\cdot}10^{-4}$	0.72	0.066	0.13
Single trees (n=213, ch. 5)	1.2	7.5	3.8	1.17	– -	– -	– -	– -
Forest (n=36, ch. 4, 6)	– -	– -	– -	– -	0.005	0.612	0.039	0.11

a. σ is the standard deviation, ch. chapter

8.2 Spatial floodplain roughness parameterization using airborne remote sensing

This study has focused on the spatial mapping of input parameters for roughness models at the spatial scale of a floodplain. Using the roughness model of Baptist (2005), vegetation height and density are the two parameters to map. Even though few papers reported on the extraction of these hydrodynamic parameters of vegetation in winter, the literature review and the Duursche Waarden case study (Chapter 2) made ALS a promising technique.

Results
For herbaceous vegetation, new methods were developed to label laser hits as vegetation points or ground points. The inflection method (Fig. 3.2) proved most successful for vegetation height prediction, the threshold method for vegetation density. The main contribution of ALS to the extraction of forest vegetation density is the improved explained variance and the fact that ALS is able to remotely sense the vegetation up to the level of inundation during peak flow. This is contrary to spectral remote sensing data that describes mostly the top of the canopy. No translation needs to be made from canopy structure to vegetation density in the height interval just above the forest floor. A new method was developed, which remodels invalid points. The invalid points mostly represent the wet or moist ground surface and, therefore, alter the vertical point distribution (Fig. 4.5, 4.8). These points are remodeled to ground level before the computation of the laser parameters that predict vegetation density. Point remodeling is essential to all empirical models that use descriptors of the complete vertical point distribution as regressors, such as percentiles.

In chapter 5, a new single tree delineation method is presented that uses clustering and iterative cross section analyses. This method improves a current clustering method for single tree delineation (Morsdorf *et al.* 2004) by classifying the cross sections between cluster maxima as belonging to either one or two trees (Fig. 5.4, 5.5). The advantage of this method is that, for a specific vegetation type, a training set can be created manually, which may be used in a subsequent supervised classification to delineate any dataset of that forest type. In this study, it was used to create homogeneous areas of non-woody herbaceous vegetation.

ALS showed a strong predictive power for vegetation structure estimation as judged from the linear regression models that were established in this study:
1. Herbaceous vegetation height (R^2 = 0.74-0.88, RSE = 0.16-0.11 m, n = 31-12, Chapter 3)
2. Herbaceous vegetation density (R^2 = 0.51, RSE = 0.08 m^{-1}, n = 43, Chapter 3)
3. Forest vegetation density (R^2 = 0.66, RSE = 0.016 m^{-1}, n = 22, Chapter 4)
4. Single trees height (R^2 = 0.41, RSE = 0.84 m, n = 86, Chapter 5)

This shows that vegetation height and density of herbs and vegetation density of deciduous floodplain forest can be mapped accurately using ALS. The predictive power for herbs under leaf-off condition equals the predictive power of comparable estimates in forestry (Chapter 2), which is a good achievement, given the small size of the vegetation stalks of the herbs in winter. These results are obtained with a point density of 15 points m^{-2} and do not improve with higher point densities. Higher point densities, therefore, seem unnecessary for herbaceous vegetation.

The strength of these relations and the estimate of the residual standard error are indicators of the high accuracy of these methods. This is an important improvement compared to a method based on ecotopes and a lookup-table, which explained only 34 percent of the field variation for forest vegetation density. Based on an earlier study of Asselman (2002), the river managers in the Netherlands decided not to continue research into the extraction of vegetation structure from ALS data, because the strength of the relations were too low (Jesse *et al.* 2002). The results of this thesis rebut that conclusion.

At the spatial scale of a floodplain, more land cover classes than herbaceous vegetation have to be taken into account. The first-return ALS data proved unable to extract reliable estimates of structural characteristics of water, sand, meadows or paved areas. A new way of fusing ALS data with CASI multispectral data was developed, which comprised a segmentation and classification of the fused dataset (Chapter 5). This method proved successful in classifying floodplain land cover (KHAT = 0.78), because sand, meadow, paved areas and water have such widely different spectral signatures. For each land cover class, a specific method was applied, which was based on ALS in case of herbs and forest, and based on a lookup table for other classes. These methods clearly show the within-class variation of vegetation height and density for herbaceous vegetation and forest (Fig. 5.6). The accuracy of these predicted vegetation structural parameters is given by the residual standard error of the respective regression models. Concluding, input parameters for floodplain roughness can be mapped accurately and in a highly automated way using a combination of ALS and CASI (Compact Airborne Spectral Imager) data.

Compared to other studies that used ALS for roughness parameterization, this paper specifically takes the vegetation density into account. Cobby *et al.* (2001) and Mason *et al.* (2003) only used vegetation height as required for the roughness models of Kouwen (1988) and Kouwen & Fathi-Moghadam (2000). They also apply their regression models to meadows. Independent of the roughness model used, a classification of the land cover should be applied to exclude non-vegetated parts of the floodplain. I recommend to exclude meadows from ALS data processing as well, because the signal to noise ratio is around 0.25 (4 cm vegetation height verses 16 cm residual standard error).

The effects of two different roughness parameterizations on water flow were evaluated in a Delft3D-flow model application of the '*Gamerensche Waard*' floodplain. Significant differences in water flow velocity showed up, which is relevant for morphological modeling or aquatic habitat mapping. Water level differences were less affected due to the low fractional discharge over the floodplain and the geographic position of the floodplain close to the river mouth.

Further research

The portability of the empirical regression models proved low, which was implied in the many different regression models available for forest structure extraction and vegetation height (Chapter 2 and 3; Hopkinson *et al.* 2004). The need for repeatedly establishing the empirical relations reduces the applicability of ALS as a standard mapping tool for vegetation structure. The portability could be increased by field calibration, which would incorporate the ALS measurements of standard geometrical objects or plants, measured from different flying heights and scan angles (Wotruba *et al.* 2005). Over time, a database could be filled with descriptive

parameters of these calibration tests and empirical relations for vegetation characteristics, which would allow establishing relations between the two. Additional information could be acquired also, if the average energy intensity within the laser footprint would be attributed to each laser point. This would be a more informative parameter than the current dimensionless reflection intensity.

Increased accuracy of the predictions is to be expected on the one hand from better field data: (1) a higher positional accuracy of the field reference plots using dGPS might reduce the prediction error and (2) an estimate of the vegetation density as a function of height above the ground surface would facilitate the comparison with the vertical distribution of laser points. Parallel photography (Chapter 6) might enable such a comparison. On the other hand, a more adequate set-up of the aerial data acquisition might improve the vegetation structure estimates, which is related to sensor orientation, data capture of the laser receiver and timing of the airborne missions.

The sensor orientation affects the hydrodynamic vegetation density estimates. Hydrodynamic vegetation density describes the horizontal obstruction of the vegetation for flowing water, whereas the vertical distribution of the laser hits depends on the detectability of the vegetation in the direction of the laser pulses, which is primarily vertical. More accurate estimates of vegetation density might be obtained when the laser scanner would be oriented in a more forward looking direction, in which case the flow direction and scan direction would coincide to a larger extent (Chapter 4). This would be possible with a portable ALS system as presented by Skaloud *et al.* (2005).

The data capture of the laser receiver determines what information of the laser return is being recorded. Within this study, first-return, small-footprint ALS data was used with a high point density. Other systems are able to record multiple discrete peaks of one returned laser pulse or even the full waveform (Baltsavias 1999). However, to register more than one pulse, a certain height interval between the first and second peak is required, otherwise the peaks merge into one wider peak. The minimum detectable height difference is about 0.6 m (Hug *et al.* 2004). For herbaceous floodplain vegetation in the range of 0.2 to 1.7 m as in this study, little improvements are expected from multiple return ALS data. For forest, the point density in the height interval above the forest floor is expected to increase. This is useful for vegetation density mapping, because it requires a minimum number of points (Chapter 4). Full waveform digitizing laser scanners have recently become available and provide an alternative, as they do not use a threshold. For short vegetation last echo detection (LED) seems a promising direction. The LED should return the trailing end of the last significant return of a single laser pulse. In that case, the first pulse would refer to the upper part of the vegetation and the last echo the ground surface. Using this method, a vegetation height measure can be derived from a single pulse, probably leading to less noise. This might also solve the problem for very low vegetation, because the signal to noise ratio increases.

The timing of the airborne mission influences the vertical distribution of the laser point heights as well as the spectral signature of the optical data. Future research should focus on the distinction between meadows and herbaceous vegetation, because these classes are difficult to

discern. Multitemporal spectral imagery might improve the distinction between these classes. Even relatively low resolution Landsat images may help due to its high temporal resolution (16 days).

8.3 Field vegetation density measurements

Accurate field methods to estimate hydrodynamic vegetation density are required to relate remote sensing observations to the field and to produce predictive models. Parallel Photography (PP) uses a photomosaic of the centre columns of a series of adjacent images of vegetation against a contrasting background. PP proved extremely accurate in predicting the hydrodynamic vegetation density at plot level (R^2 = 0.996, RSE = 3.7 10^{-3} m^{-1}, n=17, Chapter 6). The regression model was linear and did not deviate from the line of identity, which indicates that this method does not have to be calibrated and that portability is guaranteed. In addition, the support of this method is variable as the distance between the digital camera and the background screen is easily varied. Terrestrial laser scanning (TLS) generates a 3D point cloud based on distance measurements. TLS provided a 2D distribution of the forest vegetation density with a high accuracy (R^2 = 0.77, n = 23, RSE = 0.022 m^{-1}, Chapter 6). This method is easily extended to 3D. PP and TLS are complementary techniques in the sense that they combine high plot level accuracy and spatially distributed estimates of vegetation density.

More detailed analyses of the composite image (e.g. Zehm *et al.* 2003) and laser data might enable the distinction between stems, twigs, and leaves. Such a method should include the classification of different vegetation elements and an estimate of their size. In this way, average stem spacing or flexural rigidity might be derived from the same methods.

8.4 Roughness measurements

To quantify *in situ* hydrodynamic roughness of submerged floodplain vegetation, a novel method called ´3D float tracking´ was developed and tested. A floating platform (Fig. 7.1) is tracked using a shore-based total station, while a current meter measures the flow profile. This method is easily applied at various locations with different submerged vegetation types. The float plus equipment is transportable in a minivan, but the boat required a trailer. The top of the vegetation needs to be submerged by more than 50 cm of water to enable the float to flow freely.

The main achievement of this method is the accuracy of the water surface height determination (residual standard deviation of 0.7 mm) in the absence of waves. Combined with the depth averaged flow velocities and the water depth this enables to solve the 1D equation for free surface flow locally leading to the hydrodynamic roughness. 3D float tracking proved very suitable for inundated floodplains with limited water depth and modest flow velocities. A clear spatial pattern in roughness was the result from this analysis (Fig. 7.9e). Alternatively, 3D float tracking generates the detailed hydrodynamic data that are needed to assess the output of high-resolution hydrodynamic models, which may reduce the underdetermination of these models. Additional information might be collected, when the float is equipped with three horizontal

current profilers to model lateral gradients in the flow velocity and an echo sounder with a very narrow beam to model the vegetation height.

The derived Nikuradse equivalent roughness of meadows of 3 and 5 cm high grass is 12 and 19 cm. Klaassen & Van der Zwaard (1974) suggested to use 7 cm for meadows and Van Urk (1981) 20 cm based on *in situ* measurements. The results from this study are, therefore within the range of suggested values. The real achievement of this study is that it shows the spatial patterns in roughness, which points at the underlying processes.

The ultimate type of calibration data for hydrodynamic models would be full 2D maps of water elevation and flow velocity. One possibility is to calibrate on flood extent derived from spectral or radar remote sensing data (Bates *et al.* 1997; Bates *et al.* 2004). Flood extent is, however, insensitive to water level variations for embanked rivers during peak discharge and should therefore be applied during the rising limb of the flood peak. Further research could focus at airborne side-looking Along Track Interferometric Synthetic Aperture Radar (ATI-SAR) data. This method can measure flow velocity of the top of the water column. It has been used in oceanography to monitor spatially distributed surface flow velocities with a resolution of 10 m and resulted in flow vectors with a error of 6 cm s^{-1} (Graber *et al.* 1996; Moller *et al.* 1998). A drawback for the application of ATI-SAR in a fluvial environment is the need for information on the wave field to model the radar data into flow velocities. For a large part of the river area, this wave field is irregular due to ship-induced waves and refractions.

8.5 Integral river management

This thesis provides new field and remote sensing based methods that enable the spatially distributed and accurate parameterization of roughness input data and a method for *in situ* roughness extraction. The methods that have been developed provide some of the basic ingredients for a better estimate of the hydrodynamic roughness, which partly determines the accuracy of the predicted peak water levels and safety levels of the people living in the embanked area.

Apart from increased accuracy of the derived products from remote sensing data presented in this thesis, other landscape characteristics could be extracted from the remote sensing data. Additional data analyses could be carried out to filter floodplain topography (Vosselman 2000), to extract buildings (Baltsavias 2004) or the breaklines of embankments, groynes, and ditches (Brügelmann 2000). This could complete the data input for hydrodynamic models and optimize the use of the remote sensing data. When the scope of remote sensing data processing is widened beyond hydrodynamic modeling, the methods developed in this study may prove useful as well in coastal zone management, biomass estimations or habitat mapping (MacArthur & MacArthur 1961; Davenport *et al.* 2000; Vulink 2001; Lefsky *et al.* 2002). Multitemporal ALS monitoring of floodplains could be used to monitor vegetation succession. From the perspective of integral river management, this fundamental study created some of the building blocks to optimize protection against flooding and opens new applications of remote sensing in ecology.

Summary

Within the framework of integral river management, the exceedance probability of peak water levels is an important parameter. These local peak water levels, computed using a hydrodynamic model, are determined by the peak discharge, downstream water levels, river topography and the hydrodynamic roughness of the river bed and vegetation. Therefore, floodplain roughness parameterization is one of the key elements for safety level estimation of lowland fluvial areas. Vegetation roughness, the retardance of the flow velocity due to shear stress of the vegetation on the water, depends on a variety of vegetation structural characteristics and hydrodynamic aspects. This PhD-thesis focuses on two main goals:

1. Parameterize floodplain roughness accurately, quantitatively and spatially distributed using airborne remote sensing data.
2. Develop methods for accurate field reference data for the input and output of hydrodynamic models

Literature and case study

In literature, many studies report accurate classification of natural vegetation using multispectral or hyperspectral remote sensing data that has been combined in some cases with height information. Nevertheless, a lookup table is required to convert the vegetation classes to vegetation structure values, which leads to undesirable loss of within-class variation. In contrast, Airborne Laser Scanning (ALS) enables direct extraction of vegetation structural characteristics. Chapter 2 gives a review of the vegetation structural characteristics relevant for hydrodynamic roughness. Reliable predictions using ALS data have been reported for (1) forest height (R^2 = 0.64-0.98), (2) forest density, such as stem number, stem diameter, biomass, timber volume or basal area (R^2 = 0.42-0.93), and (3) herbaceous vegetation height in summer condition (R^2 = 0.75-0.89). No empirical relations have been reported on density of herbaceous vegetation. However, the vegetation in these studies mostly consisted of vegetation in leaf-on conditions, which is not representative for winter floods, nor did any study report on the accurate mapping of hydrodynamic vegetation density. A case study in the Duursche Waarden floodplain showed that ALS was a promising method to extract vegetation height and density of vegetation under leaf-off conditions as well.

Vegetation structure extraction from ALS

Detailed analyses on the extraction of vegetation height and density of herbaceous vegetation from ALS data are given in chapter 3. Three ALS surveys were carried out, coincident with field measurements. The laser data surveys differed in flying height, gain setting and laser diode age. Laser points were labeled as either vegetation or ground using three different methods: (1) a fixed threshold value, (2) a flexible threshold value based on the inflection point in the point height distribution, and (3) using a Gaussian distribution to separate noise in the ground surface points from vegetation. The vegetation height was best predicted by using the inflection method for

labeling and the 95 percentile of the laser point heights above the ground surface as a regressor (R^2 = 0.74 – 0.88). Vegetation density was best predicted using the threshold method for labeling and the percentage index (*PI*) as a predictor (R^2 = 0.51). *PI* computes the density of vegetation points. The results of vegetation height prediction were found to depend on the combined effect of flying height, gain setting or laser diode age. The quality of the estimation of vegetation height and density is also affected by point density, for densities lower than 15 points m^{-2}. I conclude that high resolution ALS data allows to estimate vegetation height and density of herbaceous vegetation under leaf-off condition, but field reference data remains necessary for calibration

The extraction of vegetation density of floodplain forest from ALS data is presented in chapter 4 using the same dataset as in chapter 3. Two indices to predict vegetation density from the laser data were considered: (1) Percentage Index (*PI*) of points in the height interval inundated by the water, and (2) a Vegetation Area Index (*VAI*) that corrects for occlusion from the crown area. A computer simulation, using a digital forest model, showed a minimum required number of points to accurately compute the indices, a dependency on the incidence angle, and a sensitivity of the indices for laser pulses that were send out, but not detected by the laser receiver. Two out of three datasets included many so-called invalid points. The location of these invalid points as well as incidence angles were therefore reconstructed using the known time stamp on both scanner positions and point positions. Two different assumptions were tested to assign new coordinates to all invalid points: (1) all invalid points are remodeled to ground level and (2) invalid points are remodeled to ground level when the point density ratio is high. Percentage Index (*PI*), with the invalid points remodeled by means of thresholding on the point density ratio, proved the best predictor (R^2 = 0.66) of vegetation density of deciduous floodplain forests under winter condition. The incidence angle did not add significantly to the overall explained variance of the vegetation density.

Spatial roughness parameterization and modeling

Due to the noise in the laser data, no roughness input parameters could be determined from the ALS data for sand, roads, built-up areas and meadows. To enable the floodplain-wide mapping of roughness parameters, a data fusion of ALS data with multispectral data was carried out in chapter 5. The fused data set was segmented in spatial objects and classified into nine land cover types (KHAT = 0.78). For each of these types a lookup table was applied where needed, and the vegetation structure of herbaceous vegetation and forest was determined using the relations derived in the previous chapters. Additionally, a new single tree delineation method using ALS data was developed to create homogeneous areas of non-woody herbaceous vegetation. This new method for floodplain roughness parameterization was applied to a floodplain section and the results were assessed in a hydrodynamic model. A comparison of model results was made to the current method based on manual mapping of vegetation types. The model showed small differences in water level, but significant differences in flow velocity.

Field measurements

Manual field measurements of vegetation density based on the number of stems m^{-2} and stem diameter proved subjective in case of irregular stem shapes. Two novel techniques were compared: Terrestrial Laser Scanning (TLS) and digital Parallel Photography (PP). PP consists of a series of digital photographic images of vegetation against a contrasting background. The

centre columns of all images were merged into a single composite parallel image. This mosaic was thresholded to determine the fractional coverage of the vegetation, which is converted to vegetation density using the optical point quadrate method. TLS was carried out using a Leica HDS3000 time of flight laser scanner. Data processing of TLS data consisted of slicing the points around breast height. In a polar grid the vegetation density was predicted, using the optical point quadrate method corrected for missing points. Both methods were compared to the field reference data. PP (R^2 = 0.996, RSE = $3.7 \cdot 10^{-3}$ m^{-1}) performed better than the TLS (R^2 = 0.77, RSE = $22 \cdot 10^{-3}$ m^{-1}). Advantage of the TLS method is the ability to provide a detailed 2D or even 3D distribution of the vegetation density. TLS and PP are, therefore, two complementary techniques.

Roughness models are rarely tested under field conditions. 3D float tracking is a new method that may fill this gap (chapter 7). It uses a floating tripod that is released on the inundated floodplain. A robotic total station tracks the float from shore, and an Acoustic Doppler Current Profiler (ADCP) mounted on the float collects flow velocity profiles and water depth data. Roughness values are derived from three methods based on (1) run-averaged values to compute the roughness based on the Chézy equation, assuming uniform flow, (2) the equation for one-dimensional free surface flow in a moving window, and (3) the zero plane displacement of the flow velocity profiles. Field measurements were carried out on two floodplain sections with a vegetation height of 0.030 (Arnhem) and 0.043 m (Dreumel). Method 1 resulted in a Nikuradse roughness value of 0.08 m for both locations. Method 2 gave 0.12 m for Arnhem and 0.19 m for Dreumel. At the Dreumel site, ship-induced waves were present, which was an additional source of noise in the water level measurements. In Arnhem, a spatial pattern of roughness values was present, which might be related to fractional vegetation cover during the flood peak. Method 3 generated unrealistically high roughness values. 3D float tracking proved a flexible and detailed method for roughness determination in the absence of waves, which can additionally be used to calibrate high-resolution hydrodynamic models.

Future research

Recommended research may include:

1. ALS sensor reorientation to a more forward-looking direction, which increases detection of vertical stems.
2. Full waveform data analyses, including last echo detection, to parameterize low vegetation.
3. Increasing the portability by relating standardized field calibration of ALS to vegetation structure.
4. Multitemporal data analyses to discriminate between herbaceous vegetation and meadows.
5. Detailed analysis of the PP photomosaics and TLS point clouds to estimate leaf coverage and flexural rigidity of the vegetation
6. Inclusion of horizontal ADCP and small-footprint echo sounders to the 3D float tracking method.

Samenvatting

Hydrodynamische ruwheid van uiterwaardenvegetatie
Parametrisatie vanuit de lucht en validatie in het veld

In de voorgaande hoofdstukken is op wetenschappelijke wijze verslag gedaan van het promotieonderzoek naar nieuwe methoden om de structuur van uiterwaardenvegetatie te karteren. Dit proefschrift richt zich daarmee op een wetenschappelijk publiek wat tot uitdrukking komt in een strenge opbouw van de hoofdstukken, een scherpe afbakening tussen bekende kennis, toegevoegde resultaten en de interpretatie daarvan. Deze samenvatting beoogt om ook voor niet-wetenschappers, of wetenschappers met een andere achtergrond, inzicht te geven in de problematiek en de gevonden oplossingen.

Het probleem
Binnen het kader van het integraal rivierbeheer zijn de maximale verwachte hoogwaterstanden een belangrijk gegeven. Op basis van deze waterstanden wordt namelijk de hoogte van de dijken gebaseerd. De maximale waterstanden worden voorspeld met behulp van een computermodel dat de waterstroming door het rivierengebied berekent. Invoer voor zo'n model bestaat uit een bovenstroomse afvoer, benedenstroomse waterstanden, bodemhoogte en de hydrodynamische ruwheid van het zomerbed en de uiterwaarden. Hydrodynamische ruwheid is een maat voor de wrijving die het water ondervindt van de ondergrond en de vegetatie in het geval van uiterwaarden. Vegetatieruwheid wordt mede bepaald door de hoogte en dichtheid van de van de vegetatie, waarbij geldt: hoe hoger en dichter de vegetatie, hoe hoger de ruwheid, hoe lager de stroomsnelheden over de uiterwaarden en dus hoe hoger het water komt tijdens een hoogwatergolf. Daarmee is vegetatieruwheid dus één van de parameters die de veiligheid van het rivierengebied bepaald. Het blijkt echter nog knap lastig om goede kaarten te maken van de hoogte en dichtheid van vegetatie. Eén mogelijkheid is om overal in het veld te gaan meten, maar dat kost teveel tijd. Daarom moeten we zoeken naar meer geautomatiseerde methoden op basis van satellietbeelden of luchtfoto's. Daarnaast zijn er altijd nog goede veldmetingen nodig om de beelden om te zetten naar vegetatiestructuur en om de stromingsmodellen te kalibreren. Kalibreren wil zeggen dat er wordt gecontroleerd of de voorspelde modeluitkomsten wel kloppen met de werkelijkheid. Deze dissertatie richt zich op twee hoofdvragen, die beiden gerelateerd zijn aan de hydrodynamische ruwheid:

1. Is het mogelijk om de ruwheid van de uiterwaarden te karteren met een methode die kwantitatief, nauwkeurig, ruimtelijk verdeeld en geautomatiseerd is?
2. Hoe kan vegetatiedichtheid objectief worden gemeten in het veld?
3. Hoe kan de ruwheid van overstroomde vegetatie tijdens hoogwater worden bepaald?

Remote sensing

In de vakliteratuur is veel gepresenteerd over het classificeren van vegetatie met behulp van *remote sensing* beelden zoals luchtfoto's, satellietbeelden of radarbeelden. In sommige studies is deze data gecombineerd met hoogtegegevens. Hoe nauwkeurig de classificatie ook mag zijn. Uiteindelijk moeten de vegetatieklassen toch worden omgezet naar vegetatiehoogte en -dichtheidgetallen, waarbij de variatie binnen de klassen helaas wordt weggemiddeld. Laseraltimetrie omzeilt dit probleem door, vanuit een vliegtuig of helikopter, laserafstandsmetingen te doen met een extreem hoge puntdichtheid (tot 75 punten per vierkante meter in deze studie). Dit leidt tot een puntenwolk die deels de vegetatie representeert (zie figuur 2.2 en 2.6). In hoofdstuk 2 geef ik een introductie in de werking van de laseraltimetrie en een overzicht van eerdere studies naar laseraltimetrie in de bosbouw en het rivierbeheer. Daaruit blijkt dat de hoogte van het bos beter wordt voorspeld dan parameters die zijn gerelateerd aan de dichtheid. Ook voor ruigte geldt dat de hoogte goed wordt voorspeld, maar er zijn geen voorspellende modellen gevonden die de dichtheid van ruigte bepalen met laseraltimetrie. Daar komt nog bij dat de vegetatie in de meeste gevallen is bestudeerd op het moment dat ze in blad waren. Dit is niet representatief voor de Nederlandse situatie waarin overstromingen voornamelijk in de winter plaatsvinden.

Hoogte en dichtheid van ruigten

In hoofdstuk 3 wordt een gedetailleerde studie gepresenteerd naar hoe de vegetatiehoogte en -dichtheid van ruigte kan worden bepaald met behulp van laseraltimetrie. Drie laseraltimetriecampagnes zijn uitgevoerd waarbij drie parameters varieerden: de vlieghoogte, de ouderdom van de laserlamp en de mate van versterking van het inkomend signaal. Drie verschillende methoden zijn ontwikkeld en getest om het onderscheid te maken tussen laserpunten die de bodem of vegetatie representeren (zie figuur 3.2 en 3.3). Twee van deze methoden bleken het erg goed te doen voor het voorspellen van hoogte en dichtheid. De kwaliteit van de methode wordt uitgedrukt als de procentuele verklaarde variantie. Oftewel, welk deel van de variatie die je ziet in het veld, zie je ook terug in de methode op basis van remote sensing? Verklaarde variantie voor de hoogte van de ruigte varieerde tussen de 74 en 88 procent, van dichtheid werd 51 procent verklaard. Dit is een grote verdienste, aangezien de stengels van grassen en kruiden in de winter moeilijk te zien zijn met een laser scanner. Er bleken dan ook significante verschillen in gevoeligheid tussen de drie laser datasets. Daarom is calibratie van laseraltimetriedata nog steeds nodig om vegetatiestructuur te kunnen voorspellen.

Dichtheid van bos

De vegetatiedichtheid van bos wordt bepaald met laseraltimetrie in hoofdstuk 4. Ik heb twee voorspellers getest en de simpelste bleek het best te werken; de verhouding tussen het aantal laserpunten in het deel van het bos dat onder water kan komen te staan tijdens hoog water en het totaal aantal punten (zie figuur 4.8). Een nieuw probleem kwam hierbij aan de orde (zie figuur 4.3 en 4.5). Een groot aantal punten dat wordt uitgezonden wordt namelijk niet meer gedetecteerd, dat zijn zogenaamde uitvallers. Dit kan komen door een lage intensiteit van het uitgezonden signaal, in het geval van een oude laserlamp, maar ook doordat het oppervlak waar de laserpuls op terechtkomt de energie absorbeert, zoals in het geval van water. De aanwezigheid van water in de uiterwaarden varieert natuurlijk bij slootjes, maar ook waterplassen van de laatste overstroming leiden tot verschillen in absorptie. Het is dus belangrijk om rekening te houden met deze uitvallers. Eén methode is om de uitvallers terug te zetten naar de plaats waar

de energie van de laserpuls waarschijnlijk is geabsorbeerd (figuur 4.5 en 4.8). Als deze correctie wordt toegepast wordt 66 procent van de variantie verklaard tegenover slechts 28 procent voor de methode die op dit moment wordt gebruikt door Rijkswaterstaat.

Testen met een stromingsmodel

Laserdata geeft ook nogal wat ruis. Een horizontaal oppervlak geeft een puntenwolk met een verticale hoogteverschillen van 30 cm (zie figuur 2.6d). Daarom kan laseraltimetrie niet worden ingezet om ruwheidparameters te schatten voor strandjes, weilanden of water. Spectrale data, zoals in luchtfoto's of satellietbeelden, is een combinatie van blauw, groen en rood, zoals we dat met onze ogen kunnen zien en infrarood. Hiermee kan juist wel makkelijk onderscheid worden gemaakt tussen de eerdergenoemde klassen. Aan de klassen water, zand en weiland moet dan alsnog een vaste ruwheidswaarde worden gegeven, met bijbehorend verlies aan variatie binnen de klasse. Een groot voordeel is dat deze classificatie automatisch kan gebeuren in tegenstelling tot de huidige methode. In hoofdstuk 5 presenteer ik een nieuwe methode waarin ik spectrale data met laseraltimetrie data combineer om te komen tot vlakdekkende kaarten met invoergegevens voor ruwheid. Stap één bestaat uit de classificatie in landbedekkingsklassen (zie figuur 5.6a), stap twee uit het toepassen van de kennis uit de vorige hoofdstukken voor ruigten en bos (zie figuur 5.6b,c,d). In stap drie wordt aan de overige klassen een vaste waarde gekoppeld. Deze nieuwe methode heb ik vervolgens vergeleken met de methode zoals die op dit moment in Nederland wordt toegepast: handmatige classificatie op basis van luchtfoto's. Beide methoden zijn toegepast in een stromingsmodel voor een deel van de Waal, stroomafwaarts van Zaltbommel. Het bleek dat de nieuwe methode kleine verschillen gaf in waterstanden, maar grote verschillen in stroomsnelheid (zie figuur 5.10). Hieruit kan worden geconcludeerd dat de methode succesvol kan worden toegepast, maar er zijn wel betere kalibratiegegevens nodig om te kunnen zeggen (zie hoofdstuk 7) of de methode beter is dan de huidige methode.

Vegetatiedichtheid meten in het veld

Daarnaast voldeden de huidige veldmethoden om vegetatiedichtheid te meten niet. Vegetatiedichtheid is gedefinieerd als de som van de oppervlakken van de vegetatie in zijaanzicht gedeeld door het volume water waar die vegetatie in staat (figuur 2.1). Voor rechte stammen is de vegetatiedichtheid eenvoudig te bepalen door de stamdikte en het aantal stammen per vierkante meter te meten, maar bij kronkelende stammen en veel twijgjes gaat deze methode niet op. Daarom heb ik, samen met anderen, twee nieuwe methoden getest. De ene methode is op basis van digitale fotografie, waarbij vegetatie tegen een contrasterende achtergrond is gefotografeerd (zie figuur 6.2). Per opnamepunt worden ongeveer 100 foto's parallel aan elkaar gemaakt. De middelste delen van al deze foto's worden samengevoegd tot een mozaïek van samengeplakte foto's. Dit mozaïek wordt omgerekend naar vegetatiedichtheid met een bestaande formule. Deze methode geeft zeer nauwkeurige resultaten voor een meetvlak. Bijna 100 procent van de variatie wordt verklaard. De tweede methode gebruikt terrestrisch laser scannen. Hierbij wordt een laserscanner op verschillende plaatsen in het bos gezet en die meet de afstand tot alle objecten in de omgeving (zie figuur 6.8). De resulterende puntenwolk wordt op een vergelijkbare manier omgezet als bij laseraltimetrie vanuit de lucht. De nauwkeurigheid is iets lager dan bij de fotografische methode, maar geeft wel een prachtig twee-dimensionaal beeld van de vegetatiedichtheid van bos (zie figuur 6.10).

Wildwater (WW1) metingen: Stroming en verhang tijdens hoog water

Metingen tijdens hoogwater op de uiterwaarden zijn duur, afhankelijk van de grootte van de afvoer en niet vrij van gevaar, aangezien er op veel plaatsen bomen in de uiterwaarden staan. Daarom worden ruwheidsformules vooral gekalibreerd in een stroomgoot in het laboratorium. Daarnaast worden stromingsmodellen worden vooral gekalibreerd op waterstanden. Het probleem daarmee is dat met verschillende combinaties van modelinstellingen dezelfde waterstanden kunnen worden voorspeld. Dit heeft tot gevolg dat we niet goed weten of de modellen wel betrouwbaar zijn bij maatgevende afvoer. Daarom heb ik 3D *float tracking* ontwikkeld, het volgen van een drijver in drie dimensies (zie figuur 7.1). Hierbij stroomt een drijver met het water mee. Vanaf de kant wordt de positie en hoogte van de drijver bepaald met een landmeetapparaat, wat informatie geeft over het verhang van het wateroppervlak. Daarnaast geeft een snelheidsmeter onder de drijver informatie over de verdeling van de stroomsnelheid over de waterdiepte. Dit geeft een unieke dataset, waarmee de ruwheid kan worden berekend. De verdienste van deze methode zit vooral in de precisie van het bepalen van de waterstand langs het pad dat de drijver heeft afgelegd.

'Wetenschap is nooit af'

Dit is de slogan van de Universiteit Utrecht. Dankzij de nieuwe gegevens die boven tafel zijn gekomen met dit onderzoek, kan ik nu ook heel precies de mogelijkheden aangeven voor toekomstig onderzoek. Tip van de week:

1. Aanpassen van laseraltimetrie door vanaf de helikopter niet naar beneden te scannen, maar schuin naar voren. Dan 'zie' je de vegetatie beter.
2. Andere type laserdata gebruiken door van de uitgezonden laserpuls alle terugkomende informatie op te slaan en niet alleen één punt.
3. Calibratie van laseraltimetrie standaardiseren zodat voorspellers voor vegetatiestructuur overal kunnen worden toegepast.
4. Gebruik maken van spectrale data die op verschillende momenten zijn opgenomen.
5. Extra stroomsnelheidsmeters en waterdieptemeters op de drijver voor meer gedetailleerde informatie.

List of publications

Peer review

STRAATSMA, M.W. & H. MIDDELKOOP (2006), Airborne laser scanning as a tool for lowland floodplain vegetation monitoring. *Hydrobiologia*, 565, pp. 87-103.

STRAATSMA, M.W. & H. MIDDELKOOP (in press), Extracting structural characteristics of herbaceous floodplain vegetation for hydrodynamic modeling using airborne laser scanner data. *International Journal of Remote Sensing*.

STRAATSMA, M.W. (in press), Quantitative mapping of hydrodynamic vegetation density of floodplain forests using airborne laser scanning. *Photogrammetric Engineering and Remote Sensing* pp.

STRAATSMA, M.W., J. WARMINK & H. MIDDELKOOP (submitted), Two novel methods for field measurements of hydrodynamic density of floodplain vegetation using terrestrial laser scanning and digital parallel photography. *International Journal of Remote Sensing*, pp.

To be submitted

STRAATSMA, M.W. & M.J. BAPTIST (to be resubmitted), Floodplain roughness parameterization using airborne laser scanning and spectral remote sensing. *Remote Sensing of Environment*, pp.

STRAATSMA, M.W. (to be submitted), 3D float tracking: In-situ floodplain roughness estimation.

Conference papers

STRAATSMA, M.W. (2006), Floodplain roughness mapping synergy: Lidar and spectral remote sensing. In: Kerle, N. & A.K. Skidmore (eds.). ISPRS e-proceedings, Remote sensing: From pixels to processes. Enschede, pp. 612-617.

WARMINK, J., M.W. STRAATSMA & H. MIDDELKOOP (2006), Measuring hydrodynamic vegetation density in a floodplain forest using terrestrial laser scanning. In: Koukal, T. & W. Schneider (eds.). Earsel e-proceedings, 3D Remote sensing in forestry. Vienna, pp. 55-62.

WARMINK, J., M.W. STRAATSMA & H. MIDDELKOOP (2006), Field measurements of hydrodynamic density of floodplain vegetation using terrestrial laser scanning and digital parallel photography. In: Van Os, A.G. (Eds.). NCR-days 2006. Enschede.

STRAATSMA, M.W. (2005), Quantitative mapping of hydrodynamic vegetation density of floodplain forests using airborne laser scanning. In: Vosselman, G. & C. Brenner (eds.) ISPRS Vol 36, part 3/W19, ISPRS workshop laser scanning 2005. Enschede, pp. 91-96.

STRAATSMA, M.W. (2006), Floodplain roughness mapping synergy: Lidar and spectral remote sensing. In: Weerts, H.J.T., I.L. Ritsema & A.G. Van Os (eds.). NCR 29-2006, Proceedings NCR-days 2005. Zwijndrecht, pp. 67-68.

STRAATSMA, M.W. (2005), 3D float tracking: In-situ floodplain roughness estimation. In: Makaske, B., H.P. Wolfert & A.G. Van Os (eds.). Proceedings NCR-days 2004, NCR 26-2005, Wageningen, pp. 102-103.

STRAATSMA, M.W., H. MIDDELKOOP, E. PEBESMA & C. WESSELING (2004), Mapping of vegetation characteristics using lidar and spectral remote sensing. In: Douben, N., A.G. van Os (eds.). Proceedings NCR-days 2003, NCR 24-2004, Roermond, pp. 48-50.

STRAATSMA, M.W., H. MIDDELKOOP & S. DE JONG (2003), Remote sensing, floodplain vegetation and hydraulics. In: Leuven, R.S.E.W., A.G van Os, P. Nienhuis (eds.). Proceedings NCR-days 2002, NCR 20-2003, Nijmegen, pp. 166-168.

Reports

RITZEN, M.R. & M.W. STRAATSMA (2002), Laseraltimetrie en hydraulische vegetatieruwheid van uiterwaarden (in Dutch), Masters thesis, NCR 19-2002, Delft.

References

ABER, J.D. (1979), A method for estimating foliage-height profiles in broad leaved forests. *Journal of Ecology*, 67, pp. 35-40.

ADAMS, W.M. & M.R. PERROW (1999), Scientific and institutional constraints on the restoration of European floodplains. In: Marriot, S.B. & J. Alexander (eds.), Floodplains: Interdisciplinary approaches. The Geological Society of London, London,Special Publication 163, pp. 89-97.

ANDERSEN, H.E., S.E. REUTEBUCH & G.F. SCHREUDER (2002), Bayesian object recognition for the analyses of complex forest schemes in airborne laser scanner data. In: Kalliany, R., F. Leberl & F. Fraundorfer (eds.), ISPRS Vol 34, part 3A, Photogrammetric computer vision 2002. Graz, Austria, pp. A-35 ff.

ARMANINI, A., M. RIGHETTI & P. GRISENTI (2005), Direct measurements of vegetation resistance in prototype scale. *Journal of Hydraulic Research*, 43, pp. 481-487.

ASSELMAN, N.E.M. (2002), Laser altimetry and hydraulic roughness of vegetation, further studies using ground truth. Q3139, WL | Delft Hydraulics, Delft.

BAATZ, M. & A. SCHäPE (2000a), Multi-resolution segmentation: an optimization approach for high quality multiscale image segmentation. In: Strobl, J. & T. Blaschke (eds.), Wichmann Vol XII, Angewandte Geografische Informationsverarbeitung. Heidelberg.

BAATZ, M. & A. SCHäPE (2000b), Object-oriented and multi-scale image analyses in semantic networks, 2nd International Symposium: operationalization of remote sensing. Enschede.

BALTSAVIAS, E.P. (1999a), Airborne laser scanning: basic relations and formulas. *ISPRS Journal of Photogrammetry and Remote Sensing*, 54, pp. 199-214.

BALTSAVIAS, E.P. (1999b), Airborne laser scanning: existing systems and firms and other resources. *ISPRS Journal of Photogrammetry and Remote Sensing*, 64, pp. 164-198.

BALTSAVIAS, E.P. (2004), Object extraction and revision by image analysis using existing geodata and knowledge: current status and steps towards operational systems. *ISPRS Journal of Photogrammetry and Remote Sensing*, 58, pp. 129-151.

BAPTIST, M.J. (2005), Modelling floodplain biogeomorphology, Delft Technical University, Delft, 195 pp.

BAPTIST, M.J., L.V. VAN DEN BOSCH, J.T. DIJKSTRA & S. KAPINGA (2005), Modelling the effects of vegetation on flow and morphology in rivers. *Large Rivers*, 15, pp. 339-357.

BAPTIST, M.J., V. BABOVICH, J. RODRíGUEZ UTHURBURU, M. KEIJZER, R.E. UITTENBOGAARD, A. MYNETT & A. VERWEY (in press), On inducing equations for vegetation resistance. *Journal of Hydraulic Research*.

BAPTIST, M.J., W.E. PENNING, H. DUEL, A.J.M. SMITS, G.W. GEERLING, G.E.M. VAN DER LEE & J.S.L. VAN ALPHEN (2004), Assessment of the effects of cyclic floodplain rejuvenation on flood levels and biodiversity along the Rhine River. *River Research and Applications*, 20, pp. 285-297.

BATES, P., M.G. ANDERSON, D.E. WALLING & D. SIMM (1992), Modelling floodplain flows using a two-dimensional finite element model. *Earth Surface Processes and Landforms*, 17: 575-588, pp.

BATES, P.D., K.J. MARKS & M.S. HORRITT (2003), Optimal use of high-resolution topographic data in flood inundation models. *Hydrological Processes*, 17, pp. 537-557.

BATES, P.D., M.S. HORRITT, C.N. SMITH & D.C. MASON (1997), Integrating remote sensing observations of flood hydrology and hydraulic modelling. *Hydrological Processes*, 11, pp. 1777-1795.

BATES, P.D., M.S. HORRITT, G. ARONICA & K. BEVEN (2004), Bayesian updating of flood inundation likelihoods conditioned on flood extent data. *Hydrological Processes*, 18, pp. 3347-3370.

BERZ, G., T. LOSTER & A.M. WIRTZ (2003), Topics, Annual review: Natural catastrophes 2002. 302-03631, Münchener Rückversicherungs Gesellschaft, Munich.

BESL, P.J. & N.D. MCKAY (1992), A method for registration of 3-D shapes. *IEEE transactions on pattern analysis and machine intelligence*, 14, pp. 239-256.

BEVEN, K. (2006), A manifesto for the equifinality thesis. *Journal of Hydrology*, 320, pp. 18-36.

BIENERT, A., H.G. MAAS & S. SCHELLER (2006), Analysis of the information content of terrestrial laser scanner point clouds for the automatic determination of forest inventory parameters. In: Koukal, T. & W. Schneider (eds.), 3D remote sensing in forestry. Vienna, pp. 44-49.

BIRON, P.M., A. RICHER, A.D. KIRKBRIDE, A.G. ROY & S. HAN (2002), Spatial patterns of water surface topography at a river confluence. *Earth Surface Processes and Landforms*, 27, pp. 913-928.

BLAIR, J.B., D.L. RABINE & M.A. HOFTON (1999), The Laser Vegetation Imaging Sensor: a medium-altitude, digitisation-only, airborne laser altimeter for mapping vegetation and topography. *ISPRS Journal of Photogrammetry and Remote Sensing*, 54, pp. 115-122.

BOLLWEG, A., R. BRüGELMANN, H. VAN DIJK & E. VAESSEN (2004), Laseraltimetriedata met hoge puntdichtheid voor rivierbeheer (in Dutch). AGI-GAR-2004011, Adviesdienst Geoinformatie en ICT, Delft.

BRANDTBERG, T., T.A. WARNER, R.E. LANDENBERGER & J.B. MCGRAW (2003), Detection and analysis of individual leaf-off tree crowns in small footprint, high sampling density lidar data from the eastern deciduous forest in North America. *Remote Sensing of Environment*, 85, pp. 290-303.

BROWN, J.K. (1971), A planar intersect method for sampling fuel volume and surface area. *Forest science*, 17, pp. 96-102.

BRüGELMANN, R. (2000), Automatic breakline extraction from airborne laser range data. ISPRS Vol 33, part B, XIX ISPRS congress. Amsterdam, pp. 109-114.

CAROLLO, F.G., V. FERRO & D. TERMINI (2002), Flow velocity measurements in vegetated channels. *Journal of Hydraulic Engineering*, 128, pp. 664-673.

CASAS, A., G. BENITO, V.R. THORNDYCRAFT & M. RICO (2006), The topographic data source of digital terrain models as a key element in the accuracy of hydraulic flood modelling. *Earth Surface Processes and Landforms*, 31, pp. 444-456.

CHOW, V.T. (1959), Open channel hydraulics. McGraw Hill, New York.

COBBY, D.M., D.C. MASON & I.J. DAVENPORT (2001), Image processing of airborne scanning laser altimetry data for improved river flood modeling. *ISPRS Journal of Photogrammetry and Remote Sensing*, 56, pp. 121-138

COBBY, D.M., D.C. MASON, M.S. HORRIT & P.D. BATES (2003), Two-dimensional hydraulic flood modelling using a finite-element mesh decomposed according to vegetation and topographic features derived from airborne scanning laser altimetry. *Hydrological Processes*, 17, pp. 1979-2000.

COPELAND, R.R. (2000), Determination of flow resistance coefficients due to shrubs and woody vegetation. ERDC/CHL CHETN-VIII-3, US Army Corps of Engineers.

CUSACK, G.A., M.F. HUTCHINSON & J.D. KALMA (1999), Calibrating airborne vegetation data for hydrological applications under dry conditions. *International Journal of Remote Sensing*, 20, pp. 2221-2233.

DARBY, S.E. (1999), Effect of riparian vegetation on resistance and flood potential. *Journal of Hydraulic Engineering*, 125, pp. 443-454.

DAVENPORT, I.J., R.B. BRADBURY, G.R.F. ANDERSON, J.R. HAYMAN, J.R. KREBS, D.C. MASON, J.D. WILSON & N.J. VECK (2000), Improving bird population models using airborne remote sensing. *International Journal of Remote Sensing*, 21, pp. 2705-2717.

DAVIS, J.C. (1986), Statistics and data analyses in geology. John Wiley & sons, New York, 646 pp.

DAWSON, F.H. & F.G. CHARLTON (1988), Bibliography on the hydraulic resistance of vegetated watercourses, No. 25, ISNN 0308-6739. Ambleside, Freshwater Biological Association, Occasional Publication, 25 pp.

DE BRUYN, K.M. (2005), Resilience and flood risk management: A systems approach applied to lowland rivers. PhD Thesis, Delft University of Technology, Delft, 210 pp.

DE NOOIJ, R.J.W. (2006), Integrating ecological knowledge with legal instruments for nature conservation in river management. PhD Thesis, Radboud University Nijmegen, Nijmegen, 167 pp.

DEFINIENS (2000), eCognition user guide, München.

DEN OUDEN, J.B. (1993), Het aangestroomd oppervlak van geïnundeerde ooibossen in diverse ontwwikkelingsstadia (in Dutch). IBN-rapport 039, IBN-DLO, Wageningen.

DIETRICH, W.E. & J.D. SMITH (1983), Influence of the point bar on flow through curved channels. *Water Resources Research*, 19, pp. 1173-1192.

DOWLING, R. & A. ACCAD (2003), Vegetation classification of the riparian zone along the Brisbane River, Queensland, Australia, using light detection and ranging (lidar) data and forward looking digital video. *Canadian Journal of Remote Sensing*, 29, pp. 556-563.

DRAKE, J.B., R.O. DUBAYAH, D.B. CLARK, R.G. KNOX, J.B. BLAIR, M.A. HOFTON, R.L. CHAZDON, J.F. WEISHAMPEL & S. PRINCE (2002), Estimation of tropical forest structural characteristics using large-footprint lidar. *Remote Sensing of Environment*, 79, pp. 305-319.

DUDLEY, S.J., C.D. BONHAM, S.R. ABT & J.C. FISCHENICH (1998), Comparison of methods for measuring woody riparian vegetation density. *Journal of Arid Environments*, 38, pp. 77-86.

DUEL, H., M.J. BAPTIST, & W.E. PENNING (2001), Cyclic floodplain rejuvenation. *NCR publication 14-2001,* ISSN 1568-234X, NCR, Delft.

EHLERS, M., M. GAHLER & R. JANOWSKY (2003), Automated analysis of ultra high resolution remote sensing data for biotope type mapping: new possibilities and challenges. *ISPRS Journal of Photogrammetry and Remote Sensing*, 57, pp. 315-326.

EINSTEIN, H.A. & R.B. BANKS (1950), Fluid resistance of composite roughness. *Transactions of the American Geophysical Union*, 31, pp. 603-610.

ESBJöRN-HARGENS, S. (2005), Integral ecology: the who, what and how of environmental phenomena. *World Futures*, 61, pp. 5-49.

FISCHER-ANTZE, T., T. STOESSER, P. BATES, & N.R.B. OLSEN (2001), 3D numerical modelling of open-channel flow with submerged vegetation. *Journal of Hydraulic Research*, 39, pp. 303-310.

FREEMAN, G.E., D.R. DERRICK & W.J. RAHMEYER (1996), Vegetative roughness in flood control channels. In: Proceedings of the North Americam Water and environment Congress, American society of engineers, Anaheim, CA.

FRöHLICH, C. & M. METTENLEITER (2004), Terrestrial laser scanning-new perspectives in 3D surveying. In: Thies, M., B. Koch, H. Spiecker & H. Weinacker (eds.), ISPRS Vol. 36, part 8/W2, Laser-scanners for forest and landscape assessment. Freiburg, Germany.

GERRITSEN, H. & G.K. VERBOOM (1994), The coastal modelling system. *Journal of Hydraulic Research*, 32, pp. 118-128.

GOODWIN, C.N., C.P. HAWKINS & J.L. KERSHNER (1997), Riparian Restoration in the Western United States: Overview and Perspective. *Restoration Ecology*, 5, pp. 4-14.

GORTE, B.G.H. & D. WINTERHALDER (2004), Reconstruction of laser-scanned trees using filter operations in the 3D raster domain. In: Thies, M., B. Koch, H. Spiecker & H. Weinacker (eds.), ISPRS Vol. 36, part 8/W2, Laser-scanners for forest and landscape assessment. Freiburg, Germany.

GRABER, H.C., D.R. THOMPSON & R.E. CARANDE (1996), Ocean surface features and currents measured with synthetic aperture radar interferometry an HF radar. *Journal of Geophysical Research*, 101, C11, pp. 25813-25832.

HALL, J.W., I.C. MEADOWCROFT, P.B. SAYERS & M.E. BRAMLEY (2003), Integrated flood risk management in England and Wales. *Natural Hazards Review*, 4, pp. 126-135.

HARTMANN, R., R. BRüGELMANN & A. BOLLWEG (2004), Vegetatieclassificatie uit laser en optische RS data (in Dutch). AGI/0109/GAR002, Adviesdienst Geoinformatie en ICT, Delft.

HAY, G.J., T. BLASCHKE, D.J. MARCEAU & A. BOUCHARD (2003), A comparison of three image-object methods for the multiscale analyses of landscape structure. *ISPRS Journal of Photogrammetry & Remote sensing*, 57, pp. 327-345.

HELMIö, T. (2002), Unsteady 1D flow model of compound channel with vegetated floodplains. *Journal of Hydrology*, 269, pp. 89-99.

HILL, R.A., G.M. SMITH, R.M. FULLER & N. VEITCH (2002), Landscape modelling using integrated airborne multi-spectral and laser scanning data. *International Journal of Remote Sensing*, 23, pp. 2327-2334.

HODGSON, M.E. & P. BRESNAHAN. (2004), Accuracy of airborne lidar-derived elevation: empirical assessment and error budget. *Photogrammetric Engineering and Remote Sensing*, 70, pp. 331-339.

HOLMGREN, J. & A. PERSSON (2004), Identifying species of individual trees using airborne laser scanner. *Remote Sensing of Environment*, 90, pp. 415-423.

HOLMGREN, J. & T. JONSSON, 2004. Large scale airborne laser scanning of forest resources in Sweden. In: Thies, M., B. Koch, H. Spiecker & H. Weinacker (eds.). Laser-scanners for forest and landscape assessment. ISPRS Vol. 36, part 8/W2: 157-160.

HOLMGREN, J., M. NILSSON & H. OLSSON (2003), Simulating the effect of lidar scanning angle of mean tree height and canopy closure. *Canadian Journal of Remote Sensing*, 29, pp. 623-632.

HOLMGREN, J., M. NILSSON, H. OLSSON, 2003. Estimation of tree height and stem volume on plots using airborne laser scanning. *Forest Science,* 49, pp. 419 – 428.

HOOIJER, A. & A. G. VAN OS (eds.) (2002), IRMA-SPONGE Towards sustainable flood risk management in the Rhine and Meuse basins. NCR-publication 18-2002, NCR, Delft.

HOOIJER, A., F. KLIJN, G.B.M. PEDROLI & A.G. VAN OS (2004), Towards sustainable flood risk management in the Rhine and Meuse river basins: synopsis of the findings of the IRMA-SPONGE. *River Research and Applications*, 20, pp. 343-357.

HOPKINSON, C., K. LIM, L.E. CHASMER, P. TREITZ, I.F. CREED & C. GYNAN (2004b), Wetland grass to plantation forest – estimating vegetation height from the standard deviation of lidar frequency distributions. In: Thies, M., B. Koch, H. Spiecker & H. Weinacker (eds.), ISPRS Archives Vol. 36 part 8/W2, Laser-scanners for forest and landscape assessment. Freiburg, Germany.

HOPKINSON, C., L.E. CHASMER, C. YOUNG-POW & P. TREITZ (2004a), Assessing forest metrics with a ground-based scanning lidar. *Canadian Journal of Forest Research*, 34, pp. 573-583.

HOPKINSON, C., L.E. CHASMER, G. SASS, I.F. CREED, M. SITAR, W. KALBFLEISCH & P. TREITZ (2005), Vegetation class dependent errors in lidar ground elevation and canopy height estimates in a boreal wetland environment. *Canadian Journal of Forest Research*, 31, pp. 191-206.

HOPKINSON, C., L.E. CHASMER, G. ZSIGOVICS, I.F. CREED, M. SITAR, P. TREITZ & R.V. MAHER (2004), Errors in lidar ground elevation and wetland height estimates. In: Thies, M., B. Koch, H. Spiecker &

H. Weinacker (eds.). Laser-scanners for forest and landscape assessment. ISPRS Archives, Vol. 36, part 8/W2, pp. 108-113.

HUG, C., A. ULLRICH & A. GRIMM (2004), Litemapper-5600: A waveform-digitizing lidar terrain and vegetation mapping system. In: Thies, M., B. Koch, H. Spiecker & H. Weinacker (eds.). Laser-scanners for forest and landscape assessment. ISPRS Archives, Vol. 36, part 8/W2, pp. 24-29.

HUISING, E.J. & L.M. GOMES PEREIRA (1998), Errors and accuracy estimates of laser data acquired by various laser scanning systems for topographic applications. *ISPRS Journal of Photogrammetry and Remote Sensing*, 53, pp. 245-261.

HUTHOFF, F. & D. AUGUSTIJN (2004), Sensitivity analysis of floodplain roughness in 1D flow. In: Liong, S.Y., S.I. Phoon & V. Babovich (eds.). 6th Interational conference on hydroinformatics. Singapore, Malaysia, pp. 301-308.

IPCC (2001), Climate change 2001: The scientific basis. In: Houghton, J.T., Y. Ding, D.J. Griggs, M. Noguer, P.J. Van der linden, X. Dai, K. Maskell & C.A. Johnson (eds.), IPCC, Cambridge, 83 pp.

JANS, L. (2004), Evaluatie nevengeulen Gamerense Waard 1996-2002 (in Dutch). RIZA 2004.024, RIZA, Arnhem.

JANSEN, B.J.M. & J.J.G.M. BACKX (1998), Ecotope mapping Rhine Branches-east 1997 (in Dutch). 98.054, RIZA, Lelystad.

JäRVELä, J. (2002), Flow resistance of flexible and stiff vegetation: a flume study with natural plants. *Journal of Hydrology*, 269, pp. 44-54.

JäRVELä, J. (2004), Effect of submerged flexible vegetation on flow structure and resistance. *Journal of Hydrology*, 307, pp. 233-241.

JESSE, P. (2004), Hydraulic resistance in (nature) development (in Dutch). 2003.124X, RIZA, Arnhem.

JESSE, P., D. BEYER & J.F. VAN DEN BORN (2002), Laseraltimetrie als invoer voor WAQUA (in Dutch). 2002.210X, RIZA, Arnhem.

JONCKHEERE, I., S. FLECK, K. NACKAERTS, B. MUYS, P. COPPIN, M. WEISS & F. BARET (2004), Review of methods for *in situ* leaf area index determination: Part I. Theories, sensors and hemispherical photography. *Agricultural and Forest Meteorology*, 121, pp. 19-35.

KATZENBEISSER, R. (2003). Technical note on: echo detection. Toposys GMBH, Biberach.

KAY, T.L. & J.T. KAJIYA (1986), Ray tracing complex scenes. *Computer Graphics*, 20, pp. 269-278.

KERNKAMP, H.W.J., H.A.H. PETIT, H. GERRITSEN & E.D. DE GOEDE (2005), A unified formulation for the three-dimensional shallow water equations using orthogonal co-ordinates: theory and application. *Ocean Dynamics*, 126, pp. 732-740.

KEULEGAN, G.H. (1938), Laws of turbulent flow in open channels. *Journal of Research of the National Bureau of Standards*, 21 (research paper 1151), pp. 707-741.

KILIAN, J., N. HAALA & M. ENGLICH (1996), Capture and evaluation of airborne scanner data. ISPRS Archives, Vol. 31 B3, pp. 383-388.

KLAASSEN, G.J. & J.J. VAN DER ZWAARD (1974), Roughness coefficients of vegetated flood plains. *Journal of Hydraulic Research*, 12, pp. 43-63.

KLAASSEN, G.J., C. STOLKER, E.H. VAN VELZEN & H. VERHEY (1999), Naar een ruwheidsvoorspeller voor moerasvegetatie op basis van riet en gras (in Dutch). 2000.166X, Delft Hydraulics, RIZA, Delft, Arnhem.

KLOPSTRA, D., H. BARNEVELD, J.M. VAN NOORTWIJK & E.H. VAN VELZEN (1997), Analytical model for hydraulic roughness of submerged vegetation, 27th international IAHR conference, San Francisco, pp. 775-780.

KOCH, B., U. HEYDER & H. WEINACKER (2006), Detection of individual tree crowns in airborne lidar data. *Photogrammetric Engineering & Remote Sensing*, 72, pp. 357-363.

KOPPEJAN, H. (1998), Toelichting bij de vegetatie- en structuurkaart Duursche Waarden 1996 op basis van false-color luchtfoto's (in Dutch). MDGAT 9716, Rijkswaterstaat Meetkundige Dienst, Delft.

KOUWEN, N. & M. FATHI-MOGHADAM (2000), Friction factors for coniferous trees along rivers. *Journal of Hydraulic Engineering*, 126, pp. 732-740.

KOUWEN, N. & R.M. LI (1980), Biomechanics of vegetated channel linings. *Journal of Hydraulics Divisions*, 106, pp. 1085-1103.

KOUWEN, N. & T.E. UNNY (1973), Flexible roughness in open channels. *Journal of the Hydraulics Division*, 99(HY5), pp. 713-728.

KOUWEN, N. (1988), Field estimation of biomechanical properties of grass. *Journal of Hydraulic Research*, 26, pp. 559-568.

KOUWEN, N., T.E. UNNY & H.M. HILL (1969), Flow retardance in vegetated channels. *Journal of the Irrigation and Drainage Division*, 95(IR2), pp. 329-342.

KRABILL, W., W. ABDALATI, E. FREDERICK, S. MANIZADE, C. MARTIN, J. SONNTAG, R. SWIFT, R. THOMAS, W. WRIGHT & J. YUNGEL (2000), Greenland ice sheet: High-elevation balance and peripheral thinning. *Science,* 289, pp. 428-430.

KRAUS, K. & N. PFEIFER (1998), Determination of terrain models in wooded areas with airborne laser scanner data. *ISPRS Journal of Photogrammetry and Remote Sensing*, 53, pp. 193-203.

LEFSKY, M.A., D. HARDING, W.B. COHEN, G. PARKER & H.H. SHUGART (1999b), Surface lidar remote sensing of basal area and biomass in deciduous forests of eastern Maryland, USA. *Remote Sensing of Environment*, 67, pp. 83-98.

LEFSKY, M.A., W.B. COHEN, G. PARKER & D. HARDING (2002), Lidar remote sensing for ecosystem studies. *Bioscience*, 52, pp. 19-30.

LEFSKY, M.A., W.B. COHEN, S.A. ACKER, G.G. PARKER, T.A. SPIES & D. HARDING (1999a), Lidar remote sensing of the canopy structure and biophysical properties of Douglas-fir Western Hemlock forests. *Remote Sensing of Environment*, 70, pp. 339-361.

LENDERS, H.J.R. & L. KNIPPENBERG (2005), The temporal and social dimensions of river rehabilitation: towards a multi-dimensional research perspective. *Archive für Hydrobiologie*, 15, pp. 119-131.

LEUVEN, R.S.E.W., Y. GERIG, I. POUDEVIGNE, G.W. GEERLING, L. KOOISTRA & B.G.W. AARTS (2002), Cumulative impact assessment of ecological rehabilitation and infrastructure facilities in floodplains along the middle reach of the River Waal. In: Leuven, R.S.E.W., I. Poudevigne & R.M. Teeuw (eds.). Application of Geographic Information systems and remote sensing in river studies. Backhuys Publishers, Leiden, Backhuys Publishers 247 pp.

LICHTI, D., D.J. GORDON & M.P. STEWART (2002), Ground-based laser scanners: operation, systems and application. *Geomatica*, 56, pp. 21-33.

LILLESAND, T.M. & R.W. KIEFER (1994), Remote sensing and image interpretation. John Wiley & sons, New York, 750 pp.

LIM, K., P. TREITZ, M. WULDER, B. ST-ONGE & M. FLOOD (2003), Lidar remote sensing of forest structure. *Progress in Physical Geography*, 27, pp. 88-106.

MACARTHUR, R.H. & H.S. HORN (1969), Foliage profile by vertical measurements. *Ecology*, 50, pp. 594-598.

MACARTHUR, R.H. & J.W. MACARTHUR (1961), On bird species diversity. *Ecology*, 42, pp. 594-598.

MAGNUSSEN, S. & P. BOUDEWYN (1998), Derivations of stand height from airborne laser scanner data with canopy-based quantile estimators. *Canadian Journal of Forest Research*, 28, pp. 1016-1031.

MALTAMO, M., K. EERIKAINEN, J. PITKANEN, J. HYYPPA & M. VEHMAS (2004), Estimation of timber volume and stem density based on scanning laser altimetry and expected tree size distribution functions. *Remote Sensing of Environment*, 90, pp. 319-330.

MARINE-ELECTRONICS (2006), Multi-return altimeter. http://www.marine-electronics.co.uk/brochures/altimeter/11001.pdf, date accessed 25-7-2006.

MARKS, K. & P. BATES (2000), Integration of high-resolution topographic data with floodplain flow models. *Hydrological Processes*, 14, pp. 2109-2122.

MASON, D.C., D.M. COBBY, M.S. HORRIT & P. BATES (2003), Floodplain friction parameterization in two-dimensional river food models using vegetation heights derived from airborne scanning laser altimetry. *Hydrological Processes*, 17, pp. 1711-1732.

MEANS, J.E., S.A. ACKER, D.J. HARDING, J.B. BLAIR, M.A. LEFSKY, W.B. COHEN, M.E. HARMON & W.A. MCKEE (1999), Use of large-footprint scanning airborne lidar to estimate forest stand characteristics in the Western Cascades of Oregon. *Remote Sensing of Environment*, 67, pp. 298-308.

MENENTI, M. and RITCHIE, J.C. (1994) Estimation of effective aerodynamic roughness of Walnut Gulch with laser altimeter measurements. *Water Resources Research*, 30, pp. 1329-1337.

MERTENS, W. (1989), Zur Frage hydraulischer Berechnungen naturnaher Fliessgewässer (in German). *Wasserwirtschaft*, 79, pp. 170-179.

MERTES, L.A.K. (2002), Remote sensing of riverine landscapes. *Freshwater Biology*, 47, pp. 799-816.

MERTES, L.A.K., D.L. DANIEL, J.M. MELACK, B. NELSON, L.A. MARTINELLI & B.R. FORSBERG (1995), Spatial patterns of hydrology, geomorphology, and vegetation on the floodplain of the Amazon river in Brazil from a remote sensing perspective. *Geomorphology*, 13, pp. 215-232.

MIDDELKOOP, H. & C.O.G. VAN HASELEN (1999), Twice a river: Rhine and Meuse in the Netherlands. 99.003, RIZA, Arnhem.

MIDDELKOOP, H., K. DAAMEN, D. GELLENS, W. GRABS, J.C.J. KWADIJK, H. LANG, B.W.A.H. PARMET, B. SCHäDLER, J. SCHULLA & K. WILKE (2001), Impact of climate change on hydrological regimes and water resources management in the Rhine basin. *Climatic Change*, 49, pp. 105-128.

MOLLER, D., S.J. FRASIER, D.L. PORTER & R.E. MCINTOSH (1998), Radar-derived interferometric surface currents and their relationship to subsurface currents. *Journal of Geophysical Research*, 103, C6, pp. 12839-12852.

MORSDORF, F., E. MEIER, B. KOTZ, K.I. ITTEN, M. DOBBERTIN & B. ALLGOWER (2004), LIDAR-based geometric reconstruction of boreal type forest stands at single tree level for forest and wildland fire management. *Remote Sensing of Environment*, 92, pp. 353-362.

MUSTE, M., K. YU, T. PRATT & D. ABRAHAM (2004), Practical aspects of ADCP data use for quantification of mean river flow characteristics; Part II: fixed-vessel measurements. *Flow Measurement and Instrumentation*, 15, pp. 17-28.

NÆSSET, E. (1997a), Determination of mean tree height of forest stands using airborne laser scanner data. *ISPRS Journal of Photogrammetry and Remote Sensing,* 52, pp. 49-56.

NÆSSET, E. (1997b), Estimating timber volume of forest stands using airborne laser scanner data. *Remote Sensing of Environment*, 61, pp. 246-253.

NÆSSET, E. & K.-O. BJERKNES (2001), Estimating tree heights and number of stems in young forest stands using airborne laser scanner data. *Remote Sensing of Environment*, 78, pp. 328-340.

NÆSSET, E. & T. OKLAND (2002). Estimating tree height and tree crown properties using airborne scanning laser in a boreal nature reserve. *Remote Sensing of Environment*, 79, pp. 105-115.

NÆSSET, E. (2002), Predicting forest stand characteristics with airborne scanning laser using a practical two-stage procedure and field data. *Remote Sensing of Environment*, 80, pp. 88-99.

NÆSSET, E. (2004). Effects of different flying altitudes on biophysical stand properties estimated from canopy height and density measured with a small-footprint airborne scanning laser. *Remote Sensing of Environment*, 91, pp. 243-255.

NEPF, H.M. (1999), Drag, turbulence, and diffusion in flow through emergent vegetation. *Water Resources Research*, 35, pp. 479-489.

NICHOLAS, A.P. & S.J. MCLELLAND (2004), Computational fluid dynamics modelling of three-dimensional processes on natural river floodplains. *Journal of Hydraulic Research*, 42, pp. 131-143.

NIENHUIS, P.H. & R.S.E.W. LEUVEN (2001), River restoration and flood protection: controversy or synergism? *Hydrobiologia*, 444, pp. 85-99.

NIENHUIS, P.H., A.D. BUISE, R.S.E.W. LEUVEN, A.J.M. SMITS, R.J.W. DE NOOIJ & E.M. SAMBORSKA (2002), Ecological rehabilitation of the lowland basin of the river Rhine (NW Europe). *Hydrobiologia*, 478, pp. 53-72.

NILSSON, M. (1996), Estimating tree heights and stand volume using an airborne lidar system. *Remote Sensing of Environment*, 56, pp. 1-7.

OUDE ELBERINK, S., G. BRAND & R. BRüGELMANN (2003), Quality improvement of laser altimetry DEM's. In: Maas, H.-G., G. Vosselman & A. Streilein (eds.). 3-D reconstruction from airborne laserscanner and InSAR data. ISPRS Archives, Vol. 34 3/W13, pp. 51-58.

PARKER, G.G., D.J. HARDING & M.L. BERGER (2004), A portable LIDAR system for rapid determination of forest canopy structure. *Journal of Applied Ecology*, 41, pp. 755-767.

PASCHE, E. (1984), Turbulenzmechanismen in naturnahen Fliessgewässern und die Mögligkeit ihrer mathematischen Erfassung. Mitteilung des Instituts für Wasserbau, 52 TWTH, Aachen.

PERSSON, Å., J. HOLMGREN & U. SöDERMAN (2002), Detecting and measuring individual trees using an airborne laser scanner. *Photogrammetric Engineering & Remote Sensning*, 68, pp. 925-932.

PETRYK, S. & G. BOSMAJIAN (1975), Analysis of flow through vegetation. *Journal of Hydraulics Divisions*, 101, pp. 871-884.

PFEIFER, N., B. GORTE & G. VOSSELMAN (2003), Laser altimetry and vegetation. AGI-GAP 2003-56, AGI, Delft.

PFEIFER, N., B. GORTE & S. OUDE ELBERINK (2004), Influences of vegetation on laser altimetry – analyses and correction approaches. In: Thies, M., B. Koch, H. Spiecker & H. Weinacker (eds.). Laser-scanners for forest and landscape assessment. ISPRS Archives, Vol. 36 8/W2, pp. 283-287.

POPESCU, S.C., R.H. WYNNE & R.F. NELSON (2002), Estimating plot-level tree heights with lidar: local filtering with a canopy-height based variable window size. *Computers and Electronics in Agriculture*, 37, pp. 71-95.

POSTMA, L., G.K. VERBOOM & A.E. MYNETT (2000), Towards an Open Delft3D Modelling System, Hydroinformatics 2000.

RDINSTRUMENTS (1996), Acoustic doppler current profiler, principles of operation, a practical primer, RDInstruments, San Diego, California.

RICHTER, B.D., R. MATHEWS, D.L. HARRISON & R. WIGINGTON (2003), Ecologically sustainable water management: managing river flows for ecological integrity. *Ecological Applications*, 13, pp. 206-224.

RINGROSE, S., W. MATHESON & T. BOYLE (1988), Differentiation of ecological zones in the Okavango delta, Botswana by classification and contextual analyses of Landsat MSS data. *Photogrammetric Engineering & Remote Sensing*, 54, pp. 601-608.

RITCHIE, J.C., D.L. EVANS, D. JACOBS, J.H. EVERITT & M.A. WELTZ (1993), Measuring canopy structure with an airborne laser altimeter. *Transactions of ASAE,* 36, pp. 1235-1238.

RITCHIE, J.C., M. MENENTI & M.A. WELTZ (1996), Measurements of land surface features using an airborne laser altimeter: the HAPEX-sahel experiment. *International Journal of Remote Sensing*, 17, pp. 3705-3724.

RITZEN, M.R. & M.W. STRAATSMA (2002), Laseraltimetrie en hydraulische vegetatieruwheid van uiterwaarden, NCR-publicatie, 19-2002, Delft.

ROSSO, P.H., S.L. USTIN & A. HASTINGS (2006), Use of lidar to study changes associated with Spartina invasion in San Francisco Bay marshes. *Remote Sensing of Environment*, 100, pp. 295-306.

SCHLICHTING, H. (1962), Boundary-Layer Theory. McGraw-Hill book company, New York, 802 pp.

SCHMIDT, K.S. & A.K. SKIDMORE (2003), Spectral discrimination of vegetation types in a coastal wetland. *Remote Sensing of Environment*, 85, pp. 92-108.

SCHRöDER, W. & A. NUDING (1986), Spiegellinienberechnung für einen Wildbach mit Gehölzufern (in German). *Wasserwirtschaft*, 76, pp. 388-395.

SHABALOVA, M.V., W.P.A. VAN DEURSEN & T.A. BUISHAND (2003), Assessing future discharge of the river Rhine using regional climate model integrations and a hydrological model. *Climate Research*, 23, pp. 233-246.

SILVA, W. (2003), Hoeveel (hoog)water kan ons land binnenkomen via de Rijn bij Lobith, nu en in de toekomst (in Dutch). 2003.015, RIZA, Arnhem.

SILVA, W., F. KLIJN & J. DIJKMAN (2001), Room for the Rhine branches in The Netherlands. RIZA-report 2001.031, Delft Hydraulics report R3294, RIZA, WL | Delft Hydraulics, Arnhem, Delft.

SITHOLE, G. and VOSSELMAN, G. (2004), Experimental comparison of filter algorithms for bare-earth extraction from airborne laser scanning point clouds. *ISPRS Journal of Photogrammetry and Remote Sensing*, 59, pp. 85-101

SKALOUD, J., J. VALLET, K. KELLER, G. VESSIèRE & O. KöLBL (2005), Helimap: rapid large scale mapping using handheld lidar/CCD/GPS/INS sensors on helicopters, ION GNSS Congress. Long Beach.

STOESSER, T., C.A.M.E. WILSON, P. BATES & A. DITTRICH (2003), Application of a 3D numerical model to a river with vegetated floodplains. *Journal of Hydroinformatics*, 5, pp. 99-112.

STOLKER, C., E.H. VAN VELZEN & G.J. KLAASSEN (1999), Nauwkeurigheidsanalyse stromingsweerstand vegetatie (in Dutch). 99.192x, Delft Hydraulics, RIZA, Delft, Arnhem.

STONE, B.M. & H.T. SHEN (2002), Hydraulic resistance of flow in channels with cylindrical roughness. *Journal of Hydraulic Engineering*, 128, pp. 500-506.

THIES, M., N. PFEIFER, D. WINTERHALDER & B.G.H. GORTE (2004), Three-dimensional reconstruction of stems for assessment of taper, sweep and lean based on laser scanning of standing trees. *Scandinavian Journal of Forest Research* 19, pp. 571-581.

THOMPSON, A.G., R.M. FULLER & J.A. EASTWOOD (1998), Supervised versus unsupervised methods for classification of coasts and river corridors from airborne remote sensing. *International Journal of Remote Sensing*, 19, pp. 3423-3431.

TOWNSEND, P.A. & J. WALSH (2001), Remote sensing of forested wetlands: application of multitemporal and multispectral satellite imagery to determine plant community composition and structure in southeastern USA. *Plant Ecology*, 157, pp. 129-149.

TRIMBLE (2006), Datasheet Trimble 5600 DR total station. http://trl.trimble.com/docushare/dsweb/Get/Document8889/12412E_5600_DS_0306_lr.pdf, date accessed 12-7-2006.

TSUJIMOTO, T. (1999), Fluvial processes in streams with vegetation. *Journal of Hydraulic Engineering*, 37, pp. 789-803.

VAN DER MOST, H. & M. WEHRUNG (2005), Dealing with uncertainty in flood risk assessment of dike rings in The Netherlands. *Natural Hazards*, 36, pp. 191-206.

VAN DER SANDE, C.J., S.M. DE JONG & A.P.J. DE ROO (2003), A segmentation and classification approach of IKONOS-2 imagery for land cover mapping to assist flood risk and flood damage assessment. *International Journal of Applied Earth Observation and Geoinformation*, 4, pp. 217-229.

VAN GENNIP, B. & J. BERGWERFF (2002), Ecotopen- en struweelkartering Gamerensche Waard 2002 (in Dutch). MD-GAE-2002.37, RIZA, Lelystad.

VAN RIJN, L.C. (1994), Principles of fluid flow and surface waves in rivers, estuaries, seas and oceans. Aqua publications, Amsterdam.

VAN STOKKOM, H.T.C., A.J.M. SMITS & R.S.E.W. LEUVEN (2005), Flood defense in the Netherlands a new era, a new approach. *Water International*, 30, pp. 76-87.

VAN URK, A. (1981), Hydraulische ruwheid grasland in uiterwaarden (in Dutch). WWZO 81.21, RIZA, Arnhem.

VAN VELZEN, E.H., P. JESSE, P. CORNELISSEN & H. COOPS (2003), Stromingsweerstand vegetatie in uiterwaarden (in Dutch). 2003.028, RIZA, Arnhem.

VAN WESTEN, C.J. (2005), Flood risk and safety in the Netherlands (Floris): Floris study, full report. DWW 2006-014, ISBN 90-369-5604-9, DWW, Delft.

VOSSELMAN, G. (2000), Slope based filtering of laser altimetry data., ISPRS Archives, Vol 33. pp. 935-942, Amsterdam.

VULINK, T. (2001), Hungry herds Management of temperate lowland wetlands by grazing. PhD Thesis, University of Groningen, Groningen, pp. 271-290.

WAGNER, W., A. ULRICH, T. MELZER, C. BRIESE & K. KRAUS (2004), From single pulse to full waveform digitizing laser scanners: potential and practical challenges. ISPRS Archives, Vol. 35 part B3, Istanbul

WARD, J.V. & K. TOCKNER (2001), Biodiversity: towards a unifying theme for river ecology. *Freshwater Biology*, 46, pp. 807-819.

WARMINK, J. (2007), Measuring vegetation density. MSc Thesis, Utrecht University, Utrecht, 80 pp.

WATT, P.J. & D.N.M. DONOGHUE (2005), Measuring forest structure with terrestrial laser scanning. *International Journal of Remote Sensing*, 26, pp. 1437-1446.

WEHR, A. & U. LOHR (1999), Airborne laser scanning – an introduction and overview. *ISPRS Journal of Photogrammetry and Remote Sensing*, 54, pp. 68-82.

WELTZ, M.A., J.C. RITCHIE & H. DALE FOX (1994), Comparison of laser and field measurements of vegetation height and canopy cover. *Water Resources Research*, 30, pp. 1311-1319.

WERNER, M.G.F., N.M. HUNTER & P.D. BATES (2005), Identifiability of distributed floodplain roughness values in flood extent estimation. *Journal of Hydrology*, 314, pp. 139-157.

WHEATER, H.S. (2006), Flood hazard and management: A UK perspective. *Philosophical Transactions: Mathematical, Physical and Engineering Sciences (Series A)*, 364, pp. 2135-2145.

WILBER, K. (2000), Sex, ecology and spirituality. Shambala, Boston and London, 823 pp.

WILSON, C.A.M.E. & M.S. HORRIT (2002), Measuring flow resistance of submerged grass. *Hydrological Processes*, 16, pp. 2589-2598.

WONNACOTT, T.H. & R.J. WONNACOTT (1990), Introductory Statistics. John Wiley & Sons, New York, 711 pp.

WOOLARD, J.W. & J.D. COLBY (2002), Spatial characterization, resolution, and volumetric change of coastal dunes using airborne LIDAR: Cape Hatteras, North Carolina. *Geomorphology*, 48, pp. 269-287.

WOTRUBA, L., F. MORSDORF, E. MEIER & D. NüESCH (2005), Assessment of sensor characteristics of an airborne laser scanner using geometric reference targets. In: Vosselman, G. & C. Brenner (eds.). ISPRS Archives Vol. 36, part 3/W19, ISPRS workshop laser scanning 2005, Enschede.

YU, X., J. HYYPPä & H. HYYPPä, 2004. Effects of flight altitude on tree height estimation using airborne laser scanning. In: Thies, M., B. Koch, H. Spiecker & H. Weinacker (eds.). Laser-scanners for forest and landscape assessment. ISPRS Archives, Vol. 36 8/W2, pp. 96-101.

ZEHM, A., M. NOBIS & A. SCHWABE (2003), Multiparameter analysis of vertical vegetation structure based on digital image processing. *Flora*, 198, pp. 142-160.

Curriculum Vitae

Menno Wiebe Straatsma (1974) grew up in Berkel and Rodenrijs and later in Schipluiden, a village close to Delft. From the age of 14 he was active as a white water kayaker and two years later he started to work as a kayak instructor in the Alps and in the surf zone in the Netherlands. In 1993 he passed his exam at the 'Sint Stanislas College' and studied civil engineerng for one year at the Delft Technical University.

After that, it was time to go and see the world. In 1995, Menno went to Lesotho, Africa, where he developed appropriate solar technology using locally available building materials. Additionally, he worked as a safety kayaker on the Zambezi river downstream of the Victoria Falls accompanying raft trips. In this period, aquiring and applying knowledge proved very difficult. Theefore, he decided to return to university to complete his formal studies. He studied Physical Geography at the Utrecht University, which was such a boon, because of the ease of knowledge aquisition. His special interest was in rivers and he wrote his master's thesis on hydrodynamic roughness and airborne laser scanning.

This became also the topic of his PhD research, which he started in 2002. Field data were aquiered in several floodplain sections and compared to remote sensing datasets. Results were presented at several national and international congresses in the Netherlands and Austria. He won prizes on poster design, oral presentation and scientific writing. Additional input for personal development was gained from the 'adventure in consciousness' provided by the Ridhwan school of Hameed Ali. This training can be seen as the psycho-spiritual equivalent of white-water kayaking.

Currently, Menno works at the Utrecht University on the integration of perspectives on river landscaping and their influence on flow characteristics, sediment and heavy metal deposition, natural value and food web poisoning.